Ultrafast fluorescence spectroscopy used as a probe to explore excited state photophysics of biologically and environmentally relevant systems

by

Prasun Mukherjee

A dissertation submitted to the graduate faculty

in partial fulfillment of the requirements for the degree of

DOCTOR OF PHILOSOPHY

Major: Physical Chemistry

Program of Study Committee:
Jacob W. Petrich, Major Professor
Mark S. Gordon
Mark S. Hargrove
Xueyu Song
Hans Stauffer

Iowa State University

Ames, Iowa

2008

UMI Number: 3307072

UMI Microform 3307072

ProQuest Information and Learning Company
300 North Zeeb Road
P.O. Box 1346
Ann Arbor, MI 48106-1346

Dedicated to my parents

TABLE OF CONTENTS

ACKNOWLEDGEMENT

I would like to express my heartfelt gratitude and appreciation to my research advisor, Dr. Jacob W. Petrich. It is obvious that without his invaluable guidance, constant support and help, the research works described here would never have been possible. It is my ultimate pleasure to work with him.

I would also express my humble gratitude to all my committee members, Dr. Mark S. Gordon, Dr. Mark S. Hargrove, Dr. Xueyu Song and Dr. Hans Stauffer for all their help.

I am highly grateful to all of our group members. I express my special thanks to Dr. Mintu Halder for training me in the laboratory. I thank Pramit Chowdhury and Lindsay Sanders Headley for their generous help in showing me the intrinsic details of numerous calculation and analysis methods. It has turned out to be a great experience working with Ramkrishna Adhikary and Sayantan Bose and I enjoyed sharing the workspace with them. I admit that I have been benefited a lot through the discussions with them on various basic concepts. I am thankful to Ramkrishna Adhikary for carefully reading the first two chapters of this thesis and giving helpful comments. I would also like to thank Dr. Ranjan Das, Dr. Govindarajan Krishnamoorthy, Charles Barnes, Alyse Hurd, Alex Reynolds, Frank Maistrovich, Tessa Calhoun and Erin Campbell. I have been privileged to work with all these wonderful people in the laboratory.

The research described in this thesis involves lot of collaborations. I thank Dr. Daniel W. Armstrong and his group members for providing us with the ionic liquids and helping us with chromatographic separations. For protein work, I thank Dr. Mark S. Hargrove and his group members for collaborating with us and letting us use his laboratory for our protein preparation work. Dr. Xueyu Song deserves special thanks as he always helped us with the

theoretical aspects. I am gratefully indebted to him for providing the program of "zero-time" spectrum calculation. I am thankful to Dr. William M. Atkins and Weiya D. Lu for providing us with the GST proteins. For pigment work, I thank Dr. Christopher S. Lobban, Bruce Fulton and Kamel Harrata for providing immense help. I also thank the members from NADC and Dr. Pavol Miskovsky and Dr. Zhiqun Lin for collaborating with us.

I would like to thank Dr. Basudeb Saha for helping and teaching me various experiments in Physical and Analytical Chemistry laboratory. I would also like to thank Dr. Bob Doyle for his generous support while performing the microscopy experiments. I am also very grateful to all the members of the Chemistry department for making my stay here a wonderful one. I thank all of my friends, especially Supratim Giri, Ramkrishna Adhikary, Sayantan Bose, for their company.

I am grateful to many of my teachers for building me up. I am thankful to Dr. Sambhu N. Datta (with whom I have done my Masters research) for his guidance and to Dr. Anindya Datta for helping me in choosing this laboratory for my graduate studies. Two of my college professors, Dr. Gobinda De and Dr. Anirban Misra, need special mention. I am gratefully thankful to them for guiding me during my college days. I must admit that without their constant help I would probably not ending up here.

Last but not the least I would like to express my sincere thanks to my parents for their love, support, patience and understanding. This work would never have been possible without their constant encouragement. I dedicate the thesis to my parents. My interest in Chemistry grew initially while discussing many Chemistry problems with my father. I also thank all my family members and relatives for their love and support.

CHAPTER I. GENERAL INTRODUCTION

With the help of ultrafast laser techniques there has been tremendous progress in understanding various important molecular phenomenon occurring on the nanosecond (10^{-9} s), picosecond (10^{-12} s), and even femtosecond (10^{-15} s) time regimes. The importance of such short time scale measurements can be appreciated by considering that many biological and chemical phenomena, for example, hydrogen atom (or proton) transfer and electron transfer, occur on these time scales.

This thesis mainly deals with four main topics, namely (a) understanding the differential interaction of hypericin with two different isoforms of Glutathione S-transferase (GST) proteins, (b) characterization and structure elucidation of a novel hypericin like pigment from a marine ciliate Maristentor dinoferus, (c) solvation dynamics in room temperature ionic liquids (RTILs) especially focusing on a comparison of bulk solvent versus its micellar form in water and (d) solvation dynamics in protein environments. In this chapter I will briefly overview various systems, which are studied here, with the help of the instrumentation available in our laboratory. Special emphasis was given to the current available literature and the motivation of the work discussed here.

Excited State Photophysics of Hypericin: Understanding the Nature of Non-naturally Occurring Complexes with Proteins

Hypericin (Figure I.1) is a widely occurring natural perylene quinone pigment, best known from flowering plants in the genus Hypericum. Hypericin merits attention in the scientific community because it displays a broad spectrum of light induced antitumor and

antiviral activity against several types of viruses, including the human immunodeficiency virus (HIV) [1-5].

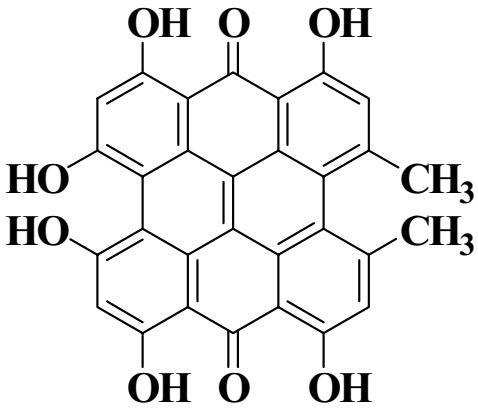

Figure I.1. The structure of Hypericin (7,14 normal form).

Photoactive molecules interact by two major pathways, namely, interacting directly with a substrate (Type I mechanisms) or producing reactive oxygen species, especially highly reactive singlet oxygen (Type II mechanisms). A schematic diagram illustrating these two mechanisms is shown in figure I.2. The basic difference between these two mechanisms lies in whether the photosensitizer first experiences the substrate or the ground state triplet oxygen in a particular environment.

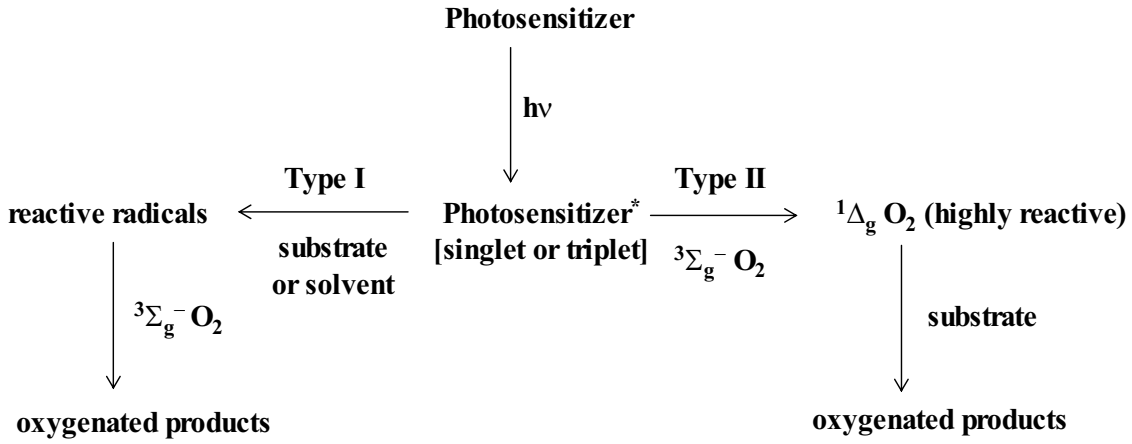

Figure I.2. Schematic diagram of Type I and Type II mechamisms in photosensitization reaction.

Hypericin and its analogs can interact through both of these pathways independently or act as some suitable combination of these two extremes. It is important to understand the relative roles of these two mechanistic pathways in a given environment.

Hypericin has a single exponential fluorescence lifetime of ~ 5.5 ns in bulk organic solvents in which it is soluble. It is to be noted that hypericin is not soluble in water and also it forms non-fluorescent aggregates in bulk water and consequently has no photodynamic action [6-8]. The triplet state lifetime of hypericin is in μs regime. The reasonably long triplet lifetime and significant quantum yield (0.35) makes hypericin a good photosensitizer [9].

Owing to diverse applications of hypericin in biological activities it would be very interesting to understand the photophysical processes that occur upon light absorption. By means of H/D substitution, investigation of methoxy analogs, and complementary studies using both transient absorption and fluorescence upconversion spectroscopies, we have argued that the major primary photophysical process in hypericin in organic solvents is excited-state intramolecular hydrogen atom transfer [10-23]. This argument was based upon the observation of a rising component in the kinetic traces of stimulated emission or fluorescence in hypericin and related analogs and the absence of the same in the corresponding deutarated and methylated analogs. The intramolecular hydrogen atom transfer is followed by intermolecular proton transfer [24-26]. We have argued that these photogenerated protons might have significant role in the photodynamic therapy of hypericin [4]. However, in light of the photodynamic therapy (PDT) it is of utmost importance to understand the interaction of hypericin with various biologically important macromolecules. The literature on this important aspect is rather sparse.

Earlier we have extensively studied the photophysics of hypericin complexed with human serum albumin (HSA) [22]. From this study it was demonstrated that hypericin forms a rigid complex with HSA having 1:1 binding stoichiometry. It has been shown that in HSA:Hyp = 1:1 complex the intramolecular hydrogen atom transfer is completely impeded as evidenced by the absence of rise time in the emission trace. Based on this observation it was proposed that hypericin binds to HSA by means of a specific hydrogen-bonded interaction between its carbonyl oxygen and the N_1-H of the single tryptophan residue (W214) in the IIA subdomain of HSA.

Although various groups have investigated the interaction of hypericin with HSA [6,22,27-33], detailed studies on the interaction of hypericin with other biomolecules are not widely available in the literature. Recently Atkins and coworkers have shown that hypericin can form complexes with different isoforms of Glutathione S-Transferases (GSTs), namely A1-1 and P1-1, with submicromolar binding affinity [34]. Most interestingly it has been demonstrated that these two isoforms can tune hypericin photophysics differently. By means of electrospray ionization mass spectrometry (ESI-MS) they have demonstrated while hypericin complexed with A1-1 is susceptible to light induced oxidation, corresponding P1-1 complex resists oxidation significantly. With this result in hand we aim to understand the photophysics of hypericin in complex with these proteins. It is clear that interaction with a protein modifies the photophysics of hypericin, and understanding the molecular basis of this interaction is one of the outstanding problems in elucidating the function of hypericin and hypericin-like chromophores.

Photomovements in Ciliates: Structure Elucidation of Novel Hypericin Like Pigment

Many protists respond positively or negatively to light in order to acquire food, to avoid predators, or to avoid direct harmful effects of irradiation. Ciliates have cilia and photoreceptors distributed all over the cell surface. Before proceeding on this topic it would be helpful to define a few relevant terms. Phototaxis is movement oriented to the direction of light and can be positive or negative. Phototaxis and other behavioral responses to light can result in photoaccumulation in bright light or photodispersal into dim light or darkness. A photophobic reaction is an abrupt stop, reversal and turn in response to a rapid increase (step-up) or decrease (step-down) in the light flux [35-37].

Photoresponse in two species, namely, Stentor coeruleus and Blepharisma japonicum were extensively studied [36,38-48]. Both of these species show abrupt photophobic response. The major pigments from these species has also been characterized [49,50]. Structures of these pigments are shown in figure I.3. To date these are the only two pigments that have been structurally characterized from the ciliates. Other heterotrichs are known to have spectrally similar pigments but the structures have not been determined. Some other Stentor species have both pigment and symbiotic green algae (zoochlorellae) and are positively phototactic, but neither their photobiology nor their pigment structures have been studied.

Recently Lobban and coworkers discovered the marine ciliate, Maristentor dinoferus [51,52], which is prominently pigmented and also contains some 600 endosymbiotic golden algal cells (zooxanthellae). It is positively phototactic. Initial observations on the Maristentor pigment [51,52] showed that the pigment is fluorescent and has a UV-visible absorption spectrum similar to hypericin and stentorin. Here we report the elucidation of the structure of the chromophore and its spectral properties. Maristentorin is interesting both as

a novel analog of hypericin and as a new member of the multifunctional pigments from stentorids. For more detailed information on this interesting topic readers are referred to a recent review by Lobban et al. and references therein [53].

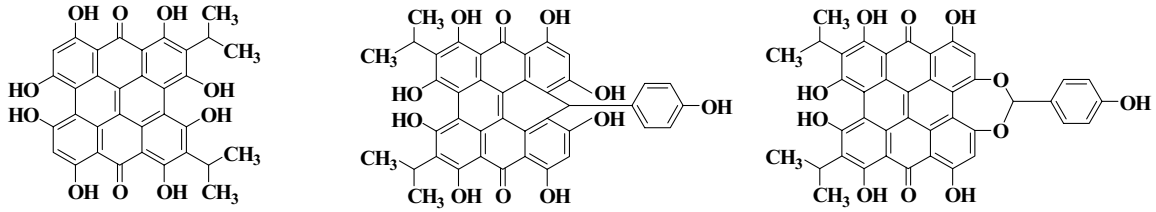

Figure I.3. The structures of (a) stentorin, (b) blepharismin C, (c) oxyblepharismin C. For the structure of hypericin refer to figure I.1.

Solvation Dynamics

Solvents play a major role in various chemical reactions. Solvents usually change the reaction pathways compared to that in gas phase. This is known as static solvation [54]. Solvation dynamics refers to solvation phenomena that change with time. Detailed insight into the time scale of solvation dynamics has important consequence in understanding the rates of chemical reactions in liquids, especially electron transfer and various charge transfer reactions [55-68].

Typically a fluorophore resides in the ground electronic state at room temperature and is in equilibrium with the surrounding solvent molecules. Upon excitation with light the molecule absorbs a photon and goes to the excited state. This creates an instantaneous change in the dipole moment of the molecule, and the system is placed in a non-equilibrium

configuration. The solvent molecules now must reorient themselves so as to minimize the total energy of the system. The process of this solvent stabilization towards a new equilibrium state is known as dynamic solvation; and, as it occurs the emission spectrum changes with time. This results in a time dependent fluorescence Stokes shift (TDFSS). The corresponding spectra are known as time resolved emission spectra (TRES). At earlier times one monitors emission from initially excited states and hence the spectrum appears at higher energies. On the other hand, as time progresses the initially excited state gets relaxed and one monitors emission from the relaxed state and consequently the spectrum shifts to lower energies. A schematic diagram illustrating solvation dynamics is shown in figure I.4. Detailed discussions on the concept of solvation dynamics experiments can be found in references [69,70].

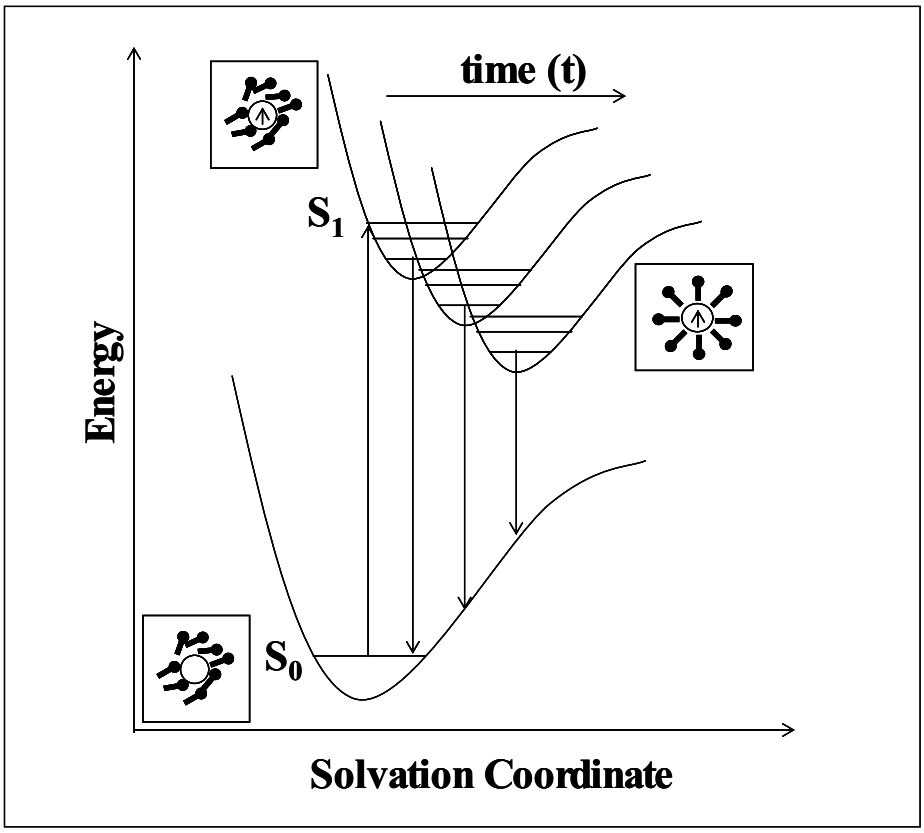

Figure I.4. A schematic diagram illustrating solvation dynamics.

Solvation dynamics is an active area of both experimental [68,71-92] and theoretical [91,93-98] research. Here I will mainly focus on solvation dynamics in two very different environments, namely, room temperature ionic liquids (RTILs) and monomeric hemeproteins.

We use coumarin 153 (C153) as our solvatochromic probe (figure I.5). The choice of C153 was based on the following considerations. First, there is a significant change in dipole moment (~ 7 D) of C153 upon excitation. Second, C153 is a reasonably rigid molecule. Third, C153 shows a significant red shift on changing the polarity of the surrounding solvent media. For example, there is a shift in fluorescence emission peak maxima from 447 to 536 nm on going from n-hexane to methanol. Fourth, the photophysics of C153 is known to have no contamination from other excited states. Due to these factors C153 has been extensively used in solvation dynamics study involving bulk homogeneous solvents [68,84,99] to restricted heterogeneous systems, for example, micelle [100-102], reverse micelle and related systems [103-105] and in proteins [106-108].

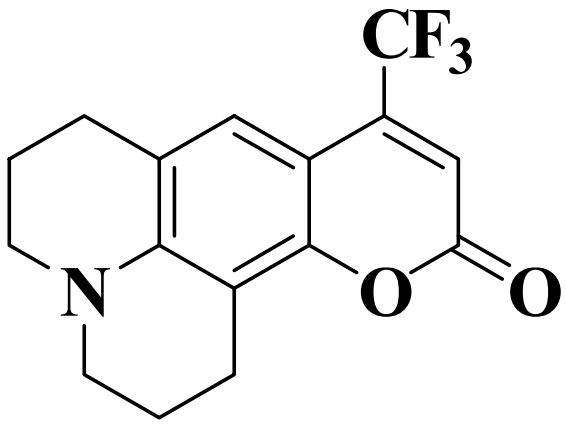

Figure I.5. Structure of coumarin 153 (C153).

Room Temperature Ionic Liquids (RTILs)

Room temperature ionic liquids (RTILs) are salts, usually composed of an organic cation and an inorganic anion that are liquid at room temperature or at reasonably low temperature. These systems are different than ionic solutions where an external solvent is necessary to dissolve the ions of the solute. As the name suggests these compounds are liquid at room temperature. However, in the scientific community ionic liquids having melting point less than 100^{o}C are considered as RTIL, because they can be used as solvents under conventional organic liquid phase reaction conditions [109]. It should be noted that 100^{o}C is just a convenient temperature and no special significance is associated with this temperature [110]. One of the earlier known ionic liquid was ethyl ammonium nitrate [$EtNH_3^+$][NO_3^-], the synthesis of which was reported in 1914 [111]. Despite the fact that ionic liquids were reported in the literature earlier it was not until very recently these systems received much attention in scientific research. Although the haloaluminate based ionic liquids were reported since the 1950s [112,113] their use was limited due to air and moisture sensitivity. Very recently there is a growing body of literature on air and moisture stable ionic liquids which have attracted the attention in scientific community [110,114-116]. These salts are typically based on organic cations such as alkylimidazolium [$R_1R_2R_3IM^+$], N-alkyl pyridinium [R_1Py^+], tetraalkyl ammonium [$R_1R_2R_3R_4N^+$] or tetraalkyl phosphonium [$R_1R_2R_3R_4P^+$] where R represents alkyl groups which could be same or different in a given ion and inorganic anions such as halides [X^-], hexafluoro phosphate [PF_6^-], tetrafluoro borate [BF_4^-] or bis-trifluoromethyl sulfonyl imide [NTf_2^-]. The structures of the common cations and anions that comprise ionic liquids are shown in figure I.6.

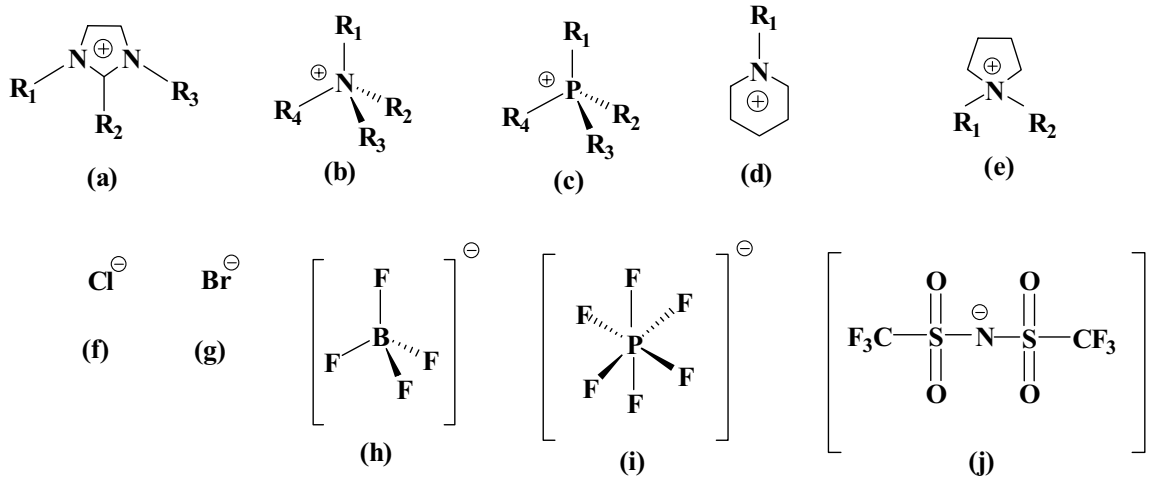

Figure I.6. Structures of commonly used cations (a) alkylimidazoliums, (b) alkylammoniums, (c) alkylphosphoniums, (d) alkylpyridiniums, (e) alkylpyrrolidiniums, and anions (f) chloride, (g) bromide, (h) tetrafluoroborate [BF_4^-], (i) hexafluorophosphate [PF_6^-], (j) bis[(trifluoromethyl)-sulfonyl]imide [NTf_2^-].

RTILs find wide applications in organic systhesis [114,116-128], in liquid-liquid extractions [129,130], in electrochemical studies [131] and as ultralow volatility liquid matrixes for matrix assisted laser desorption/ionization mass spectrometry [132]. They have negligible vapor pressure, thus making them "green" solvents by reducing the volatile organic content in the environment. They also have stability over a wide range of temperature as well a huge liquidus range. Perhaps the most important aspect of ionic liquids is to tune their physical properties by varying the cationic or the anionic moiety. This is the basis that the RTILs are often designated as "designer solvent" [133].

The synthesis of ionic liquids is mainly comprised of two main reactions, namely the quarternization followed by the metathesis step [109]. A general schematic outline of ionic liquid synthesis is shown in scheme I.

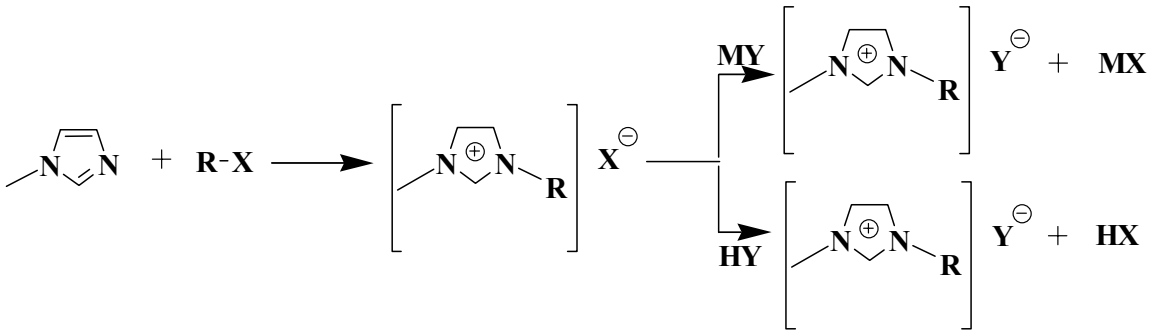

Scheme I.

For example, to synthesize [BMIM$^+$][NTf$_2^-$], first [BMIM$^+$][Cl$^-$] is produced by refluxing equimolar amounts of 1-methylimidazole with 1-chlorobutane at 70°C for 72 h. The resulting [BMIM$^+$][Cl$^-$] is washed with ethyl acetate and dried under vacuum. [BMIM$^+$][NTf$_2^-$] is produced by reacting equimolar amount of [BMIM$^+$][Cl$^-$] and N-lithiotrifluoromethanesulfonimide (LiNTf$_2$) in water and stirred for 12 h. The aqueous portion is removed and the resulting [BMIM$^+$][NTf$_2^-$] is washed with water. The IL is then dried under vacuum [134].

Considering the wide applications of RTILs, it is an obvious concern to understand the nature of the interactions of these interesting solvents with various dissolved solutes, in particular the relative contribution of individual ions on the solvation response. Here I will briefly discuss the current literature on this growing topic. To gain insight into this new class of fascinating solvents attempt were made to determine the polarity of these media. RTILs were found to be more polar than acetonitrile, but less polar than methanol as determined by the $E_T(30)$ scale, typically in most cases the values are comparable to that in short chain alcohols [135]. Also, they appear within a very short range in the polarity scale. Clearly the single polarity parameter in ionic liquids is not very helpful considering that ionic liquids are known to tune the rates of chemical reactions differently. For example, although

[$BMIM^+$][PF_6^-] and [$BMIM^+$][BF_4^-] have similar polarity parameters in the $E_T(30)$ scale they are known to affect a given chemical reaction in a different manner [123,124]. It is of interest that the dielectric constant (which is a measure for the bulk polarity of a solvent) as determined by Weingärtner and coworkers [136] by dielectric relaxation spectroscopy falls in the region of 8.8-15.2 differs significantly than that observed from the empirical polarity scales like $E_T(30)$ parameter. From this observation it might be reasonable to assume that the microscopic polarity in RTILs is in general higher compared to the bulk polarity. Anderson et al. [115] characterized a wide range of ionic liquids using an empirical relationship proposed by Abraham and coworkers [137-139] which considers the interaction with n and π electrons, dipolarity or polarizabilty, hydrogen bond acidity, hydrogen bond basicity and dispersion effects. However, to understand the rates of various chemical reactions in ionic liquids it is of extreme importance to understand the dynamic aspect of solvation in these systems.

Towards this goal, Huppert and coworkers have investigated the solvation dynamics of molten tetraalkyl ammonium salts and concluded that the solvation is biphasic, where the components are related to the transport properties of the ions which consequently relate to the relative size of the constituent ions. As in most cases the cations are larger in size than the anions, according to the Huppert model, it is the anion which is responsible for the faster part of response, and the cation is the sole contributor for the slower response [140-143]. This idea was slightly modified by Samanta and coworkers who has argued that while the faster response is due to the anions the origin of slower part is due to the collective motion of the cations and anions [144-146]. Maroncelli and coworkers however emphasized the solvation event in ionic liquids as being non-exponential in nature which could be best described by stretched exponential functions (in analogy to glass forming liquids) [147-149]. These authors

emphasized the contribution of cationic moiety for the faster response in solvation [147,148], which was proposed on the basis of observation of ~ 50 % solvation occurring within ~ 5 ps in imidazolium based RTILs and the corresponding absence of similar response in ammonium and phosphonium based RTILs. From this they have proposed that the ultrafast component in imidazolium salts are originating from the small amplitude motions of cations which are closer to the probe molecule and is being facilitated by the coplanarity of the imidazolium ring along with the fluorophore. Later they have observed that presence of imidazolium cations is not a prerequisite to observe an ultrafast component [150-152] as with improved time resolution they were able to observe nearly full solvation response from an imidazolium based ionic liquid, also the ultrafast component was observed in pyrrolidinium and ammonium based ionic liquids. In a comparison of $[BMIM^+][PF_6^-]$, $[BMIM^+][NTf_2^-]$ and $[BMIM^+][CTf_3^-]$ they found a correlation between the initial faster solvation response and the size and/or mass of the anion, that is, the faster part of the response increases in the order $CTf_3^- < NTf_2^- < PF_6^-$ [150]. They concluded that the anion might be responsible for this part of the response [150-152]. Based on this, they have proposed that the initial part of the solvation response might be attributed to the translational adjustment of ions within the first solvation shell upon excitation of the probe where the slower part is a reflection of the diffusive response of the cations and anions [152]. However, they stress special importance to phosphonium based ionic liquids owing to their large size and corroborate this with the non-observance of the ultrafast component in these systems [148,153]. We, on the other hand, have suggested that the polarizability of the cation might be responsible for the early time solvation response. This conclusion was based on the observation of similar faster solvation component in ionic liquid $[BMIM^+][PF_6^-]$ and its pure organic counterpart butyl imidazole

(BuIm) [134]. Following this we have studied several imidazolium based ionic liquids where we have also demonstrated that significant amount of solvation in imidazolium based solvents occurs in an ultrafast time scale [154]. On the other hand, Vauthey and coworkers have studied solvation dynamics of C153 by fluorescence upconversion spectroscopy in two imidazolium ionic liquids and have concluded that only 10-15 % of solvation occurs within 10 ps [155]. Castner and coworkers have compared the dynamics of a RTIL with an equimolar mixture of its constituents [156]. Intermolecular dynamics and the time scales of different relaxation processes were explored by femtosecond time resolved optical Kerr effect spectroscopy [157-160].

Several simulation studies have been performed towards an understanding of the solvation response in RTILs [161-166]. Based on a model diatomic solute, Shim et al. proposed that a fast response results due to the translational motion of anion whereas the slower response is due to the collective diffusional motion of the cation and anion [161]. Kobrak and Znamenskiy however assigned the ultrafast response as due to the collective cation-anion motion [164,165]. In this study they used betaine-30 as the dye molecule, which is obviously a more realistic comparison with the experimental solvation probe compared to the small diatomic solute used by Shim et al. [161]. Recently Shim et al. proposed that the ultrafast component depends on the local density of ions near the probe molecule [162,163].

Clearly at this point the literature on the mechanism of solvation response in RTILs is rather contradictory and more studies are required for a proper understanding of the behavior of this fascinating class of solvents. To explore the effect of cation on the solvation response in RTILs, we propose to compare the solvation dynamics of a probe in bulk ionic liquid and the corresponding micelle in water where the cationic part of the ionic liquid is responsible to

form the micelle. Ionic liquids are shown to form micelles in water or act as a conventional media in which different known surfactants can form micelle (for a more detailed discussion refer to the micelle section). Initially we have focused on an imidazolium based ionic liquid and later extended similar studies to phosphonium based ionic liquids. Sarkar and coworkers have studied solvation dynamics in ionic liquid micelle and microemulsions [101,104,105,167]. They reported a slower solvation response in these media compared to that of in the bulk environment. Bhattacharyya and coworkers have also studied solvation response in ionic liquid microemulsions [168]. In the course of the study with phosphonium based ionic liquids we realize that our results were somewhat in disagreement with the corresponding results found by Maroncelli and coworkers on related systems [147,148,153]. Towards this goal, we have extensively discussed on the possible sources of this discrepancy with special emphasis on the construction of C(t) using various methodologies.

An important issue is to understand the effects of impurity in RTILs. It has been reported that presence of small amount of impurities like water, chloride ion can affect the physical properties and solvation characteristics in RTILs. In an excellent study Bright and coworkers have explored the effect of water by studying the solvation of Prodan in $[BMIM^+][PF_6^-]$ where there was an ~ 40 % decrease in average solvation time observed on going from 50 ppm to 1.8 % water [169]. On the other hand, Maroncelli and coworkers proposed that C153 is fortuitously insensitive towards the presence of small amount of water possibly because of its hydrophobic nature [148]. Sarkar and coworkers have also explored the solvation dynamics in several binary solvents, one of which was an ionic liquid [170]. They have reported a decrease in solvation time in the binary solvent mixture compared to that in the pure ionic liquid. Another challenging task is to synthesize optically pure (that is, non-

fluorescent) ionic liquids as most often these solvents show color. While Samanta and coworkers have argued that the color in ionic liquid might be intrinsic [171,172], we have adopted a method to decolorize the RTILs based on a methodology published recently [173]. In most of the cases this method successfully removes the coloring impurities and generates colorless ionic liquid. A recent study by Burrell et al. also demonstrated that it is possible to prepare non-fluorescent ionic liquids by proper means [174]. Among other possible reasons, the coloration of ionic liquids probably occurs because of the somewhat impure nature of the starting materials or the formation of different side products during synthesis. The identity of these colored impurities is still not very clear as these are not characterized by different analytical techniques like NMR and mass spectroscopy or by different chromatography. Based on this one might assume that whatever the impurities are these are present in very small amount but they do possess high extinction coefficient [173].

Dielectric Relaxation in Protein Environment

Proteins are complex heterogeneous media with important biological functions. To understand the dielectric relaxation in protein environments has been a challenging task. Much effort has been devoted to understanding this complicated topic [63,72,82,88-91,108,175-187]. There are two known theoretical approaches, namely the full atomistic model [188,189] which considers the detailed microscopic interactions. Although this model has potential to give more subtle information on protein response this is computationally expensive and in most cases hard to perform. On the other hand, the simple continuum (SC) model treats the protein environment as a bulk dielectric medium and hence cannot extract all necessary information [190-192]. It is our ultimate goal to develop an intermediate model which could

account for the heterogeneity of the protein environment as well as computationally viable. Towards this goal Song [193] has developed a model which assigns an intrinsic polarizability to each of the twenty naturally occurring amino acids. According to this model it is assumed that the amino acids can be represented by these assigned polarizabilities in any protein.

To validate this model it is important to study a model system experimentally. The basic idea is to measure the solvation dynamics and compare the experimentally observed solvation correlation function to that obtained from the theoretical calculations. Much effort was devoted from our group to characterize a model system for this purpose. Earlier based on Job's plot analysis, circular dichroism, capillary electrophoresis, molecular dynamics simulation, steady-state fluorescence and time resolved fluorescence anisotropy measurements we have proposed that C153-apomyoglobin (protein without the prosthetic heme group) as the model system to study the dielectric relaxation in proteins environment [194]. To further characterize this system we have extended this work in more detail. The idea is to demonstrate that C153 binds to the hydrophobic heme pocket of apomyoglobin and there is negligible non-specific interaction in this binding. To verify this we have undertaken binding studies of C153 based on Job's plot in apoprotein and compare those to that of in holoprotein (proteins containing the prosthetic heme group). Similar experiments were also performed with 1,8-anilinonaphthalene sulfonate (1,8-ANS) as the fluorescent dye molecule. While 1,8-ANS being known extensively for it's binding characteristics to the hydrophobic protein interiors with high quantum yield [195] the consideration of this was also influenced by the known NMR structure of this probe with apomyoglobin [196]. Having characterized the apomyoglobin-C153 complex as a model system to study the solvation dynamics in protein environment it was our immediate goal to study the solvation dynamics of this complex.

While performing these experiments we have extended similar work to a related monomeric hemeprotein apoleghemoglobin which is found in root nodules of leguminous plants.

Understanding our results from solvation dynamics experiments in apohemeproteins requires a thorough knowledge on the current available literature. A more fundamental question is probably to understand the role of water in protein solvation; more specifically whether the water molecules behave in a similar fashion compared to bulk water or they have some distinct properties. Towards this end I would like to discuss briefly on the current available literature on solvation dynamics in bulk water as well as in protein environments.

A. Bulk Water Solvation

Solvation in bulk water was first studied by Jarzeba et al. on the femtosecond time scale using fluorescence upconversion spectroscopy with a time resolution of 280 fs [74]. Using 7-(dimethylamino)coumarin-4-acetate ion as the probe molecule they have concluded that solvation in water can be best described by a biexponential function with time constants of 0.16 and 1.2 ps respectively. In an excellent study Fleming and coworkers undertook the solvation of a C343 salt in water with 100-110 fs time resolution [76]. From this study they concluded that the measured solvation response is well represented by a Gaussian component $a_g \exp(-\frac{1}{2}\omega_g^2 t^2)$ with frequency 38.5 ps^{-1} followed by a sum of two decaying exponentials with time constants 126 and 880 fs respectively. These studies confirm that solvation by water occurs on a femtosecond time scale. The study of Fleming and coworkers was the first experimental demonstration of the dominant inertial response (<50 fs) in water which was supported by different molecular dynamics simulation in bulk solvents [93,197-203].

B. Solvation in Protein Environment

Although there is a voluminous literature that exists on solvation in protein environments, I will focus only on the key features that point toward the different understanding on this rather complicated interaction.

Dielectric relaxation in apomyoglobin was earlier studied by Bashkin et al. [63] and Boxer and coworkers [177]. Fleming and coworkers studied the solvation response of eosin in lysozyme and compared them to that of in bulk water by three pulse photon echo peak shift (3-PEPS) spectroscopy [91,204]. They found that while the response in bulk water is represented by the sum of exponentially decaying functions with time constants 17 fs (0.73), 330 fs (0.15) and 3 ps (0.12) respectively with the relative amplitudes mentioned in the parentheses, the corresponding values for the protein-probe complex were found to be 18 fs (0.69), 310 fs (0.09), 7 ps (0.08) and 135 ps (0.08) respectively. The existence of very similar ultrafast component observed in both systems led the authors to conclude that the majority of solvation in the protein's hydrophobic pocket is bulk type. Although there is a dependence of the long time component on the time scale of the experiment, that is, this component gets lengthened on increasing the full time window of the experiment, the relative amplitude was never observed to be > 10 %, suggesting even if some relatively longer component of solvation is present in protein environments the contribution of this is significantly small.

On the other hand, Zewail and coworkers have extensively studied solvation dynamics in protein environments by monitoring spectral shift of surface exposed tryptophan intrinsic fluorescence by fluorescence upconversion spectroscopy [89,90,180-182]. From their experiments they could not resolve any ultrafast component in proteins which was present in bulk solvent. These authors emphasized that the response in protein environments lacks the

ultrafast component and is considerably slower compared to the bulk solvent. Based on their observations they have proposed a new model described as "biological water" which hypothesizes a dynamic equilibrium between bound and free water molecules on the surface of the biomolecule. Bhattacharyya and coworkers have also emphasized on the slower part of the response in protein environments and argued on the presence of biological water [72,82,108,183,184], the concept of which was originally proposed by Bagchi and coworkers [205,206]. However we do not believe on the existence of this special type of water and the discussions on this topic can be found in the relevant sections of this thesis.

Recently Boxer and coworkers [187] have undertaken a detailed study on dielectric relaxation in protein by monitoring the fluorescence of synthetic amino acid ALADAN in seven different sites with wide spatial variations of the B1 domain of streptococcal protein G (GB1). From this study they have concluded that all sites are capable of showing an initial ultrafast component comparable to that of in bulk environment which is followed by a slower response, although there is some correlation of the amplitude of the ultrafast component with the location of the fluorophore inside the protein.

Micelle

Surfactants are amphiphilic molecules which contains a polar head group and a non-polar tail in their structure. Normal micelles are formed due to the aggregation of surfactant molecules in polar solvents, water being the most common one. A simple representation of micelle formation is as follows $nS \leftrightarrow S_n$, where S is the surfactant and n is the degree of association (commonly known as aggregation number of the micelle). Formation of micelle is spontaneous and is thermodynamically controlled, that is, $\Delta G^0_{mic} < 0$. The major driving

force in the micellization process comes from a large positive value of ΔS^0, ΔH^0 being either positive or negative. There is a certain concentration and temperature above which the surfactant molecules form micelles, which are known as critical micelle concentration (CMC) and "Krafft temperature" respectively. Other polar solvents such as methanol, acetonitrile can also be used to form micelles [207-210]. There are numerous physical parameters such as surface tension, conductivity, osmotic pressure and turbidity, to name a few, which change drastically upon micelle formation. Generally at or near the CMC value there is a change in slope of the physical observable. Recently it has been demonstrated that ionic liquids are also capable of forming micelle in water [211-214]. Also different known surfactants can form micelle in ionic liquids [209,213,215], where the ionic liquids act as the solvent.

Normal micelles are composed of three distinct regions, namely, the hydrocarbon core, the Stern layer and the Gouychapman layer. The hydrocarbon core consists of the long hydrophobic chain of the surfactant molecule; the Stern layer consists of the polar headgroups, counter ions and water molecules. Stern layer is immediately surrounded by the Gouychapman layer. Thus the micellar environment is considerably heterogeneous in nature and there occurs a polarity gradient through space. Micelles can be cationic, anionic, and neutral. Typical examples of these are cetyl trimethyl ammonium bromide (CTAB), sodium dodecyl sulfate (SDS) and Brij-35, Triton X-100 respectively. A schematic diagram of normal cationic micelle is shown in figure I.7.

Micelles are important owing to their ability to dissolve various organic molecules which are otherwise insoluble in bulk solvent. This property has found wide applications in the soap and detergent industry in dissolving dirt particles. Considerable interest resides on

the exploration of the location of dissolved solutes inside the micelle. Towards this goal various spectroscopic tools like fluorescence, NMR is found to be useful. Micelles have also gained great interest in scientific research owing to the possibility to mimic biologically important systems like enzymes and membranes. In the work presented in this thesis, we attempted to understand the role of the cation on the faster response of solvation in ionic liquid, the motivation of which is discussed in the earlier section in details. In understanding our experimental observations we have also focused on the exploration of the plausible location of the probe in the micelle based on fluorescence quenching experiments.

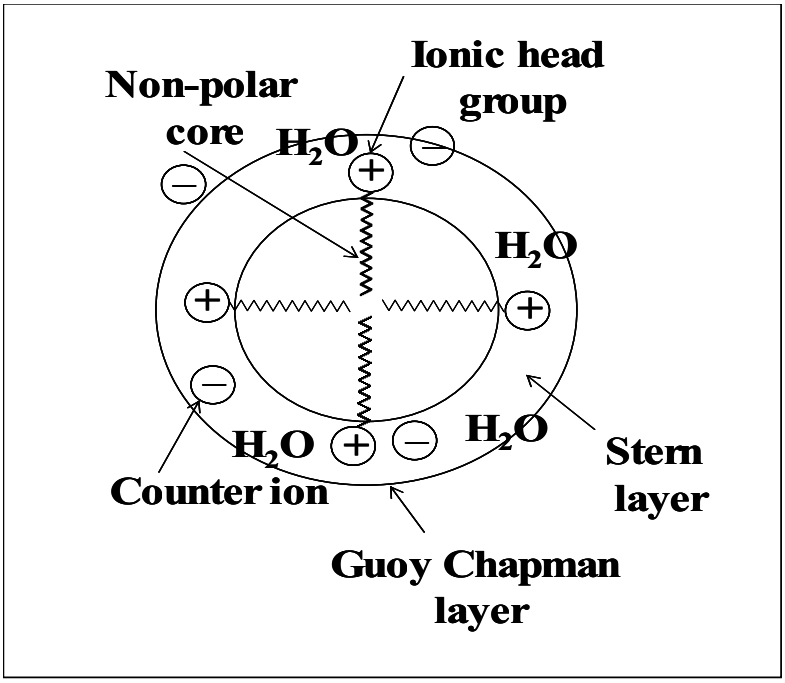

Figure I.7. Schematic diagram of a normal cationic micelle.

Thesis Organization

Following a general introduction on the various systems studied in the thesis presented in this chapter the remaining chapters are organized in the following way.

Chapter II. Experimental details alongwith the methods of data analysis.

Chapter III. Interaction of hypericin with two different isoforms of Glutathione S-transferase (GST) proteins.

Chapter IV. Characterization and structure elucidation of a novel hypericin like pigment from a marine ciliate Maristentor dinoferus.

Chapter V. Study on the comparison of solvation dynamics between bulk imidazolium ionic liquid with its micelle in water.

Chapter VI. Extension of the work described in chapter V undertaking similar studies in a phosphonium based ionic liquid. Several considerations on the construction of solvation correlation function, C(t) is also discussed.

Chapter VII. Characterization of a model system to study the dielectric relaxation in proteins.

Chapter VIII. Study of solvation dynamics in two monomeric hemeproteins, namely apomyoglobin and apoleghemoglobin. Some critical aspects on the construction of C(t) is also discussed.

Chapter IX. General conclusions from the work presented in the thesis.

References

(1) Durán, N.; Song, P. S. Photochem. Photobiol. 1986, 43, 677.

(2) Lown, J. W. Can. J. Chem. 1997, 75, 99.

(3) Diwu, Z. Photochem. Photobiol. 1995, 61, 529.

(4) Kraus, G. A.; Zhang, W. J.; Fehr, M. J.; Petrich, J. W.; Wannemuehler, Y.; Carpenter, S. Chem. Rev. 1996, 96, 523.

(5) Falk, H. Angew. Chem., Int. Ed. 1999, 38, 3117.

(6) Senthil, V.; Longworth, J. W.; Ghiron, C. A.; Grossweiner, L. I. Biochem. Biophys. Acta. 1992, 1115, 192.

(7) Senthil, V.; Jones, L. R.; Senthil, K.; Grossweiner, L. I. Photochem. Photobiol. 1994, 59, 40.

(8) Burel, L.; Jardon, P. J. Chim. Phys. Phys.-Chim. Biol. 1996, 93, 300.

(9) Darmanyan, A. P.; Burel, L.; Eloy, D.; Jardon, P. J. Chim. Phys. 1994, 91, 1774.

(10) Gai, F.; Fehr, M. J.; Petrich, J. W. J. Am. Chem. Soc. 1993, 115, 3384.

(11) Gai, F.; Fehr, M. J.; Petrich, J. W. J. Phys. Chem. 1994, 98, 8352.

(12) Gai, F.; Fehr, M. J.; Petrich, J. W. J. Phys. Chem. 1994, 98, 5784.

(13) Das, K.; English, D. S.; Fehr, M. J.; Smirnov, A. V.; Petrich, J. W. J. Phys. Chem. 1996, 100, 18275.

(14) Das, K.; English, D. S.; Petrich, J. W. J. Am. Chem. Soc. 1997, 119, 2763.

(15) Das, K.; Smirnov, A. V.; Snyder, M. D.; Petrich, J. W. J. Phys. Chem. B 1998, 102, 6098.

(16) Das, K.; Dertz, E.; Paterson, J.; Zhang, W.; Kraus, G. A.; Petrich, J. W. J. Phys. Chem. B 1998, 102, 1479.

(17) Das, K.; Ashby, K. D.; Wen, J.; Petrich, J. W. J. Phys. Chem. B 1999, 103, 1581.

(18) English, D. S.; Das, K.; Ashby, K. D.; Park, J.; Petrich, J. W.; Castner, E. W. J. Am. Chem. Soc. 1997, 119, 11585.

(19) Das, K.; English, D. S.; Petrich, J. W. J. Phys. Chem. A 1997, 101, 3241.

(20) English, D. S.; Zhang, W.; Kraus, G. A.; Petrich, J. W. J. Am. Chem. Soc. 1997, 119, 2980.

(21) Smirnov, A. V.; Das, K.; English, D. S.; Wan, Z.; Kraus, G. A.; Petrich, J. W. J. Phys. Chem. A 1999, 103, 7949.

(22) Das, K.; Smirnov, A. V.; Wen, J.; Miskovsky, P.; Petrich, J. W. Photochem. Photobiol. 1999, 69, 633.

(23) Petrich, J. W. Int. Rev. Phys. Chem. 2000, 19, 479.

(24) Fehr, M. J.; Mccloskey, M. A.; Petrich, J. W. J. Am. Chem. Soc. 1995, 117, 1833.

(25) Sureau, F.; Miskovsky, P.; Chinsky, L.; Turpin, P. Y. J. Am. Chem. Soc. 1996, 118, 9484.

(26) Chaloupka, R.; Sureau, F.; Kocisova, E.; Petrich, J. W. Photochem. Photobiol. 1998, 68, 44.

(27) Lavie, G.; Mazur, Y.; Lavie, D.; Prince, A. M.; Pascual, D.; Liebes, L.; Levin, B.; Meruelo, D. Transfusion 1995, 35, 392.

(28) Liebes, L.; Mazur, Y.; Freeman, D.; Lavie, D.; Lavie, G.; Kudler, N.; Mendoza, S.; Levin, B.; Hochster, H.; Meruelo, D. Anal. Biochem. 1991, 195, 77.

(29) Falk, H.; Meyer, J. Monatsh. Chem. 1994, 125, 753.

(30) Miskovsky, P.; Jancura, D.; Sanchez-Cortes, S.; Kocisova, E.; Chinsky, L. J. Am. Chem. Soc. 1998, 120, 6374.

(31) Miskovsky, P.; Hritz, J.; Sanchez-Cortes, S.; Fabriciova, F.; Ulicny, J.; Chinsky, L. Photochem. Photobiol. 2001, 74, 172.

(32) Uzdensky, A. B.; Iani, V.; Ma, L. W.; Moan, J. Photochem. Photobiol. 2002, 76, 320.

(33) Schwarzinger, B.; Falk, H. Monatsh. Chem. 2003, 134, 1353.

(34) Lu, W. D.; Atkins, W. M. Biochemistry 2004, 43, 12761.

(35) Sgarbossa, A.; Checcucci, G.; Lenci, F. Photochem. Photobiol. Sci. 2002, 1, 459.

(36) Sgarbossa, A.; Lucia, S.; Lenci, F.; Gioffré, D.; Checcucci, G. J. Photochem. Photobiol. B 1995, 27, 243.

(37) Ntefidou, M.; Iseki, M.; Watanabe, M.; Lebert, M.; Häder, D.-P. Plant Physiol. 2003, 133, 1517.

(38) Sobierajska, K.; Fabczak, H.; Fabczak, S. J. Photochem. Photobiol. B 2006, 83, 163.

(39) Fabczak, H. Acta Protozool. 2000, 39, 171.

(40) Song, P.-S. J. Photosci. 1999, 6, 37.

(41) Song, P.-S. Hypericin-like photoreceptors. In Handbook of Photosensory Receptors; Spudich, J. L., Briggs, W. R., Eds.; Wiley VCH: Weinheim, Germany, 2005; pp 417.

(42) Song, P.-S. Biochim. Biophys. Acta 1981, 639, 1.

(43) Scevoli, P.; Bisi, F.; Colombetti, G.; Ghetti, F.; Lenci, F.; Passarelli, V. J. Photochem. Photobiol. B 1987, 1, 75.

(44) Matsuoka, T. J. Protozool. 1983, 30, 409.

(45) Plaza, P.; Mahet, M.; Martin, M. M.; Angelini, N.; Malatesta, M.; Checcucci, G.; Lenci, F. Photochem. Photobiol. Sci. 2005, 4, 754.

(46) Kraml, M.; Marwan, W. Photochem. Photobiol. 1983, 37, 313.

(47) Song, P.-S.; Häder, D.-P.; Poff, K. L. Photochem. Photobiol. 1980, 32, 781.

(48) Menzies, E.; Das, N.; Wood, D. C. Photochem. Photobiol. 2004, 80, 401.

(49) Tao, N.; Orlando, M.; Hyon, J. S.; Gross, M.; Song, P.-S. J. Am. Chem. Soc. 1993, 115, 2526.

(50) Checcucci, G.; Shoemaker, R. S.; Bini, E.; Cerny, R.; Tao, N.; Hyon, J. S.; Gioffre, D.; Ghetti, F.; Lenci, F.; Song, P. S. J. Am. Chem. Soc. 1997, 119, 5762.

(51) Lobban, C. S.; Schefter, M.; Simpson, A. G. B.; Pochon, X.; Pawlowski, J.; Foissner, W. Mar. Biol. 2002, 140, 411.

(52) Lobban, C. S.; Schefter, M.; Simpson, A. G. B.; Pochon, X.; Pawlowski, J.; Foissner, W. Mar. Biol. 2002, 141, 207.

(53) Lobban, C. S.; Hallam, S.; Mukherjee, P.; Petrich, J. W. Photochem. Photobiol. 2007, 83, 1074.

(54) Maroncelli, M.; Macinnis, J.; Fleming, G. R. Science 1989, 243, 1674.

(55) Calef, D. F.; Wolynes, P. G. J. Phys. Chem. 1983, 87, 3387.

(56) Truong, T. B. J. Phys. Chem. 1984, 88, 3906.

(57) Sumi, H.; Marcus, R. A. J. Chem. Phys. 1986, 84, 4894.

(58) Kahlow, M. A.; Kang, T. J.; Barbara, P. F. J. Phys. Chem. 1987, 91, 6452.

(59) Zusman, L. D. Chem. Phys. 1988, 119, 51.

(60) Blackbourn, R. L.; Hupp, J. T. J. Phys. Chem. 1988, 92, 2817.

(61) Kosower, E. M.; Huppert, D. Ann. Rev. Phys. Chem. 1986, 37, 127.

(62) Marcus, R. A. J. Phys. Chem. 1989, 93, 3078.

(63) Bashkin, J. S.; Mclendon, G.; Mukamel, S.; Marohn, J. J. Phys. Chem. 1990, 94, 4757.

(64) Bagchi, B.; Chandra, A.; Fleming, G. R. J. Phys. Chem. 1990, 94, 5197.

(65) Weaver, M. J. Chem. Rev. 1992, 92, 463.

(66) Raineri, F. O.; Friedman, H. L. Adv. Chem. Phys. 1999, 107, 81.

(67) Hynes, J. T. Charge Transfer Reactions and Solvation Dynamics. In Ultrafast Dynamics of Chemical Systems, 1994; Vol. 7; p 345.

(68) Maroncelli, M.; Fleming, G. R. J. Chem. Phys. 1987, 86, 6221.

(69) Lakowicz, J. R. Principles of fluorescence spectroscopy, 2nd ed.; Springer: New York, 2004.

(70) Nitzan, A. Chemical Dynamics in Condensed Phases Relaxation, Transfer and Reactions in Condensed Molecular Systems; Oxford University Press Inc.: New York, 2006.

(71) Bhattacharyya, K. Acc. Chem. Res. 2003, 36, 95.

(72) Bhattacharyya, K.; Bagchi, B. J. Phys. Chem. A 2000, 104, 10603.

(73) Simon, J. D. Acc. Chem. Res. 1988, 21, 128.

(74) Jarzeba, W.; Walker, G. C.; Johnson, A. E.; Kahlow, M. A.; Barbara, P. F. J. Phys. Chem. 1988, 92, 7039.

(75) Chapman, C. F.; Maroncelli, M. J. Phys. Chem. 1991, 95, 9095.

(76) Jimenez, R.; Fleming, G. R.; Kumar, P. V.; Maroncelli, M. Nature 1994, 369, 471.

(77) Reynolds, L.; Gardecki, J. A.; Frankland, S. J. V.; Horng, M. L.; Maroncelli, M. J. Phys. Chem. 1996, 100, 10337.

(78) Sarkar, N.; Datta, A.; Das, S.; Bhattacharyya, K. J. Phys. Chem. 1996, 100, 15483.

(79) Datta, A.; Mandal, D.; Pal, S. K.; Das, S.; Bhattacharyya, K. J. Mol. Liq. 1998, 77, 121.

(80) Mandal, D.; Datta, A.; Pal, S. K.; Bhattacharyya, K. J. Phys. Chem. B 1998, 102, 9070.

(81) Shirota, H.; Horie, K. J. Phys. Chem. B 1999, 103, 1437.

(82) Nandi, N.; Bhattacharyya, K.; Bagchi, B. Chem. Rev. 2000, 100, 2013.

(83) Levinger, N. E. Curr. Opi. Coll. Int. Sci. 2000, 5, 118.

(84) Horng, M. L.; Gardecki, J. A.; Papazyan, A.; Maroncelli, M. J. Phys. Chem. 1995, 99, 17311.

(85) Horng, M. L.; Gardecki, J. A.; Maroncelli, M. J. Phys. Chem. A 1997, 101, 1030.

(86) Pal, S. K.; Zhao, L.; Zewail, A. H. Proc. Natl. Acad. Sci. U. S. A. 2003, 100, 8113.

(87) Pal, S. K.; Peon, J.; Zewail, A. H. Proc. Natl. Acad. Sci. U. S. A. 2002, 99, 15297.

(88) Pal, S. K.; Peon, J.; Bagchi, B.; Zewail, A. H. J. Phys. Chem. B 2002, 106, 12376.

(89) Pal, S. K.; Peon, J.; Zewail, A. H. Proc. Natl. Acad. Sci. U. S. A. 2002, 99, 1763.

(90) Peon, J.; Pal, S. K.; Zewail, A. H. Proc. Natl. Acad. Sci. U. S. A. 2002, 99, 10964.

(91) Jordanides, X. J.; Lang, M. J.; Song, X.; Fleming, G. R. J. Phys. Chem. B 1999, 103, 7995.

(92) Ghosh, S.; Mandal, U.; Adhikari, A.; Dey, S.; Bhattacharya, K. Int. Rev. Phys. Chem. 2007, 26, 421.

(93) Maroncelli, M.; Fleming, G. R. J. Chem. Phys. 1988, 89, 5044.

(94) Chandra, A.; Bagchi, B. Chem. Phys. Lett. 1990, 165, 93.

(95) Song, X. Y.; Chandler, D.; Marcus, R. A. J. Phys. Chem. 1996, 100, 11954.

(96) Song, X.; Chandler, D. J. Chem. Phys. 1998, 108, 2594.

(97) Van der Zwan, G.; Hynes, J. T. J. Phys. Chem. 1985, 89, 4181.

(98) Bagchi, B.; Oxtoby, D. W.; Fleming, G. R. Chem. Phys. 1984, 86, 257.

(99) Maroncelli, M. J. Mol. Liq. 1993, 57, 1.

(100) Kumbhakar, M.; Nath, S.; Mukherjee, T.; Pal, H. J. Chem. Phys. 2004, 121, 6026.

(101) Chakraborty, A.; Seth, D.; Chakrabarty, D.; Setua, P.; Sarkar, N. J. Phys. Chem. A 2005, 109, 11110.

(102) Kumbhakar, M. J. Phys. Chem. B 2007, 111, 12154.

(103) Partha, H.; Chakrabarty, D.; Sarkar, N. Chem. Phys. Lett. 2003, 371, 553.

(104) Chakrabarty, D.; Seth, D.; Chakraborty, A.; Sarkar, N. J. Phys. Chem. B 2005, 109, 5753.

(105) Seth, D.; Chakraborty, A.; Setua, P.; Sarkar, N. Langmuir 2006, 22, 7768.

(106) Dutta, P.; Sen, P.; Halder, A.; Mukherjee, S.; Sen, S.; Bhattacharyya, K. Chem. Phys. Lett. 2003, 377, 229.

(107) Mondal, S. K.; Roy, D.; Sahu, K.; Mukherjee, S.; Halder, A.; Bhattacharyya, K. J. Mol. Liq. 2006, 124, 128.

(108) Sahu, K.; Mondal, S. K.; Ghosh, S.; Roy, D.; Sen, P.; Bhattacharyya, K. J. Phys. Chem. B 2006, 110, 1056.

(109) Seddon, K. R.; Stark, A.; Torres, M.-J. Pure Appl. Chem. 2000, 72, 2275.

(110) Seddon, K. R. Nature (Materials) 2003, 2, 363.

(111) Walden, P. P. Bull. Acad. Imper. Sci. (St. Petersburg) 1914, 405.

(112) Hurley, F. H.; Wier, T. P. J. Electrochem. Soc. 1951, 98, 203.

(113) Hurley, F. H.; Wier, T. P. J. Electrochem. Soc. 1951, 98, 207.

(114) Welton, T. Chem. Rev. 1999, 99, 2071.

(115) Anderson, J. L.; Ding, J.; Welton, T.; Armstrong, D. W. J. Am. Chem. Soc. 2002, 124, 14247.

(116) Wilkes, J. S.; Zaworotko, M. J. J. Chem. Soc., Chem. Commun. 1992, 965.

(117) Adams, C. J.; Earle, M. J.; Roberts, G.; Seddon, K. R. Chem. Commun. 1998, 2097.

(118) Earle, M. J.; McCormac, P. B.; Seddon, K. R. Chem. Commun. (Cambridge) 1998, 2245.

(119) Dyson, P. J.; Ellis, D. J.; Parker, D. G.; Welton, T. Chem. Commun. (Cambridge) 1999, 25.

(120) Leadbeater, N. E.; Torenius, H. M. J. Org. Chem. 2002, 67, 3145.

(121) Mann, B. E.; Guzman, M. H. Inorg. Chim. Acta 2002, 330, 143.

(122) Wasserscheid, P.; Keim, W. Angew. Chem., Int. Ed. 2000, 39, 3772.

(123) Reynolds, J. L.; Erdner, K. R.; Jones, P. B. Org. Lett. 2002, 4, 917.

(124) Nara, S. J.; Harjani, J. R.; Salunkhe, M. M. Tetrahedron Lett. 2002, 43, 2979.

(125) Yao, Q. Org. Lett. 2002, 4, 2197.

(126) Fletcher, K. A.; Pandey, S.; Storey, I. K.; Hendricks, A. E.; Pandey, S. Anal. Chim. Acta 2002, 453, 89.

(127) Grodkowski, J.; Neta, P. J. Phys. Chem. A 2002, 106, 5468.

(128) Handy, S. T.; Zhang, X. Org. Lett. 2001, 3, 233.

(129) Huddleston, J. G.; Rogers, R. D. Chem. Commun. 1998, 1765.

(130) Dai, S.; Ju, Y. H.; Barnes, C. E. J. Chem. Soc., Dalton Trans. 1999, 1201.

(131) Dickinson, V. E.; Williams, M. E.; Hendrickson, S. M.; Masui, H.; Murray, R. W. J. Am. Chem. Soc. 1999, 121, 613.

(132) Armstrong, D. W.; Zhang, L.-K.; He, L.; Gross, M. L. Anal. Chem. 2001, 73, 3679.

(133) Rogers, R. D.; Seddon, K. R. Science 2003, 302, 792.

(134) Chowdhury, P. K.; Halder, M.; Sanders, L.; Calhoun, T.; Anderson, J. L.; Armstrong, D. W.; Song, X.; Petrich, J. W. J. Phys. Chem. B 2004, 108, 10245.

(135) Aki, S. N. V. K.; Brennecke, J. F.; Samanta, A. Chem. Commun, (Cambridge) 2001, 413.

(136) Wakai, C.; Oleinikova, A.; Ott, M.; Weingärtner, H. J. Phys. Chem. B 2005, 109, 17028.

(137) Abraham, M. H.; Whiting, G. S.; Doherty, R. M.; Shuely, W. J. J. Chromatogr. A 1990, 518, 329.

(138) Abraham, M. H.; Whiting, G. S.; Andonian-Haftvan, J.; Steed, J. W. J. Chromatogr. A 1991, 588, 361.

(139) Abraham, M. H.; Whiting, G. S.; Doherty, R. M.; Shuely, W. J. J. Chromatogr. A 1991, 587, 213.

(140) Bart, E.; Meltsin, A.; Huppert, D. J. Phys. Chem. 1994, 98, 3295.

(141) Bart, E.; Meltsin, A.; Huppert, D. J. Phys. Chem. 1994, 98, 10819.

(142) Bart, E.; Meltsin, A.; Huppert, D. Chem. Phys. Lett. 1992, 200, 592.

(143) Bart, E.; Meltsin, A.; Huppert, D. J. Phys. Chem. 1995, 99, 9253.

(144) Karmakar, R.; Samanta, A. J. Phys. Chem. A 2002, 106, 4447.

(145) Karmakar, R.; Samanta, A. J. Phys. Chem. A 2002, 106, 6670.

(146) Karmakar, R.; Samanta, A. J. Phys. Chem. A 2003, 107, 7340.

(147) Arzhantsev, S.; Ito, N.; Heitz, M.; Maroncelli, M. Chem. Phys. Lett. 2003, 381, 278.

(148) Ito, N.; Arzhantsev, S.; Heitz, M.; Maroncelli, M. J. Phys. Chem. B 2004, 108, 5771.

(149) Ito, N.; Arzhantsev, S.; Maroncelli, M. Chem. Phys. Lett. 2004, 396, 83.

(150) Arzhantsev, S.; Hui, J.; Naoki, I.; Maroncelli, M. Chem. Phys. Lett. 2006, 417, 524.

(151) Arzhantsev, S.; Hui, J.; Baker, G. A.; Naoki, I.; Maroncelli, M. "Solvation dynamics in ionic liquids, results from ps and fs emission spectroscopy." Femtochemistry VII, 2005.

(152) Arzhantsev, S.; Jin, H.; Baker, G. A.; Maroncelli, M. J. Phys. Chem. B 2007, 111, 4978.

(153) Jin, H.; Baker, G. A.; Arzhantsev, S.; Dong, J.; Maroncelli, M. J. Phys. Chem. B 2007, 111, 7291.

(154) Headley, L. S.; Mukherjee, P.; Anderson, J. L.; Ding, R.; Halder, M.; Armstrong, D. W.; Song, X.; Petrich, J. W. J. Phys. Chem. A 2006, 110, 9549.

(155) Lang, B.; Angulo, G.; Vauthey, E. J. Phys. Chem. A 2006, 110, 7028.

(156) Shirota, H.; Castner, E. W., Jr. J. Phys. Chem. A 2005, 109, 9388.

(157) Hyun, B.-R.; Dzyuba, S. V.; Bartsch, R. A.; Quitevis, E. L. J. Phys. Chem. A 2002, 106, 7579.

(158) Giraud, G.; Gordon, C. M.; Dunkin, I. R.; Wynne, K. J. Chem. Phys. 2003, 119, 464.

(159) Cang, H.; Li, J.; Fayer, M. D. J. Chem. Phys. 2003, 119, 13017.

(160) Shirota, H.; Funston, A. M.; Wishart, J. F.; Castner, E. W., Jr. J. Chem. Phys. 2005, 122, 184512.

(161) Shim, Y.; Duan, J.; Choi, M. Y.; Kim, H. J. J. Chem. Phys. 2003, 119, 6411.

(162) Shim, Y.; Choi, M. Y.; Kim, H. J. J. Chem. Phys. 2005, 122, 044510.

(163) Shim, Y.; Choi, M. Y.; Kim, H. J. J. Chem. Phys. 2005, 122, 044511.

(164) Znamenskiy, V.; Kobrak, M. N. J. Phys. Chem. B 2004, 108, 1072.

(165) Kobrak, M. N.; Znamenskiy, V. Chem. Phys. Lett. 2004, 395, 127.

(166) Kobrak, M. N. J. Chem. Phys. 2006, 125, 064502.

(167) Seth, D.; Chakraborty, A.; Setua, P.; Sarkar, N. J. Phys. Chem. B 2007, 111, 4781.

(168) Adhikari, A.; Sahu, K.; Dey, S.; Ghosh, S.; Mandal, U.; Bhattacharyya, K. J. Phys. Chem. B 2007, 111, 12809.

(169) Baker, S. N.; Baker, G. A.; Munson, C. A.; Chen, F.; Bukowski, E. J.; Cartwright, A. N.; Bright, F. V. Ind. Eng. Chem. Res. 2003, 42, 6457.

(170) Chakrabarty, D.; Chakraborty, A.; Seth, D.; Sarkar, N. J. Phys. Chem. A 2005, 109, 1764.

(171) Paul, A.; Mandal, P. K.; Samanta, A. Chem. Phys. Lett. 2005, 402, 375.

(172) Samanta, A. J. Phys. Chem. B 2006, 110, 13704.

(173) Earle, M. J.; Gordon, C. M.; Plechkova, N. V.; Seddon, K. R.; Welton, T. Anal. Chem. 2007, 79, 758.

(174) Burrell, A. K.; Del Sesto, R. E.; Baker, S. N.; McCleskeya, T. M.; Baker, G. A. Green Chem. 2007, 9, 449.

(175) Sheppard, R. J.; Grant, E. H.; South, G. P. Dielectric Behavior of Biological Molecules, first edition; Oxford University Press: Clarendon, 1978.

(176) Pethig, R. Annu. Rev. Phys. Chem. 1992, 43, 177.

(177) Pierce, D. W.; Boxer, S. G. J. Phys. Chem. 1992, 96, 5560.

(178) Homoelle, B. J.; Edington, M. D.; Diffey, W. M.; Beck, W. F. J. Phys. Chem. B 1998, 102, 3044.

(179) Fraga, E.; Loppnow, G. R. J. Phys. Chem. B 1998, 102, 7659.

(180) Qiu, W.; Kao, Y.-T.; Zhang, L.; Yang, Y.; Wang, L.; Stites, W. E.; Zhong, D.; Zewail, A. H. Proc. Natl. Acad. Sci. U. S. A. 2006, 103, 13979.

(181) Qiu, W.; Zhang, L.; Okobiah, O.; Yang, Y.; Wang, L.; Zhong, D.; Zewail, A. H. J. Phys. Chem. B. 2006, 110, 10540.

(182) Pal, S. K.; Zewail, A. H. Chem. Rev. 2004, 104, 2099.

(183) Pal, S. K.; Mandal, D.; Sukul, D.; Sen, S.; Bhattacharyya, K. J. Phys. Chem. B 2001, 105, 1438.

(184) Guha, S.; Sahu, K.; Roy, D.; Mondal, S. K.; Roy, S.; Bhattacharyya, K. Biochemistry 2005, 44, 8940.

(185) Li, T.; Hassanali, A. A.; Kao, Y.-T.; Zhong, D.; Singer, S. J. J. Am. Chem. Soc. 2007, 129, 3376.

(186) Nilsson, L.; Halle, B. Proc. Natl. Acad. Sci. U. S. A. 2005, 102, 13867.

(187) Abbyad, P.; Shi, X.; Childs, W.; McAnaney, T. B.; Cohen, B. E.; Boxer, S. G. J. Phys. Chem. B 2007, 111, 8269.

(188) Zheng, C.; Wong, C. F.; McCammon, J. A.; Wolynes, P. G. Chem. Scripta 1989, 29A, 171.

(189) Simonson, T. Proc. Natl. Acad. Sci. U. S. A. 2002, 99, 6544.

(190) Marcus, R. A.; Sutin, N. Biochim. Biophys. Acta 1985, 811, 265.

(191) King, G.; Warshel, A. J. Chem. Phys. 1989, 91, 3647.

(192) Bader, J. S.; Kuharski, R. A.; Chandler, D. J. Chem. Phys. 1990, 93, 230.

(193) Song, X. J. Chem. Phys. 2002, 116, 9359.

(194) Chowdhury, P. K.; Halder, M.; Sanders, L.; Arnold, R. A.; Liu, Y.; Armstrong, D. W.; Kundu, S.; Hargrove, M. S.; Song, X.; Petrich, J. W. Photochem. Photobiol. 2004, 79, 440.

(195) Stryer, L. J. Mol. Biol. 1965, 13, 482.

(196) Cocco, M. J.; Lecomte, J. T. J. Protein Sci. 1994, 3, 267.

(197) Impey, R. W.; Madden, P. A.; McDonald, I. R. Molec. Phys. 1982, 46, 513.

(198) Bader, J. S.; Chandler, D. Chem. Phys. Lett. 1989, 157, 501.

(199) Maroncelli, M. J. Chem. Phys. 1991, 94, 2084.

(200) Carter, E. A.; Hynes, J. T. J. Chem. Phys. 1991, 94, 5961.

(201) Fonseca, T.; Ladanyi, B. M. J. Phys. Chem. 1991, 95, 2116.

(202) Muiño, P. L.; Callis, P. R. J. Chem. Phys. 1994, 100, 4093.

(203) Barnett, R. B.; Landman, U.; Nitzan, A. J. Chem. Phys. 1989, 90, 4413.

(204) Lang, M. J.; Jordanides, X. J.; Song, X.; Fleming, G. R. J. Chem. Phys. 1999, 110, 5884.

(205) Nandi, N.; Bagchi, B. J. Phys. Chem. B 1997, 101, 10954.

(206) Nandi, N.; Bagchi, B. J. Phys. Chem. A 1998, 102, 8217.

(207) McIntire, G. L. CRC Anal. Chem. 1990, 2, 257.

(208) Fendler, J. H.; Fendler, E. J. Catalysis in Micellar and Macromolecular Systems; Academic Press: New York, 1975.

(209) Anderson, J. L.; Pino, V.; Hagberg, E. C.; Sheares, V. V.; Armstrong, D. W. Chem. Commun. 2003, 19, 2444.

(210) Fletcher, K. A.; Pandey, S. Langmuir 2004, 20, 33.

(211) Trewyn, B. G.; Whitman, C. M.; Lin, V. S. Y. Nano Lett. 2004, 4, 2139.

(212) Miskolczy, Z.; Sebok-Nagy, K.; Biczok, L.; Gokturk, S. Chem. Phys. Lett. 2004, 400, 296.

(213) Merrigan, T. L.; Bates, E. D.; Dorman, S. C.; Davis, J. H., Jr. Chem. Commun. 2000, 2051.

(214) Friberg, S. E.; Yin, Q.; Pavel, F.; Mackay, R. A.; Holbrey, J. D.; Seddon, K. R.; Aikens, P. A. J. Dispersion Sci. Technol. 2000, 21, 185.

(215) Hoffmann, M. M.; Heitz, M. P.; Carr, J. B.; Tubbs, J. D. J. Dispersion Sci. Technol. 2003, 24, 155.

CHAPTER II. EXPERIMENTAL AND CALCULATION METHODS

The work presented in this thesis mainly involves the use of steady-state and time-resolved fluorescence measurements. In this chapter, I will discuss the different methods that are employed.

Generation of Laser Pulses

There are several types of processes which result in the generation of pulsed output from a laser. The most commonly used techniques are cavity dumping, Q-switching, and mode-locking. Excellent reviews on these topics can be found [1,2]. Generation of ultrashort pulses has several advantages. First, as the temporal resolution is very high for these pulses they are generally obtainable with high instantaneous irradiance. Second, these pulses can be used to explore relevant chemical and biological phenomenon which occurs in comparable time scales.

Cavity dumping is a method where the energy stored in a laser cavity is rapidly emptied. This can be accomplished by making the two end mirrors of the laser cavity to be fully reflective and a third mirror is used which serves the purpose to get the reflected light out of the cavity. An acousto-optic modulator is generally used for this purpose, which typically generates a frequency in the order of MHz.

Q-switching is a technique where the Q-factor of a laser is first decreased and then suddenly increased by proper means. This can be accomplished by incorporating a shutter or some appropriate device (which acts as a shutter) within the laser cavity so as to increase the loss per round trip of the radiation, at this point, significant population inversion occurs without stimulated emission from the cavity. Now if the shutter is opened so that the cavity

can act as a resonator the energy stored in the cavity will result an intense burst of light. The most commonly used techniques for this employs the use of a rotating end mirror, a Pockel cell or a saturable absorber cell. This technique is generally capable to generate pulses of nanosecond duration.

The third method of generating pulsed outputs is mode-locking and perhaps this is the most widely used method in ultrafast spectroscopy as this method can generate pulses with picosecond and even with femtosecond time resolution. Before going into the discussion of mode-locking I will briefly describe about the cavity modes of a laser.

The range of frequencies in which a laser operates is known as the gain bandwidth of that laser. For a Ti-sapphire laser the gain bandwidth is about 128 THz which corresponds to ~ 300 nm around 800 nm (which is the central wavelength of this laser). The other factor that determines the frequency range comes from the arrangement of the oscillating cavity of the laser. Typically the laser cavity is designed according to the Fabry-Perot arrangement, which is attained by placing two flat mirrors facing each other surrounding the laser cavity. When light travels in the laser cavity it creates constructive and destructive interferences. This results in the formation of standing wave condition which satisfies the relation

$$\mathbf{L} = \frac{\mathbf{N}\lambda}{\mathbf{2}} \qquad \textbf{(II.1)}$$

where L is the distance between the two mirrors, λ is the wavelength of light and N is an integer. Typically the distance between the two mirrors is very large (in the order of centimeter) compared to the wavelength of light (in the order of nanometer) so the value of N is very large and this value defines the mode order. The frequency separation between any two adjacent modes (that is, between N and N + 1) is given by

$$\Delta\nu = \frac{\mathbf{c}}{\mathbf{2L}} \tag{II.2}$$

where c is the velocity of light and L is the separation between the two mirrors. For a Ti-sapphire laser cavity with a separation distance of 30 cm between the mirrors the number of allowed modes will be ~ 250000.

In general, these modes oscillate in a random way (that is, without maintaining any particular phase relationship between them) in a continuous wave laser. If these modes are made to operate in such a way so that they maintain a constant phase relationship with the adjacent modes (L), so that,

$$\varphi_{\mathrm{L}} - \varphi_{\mathrm{L-1}} = \varphi \tag{II.3}$$

then the laser modes will periodically produce a constructive interference together, this creates an intense burst of light and results a pulsed output from the laser. Such a situation is known as mode-locked condition for a laser. So mode-locking a laser mean to produce a constant phase relationship between adjacent modes in its cavity. The mode-locked output appears as a train of pulses. The frequency domain and time domain representations of mode-locked output are shown in figure II.1. The separation time between the pulses is given by

$$\tau = \frac{\mathbf{2L}}{\mathbf{c}} \tag{II.4}$$

This is the time required for one round trip in the resonating cavity. The duration of each pulse is given by the number of modes oscillating in the laser cavity. For N modes oscillating in a laser cavity with phase relationship and with a frequency separation $\Delta\nu$, the overall mode-locked bandwidth is given by $N\Delta\nu$. In this case, the pulse duration is given by

$$\Delta t = \frac{2\pi}{N\Delta\nu} \qquad \text{(II.5)}$$

which implies that wider the pulse narrower will be the pulsed output.

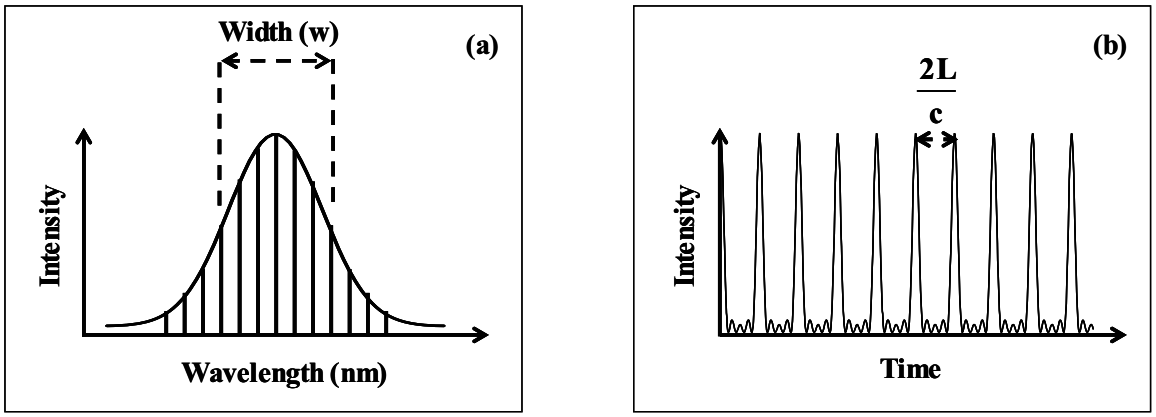

Figure II.1. Schematic representation of mode-locked output in (a) frequency and (b) time domain. Note that the output appears as a pulse train.

For a pulse with Gaussian temporal profile

$$\Delta t = \frac{0.441}{N\Delta\nu} \qquad \text{(II.6)}$$

where Δt is the minimum possible pulse duration and the factor 0.441 is known as the time bandwidth product of the pulse.

There are two major ways by which one can attain mode-locking, namely the active and passive methods. In the active method typically an external signal is used to modulate the intra-cavity light whereas in the passive method no external signal is required and this method depends on the self-modulation which is attained by placing some suitable material inside the laser cavity.

There are various ways to obtain mode-locking using the active method, namely by amplitude modulation, frequency modulation and synchronized pumping. Amplitude modulation is generally attained by placing an acousto-optic modulator inside the laser

cavity. The modulation frequency is chosen in such a way that it matches the spacing between two adjacent modes in the laser cavity. Under this circumstances side bands are generated which matches the frequency of the two adjacent modes. With sufficiently strong modulation all modes would be synchronized. Frequency modulation acts in a similar fashion as to the amplitude modulation, in this case typically an electro-optic modulator is used and the modulation frequency is matched with the round trip time in the cavity. In the synchronized method of mode-locking the pump source is itself mode-locked. This type of mode-locking requires an accurate matching of the pump laser and the driven laser.

The passive method of mode-locking usually employs the use of a saturable absorber inside the laser cavity. Organic dye molecules and semiconductors are often used as saturable absorbers. The dye molecules are in general of very short excited state lifetime and this value is important to attain pulse of short duration. The use of saturable absorber relies on non-linear increase in transmission with increase in intensity of the light. This method generates pulse of short temporal duration because this attenuates the low intensity light and transmits only the sufficiently high intensity light. The other type of attaining passive mode-locking is by Kerr lens mode-locking (KLM) which is based on the optical Kerr effect. Optical Kerr effect (OKE) is defined by the intensity dependent change of refractive index in some materials, for example, quartz or sapphire. So we have, $n = n(I)$, alternately,

$$n = n_0 + n_2 I \qquad \text{(II.7)}$$

where n_2 is a positive coefficient which depends on the nature of the material. For example, for sapphire $n_2 \cong 3.45 \times 10^{-16}$ cm^2/W. In a solid, OKE originates from the deformation of the atom's electron cloud; the response of this comes from the rotation of outermost electrons of the atom and is considerably fast, typically in the range of femtosecond time regime. Now

if we assume that the beam intensity has a non-uniform transverse profile, for example, Gaussian, then the intensity at the beam center will be more than that in the wings. In this case, one can show that the non-linear phase shift acquired of the medium can be represented by a parabolic function. This is the underlying reason for the origination of lens effect. Indeed, upon increasing the beam power beyond a critical value the induced lens may lead to beam focusing, thereby introducing self-focusing. The principle behind the KLM is illustrated in figure II.2.

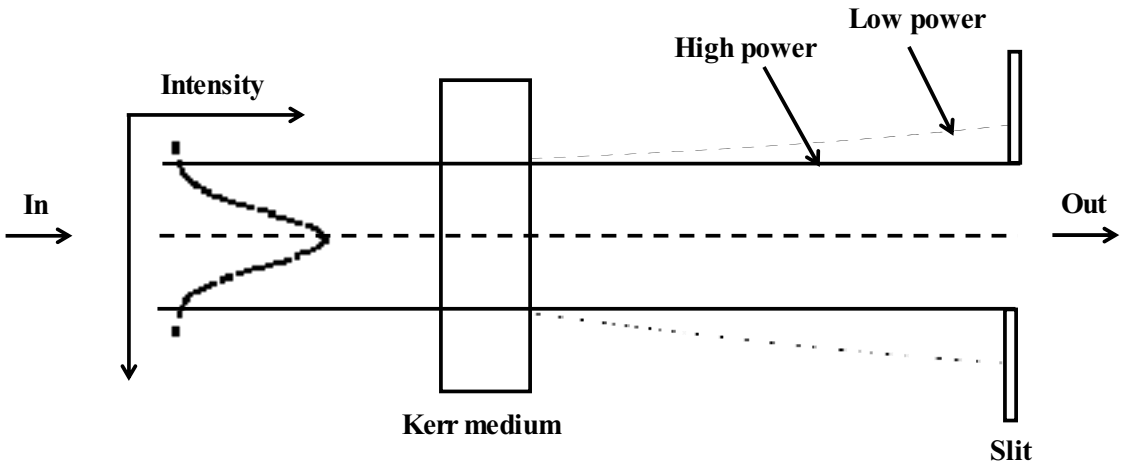

Figure II.2. Illustration of the basic principle of Kerr lens mode-locking.

Group Velocity Dispersion

A most common example of dispersion is separating white light with a prism into its constituent colors. Different components of light have different frequencies. The index of refraction is wavelength dependent. For normal dispersion, we have, $\frac{dn}{d\lambda} < 0$ which means refractive index decreases with increase in wavelength of the light. So, blue light experiences a greater index of refraction than that of the red light while passing through glass, thereby creating a phase velocity difference between the constituent colors. This is

why blue light bends more while traversing a prism. Dispersion can either be spatial or temporal. In the following sections we will consider the case of temporal dispersion, also commonly known as chirp, based on the analogy of bird sound.

Equation (II.3) can also be represented as $\varphi_1 = l\varphi$. Under this condition, the pulse is transform limited. If we consider

$$\varphi_1 = l\varphi_1 + l^2\varphi_2 \qquad \text{(II.8)}$$

where φ_1 and φ_2 are two constants. For a Gaussian amplitude function, E(t) can be represented by

$$E(t) = \exp(-\alpha t^2)\exp[i(\omega_0 t + \beta t^2)] \qquad \text{(II.9)}$$

where α and β are constants. The presence of the non-linear term in equation (II.9) gives rise to the βt^2 phase term in E(t) expression. In this case, the instantaneous carrier frequency of the wave, $\omega(t)$ can be represented by

$$\omega(t) = \frac{d}{dt}(\omega_0 t + \beta t^2) = \omega_0 + 2\beta t \qquad \text{(II.10)}$$

The term $2\beta t$ is the frequency chirp. If $\beta \neq 0$, $\Delta\tau\Delta\nu > 0.441$.

The electric field of a wave propagating along the z-direction in a transparent medium can be represented by

$$E = A_0 \exp[i(\omega t - \beta z)] \qquad \text{(II.11)}$$

The phase velocity of a wave is

$$v_{phase} = \frac{dz}{dt} = \frac{\omega}{\beta} \qquad \text{(II.12)}$$

and the group velocity is

$$v_g = \left(\frac{d\omega}{d\beta}\right) \qquad \text{(II.13)}$$

The frequency dependent phase of an ultrafast pulse is given by

$$\varphi(\omega) = \varphi(\omega_0) + \left(\frac{d\varphi}{d\omega}\right)_{\omega_0}(\omega - \omega_0) + \frac{1}{2!}\left(\frac{d^2\varphi}{d\omega^2}\right)_{\omega_0}(\omega - \omega_0)^2 + ... \qquad \text{(II.14)}$$

In this expression the first term is the propagation vector of the pulse centered at ω_0. The second term is the inverse of group velocity (v_g), the third term describes the deviation of pulse shape from transform limited value and is known as group velocity dispersion, a non-zero value of which indicates that the pulse is chirped.

In general, common optical components induce a positive or normal dispersion. To overcome this typically one uses a set of prism pair (total four prisms) inside the laser cavity to introduce negative dispersion in the system [3], this is equivalent to anomalous dispersion. Schematic diagram of the arrangement is shown in figure II.3. The prisms are arranged in such a way so that the entrance face of prism I is parallel to the exit face of prism II and vice versa. The plane indicated by dashed line in figure II.3 is perpendicular to the optical path between prisms II and III, also this plane is situated at halfway distance between the prisms. This is a plane of symmetry for the light paths. The first prism disperses the beam and the second one collimates the beam. The angular dispersion of the prism is such that the two light pulses that enter the prism I at the same time and in the same direction travels different path. The output from the prism II is spatially chirped, this chirping is removed by the second prism pair which restores the original pulse profile. The incident light path at prism I is collinear to that of the transmitted light from prism IV. As there is a plane of symmetry between prism II and III one can also just use first two prisms in a resonator having two

mirrors with one flat mirror located at the position of this plane of symmetry. It is also common to use prism pair outside the laser cavity to attain external compensation.

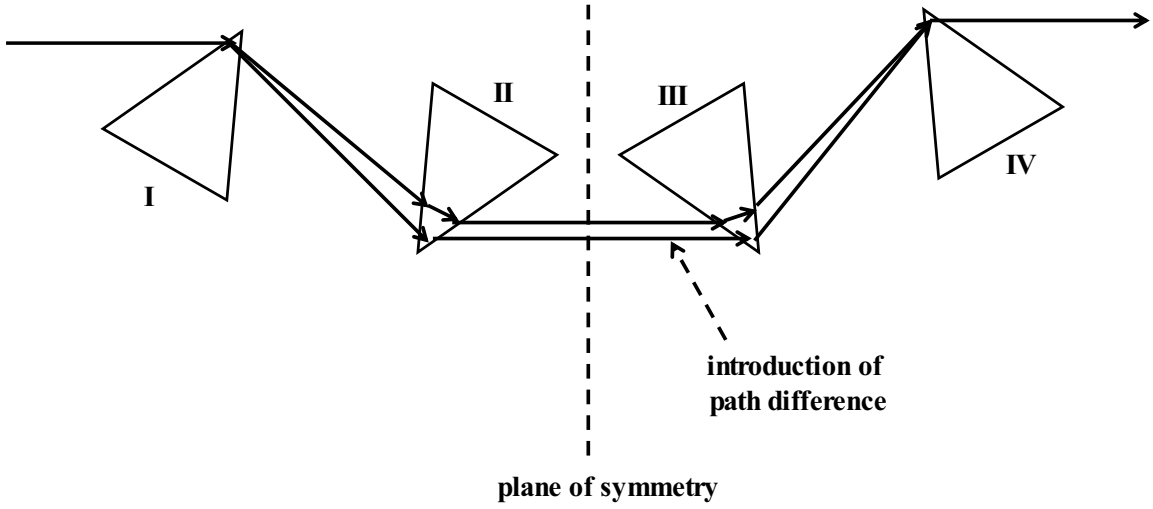

Figure II.3. Schematic arrangement for dispersion compensation by introducing prism pairs.

Ti-Sapphire Oscillator

The Ti-sapphire oscillator in our laboratory is based on the Kapteyn-Murnane design [4]. A schematic diagram of the oscillator is shown in figure II.4.

The gain medium of the oscillator consists of sapphire (Al_2O_3) crystal which is doped with 0.1 % titanium ions. There is a strong interaction between the titanium ions and the host lattice, which in combination to the energy levels of titanium ions gives rise to a broadband emission from this laser. The oscillator is usually pumped by a green laser having an output of ~ 514-532 nm. This is accomplished by the argon ion laser (514.5 nm) or frequency doubled Nd:YAG, Nd:YLF and Nd:YVO_4 (527-532 nm) laser. In our lab we use Spectra Physics Millennia V diode based continuous wave (CW) Nd:YVO_4 laser (532 nm) which runs with a power of 5 W. Extreme care must be taken so that this intense green light is not

exposed directly to eye and skin. The oscillator is tunable over a wide a range of 660-1180 nm [5]. The broad bandwidth of the laser makes it suitable to use for ultrafast pulse generation and amplification [6]. Best performance from the oscillator is usually obtained at ~ 800 nm. Details of the optimization procedure from scratch can be obtained in some of the earlier works [7,8]. Here I will mainly focus on the daily optimization procedure.

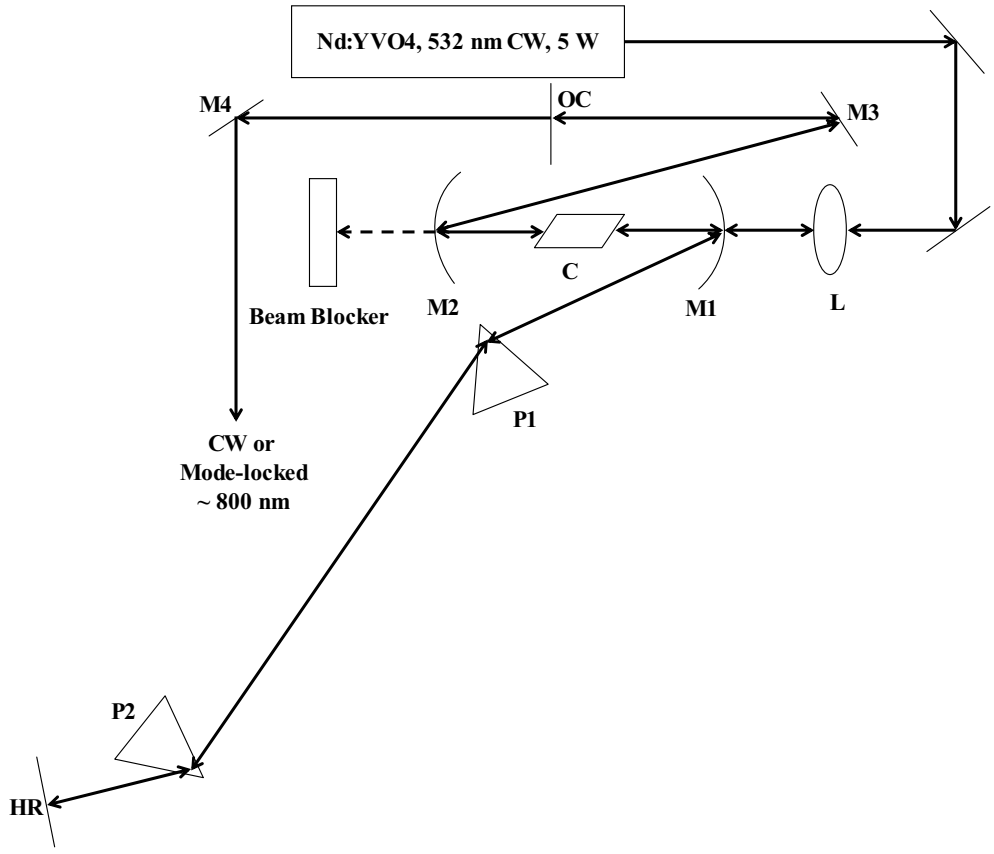

Figure II.4. Schematic representation of the Ti-sapphire oscillator used in our laboratory.

For routine use it is only required to optimize the two end mirrors of the oscillator, that is, the output coupler (OC) and the high reflector (HR). This can be done by monitoring the output power of the continuous wave (CW) red light by a power meter. First, the CW power should be maximized by careful optimization of the end mirrors. Care should be taken

at this step because abrupt tweaking of these mirrors might result in the loss of lasing from the oscillator. So it is recommended to adjust these mirrors minutely and also it is better to track the direction of rotation of the knobs in mind so that it is easier to return to the initial position. With proper optimization the CW output power of the red beam should be ~ 500-550 mW, even in some cases output power of ~ 700-800 mW might also be obtained. If the CW output power is too low (≤ 350 mW), it may be better to clean the optics with Kodak lens cleaning paper dampened with analytical grade methanol. This works better for cleaning purpose and use of other tissue papers might result unwanted scratch on the optics. It is advisable to first clean the crystal and the prism pair carefully and then checking the power, if doing this does not improve the output power then it is required to clean the curved mirrors and the end mirrors. Cleaning should be done very carefully so that the optics are not disturbed by any means. Second, the laser should get mode-locked at this stage which is usually accomplished by a small back and forth translation of either M1 or M2 in the oscillator cavity. There is no rule of thumb about which mirror would work better to get mode-locking, sometimes one or the other works better. Sometimes the laser might not get mode-locked with a maximized CW power. This usually happens when the power is very high (≥ 650 mW), in that case it is recommended to lower the power by adjusting the end mirrors properly and then try to mode-lock the laser again. Mode-locking is usually tracked by an oscilloscope. Once a good mode-locking profile is obtained the system is ready to generate the proper excitation source (~ 400 or ~ 266 nm).

For daily optimization it is not required to adjust other optical components except the end mirrors inside the oscillator cavity. It is a good practice to run and optimize the laser on a daily basis. If the laser is not turning on for a period of couple of days it might loose

lasing. If this happens then before starting with the alignment it is recommended to make a note on the main and Vernier scale readings on each optical component inside the oscillator cavity, this is advisable so that it is easier to go back to the initial condition easily. Here I will try to describe the key steps which might be adopted in absence of lasing. First, check whether the fluorescence spot is reaching the high reflector on the far end of the oscillator cavity. This can be checked by blocking the red beam with a business card in between M3 and output coupler and monitor for any change in intensity of the red beam on the high reflector. The fluorescence spot is very weak so it might be required to switch off all room lights while doing this. If a change in intensity of the red beam is observed on the high reflector upon blocking the beam you are fine with the near end of the oscillator. On the other hand, if no change in intensity is observed it is necessary to align the spot in between M3 and the output coupler and continuously monitor the spot on the high reflector. During the alignment procedure it might be helpful to insert the prism pair into the light path significantly by translating these with the Vernier scales so that missing the lasing condition is minimal. Second, once the fluorescence spot reaches the high reflector it is to be monitored whether the reflected spot travels through P_1 and reaches the output coupler. This is accomplished by adjusting the knobs in the high reflector. Once this is done the laser should give lasing, although it sometimes becomes a matter of luck to reach the optimum lasing condition. When the laser starts lasing it is recommended to place the prisms to their initial positions and follow the procedure described earlier to achieve mode-locking. Although there are other rigorous means to align the oscillator cavity which deals with the measurements of lengths between the optical components [7], I found the method described above less time consuming and hence helpful.

Time Correlated Single Photon Counting (TCSPC)

Time Correlated Single Photon Counting (TCSPC) is a very powerful tool to measure fluorescence lifetimes. Several books and reviews deal with this topic [9-13]. Here I will present a brief overview on this topic and also discuss the experimental set-up that we use in our laboratory for TCSPC experiments.

A. Basic Principle

Pulsed excitation is used to excite the sample. Following excitation the fluorophore emits from the excited state and one can monitor the decay of the species. The fluorophore usually decays exponentially (assuming first order kinetics)

$$-\frac{d}{dt}[^1S^*] = k[^1S^*] \qquad \Rightarrow [^1S^*]_t = [^1S^*]_0 \exp(-t/\tau) \qquad \text{(II.15)}$$

where $[^1S^*]_x$ and τ are the excited state polulations of the fluorophore at time x and fluorescence lifetime respectively. In TCSPC experiments the time delays between individual photons from fluorescence and the excitation pulse is recorded. This technique relies on the fact that the probability distribution for emission of a single photon after an excitation event yields the actual intensity of photons against time distribution of all the photons emitted as a result of the excitation [9]. Emitted photons are typically routed through a series of components, namely, the constant fraction discriminator (CFD), time to amplitude converter (TAC) and analog to digital converter (ADC). After signal processing in the ADC the fluorescence intensity decays are typically collected by a multichannel analyzer (MCA).

Samples are generally excited with a pulsed laser source with reasonably high repetition rate. This repetition rate is crucial for the working mode of the TCSPC set-up as

will be described later. Due to the excitation some of the fluorophores will go to the excited state and consequently fluoresce. The detector, which is generally a photomultiplier tube (PMT) or a multichannel plate (MCP) or an avalanche photodiode (APD), detects the photon. After the detector signal is processed through a pre-amplifier and then enter into the TCSPC electronics where signal processing occurs. A threshold value is set in the CFD so that it discards spurious signals below this limit. This limit should be set in such a way so that it rejects the background noise and only collects fluorescent photons. Signal processing in CFD makes the output signal independent of pulse height. The output of CFD is then fed into the TAC which is the central unit of the TCSPC operation. TAC works as a very fast stop watch which works in a START-STOP mode. In the normal mode of TAC operation the laser pulse starts this time clock in the TAC and the first fluorescent photon ends the clock. A capacitor gets charged when the START signal arrive the TAC and the fluorescent photon stops this charging and resets the capacitor to its initial position which is ready for the next START signal. It should be noted here that all excitation pulses are rejected unless the clock is stopped by the first fluorescent photon. So in one cycle only one pair of excitation pulse and fluorescent photon is involved. All other pulses are rejected during this period of time. This time duration in which the TAC is not operative towards other excitation and fluorescence events is known as the dead time of the TAC. The STOP signal ensures the next fruitful excitation event to occur. Our excitation source is a high repetition rate laser which has important consequences in choosing the mode of TAC operation. If the TAC is operated in the normal mode then the detector will be very busy in detecting the START pulses due to the very high repetition rate of the laser source but never gets stopped. This results in a very long dead time and hence inefficient experimental set-up. To circumvent

this problem the TAC is typically operated in the reverse mode where the first fluorescent photon starts the capacitor charging in the TAC and light source stops the charging of the capacitor. In a real photon counting experiment one collects a large number of these START-STOP cycles and this results the complete histogram of the fluorescence decay of the sample under investigation. We use MCP-PMT as the detector in TCSPC experiments. This has several advantages over the normal PMTs or APDs. While traditional PMTs have larger transit time spread (TTS), the time required for a photon ejected from the cathode to reach the anode, MCP-PMTs are advantageous in this particular sense. The TTS is significantly smaller in MCP-PMTs and hence advantageous. On the other hand, APDs generally have longer instrumental response.

B. TCSPC Experimental Set-up used in our Laboratory

A schematic diagram of the TCSPC set-up is shown in figure II.5. For TCSPC experiments we use a homemade mode-locked Ti-sapphire oscillator as our laser source. The laser was tunable from 780 to 900 nm with a repetition rate of 82 MHz. The oscillator was pumped by a diode laser from Spectra Physics Millennia Vs which was run at 5 W. Typically with proper optimization in the oscillator cavity we get a mode-locked output power of ~ 500-600 mW. The fundamental from the Ti-sapphire oscillator was modulated by a Pockels cell (Model 350-160, Conoptics Inc. with Conoptics Model: 25D driver) to reduce the repetition rate to about 8.8 MHz and was subsequently frequency doubled by focusing tightly into a 0.4-mm BBO crystal. The resulting blue light, which had a central wavelength of ~ 407 nm, is used as the excitation source for our samples. Samples were excited with vertically polarized light. A half-wave plate before the vertical polarizer is used to make polarization of excitation pulse vertical. The fluorescence decays were collected by

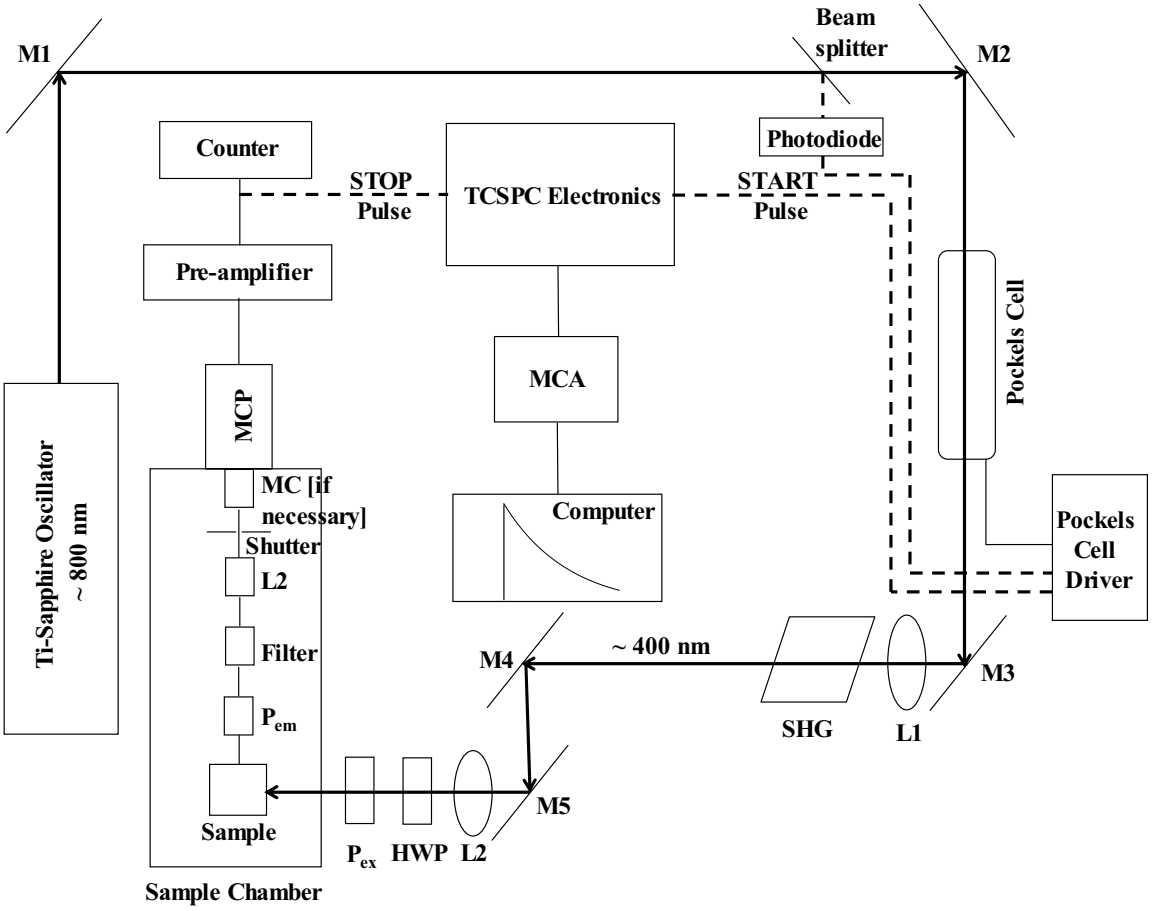

Figure II.5. Schematic diagram of the TCSPC experimental set-up used in our laboratory.

setting the emission polarizer at the magic angle, 54.7°, with respect to the vertical. This arrangement minimizes the effect of rotational diffusion in the observed traces. Emission was collected either on the entire emission band of the fluorophore (for lifetime measurements) or through a single monochromator (ISA H10) fitted with a slit having an 8-nm band pass (for solvation dynamics experiments). Hamamatsu MCP-PMT (Model: R3809U-50) was used as the detector. The output of detector was fed into an EG&G ORTEC 1 GHz pre-amplifier (Model: 9306-P) before it was processed in the TCSPC electronics. This unit was comprised of the EG&G ORTEC NIM unit (Model: 4001A), which was equipped with Tennelec Quad CFD (Model: TC 455), ORTEC TAC (Model: 457)

and ADC. The delay lines were comprised of ORTEC 425A and Tennelec TC 412A respectively. The output from the ADC was processed through the ORTEC Trump PCI card which was directly installed in the computer. The instrument-response function of the apparatus had a full-width-at-half-maximum (fwhm) of ≤ 100 ps.

Recent modifications in the TCSPC experimental set-up include the replacement of NIM-style electronics by the Becker & Hickl (B&H) photon counting module Model SPC-630 [12]. This module replaces all electronic parts (that is the CFD, TAC, ADC) in a miniaturized form, thus making it more compact. The connection is also relatively straightforward. There are two inputs in the B&H module, namely the SYNC and CFD. A schematic diagram of the connection is shown in figure II.6.

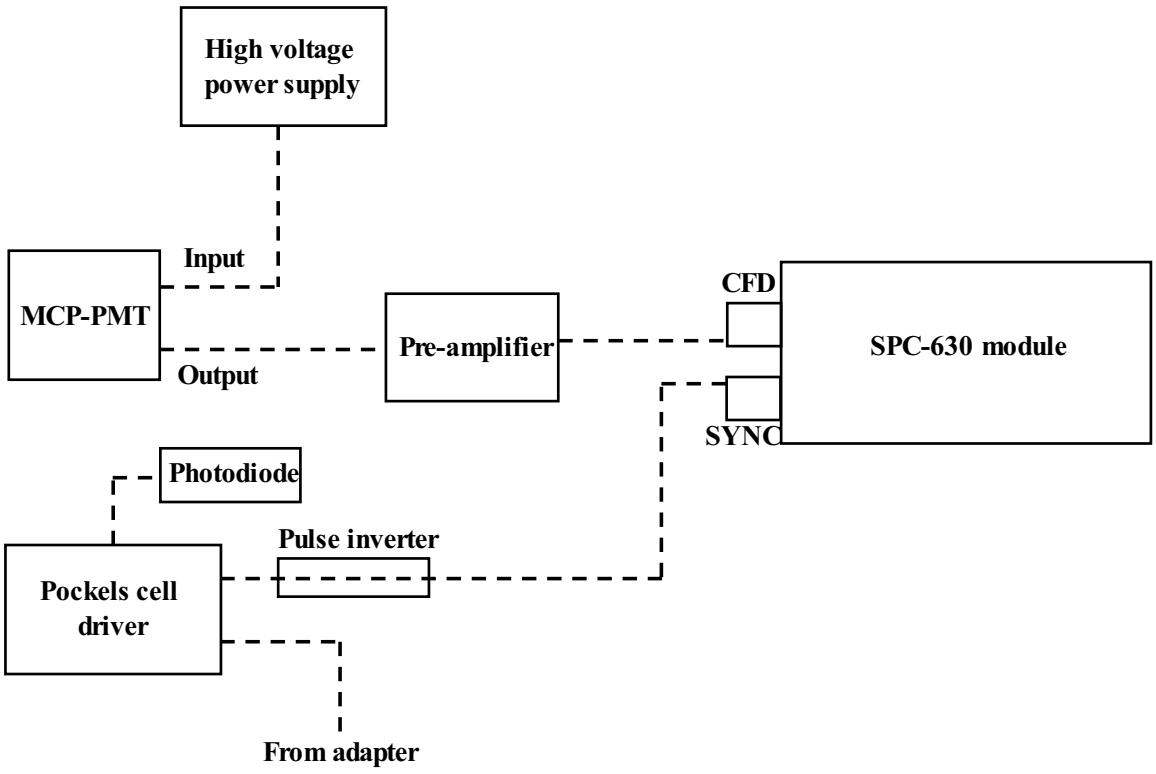

Figure II.6. Schematic representation of the connection for TCSPC experiments using Becker & Hickl photon counting module.

The SYNC channel is connected with the Pockels cell driver which is driven by a photodiode, a pulse inverter (Model: EG&G Inc. Inverting Transformer IT 100) is used in this path. The CFD channel is connected with the MCP-PMT detector. In this mode of operation the delay lines are exclusively maintained by the length of the cables in the SYNC and CFD channels. The length of these two cables is extremely important to acquire the required time window. In the CFD channel our previous ORTEC pre-amplifier has also been replaced by B&H pre-amplifier (Model: HFAC-26dB 0.3 μA), which was found necessary to minimize the background noise. An important factor is to set the CFD threshold value correctly in the module. The value is set in such a way so that the module does not detect the background noise and only collects the fluorescence from the sample. In our laboratory we found ~ –50 mV as the optimum value for the CFD threshold. With this modified system the fwhm of the instrument-response function of the apparatus is ~ 40-45 ps. A change in the time window might require some adjustments in the cable lengths and if this is done corresponding adjustments in the CFD threshold might be necessary. A time window varying between 3.3 ns and 2 μs can be obtained with a maximum number of possible counts of 65535 ($2^{16} - 1$) at the peak channel. The number of channels can be as high as 4096, which gives a maximum possible resolution of 813 fs per channel.

Tripler

A. Basic Principle

Recently we have acquired a commercial tripler (Model: U-Oplaz Technologies Time Plate® Tripler Model TP-2000B, U. S. Patent # 5,852, 620) which can be used to obtain ~ 400 nm and ~ 266 nm simultaneously. For a detailed discussion on the installation and

operation of the tripler readers are suggested to consult the manual supplied by the company. Here I will briefly discuss the basic principle alongwith the daily optimization procedure.

The third harmonic generation is based on the principle of second harmonic followed by sum frequency generation. This can be illustrated as follows.

$$\nu_1 + \nu_1 \Rightarrow \nu_2 \qquad \text{(II.16)}$$

$$\nu_1 + \nu_2 \Rightarrow \nu_3 \qquad \text{(II.17)}$$

where ν_1, ν_2 and ν_3 are the fundamental, second and third harmonic respectively. First, blue (~ 400 nm) light is generated from the fundamental red (~ 800 nm) light. Second, the second harmonic is mixed with the fundamental in an appropriate crystal to generate the third harmonic (~ 266 nm) by sum frequency generation. After the second harmonic generation there is a time delay between the ~ 800 and ~ 400 nm light due to the group velocity dispersion of the crystal and the associated optics. This time delay must be properly compensated for an effective THG.

Traditionally THG involves the use of delay lines which is based on first separating the fundamental and the second harmonic by a beam splitter, then one of them is traveled through a different distance compared to the other one followed by recombining the two pulses in another beam splitter. Although this method is widely used in ultrafast spectroscopy it has some limitations owing to the requirement of long delay lines which needs a large laboratory space. The tripler we currently acquired from Oplaz Technologies is superior in this respect due to its compact nature. In this set-up the traditional delay line is replaced by a time plate which is a tunable time delay device for time compensation. It is composed of a birefringence crystal which can be adjusted by a rotational stage. A schematic

diagram of the arrangement is shown in figure II.7. The crystal has the ordinary axis along the z-axis and the extraordinary axis along the x-y plane. The fundamental and the second harmonic are polarized perpendicular to each other, that is, when these two pulses travel the time plate they appear as a combination of ordinary and extraordinary light. The two pulses will travel through the time plate with different speed owing to the difference in their refractive index. As a result of this a time delay is generated when these two pulses travel the time plate, where the extent of the time delay is determined by the rotation angle, cutting angle, the thickness and the refractive indices of the crystal in the time plate. The time plate is designed in such a way so that rotation of the crystal results a tunable time delay. In this set-up the separation and recombination steps are no longer required and hence the longer delay lines are no longer necessary.

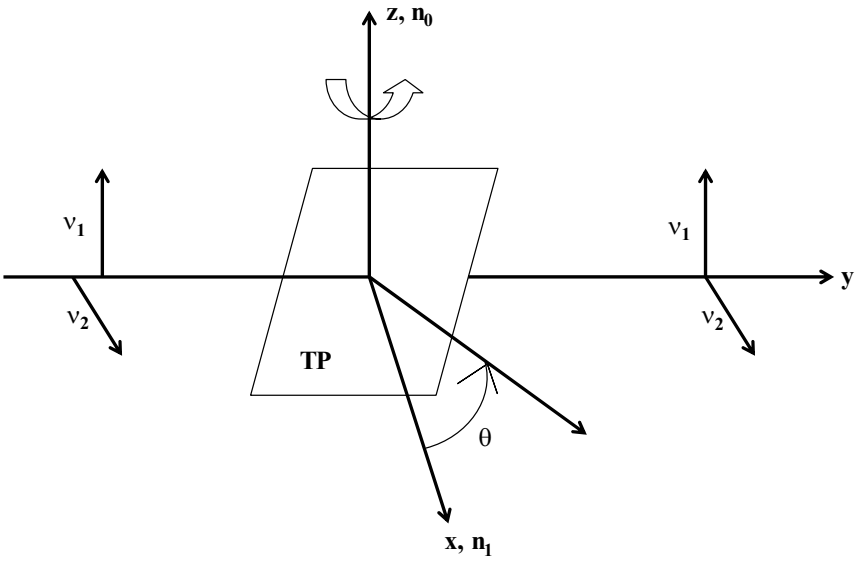

Figure II.7. A schematic representation of the time plate used in the tripler. The figure has been adapted from the manual supplied by the company.

B. Optimization of the Tripler

A schematic diagram of the tripler is shown in figure II.8.

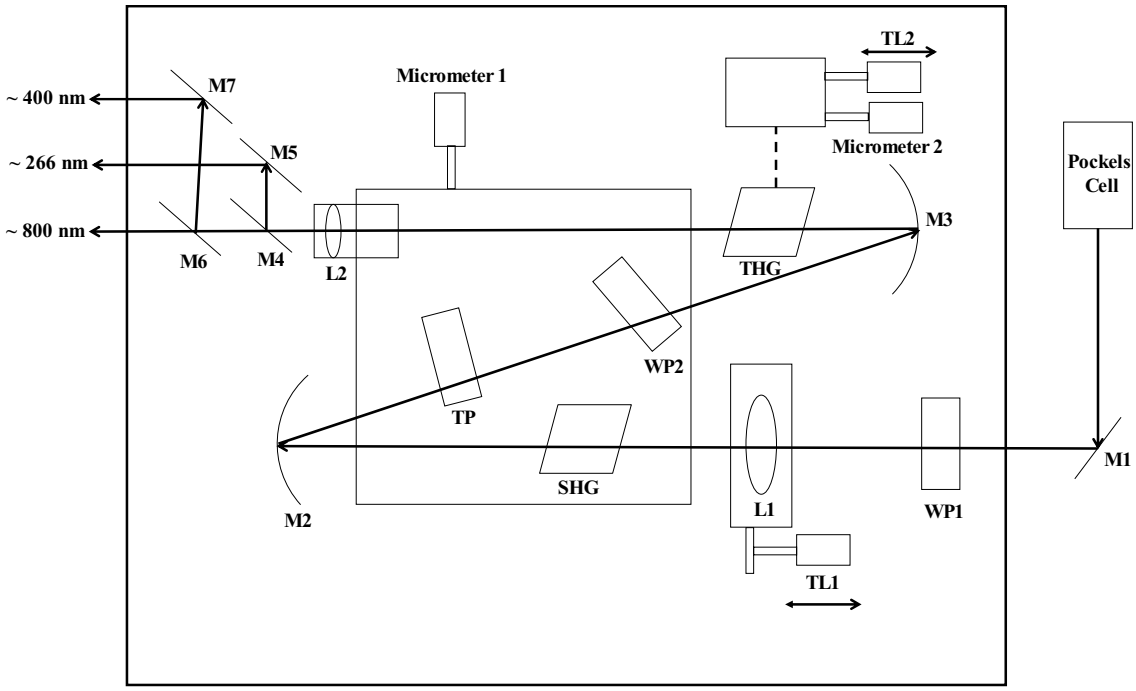

Figure II.8. Schematic diagram of the tripler (Model: U-Oplaz Technologies Time Plate® Tripler Model TP-2000B, U. S. Patent # 5,852, 620) used in our laboratory.

For routine optimization the following steps might be performed. First, the Pockels cell should be properly aligned so that the incident red beam in the tripler is well shaped. Second, the blue light is maximized by carefully adjusting M1 and TL1. This can be done by placing a business card after the SHG. At this point blue light should come out from M7. If there is enough blue light after the SHG but the output blue beam is very weak this means that the TP is not properly aligned in the light path. If this is the case, the micrometer 1 should be slightly adjusted to maximize the output blue light. Third, once this is done, the THG is properly aligned by carefully adjusting micrometer 2 and TL2. The resultant third harmonic beam is generally of very weak intensity, so it might be necessary to work in a

completely dark room to monitor the UV (~ 266 nm in this case). As UV light is invisible it is generally monitored by checking the fluorescence in a business card. Unconverted blue light is generally mixed with the output UV, so it is required to filter out the blue light by placing a UV pass filter in the middle port. Anything passes this filter should be in the UV region. To further make sure this light should be checked by blocking the beam with a normal glass. Glass should absorb the UV light completely. Once it is ensured that the output beam is purely UV and not contaminated by unconverted blue the beam is ready to use for exciting the sample. The UV output from the tripler is vertically polarized.

Fluorescence Upconversion Spectroscopy

A. Basic Concepts

The instrument response function of our TCSPC experimental set-up has a full width at half-maximum (FWHM) of $\leq$ 100 ps. To investigate more rapid phenomenon we need to increase the time resolution of the experiment. Fluorescence upconversion is one of the valuable techniques that provides ~ femtosecond time resolution and thus gives an opportunity to monitor the processes that occur in this time regime. In this section I will briefly discuss the basic principles associated with fluorescence upconversion experiments.

The basic idea of fluorescence upconversion experiment relies on the concept of pump probe experiments. Typically in a two color pump probe experiment one pulse is used to excite the sample and the other one is used to as a probe the signal from the sample. However, the signal from a pump probe experiment might have contribution from stimulated emission, excited state absorption and ground state bleaching. This often complicates the interpretation of the observed signal when some of these above mentioned effects are present

simultaneously. On the other hand, as unconversion technique only detects spontaneous emission, it is not contaminated by the other contributions and hence is obviously more preferable when one is interested in detecting fluorescence from the sample.

In an upconversion experiment one pulse excites the sample at time t = 0 and generates fluorescence, the other pulse is used to gate the fluorescence. Generally an angle tuned non-linear crystal is used to mix the fluorescence and the gate pulse, in this process the frequency of the output signal gets higher. For example, mixing of 800 nm light with 400 nm light results an output of 266 nm, that is, in this sum frequency generation the signal gets upconverted in frequency. The availability of various UV sensitive photomultiplier tubes makes upconversion a feasible process. One of these two pulses experiences a fixed delay and the other one is passed through a variable delay line. There is no restriction on this choice. In our laboratory we pass the blue light trough a variable delay line and the red light is passed though a fixed delay line. A very important criterion for effective sum frequency generation is to satisfy the condition of phase matching. This means that we need to satisfy the following conditions

$$\nu_F + \nu_P = \nu_S \qquad \text{(II.18)}$$

$$\vec{k}_F + \vec{k}_P = \vec{k}_S \qquad \text{(II.19)}$$

where ν and $\vec{k}$ are the frequency and the wave vectors and F, P and S denotes fluorescence, pump and upconverted signal respectively. A detailed discussion on the frequency mixing is given in references [14,15]. This means the phenomenon of phase matching only occurs when the pump pulse is present in the crystal, in this way it serves as a gate and gives a time

resolution comparable to the pulse width of the laser pulse. Schematic diagrams illustrating the fluorescence upconversion process is shown in figure II.9.

In this context it is worth to mention about the nature of the crystal. Typically the crystals used are non-centrosymmetric and hence birefringent, that is, they have different refractive indices along the three axis of propagation. Typically these crystals decompose light into two components, namely the ordinary (o) and the extraordinary (e) lights. The extent of birefringence is defined by

$$\Delta n = n_e - n_o \qquad \text{(II.20)}$$

where n is the refractive index. Crystals are often uniaxial, that is, they contain only one optical axis. Examples are calcite and sapphire, to name a few. Although biaxial crystals exist, for example, epsom salt, perovskite to name a few. In the current discussion I will mainly focus on the uniaxial crystals in which the optical axis is along the z-direction and $n_x = n_y = n_o$, $n_z = n_e$.

It can be shown that the phase matching condition reduces to

$$\frac{1}{n_i^2} = \frac{\sin^2\theta}{n_{e,i}^2} + \frac{\cos^2\theta}{n_{o,i}^2} \qquad \text{(II.21)}$$

The uniaxial crystals are said to be positive if $\Delta n > 0$, negative if $\Delta n < 0$. In our laboratory we use beta-barium borate (β-BaB_2O_4, commonly known as BBO) crystal which is a negative uniaxial crystal. The corresponding Sellmeir's equation (which defines the variation of refractive indices with wavelength) are

$$n_o^2 = 2.7359 + \frac{0.01878}{\lambda_2 - 0.01822} - 0.01354\lambda^2 \qquad \text{(II.22)}$$

$$\text{and } n_e^2 = 2.3753 + \frac{0.01224}{\lambda^2 - 0.01667} - 0.01516\lambda^2 \qquad \text{(II.23)}$$

BBO crystals can either be of type-I or type-II. Type I crystals mix lights of parallel polarization, whereas type II refers to mixing of lights having perpendicular polarization. It can be shown that for the phase matching condition to be satisfied in a negative uniaxial crystal the sum frequency ray light must be an e-ray; on the other hand, the opposite is true for the corresponding positive crystal. This implies that in type I BBO crystal the matching will be of the type oo-e and in type II the matching will be eo-e or oe-e.

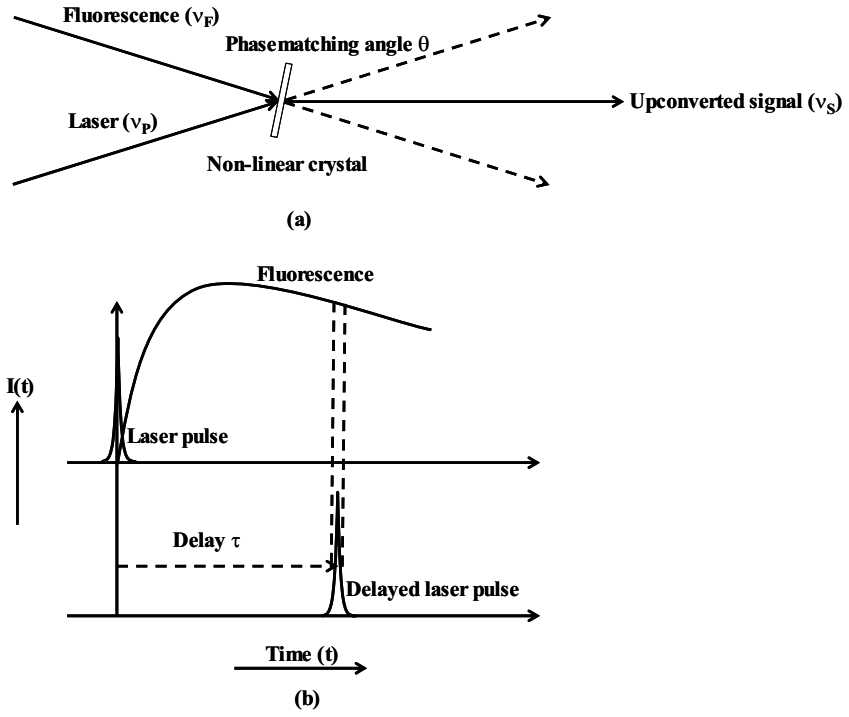

Figure II.9. Schematic diagram showing the basic principle of (a) phase matching and (b) fluorescence upconversion procedure. The figure has been adapted from reference [16].

B. Fluorescence Upconsersion in our Laboratory

Fluorescence upconversion measurements can be performed with either the amplified or unamplified Ti:sapphire systems. The experiments described in this thesis were

performed with the unamplified system. Discussion on the amplified set-up can be found in references [7,8,17,18]. A schematic diagram of the fluorescence upconversion set-up using the unamplified Ti-sapphire oscillator system is shown in figure II.10. The fundamental output from the Ti-sapphire oscillator which is centered ~ 815 nm was frequency doubled by a type-I LBO crystal (2 mm). The frequency-doubled blue pulses (~ 407 nm) were separated from the fundamental by a dielectric mirror coated for 400 nm and were focused onto a rotating cell containing the sample using a 5-cm convex lens. The remaining fundamental red beam was used as the gate to upconvert fluorescence emission. Fluorescence was collected by an LMH-10x microscopic objective (OFR Precision Optical Products) coated for near UV transmission. The gate and the emission are focused by a quartz lens (12 cm) onto a type-I 0.4-mm BBO crystal (MgF_2 coated, cut at 31°, and mounted by Quantum Technology, Inc.). The polarization of both the gate and excitation source was controlled with a set of zero-order half-wave plates for 800 and 400 nm, respectively. The upconverted signal was then directed into an H10 (8 nm/mm) monochromator (Jobin Yvon/Spex Instruments S. A. Group) with a 5-cm convex lens coupled to a Hamamatsu R980 PMT equipped with a UG11 UV-pass filter and operated at maximum sensitivity. The PMT output was fed into a lock-in amplifier (Stanford Research Systems, Model: SR830 DSP). The detection system is based on using a beam chopper and the lock-in amplifier (commonly known as phase sensitive detector). The chopper imposes a square-wave modulation (1 kHz) to the exciting blue light. The lock-in amplifier is fed two signals, first one is the control signal which comes from a detector connected to the chopper and the second one is the response signal which comes from the PMT. Lock-in amplifier selectively amplifies the components of the reference signal which is of the same frequency to that of the control signal. This mode of operation

generates a high S/N ratio. To give a variable delay to the exciting blue pulses a translation stage (Compumotor) with a resolution of 0.006 mm/step was used. The signal was collected in a computer with an interfacing card from Keithley Metrabyte (DAS 800) drives the motor. The instrument-response function is obtained by collecting the cross-correlation function of the blue and red pulses; the resulting third harmonic intensity is plotted against delay time. Generally this was done by just placing the solvent (that is, without the fluorophore) in the rotating sample cell. The instrument function was having a fwhm of ~ 300 fs.

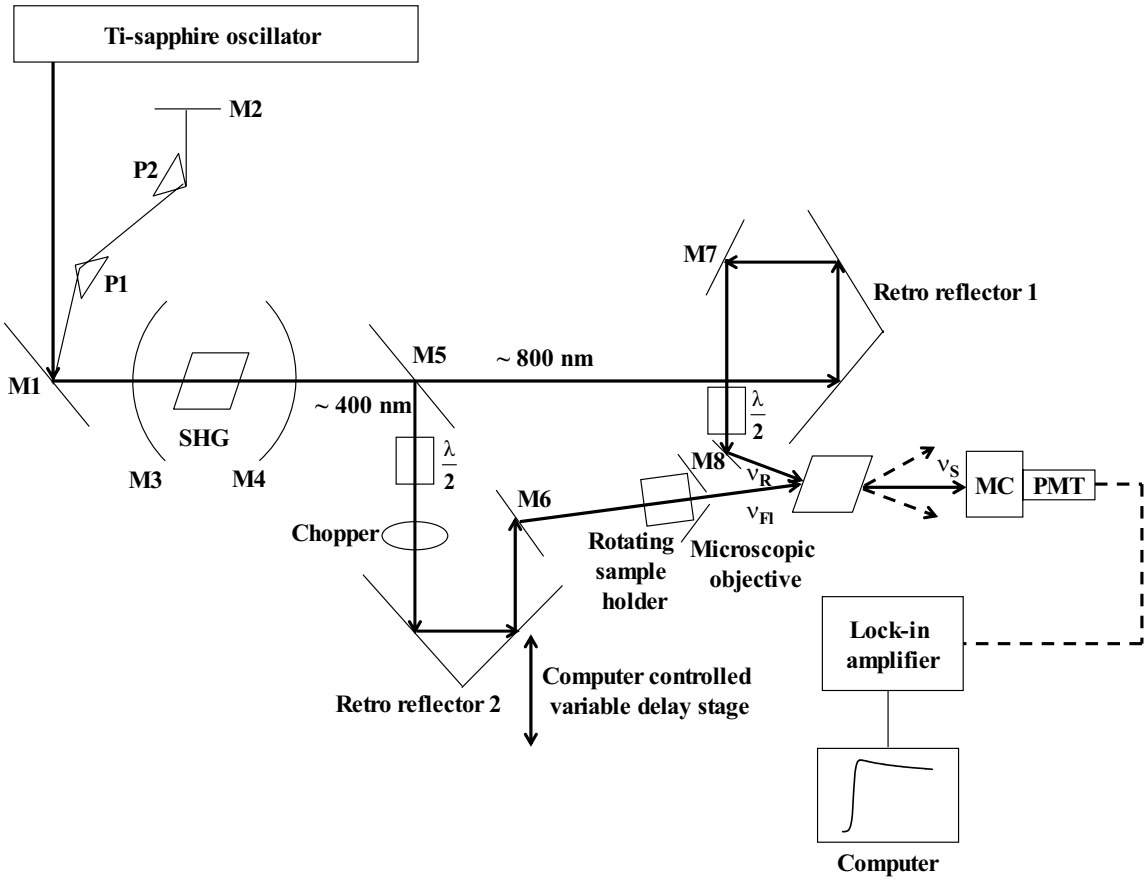

Figure II.10. Schematic diagram of the fluorescence upconversion set-up in our laboratory using the unamplified Ti-sapphire oscillator system.

Discussion of the construction of the fluorescence upconversion apparatus can be found elsewehere [18]. To run any upconversion experiment it is of basic necessity to obtain

the time zero. In our laboratory we generally use C153 in methanol solution for optimizing the set-up. As discussed earlier it is of utmost importance to satisfy the condition of phase matching condition properly in the angle tuned upconverting crystal. If the signal is obtained but it is having a lesser intensity then it might be a good idea to check the overlap of the fluorescence spot and the gate (red) beam and try to maximize the overlap by adjusting M8. If the signal is completely missing in the first place, then it is extremely important to carefully measure the path length of the red and blue beams separately by a measuring tape. These two distances should match exactly to have an optimum phase matching condition. If the distances do not match then the difference should be adjusted by varying the length of the blue beam, because in the current set-up the blue beam is attached to the variable delay line and the red beam is adjusted by a fixed delay line. The length of the blue path can be adjusted by translating the stage in the correct direction and then taking the scan after overlapping the fluorescence spot with the red beam in the upconverting crystal. If the translation stage is not in a situation to move further then the adjustments should be done by slightly adjusting the mirrors. While scanning it might be better to try with a longer time scale and even in some cases to scan in the negative time axis to see the existence of time zero. In the length matched condition with proper overlap one should see the time zero, might be with lesser intensity, which can necessarily be adjusted by the M8.

Calculation of Reorganization Energy

Reorganization energy (λ) is one of the most important parameters associated with the solvation dynamics experiments, which is widely used as a measure of the strength of interactions between a chromophore and its surrounding dielectric media. Traditionally λ is

taken as half of the Stokes shift which is the difference in peak maxima of the corresponding absorption and emission spectra. So we have,

$$\lambda = \frac{1}{2}\hbar[\max\{\sigma_a(\nu)\} - \max\{\sigma_f(\nu)\}] \qquad \text{(II.24)}$$

where $\max\{\sigma_{a,f}(\nu)\}$ is the maximum of the absorption (or excitation) and emission spectra respectively, on a wavenumber scale. However, equation (II.24) is valid if the absorption and emission spectra are Gaussian. For most of the fluorophores however this is not the case, that is, spectra deviates significantly from Gaussian shape. Consequently equation (II.24) is not valid. Song and coworkers have developed a methodology for the calculation of λ which implicitly takes care of the actual shape of the corresponding spectra [19] according to the following equation

$$\lambda = \hbar \frac{\int_0^\infty d\nu[\sigma'_a(\nu) - \sigma'_f(\nu)]\nu}{\int_0^\infty d\nu[\sigma'_a(\nu) + \sigma'_f(\nu)]} \qquad \text{(II.25)}$$

where $\sigma'_{a,f}$ are the absorption (or excitation) and emission spectral line-shapes, respectively.

Here we will discuss the methodology for the calculation of λ from the experimental absorption (or excitation) and emission spectra. First, experimentally observed normalized absorption (or excitation) and emission spectra are manipulated so that couple of data points at the extreme red edge of the emission spectrum is set equal to zero. Generally this is accomplished by subtracting the intensity value at the extreme red edge from the whole spectrum and renormalizing it to unity. Second, these spectra are converted to the corresponding spectral line-shapes according to equation (II.26) and (II.27) and renormalizing to unity.

$$\sigma'_{a}(\nu) = \frac{\sigma_{a}(\nu)}{\nu} \qquad \textbf{(II.26)}$$

$$\sigma'_{f}(\nu) = \frac{\sigma_{f}(\nu)}{\nu^{3}} \qquad \textbf{(II.27)}$$

This transformation is necessary so as to make the experimentally observed absorption (or excitation) and emission curves compatible with the respective Einstein's coefficients. Third, the absorption (or excitation) and emission spectral line-shapes are manipulated so as to permit their addition and subtraction. This procedure requires an interpolation of the corresponding spectral line-shapes into equally spaced data points. Typically we use a spacing of 20 cm^{-1} between consecutive data points in each curve. Fourth, the curve crossing point is carefully estimated by eye inspection. For this it might be required to zoom in the curve crossing region. This curve crossing frequency indicates the frequency associated with the 0-0 transition in a particular system. This characteristic frequency has to be subtracted from the wavenumber scales, so that the curve crossing point appears at zero in the abscissa. Fifth, an appropriate number of zeros are added to the high energy end of the emission curve and the low energy end of the absorption (or excitation) curve so as to allow the addition and subtraction in the entire spectral region. At this point it is always better to check the maximum intensities in the corresponding curves and if necessary, they should be renormalized to unity. Sixth, value of λ can now be calculated using equation (II.25). Typically instead of integrating from zero to infinity we integrate the numerator and denominator of equation (II.25) from negative infinity to zero. This procedure is allowed in the case of mirror image symmetry between absorption (or excitation) and emission spectra and employing this methodology avoids any contamination from higher lying excited states

in the absorption (or excitation) spectrum. All data manipulations were performed with Microcal Origin 7.0.

Experimental Procedure and Data Analysis for Solvation Dynamics Experiments

On the experimental side, the fluorescence decay of the probe molecule is collected over as much as the fluorescence spectrum as possible. The decays at the blue end of the spectrum are faster, whereas in the red edge of the spectrum there is an occurrence of growth in the fluorescence trace. The rise time is attributed to the population increase of the relaxed state which is zero at time zero (i.e. at the time of excitation). The traces are fitted to sum of exponentials where we attribute no physical significance associated to the decay parameters. Transient spectra were reconstructed from these fits by normalizing to the steady-state spectra according to

$$I(\lambda,t) = D(\lambda,t)\frac{I_{SS}(\lambda)}{\int_0^\infty D(\lambda,t)} \qquad \text{(II.28)}$$

where $D(\lambda,t)$ is the wavelength-resolved fluorescence decay, and $I_{SS}(\lambda)$ is the steady-state emission intensity at a given wavelength. The origin of equation (II.28) is discussed below [11,20].

$$I(\lambda,t) = A(\lambda)B(t) \qquad \text{(II.29)}$$

Typically B(t) is expressed as a sum of decaying exponentials. So,

$$B(t) = \sum_i a_i \exp(-t/\tau_i) \qquad \text{(II.30)}$$

The steady-state fluorescence intensity is the time integrated intensity of the decay traces, which implies

$$I_{SS}(\lambda) = \int_0^\infty I(\lambda,t)dt = A(\lambda)\int_0^\infty B(t)dt$$

$$\Rightarrow A(\lambda) = \frac{I_{SS}(\lambda)}{\int_0^\infty B(t)dt} = \frac{I_{SS}(\lambda)}{\sum_i a_i \tau_i} \qquad \textbf{(II.31)}$$

So equation (II.28) transforms to

$$I(\lambda,t) = \frac{I_{SS}(\lambda)\sum_i a_i \exp(-t/\tau_i)}{\sum_i a_i \tau_i} \qquad \textbf{(II.32)}$$

Typically one calculates a set of new intensity decays so that the time-integrated intensity at each wavelength corresponds to the steady-state intensity at that wavelength. The time-resolved emission spectra so generated are shown in figure II.11 (assuming Gaussian line-shape function).

However, in reality for C153 these spectra deviate from Gaussian line-shape function and we have employed the traditional approach of fitting the time-resolved spectra to a log-normal function [21,22] (which represents an unsymmetrical Gaussian function, equation (II.33)),

$$y = A\exp(-0.693(\ln(1+2(x-C)\sinh(B)/D)/B)^2) \qquad \textbf{(II.33)}$$

where A, B, C and D represents the ordinate value at the peak maxima, asymmetry parameter, peak position in the abscissa and the width parameter respectively. Note that this equation merges to a Gaussian when B = 0. From these fitting parameters we extract the peak frequency, ν(t), as a function of time.

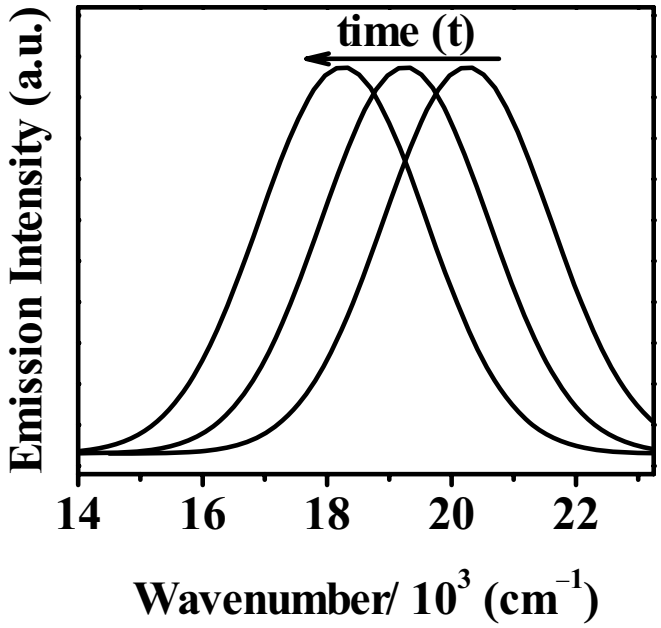

Figure II.11. Representation of typical time-resolved emission spectra assuming Gaussian line-shape function for fluorescence emission. Note that the spectrum shifts towards lower energy with increase in time.

The solvation dynamics were described by the normalized correlation function according to

$$C(t) = \frac{\nu(t) - \nu(\infty)}{\nu(0) - \nu(\infty)} \qquad \text{(II.34)}$$

where $\nu(0)$, $\nu(t)$ and $\nu(\infty)$ are the corresponding spectral peak maxima at times zero, t and infinity respectively. However, the experiments are limited to resolve the true time zero spectrum in solvation dynamics experiments due to the finite time resolution of the experiment, unless the experiment is done in super cooled liquid. An excellent recipe to calculate the time zero spectrum is provided by Fee and Maroncelli [23] where they proposed that the time zero spectrum can be calculated from the non-polar absorption (excitation), non-polar emission and polar absorption (excitation) spectra. This procedure involves taking the spectrum of the probe in a nonpolar solvent, convoluting this spectrum with a broadening

function, such as a Gaussian and shifting it until it superimposes on the polar spectrum, and then projecting this down into an emission spectrum. We have adopted this methodology to compute the time zero spectrum. $\nu(\infty)$ is typically considered as the peak maxima of the corresponding steady-state spectrum and $\nu(t)$ values are obtained from the lognormal fits of the corresponding time resolved emission spectra, which accounts well for the spectral band shape of C153 in polar solvents [21,22].

According to simple continuum (SC) theory the dielectric constant of a liquid can be represented by the Debye dispersion

$$\varepsilon(\omega) = \varepsilon_\infty + \frac{\varepsilon_0 - \varepsilon_\infty}{1 + i\omega\tau_D} \qquad \textbf{(II.35)}$$

where $\varepsilon(\omega)$ is the frequency dependent dielectric constant of the bulk solvent, ε_∞ is the high frequency dielectric constant and τ_D is the Debye relaxation time. The decay of the solvation correlation function C(t) can be best described by

$$C(t) = \exp(-t/\tau_L) \qquad \textbf{(II.36)}$$

where τ_L is the longitudinal relaxation time of the solvent which is related to τ_D according to the following equation

$$\tau_L = \left(\frac{\varepsilon_\infty}{\varepsilon_0}\right)\tau_D \qquad \textbf{(II.37)}$$

For dipoles equation (II.37) modifies to

$$\tau_L = \left(\frac{2\varepsilon_\infty + \varepsilon_c}{2\varepsilon_0 + \varepsilon_c}\right)\tau_D \qquad \textbf{(II.38)}$$

For most polar solvents, $\left(\frac{\varepsilon_\infty}{\varepsilon_0}\right) < 1$ consequently τ_L is much shorter than τ_D.

Although the prediction of dielectric continuum theory is quite simple as it predicts a single exponential decay time for solvation response, the experimental outcome most often is rather complex. This is even true for an ideal solvatochromic probe such as coumarin 153 (C153), photophysics of which is known to have no contamination from other competing processes (refer to chapter I for a discussion). Solvation dynamics experiments of C153 in bulk organic solvents yields a distribution of relaxation times, which varies between two extremes τ_L and τ_D and is believed to be due to the molecularity of the solvent [21] (that is, in reality solvent and solute molecules are comparable in size). This signifies that the solvent molecules behave more like discrete particles which are comparable to the solute molecule in size. This aspect is completely ignored in SC theory where the solvent molecules are considered as being structureless entities. The deviation from single exponential solvation response can be visualized by the introduction of multiple Debye relaxation terms (equation (II.39)) or some modified forms of equation (II.35), which is illustrated in the Cole-Cole and Cole-Davidson forms [24].

$$\varepsilon(\omega) = \varepsilon_{\infty_n} + \sum_{i=1}^{n} \frac{(\varepsilon_{0_i} - \varepsilon_{\infty_i})}{(1 + i\omega\tau_i)} \qquad \textbf{(II.39)}$$

From the theoretical point of view, the dynamical mean sphere approximation (DMSA) treats this issue in a more relevant way which considers both solute and solvent molecules as being hard spheres [25-28] which consequently allows a finite value of solute to solvent size ratio.

Calculation of the "Zero-time" Emission Spectrum

Inspection of equation (II.34) reveals that the nature of C(t) depends upon three parameters, namely, $\nu(0)$, $\nu(t)$ and $\nu(\infty)$ respectively. Considering $\nu(0)$ as the extrapolated time zero spectrum from equation (II.28) has serious limitations on the construction of C(t) because due to the finite time resolution associated with optical experiments it is not possible to determine the true position of the "zero-time" spectrum accurately. As a consequence of this the extrapolated "zero-time" spectrum obtained from an experiment with 100 fs time resolution might be shifted towards higher energy compared to that obtained from an experiment with 100 ps time resolution.

Fee and Maroncelli [23] has developed a methodology to estimate the "zero-time" spectrum associated with solvation dynamics experiments. This hypothetical spectrum corresponds to a fluorescent probe after it has undergone intramolecular events contributing to its relaxation and before it has been altered by interactions with the solvent. So this methodology relies on the assumption that the intramolecular vibrational relaxation and solvent relaxation is separated in the time regime which is indeed a very good approximation in most of the cases considering solvation dynamics in polar solvents. Here I will discuss briefly the method discussed in the paper by Fee and Maroncelli [23] on this topic.

The key ingredients for the "zero-time" spectrum calculation in a polar solvent is to take the absorption (or excitation) and emission spectrum of the fluorophore in a non-polar solvent and the absorption (or excitation) spectrum in the polar solvent under investigation. We use hexane as the non-polar solvent. The basic principle of this method is to assume that the electronic origin of the absorption (or excitation) and emission spectrum is same in absence of any solvent relaxation. This can be accomplished by convoluting the non-polar

absorption (or excitation) spectrum with a broadening function, such as a Gaussian and shifting it until it superimposes on the polar absorption (or excitation) spectrum. Under this condition, the non-polar emission spectrum is the best estimate for the "zero-time" spectrum in the polar solvent under interest. The details calculation of this considers the inhomogeneous line broadening in polar solvent and assumes the homogeneous counterpart is same in both non-polar and polar solvent.

The absorption (or excitation) and emission spectrum of the fluorophore in non-polar solvent is converted to the corresponding line-shapes according to equations (II.40) and (II.41).

$$\mathbf{g}(\nu) \propto \frac{\mathbf{A}_{np}(\nu)}{\nu} \tag{II.40}$$

$$\mathbf{f}(\nu) \propto \frac{\mathbf{F}_{np}(\nu)}{\nu^3} \tag{II.41}$$

where A_{np} and F_{np} are the absorption (or excitation) and emission spectrum in the non-polar solvent, $g(\nu)$ and $f(\nu)$ being the corresponding line-shapes. Within a site-dependent shift δ the inhomogeneously broadened polar absorption spectrum is represented by

$$\mathbf{A}_p(\nu) \propto \nu \int \mathbf{g}(\nu - \delta)\, \mathbf{p}(\delta)\mathbf{d}\delta \tag{II.42}$$

where $p(\delta)$ is the distribution of solutes among sites (spectral shifts) and is approximated as

$$\mathbf{p}(\delta) = \frac{1}{(2\pi\sigma^2)^{-\frac{1}{2}}} \exp[-(\delta - \delta_0)^2 / 2\sigma^2] \tag{II.43}$$

where δ_0 is the polar solvent induced average shift and σ is the variance of the Gaussian distribution. At this point one can calculate the "zero-time" spectrum in the polar solvent under investigation according to

$$\mathbf{F_P}(\nu, \mathbf{t} = \mathbf{0}; \nu_{ex}) \propto \nu^3 \nu_{ex} \times \int \mathbf{g}(\nu_{ex} - \delta)\, \mathbf{p}(\delta)\, \mathbf{f}(\nu - \delta)\mathbf{k_{rad}}(\delta)\mathbf{d}\delta \qquad \textbf{(II.44)}$$

where k_{rad} is the radiative rate constant and is calculated according to

$$\mathbf{k_{rad}}(\delta) \propto \frac{\int \mathbf{f}(\nu - \delta)\nu^3 \mathbf{d}\nu}{\int \mathbf{f}(\nu - \delta)\mathbf{d}\nu} \qquad \textbf{(II.45)}$$

Equation (II.44) states that the "zero-time" spectrum in polar solvent is the convolution of the solvent distribution initially transferred to the excited state $[\mathbf{g}(\nu_{ex} - \delta)\, \mathbf{p}(\delta)]$ and the fluorescence intensity function$[\, \mathbf{f}(\nu - \delta)\mathbf{k_{rad}}(\delta)]$. Note that equation (II.44) is applicable for any excitation frequency (ν_{ex}).

Validity of this calculation was tested experimentally by comparing the emission spectrum of a given fluorophore in a glass environment where no solvent relaxation is expected and a very good agreement ($\Delta \sim 200$ cm^{-1}) was observed between the calculated "zero-time" spectrum and the experimental spectrum [23]. We have also checked its validity using a different method for estimating the "zero-time" reorganization energy [29].

Fee and Maroncelli also proposed a method to calculate the "zero-time" spectral position according to the following equation

$$\nu^{\mathbf{P}}{}_{\mathbf{em}}\ (\mathbf{0}) = \nu^{\mathbf{P}}{}_{\mathbf{abs}} - (\nu^{\mathbf{nP}}{}_{\mathbf{abs}} - \nu^{\mathbf{nP}}{}_{\mathbf{em}}) \qquad \textbf{(II.46)}$$

where P and nP refer to polar and nonpolar solvents, respectively. Without dealing with the rigorous calculation that accounts for the inhomogeneous broadening of the polar absorption (or excitation) spectrum equation (II.46) just equals the difference of the absorption (or excitation) and emission spectrum in the non-polar solvent with the corresponding difference in the polar absorption (or excitation) and "zero-time" spectrum. Although equation (II.46) oversimplifies the whole story we recommend the rigorous methodology to calculate the

"zero-time" spectrum because it appears that the success of this oversimplification resides on a very careful choice of spectral position. Consideration of this and a comparison with the rigorous method is presented in chapter VI in the context of our work of solvation dynamics of C153 in phosphonium based ionic liquids and their micelle in water. Also it appears that the choice of this spectral position is probe specific, that is, sometimes ν_{md} results in reliable values, in some other cases ν_{+} gives better estimate, ν_{md} being the midpoint frequency of the spectrum and is defined as $\nu_{md} = (\nu_{+} + \nu_{-})/2$, where ν_{+} and ν_{-} are the midpoint frequencies at the blue and red edges of the spectrum, respectively. Without prior knowledge of the true "zero-time" spectrum it is sometimes difficult to predict which of these choices would give reliable information.

References

(1) Andrews, D. L. Applied laser spectroscopy : techniques, instrumentation, and applications; VCH: New York, 1992.

(2) Svelto, O. Principles of lasers, 2nd ed.; Plenum Press: New York, 1982.

(3) Martinez, O. E.; Gordon, J. P.; Fork, R. L. Opt. Soc. Am. 1984, 1, 1003.

(4) Asaki, M. T.; Huang, C.-P.; Garvey, D.; Zhou, J.; Kapteyn, H. C.; Murnane, M. M. Opt. Lett. 1993, 18, 977.

(5) Hecht, J. An entry level guide, 2nd Ed. ed.; IEEE Press, p.238.

(6) Spence, D. E.; Kean, P. N.; Sibbett, W. Opt. Lett. 1991, 16, 42.

(7) English, D. S. Elucidation of the Primary Photophysical Processes in the Light-Activated Antiviral Agents, Hypericin and Hypocrellin, Iowa State University, 1998.

(8) Park, J. Photophysics amd light induced photobiology of antiviral and antitumor agents, hypericin and hypocrellin, Iowa State University 2001.

(9) O'Connor, D. V.; Phillips, D. Time-correlated single photon counting; Academic Press, 1984.

(10) Fleming, G. R. Chemical applications of ultrafast spectroscopy; Oxford University Press, 1985.

(11) Lakowicz, J. R. Principles of fluorescence spectroscopy, 2nd ed.; Springer: New York, 2004.

(12) Becker, W. The bh TCSPC Handbook, 2nd Ed. ed.; Becker & Hickl GmbH: Berlin, 2006.

(13) Edinburgh Instruments Ltd. What is TCSPC ? (Time Correlated Single Photon Counting) (Technical Note).

(14) Zernike, F.; Midwinter, J. E. Applied Nonlinear Optics; Wiley: New York, 1973.

(15) Shen, Y. R. The Principles of Nonlinear Optics; Wiley: New York, 1984.

(16) Shah, J. IEEE J. Quant. Elec. 1988, 24, 276.

(17) Chowdhury, P. K. Picosecond time resolved spectroscopy used as a tool to probe excited state photophysics of biologically and environmentally relevant systems, Iowa State University, 2004.

(18) Smirnov, A. V. Primary Photoprocesses of light-activated antiviral and antitumor agents, hypericin and hypocrellin, Iowa State University, 1999.

(19) Jordanides, X. J.; Lang, M. J.; Song, X.; Fleming, G. R. J. Phys. Chem. B 1999, 103, 7995.

(20) Dutta, A. Study of solvation dynamics and intramolecular proton transfer process using a picosecond laser, Indian Association for the Cultivation of Science, 1998.

(21) Maroncelli, M.; Fleming, G. R. J. Chem. Phys. 1987, 86, 6221.

(22) Horng, M. L.; Gardecki, J. A.; Papazyan, A.; Maroncelli, M. J. Phys. Chem. 1995, 99, 17311.

(23) Fee, R. S.; Maroncelli, M. Chem. Phys. 1994, 183, 235.

(24) Maroncelli, M. J. Mol. Liq. 1993, 57, 1.

(25) Wolynes, P. G. J. Chem. Phys. 1987, 86, 5133.

(26) Rips, I.; Klafter, J.; Jortner, J. J. Chem. Phys. 1988, 89, 4288.

(27) Rips, I.; Klafter, J.; Jortner, J. J. Chem. Phys. 1988, 88, 3246.

(28) Nichols III, A. L.; Calef, D. F. J. Chem. Phys. 1988, 89, 3783.

(29) Headley, L. S.; Mukherjee, P.; Anderson, J. L.; Ding, R.; Halder, M.; Armstrong, D. W.; Song, X.; Petrich, J. W. J. Phys. Chem. A 2006, 110, 9549.

CHAPTER III. INTERACTION OF GLUTATHIONE S-TRANSFERASE WITH HYPERICIN: A PHOTOPHYSICAL STUDY

A paper published in the Journal of Physical Chemistry B

M. Halder[1], P. K. Chowdhury[1], R. Das[1], P. Mukherjee[1], W. M. Atkins[2], and J. W. Petrich[1,*]

Abstract

The photophysics of hypericin have been studied in its complex with two different isoforms, A1-1 and P1-1, of the protein glutathione S-transferase (GST). One molecule of hypericin binds to each of the two GST subunits. Comparisons are made with our previous results for the hypericin/human serum albumin complex (Photochem. Photobiol. 69, 633-645 (1999)). Hypericin binds with high affinity to the GSTs: 0.65 μM for the A1-1 isoform; 0.51 μM for the P1-1 isoform (Biochemistry 43, 12761-12769 (2004)). The photophysics and activity of hypericin are strongly modulated by the binding protein. Intramolecular hydrogen atom transfer is suppressed in both cases. Most importantly, while there is significant singlet oxygen generation from hypericin bound to GST A1-1, binding to GST P1-1 suppresses singlet oxygen generation to almost negligible levels. The data are rationalized in terms of a

---

[1] Department of Chemistry, Iowa State University, Ames, Iowa 50011.

[2] Departments of Chemistry and Medicinal Chemistry, University of Washington, Seattle, Washington 98185.

[*] Author to whom correspondence should be addressed.

simple model in which the hypericin photophysics depends entirely upon the decay of the triplet state by two competing processes, quenching by oxygen to yield singlet oxygen and ionization, the latter of these two are proposed to be modulated by A1-1 and P1-1.

Introduction

Hypericin (Figure III.1) is a major component of the botanical dietary supplement, St. John's Wort. It is a widely spread, naturally occurring perylene quinone pigment that is of great interest because of its broad spectrum of light-induced biological activities [1-5]. Here we investigate the photophysics of hypericin in complex with a biologically important protein to which it binds with high affinity, glutathione S-transferase (GST).

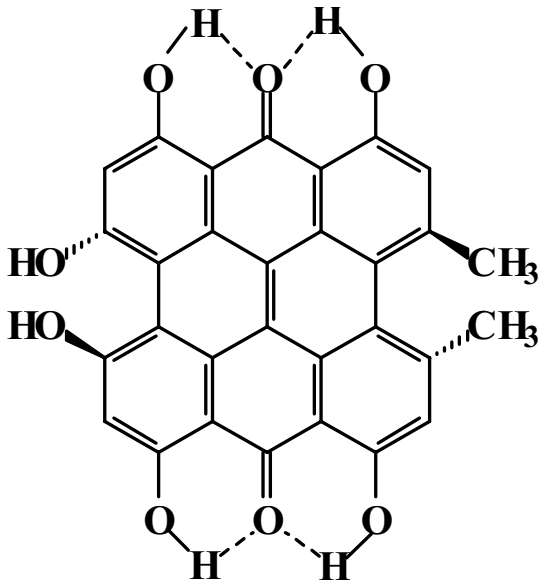

Figure III.1. Hypericin (7,14 normal form).

GSTs (Figure III.2) are biologically significant because they catalyze the conjugation of reduced glutathione (GSH) to a variety of electrophiles and thereby detoxify carcinogens, pesticides, and reactive products generated under oxidative stress. The conjugation of GSH

with a foreign compound generally results in the formation of a nontoxic product that can be readily eliminated [6]. In addition to their catalytic function, GSTs also serve as nonenzymatic binding proteins, known as ligandins, that interact with various lipophilic compounds that include steroid and thyroid hormones. Finally, reactive oxygen species can trigger apoptosis, programmed cell death, in cells. The production of GSTs, by helping to protect the cell from oxidative damage caused by reactive oxygen species, assists in obviating the induction of apoptosis [6]. Cytochrome P450, especially the form CYP3A4 which predominates in hepatic tissue, has functions similar to that of GST. It metabolizes endogenous compounds and xenobiotics. It is believed to be capable of binding multiple ligands, of the size of pyrene and we have shown that it can bind hypericin with high affinity [7]. HSA is the archetypal drug transport protein and we have studied hypericin bound to HSA extensively in the past [8]. Our hypericin/HSA results serve as a baseline reference.

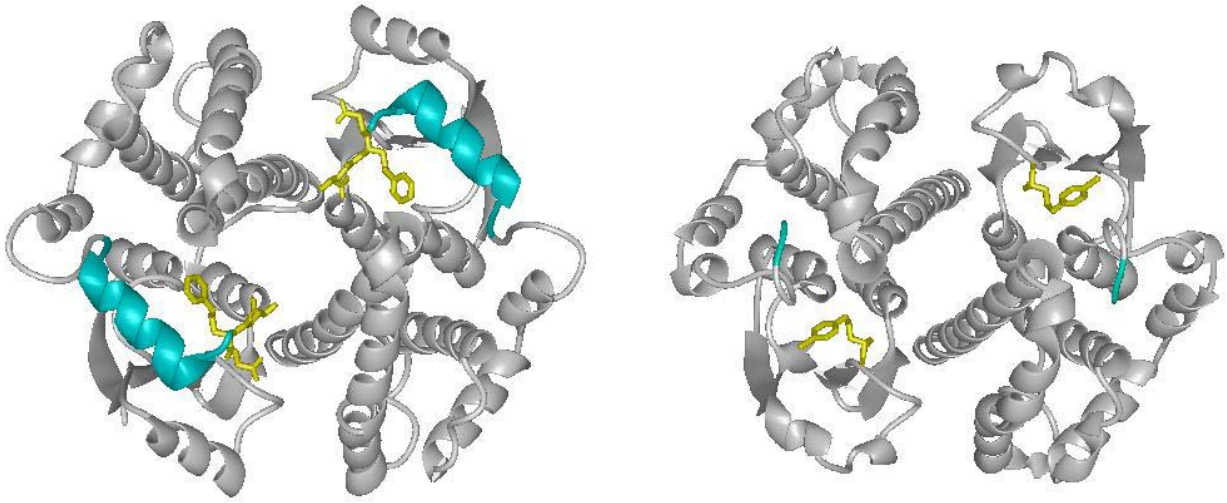

A1-1 P1-1

Figure III.2. GST isoforms: A1-1 (left); P1-1 (right). Although the two proteins are structurally very homologous, they share only 29% sequence homology [7].

The biological activity of hypericin and its analogs depends on light. Hypericin displays light-induced activity against several types of viruses, including the human immunodeficiency virus (HIV) [9-11], as well as antiproliferative and cytotoxic effects on tumor cells [12-15]. Hypericin is also a potent antidepressant [16,17], exhibits light-dependent inhibition of protein kinase C (PKC), which has been suggested to be a locus of its antiviral activity [18], and is reported to possess numerous other types of biological behavior [19-21]. Hypericin, like other anticancer drugs, also induces apoptosis [22,23]. Consequently, it is important to understand the primary photophysical processes occurring subsequent to photon absorption. Our work has produced several hypotheses concerning the excited-state H-atom transfer in these molecules, namely that excited-state intramolecular hydrogen atom displacement ultimately triggers the ejection of a proton. We have argued that the antiviral activity of hypericin remains significant in the absence of oxygen [24]. The question then arises how hypericin interacts with a cell and by what means its biological effects are exerted. Photoactive molecules are traditionally depicted as either interacting directly with a substrate (Type I mechanisms) or producing reactive oxygen species, especially singlet oxygen (Type II mechanisms) that exhibit toxicity. Clearly, hypericin and its analogs produce parallel pathways, which work either independently of the Type I and Type II mechanisms, or work in such a way as to complement them. We wish to elucidate these parallel pathways.

Owing to this light-induced biological activity, which is diverse, widespread, and important, we have been studying the early time photophysics of hypericin and its analogs [8,25-37]. By means of H/D substitution, investigation of methoxy analogs, and complementary studies using both transient absorption and fluorescence upconversion spectroscopies, we

have argued that the major primary photophysical process in hypericin in organic solvents is excited-state intramolecular hydrogen atom transfer.

Subsequent to the intramolecular H-atom transfer, there is an intermolecular proton transfer to the solvent [38-40]. This event is a reversible process in vitro, as demonstrated by the conservation of the sample optical density over the course of several cycles of pH measurement. We have suggested that these photogenerated protons may be important for understanding the light-induced biological activity of hypericin [4]. As we have discussed elsewhere [8,41-43], this H-atom transfer is not observed when hypericin is bound to HSA. Indeed, as we indicate below, this transient is not observed when hypericin is bound to either A1-1 or P1-1, which leads us to speculate upon the relative roles of singlet oxygen and photoinduced proton transfer in these systems.

Materials and Methods

GST

The expression and purification of the GSTs, the determination of their binding constants to hypericin, and the quantification of their photoinduced oxidative damage via hypericin has been thoroughly discussed by Lu and Atkins [7].

Steady-State and Time-Resolved Measurements

Steady state absorbance spectra were obtained on Perkin Elmer Lambda 18 double beam UV-visible spectrophotometer with 1-nm resolution. Steady state fluorescence spectra were obtained on a Spex Fluoromax with a 4-nm bandpass and corrected for lamp spectral intensity and detector response. For both fluorescence and absorption measurements, a 3-mm path-length quartz cuvette was used.

The apparatus for time correlated single photon counting is described elsewhere [26,27]. Fluorescence decay kinetics were recorded by exciting at 580 nm and collecting emission at > 610 nm with a cut-off filter for a maximum of 10,000 counts at the peak channel. The polarized fluorescence traces were used to obtain fluorescence anisotropy decay parameters collected to a maximum of 10,000 counts at the peak channel. Fits were considered acceptable for $\chi^2 \leq 1.2$.

Flash Photolysis

Flash photolysis experiments were performed with a system based on a 10 Hz Surelite I-10 (Continuum, Santa Clara, CA) Nd:YAG laser. The fundamental, 1064 nm, was frequency doubled, and the resulting radiation at 532 nm with an 100-mW of average power was used as the pump source. A 75-W Xe lamp (Photon Technology International, NJ) was used as a probe source. The UV from this Xe source was filtered off with a benzene solution filter. Fluorescence and scattered light were blocked by an 8-nm bandpass monochromator at 520 nm before a 1P-28 photomultiplier. Transient absorbance data were collected by a dual-channel 50- MHz Picoscope 3000 (Pico Technology Ltd., U.K).

Time-Resolved Pump Probe Absorption Spectroscopy

The instrument function of our time-correlated single photon counting system has a fwhm of 80 ps. To investigate more rapid phenomenon, better time resolution was required. This was provided by a home-made regeneratively amplified Ti-sapphire system, providing 130-fs pulses at 814 nm which was then frequency doubled and used to perform pump-probe measurements [36,43,44]. For pump probe measurements, 407 nm was used as the pump source; and a white light continuum, as the probe source. The probe wavelength was 600 nm.

Sample Preparation

A DMSO solution of Hypericin was used as the stock solution for sample preparation; the total organic content of the final sample solution was < 1% for both Hypericin/HSA and Hypericin/A1-1 or Hypericin/P1-1 in phosphate-EDTA buffer (pH 6.9). The hypericin/protein solutions were incubated for about 4-7 hours in the dark prior to steady-state, time-resolved and flash photolysis experiments. For steady-state fluorescence measurements, the solutions were prepared with a stoichiometry of 10:1 protein to hypericin with [Hyp] ~1.0×10^{-6} M. For time-resolved fluorescence studies, [Hyp] ~ 5.0×10^{-6} M, with varying amounts of protein concentrations as indicated in Table III.1 was employed. Flash photolysis experiments were performed with [Hyp] ~ 5.0×10^{-5} M with 3:1 protein to hypericin ratio. For pump probe experiments [Hyp] was kept at ~ 8.0×10^{-5} M and a 1:1 protein to hypericin ratio was maintained. (The spectra were found to be similar in case of 10:1 and 1:1 protein to hypericin ratio.)

Results and Discussion

Binding of Hypericin to GSTs and Singlet Oxygen Generation

GST binds hypericin very tightly [7]: A1-1 with K_D = 0.65 μM; P1-1 with K_D = 0.51 μM . Binding of hypericin to GSTs also inhibits their catalytic activity [7]. The submicromolar affinity with which hypericin binds to GST is the first case of high affinity binding of hypericin to a biologically important molecule that has been documented.

Our data suggest that one hypericin molecule binds to each of the two subunits comprising GST (Table III.1). Binding is determined by monitoring the average fluorescence lifetime of hypericin as a function of the GST/hypericin ratio. When GST/hypericin < 1/2, the average fluorescence lifetime decreases significantly from a

constant value of ~3.3 ns. An even more compelling indication of this binding ratio is that when it is less than 1/2, the fluorescence anisotropy decay is no longer a simple single exponential with a $\geq$ 20 ns depolarization time but takes on a second much more rapid component indicative of a chromophore loosely bound to the surface [8]. For example, when P1-1/hypericin is 1/3, $r(t) = 0.02 \exp(-t/0.98\ ns) + 0.27 \exp(-t/19\ ns)$.

Table III.1. Fluorescence Lifetimes of Hypericin Bound to GSTs [a]

	τ_1	a_1	τ_2	a_2	τ_3	$\langle\tau\rangle$ [b]
P1-1/Hyp						
10/1	**140**	**0.24**	**1860**	**0.18**	**5400**	**3500**
1/1	**170**	**0.24**	**1550**	**0.14**	**5200**	**3480**
1/1.7	**160**	**0.31**	**1560**	**0.15**	**5200**	**3100**
1/3	**210**	**0.31**	**1890**	**0.15**	**5250**	**3180** [c]
1/7	**160**	**0.51**	**1460**	**0.14**	**5230**	**2120**
1/10	**130**	**0.72**	**1100**	**0.10**	**5200**	**1140**
A1-1/Hyp						
10/1	**300**	**0.28**	**2800**	**0.17**	**5900**	**3800**
1/1	**300**	**0.34**	**2000**	**0.14**	**5400**	**3200**
1/1.7	**280**	**0.43**	**2100**	**0.13**	**5650**	**2900**
1/3	**250**	**0.68**	**1200**	**0.15**	**5450**	**1250**
1/10	**150**	**0.86**	**820**	**0.12**	**4200**	**300**

[a] All times are given in picoseconds. Fluorescence lifetimes are fit to a sum of three exponentials. In all cases, [Hyp] ~ 5.0×10^{-6} M.

[b] The error in the average fluorescence lifetime is given by $\langle\tau\rangle = \sum_i a_i \tau_i$. It is estimated to be accurate to ~ ± 15 %.

[c] This value is higher than expected given the P1-1/hypericin ratio and the corresponding results for A1-1/hypericin. Nevertheless, as we indicate in the text, under these conditions, the fluorescence anisotropy decay departs from a single exponential, indicating surface binding of the hypericin.

An intriguing observation is that the photophysical properties of hypericin can be altered upon binding to GSTs. In particular, when hypericin binds to A1-1, light-induced oxidative damage is produced, as evidenced by the mass spectrometry data obtained after 30 minutes of optical irradiation. On the other hand, no such oxidative damage is observed for P1-1. Figure III.3 compares photosensitized oxidation by hypericin of HSA, A1-1, and P1-1 [7]. While P1-1 is essentially impervious to oxidative damage, both HSA and A1-1 are extremely susceptible.

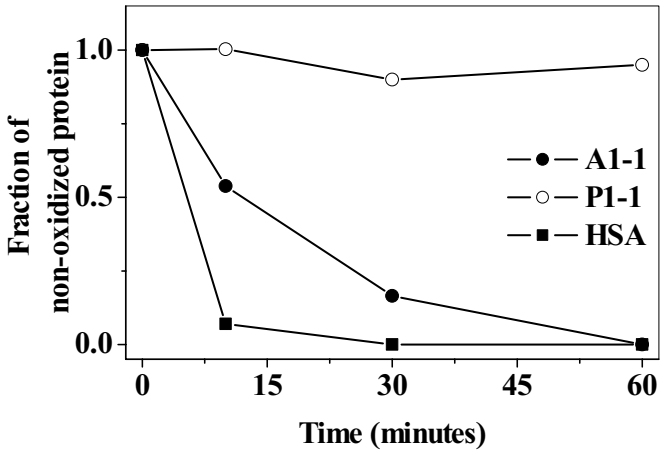

Figure III.3. Protein oxidation from light-activated bound hypericin. Details of the experiment are given by Lu and Atkins [7].

Photophysics of Hypericin Bound to GSTs

As noted in the Introduction, we have argued that one of the primary processes deactivating the excited-state singlet of hypericin in bulk organic solvent is intramolecular hydrogen atom transfer. The signature of this process is the rise time in the kinetics, as indicated in Figure III.4 for hypericin in DMSO. This process is not, however, observed

when hypericin is bound to HSA [8]. We interpreted this result in terms of hypericin binding to a tryptophan residue in HSA that inhibited its H-atom transfer. Given that intramolecular H-atom transfer is impeded in hypericin/HSA and that light-induced protein oxidation of hypericin/HSA is more similar to that of hypericin/A1-1 than to hypericin/P1-1, it was our original expectation that the photophysics of hypericin/A1-1 should more nearly resemble that of hypericin/HSA than that of hypericin/P1-1. This expectation was not, however, borne out uniformly by subsequent experiment: the singlet kinetics (Figure III.4) and fluorescence intensities (Figure III.5) of hypericin/P1-1 more closely resemble those of hypericin/HSA. On the other hand, the long-time kinetics (Figure III.6) indicate that the population of hypericin radical ion in A1-1 is essentially identical to that generated in complex with HSA and about a factor of two less than that obtained in complex with P1-1.

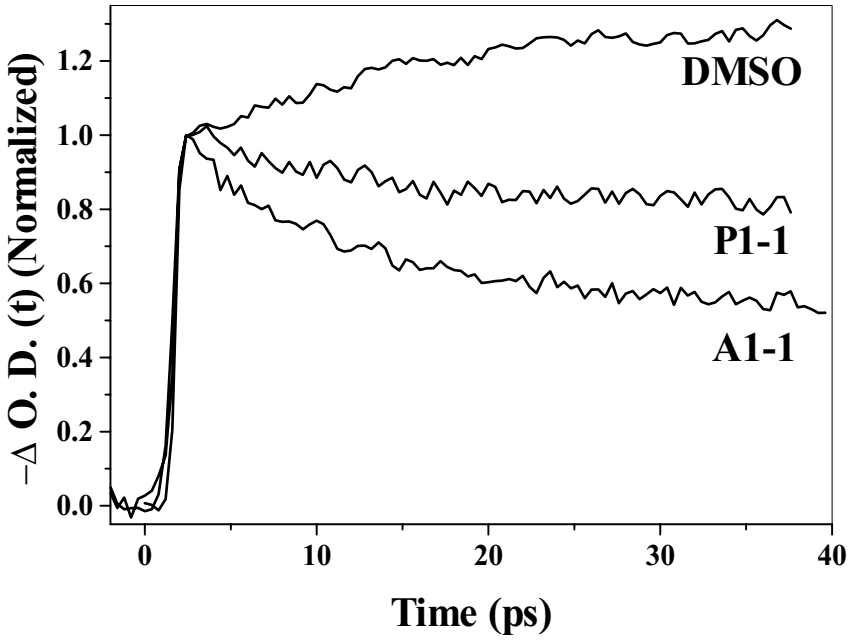

Figure III.4. Singlet kinetics of hypericin. The probe wavelength is 600 nm. Only hypericin in DMSO exhibits the ~10-ps rise time attributed to excited-state intramolecular H-atom transfer. Note that the hypericin/P1-1 trace is nearly flat on the 40-ps time scale, more like that of hypericin/HSA [8] than of hypericin/A1-1.

We note that the data presented in Figure III.4 are transient absorption data, which detect both stimulated emission, induced absorption, and ground-state bleaching. Consequently, there is always the possibility that the interpretation of the observed kinetics is complicated by several simultaneous phenomena. The interpretation of the GST data is based upon our failure to see a rise time for the 1:1 complex of hypericin:HSA in not only transient absorption but also fluorescence upconversion experiments [8], the latter of which only detect emission from the lowest singlet state.

The long-time kinetics do not reflect the decay of the triplet, T_1. Indeed, we do not detect a transient triplet species for hypericin bound to these proteins in our experiments.

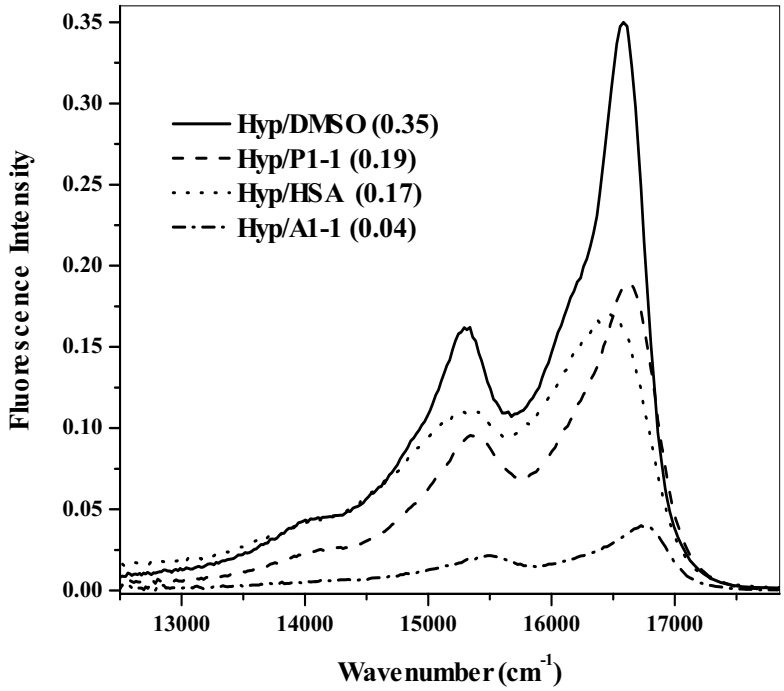

Figure III.5. Absolute hypericin fluorescence intensity vs. wavenumber. The integrated intensities on the energy (wavenumber) scale provide the fluorescence quantum yields (determined from these spectra), which are given in parentheses in the Figure. Again, note that the fluorescence quantum yield of hypericin/P1-1 is more like that of hypericin/HSA than that of hypericin/A1-1. The samples were excited at 550 nm.

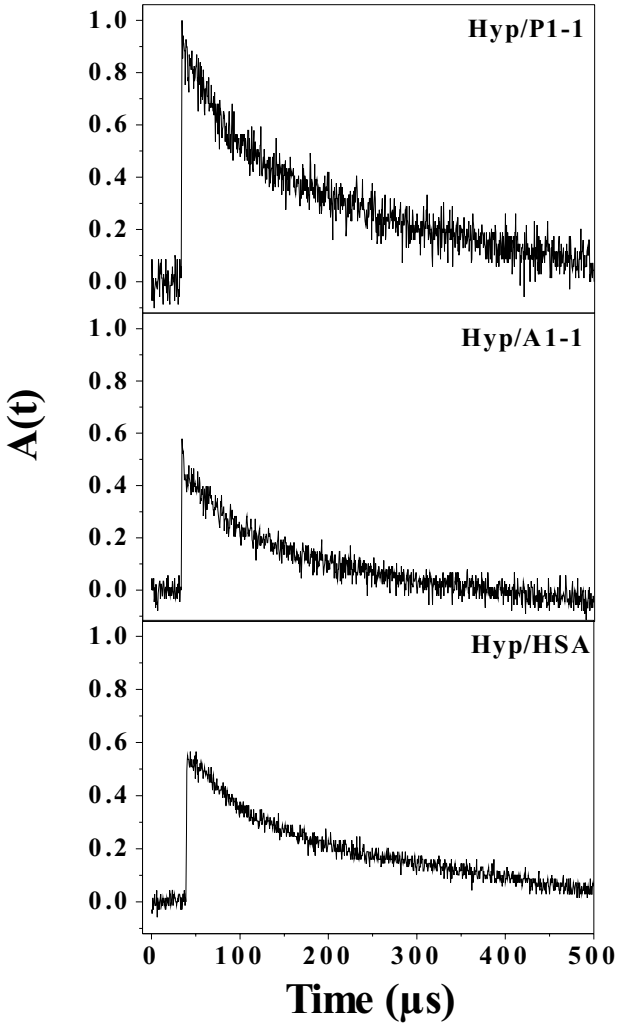

Figure III.6. Room-temperature, long-time kinetics of hypericin, reflecting the behavior of the hypericin anion. For laser flash photolysis experiments, samples were pumped at 532 nm and the transient was probed after a monochromator set at 520 nm (see experimental details). For all the samples [Hyp] ~ 5.0×10^{-5} M with 3:1 protein to hypericin ratio. The solutions were prepared in phosphate-EDTA buffer (pH 6.9) for both GSTs and HSA. The traces are scaled to their relative intensity, with the trace for Hyp/P1-1 normalized to unit intensity at time zero. These results were reproduced three times using a different protein preparation for each experiment. For the long-time kinetics, the intensity of the hypericin/A1-1 signal is essentially identical to that of hypericin/HSA. In the context of earlier work by ourselves [38], Falk and coworkers [46], and especially Jardon and coworkers [47,48], we attribute the origin of these long-lived transients to the deprotonation of the hypericin triplet. Jenks and coworkers [49] have observed similar transients arising from reduction and oxidation of triplet by electron acceptors and donors. It is unlikely that the long-lived kinetics can be attributed to the triplet. Assuming a diffusion-controlled reaction and an oxygen concentration at atmospheric pressure of ~0.2 mM [50], the time constant for triplet decay resulting from oxygen quenching is estimated to be on the order of 5 μs.

The lifetime of hypericin triplet in an air saturated solution at room temperature is expected to be ≤ 1 μs, depending on the solvent (see the caption to Figure III.6). No component of this duration is observed. We have previously observed such long-lived species of hypericin and its analogs in micelles [45]. Jardon and coworkers have discussed long-lived hypericin transients in terms of deprotonation of the hypericin triplet to form the anion [47,48], and we [38] have shown that triplet hypericin is a proton donor. It thus seems reasonable to attribute the long-lived transient to a deprotonated species originating from the triplet, Hyp^-, and in the following discussion we refer to this species as a deprotonated or anionic form of hypericin.

It may be argued that hypericin bound to P1-1 is not accessible to oxygen and that this explains the absence of oxidative damage in the complex. This is unlikely. First, the structural homology of the two proteins (Figure III.2) suggests that hypericin binds similarly to both. Second, a more quantitative indication is given by Stern-Volmer fluorescence quenching experiments [7]. Using iodide as a quencher, quenching constants of 4.3, 8.3, and 1.9 M^{-1} were obtained for hypericin bound to A1-1, P1-1, and HSA, respectively [7]. These results indicate that hypericin bound to all three of these proteins is accessible to fluorescence quenchers and that, in fact, it is even slightly more accessible when bound to P1-1 than to the other two proteins.

The unanticipated behavior of the singlet kinetics and the fluorescence quantum yields originally proved quite puzzling in light of the hypericin activity. They, however, can be rationalized by considering the following points.

1. The intersystem crossing rate, k_{ISC}, must be 5 times larger for hypericin/A1-1 than for hypericin/P1-1 in order to explain the fluorescence quantum yield and the singlet decay data: $\Phi_T^{A1-1} = 5 \cdot \Phi_T^{P1-1}$ (Figures III.4 and III.5).

2. Note that the anion intensity of hypericin/A1-1 is about 2 times smaller than that of hypericin/P1-1: $2 \cdot \Phi_{ion}^{A1-1} = \Phi_{ion}^{P1-1}$ (Figure III.6).

3. The data in Figure III.3 highlighting photosensitized oxidation of protein imply that hypericin/A1-1 makes at least 10 times more singlet oxygen than hypericin/P1-1: $\Phi_{\Delta}^{A1-1} = 10 \cdot \Phi_{\Delta}^{P1-1}$. Consequently, we can rationalize hypericin/A1-1 being about 10 times more reactive than hypericin/P1-1.

4. We make the reasonable assumption that singlet oxygen and hypericin anion are produced only by the triplet and that their respective yields, Φ_{ion} and Φ_{Δ}, are given by the standard expressions:

$$\Phi_{ion} = \Phi_T \cdot \frac{k_{ion}}{k[O_2] + k_{ion}} \quad \text{and} \quad \Phi_{\Delta} = \Phi_T \cdot \frac{k[O_2]}{k[O_2] + k_{ion}},$$

where we assume that $k[O_2]$ is the same for all the proteins considered here. Taking the ratios of the respective yields,

$$\frac{\Phi_{ion}^{A1-1}}{\Phi_{ion}^{P1-1}} = \frac{\Phi_T^{A1-1}}{\Phi_T^{P1-1}} \cdot \frac{k_{ion}^{A1-1}}{k_{ion}^{P1-1}} \cdot \frac{k[O_2] + k_{ion}^{P1-1}}{k[O_2] + k_{ion}^{A1-1}} \quad \text{and} \quad \frac{\Phi_{\Delta}^{A1-1}}{\Phi_{\Delta}^{P1-1}} = \frac{\Phi_T^{A1-1}}{\Phi_T^{P1-1}} \cdot \frac{k[O_2] + k_{ion}^{P1-1}}{k[O_2] + k_{ion}^{A1-1}},$$

from which we conclude that

$$20 = \frac{\Phi_{\Delta}^{A1-1}}{\Phi_{\Delta}^{P1-1}} \cdot \frac{\Phi_{ion}^{P1-1}}{\Phi_{ion}^{A1-1}} = \frac{k_{ion}^{P1-1}}{k_{ion}^{A1-1}}.$$

In other words, because the triplet state of hypericin is much more susceptible to decay into the anion when it is bound to P1-1 than to A1-1 or HSA, it generates considerably less singlet oxygen when complexed to P1-1 than to the two latter proteins. The origin of this difference can only be attributed to the amino acids surrounding hypericin in the various proteins and their effect on the excited-state photophysics of hypericin. An energy level diagram summarizing these processes is given in Figure III.7.

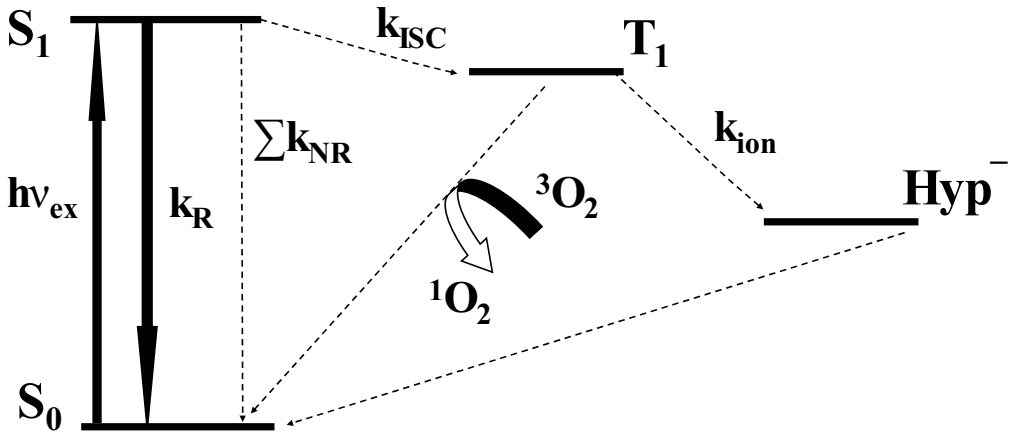

Figure III.7. Electronic energy levels of hypericin and their deactivation processes. k_R is the radiative rate of the first excited singlet and Σ k_{NR} is the sum of all the nonradiative processes deactivating this state except for k_{ISC}, the intersystem crossing rate, which is specifically indicated, taking the singlet to the triplet. At room temperature, we suggest that the triplet state decays predominantly by deprotonation to form the anion, k_{ion}, or by interaction with ground-state oxygen to form singlet oxygen, $k[^3O_2]$.

Conclusions

While the argument given above provides a pleasing rationalization of the kinetic and steady-state data and renders it consistent with the light-induced biological reactivity of hypericin in different protein environments, it is important to note that the atomistic details of A1-1 and P1-1 giving rise to these differences must still be resolved. This is a main goal of current work in progress.

An interesting consequence of this work is that it suggests that insofar as the long-lived transient species depicted in Figure III.6 can be attributed to the hypericin anion originating from the triplet, Hyp^-, even if there is no intramolecular H-atom transfer in the singlet state for hypericin bound to HSA, A1-1, or P1-1, the corresponding triplet state is still able to liberate a proton.

To date, the bulk of the photophysical studies of hypericin has been carried out in homogeneous organic solution. Studying the light-induced activity of hypericin in complex with biologically important proteins will contribute to an appreciation of both its therapeutic utility as well as its possible toxicity.

Acknowledgements

JWP was supported by grant number P01 ES012020 from the National Institute of Environmental Health Sciences (NIEHS) and the Office of Dietary Supplements (ODS), NIH. Its contents are solely the responsibility of the authors and do not necessarily represent the official views of the NIEHS, NIH. WMA was supported by the UW NIEHS sponsored Center for Ecogenetics and Environmental Health, Grant NIEHSP30ES07033 and by National Institutes of Health Grant GM62284. We thank Mr. Weiya D. Lu for providing GST for this work.

References

(1) Durán, N.; Song, P. S. Photochem. Photobiol. 1986, 43, 677.

(2) Lown, J. W. Can. J. Chem. 1997, 75, 99.

(3) Diwu, Z. Photochem. Photobiol. 1995, 61, 529.

(4) Kraus, G. A.; Zhang, W. J.; Fehr, M. J.; Petrich, J. W.; Wannemuehler, Y.; Carpenter, S. Chem. Rev. 1996, 96, 523.

(5) Falk, H. Angew. Chem., Int. Ed. 1999, 38, 3117.

(6) Adman, E. T.; Le Trong, I.; Stenkamp, R. E.; Nieslanik, B. S.; Dietze, E. C.; Tai, G.; Ibarra, C.; Atkins, W. M. Proteins: Struc. Func. Gen. 2001, 42, 192.

(7) Lu, W. D.; Atkins, W. M. Biochemistry 2004, 43, 12761.

(8) Das, K.; Smirnov, A. V.; Wen, J.; Miskovsky, P.; Petrich, J. W. Photochem. Photobiol. 1999, 69, 633.

(9) Meruelo, D.; Lavie, G.; Lavie, D. Proc. Natl. Acad. Sci. U. S. A. 1988, 85, 5230.

(10) Lenard, J.; Rabson, A.; Vanderoef, R. Proc. Natl. Acad. Sci. U. S. A. 1993, 90, 158.

(11) Hudson, J. B.; Zhou, J.; Chen, J.; Harris, L.; Yip, L.; Towers, G. H. N. Photochem. Photobiol. 1994, 60, 253.

(12) Anker, L.; Gopalakrishna, R.; Jones, K. D.; Law, R. E.; Couldwell, W. T. Drugs Future 1995, 20, 511.

(13) Couldwell, W. T.; Gopalakrishna, R.; Hinton, D. R.; He, S.; Weiss, M. H.; Law, R. E.; Apuzzo, M. L. Neurosurgery 1994, 35, 705.

(14) Zhang, W.; Anker, L.; Law, R. E.; Hinton, D. R.; Gopalakrishna, R.; Pu, Q.; Gundimeda, U.; Weiss, M. H.; Couldwell, W. T. Clin. Cancer Res. 1996, 2, 843.

(15) Zhang, W.; Law, R. E.; Hinton, D. R.; Couldwell, W. T. Cancer Lett. 1997, 120, 31.

(16) Linde, K.; Ramirez, G.; Mulrow, C. D.; Pauls, A.; Weidenhammer, W.; Melchart, D. Br. Med. J 1996, 313, 253.

(17) Suzuki, O. K.; Oya, M.; Bladt, S.; Wagner, H. Planta Med. 1984, 50, 272.

(18) Takahashi, I. N. S.; Kobayashi, E.; Nakano, H.; Suziki, K.; Tamaoki, T. Biochem. Biophys. Res. Commun. 1989, 165, 1207.

(19) Andreoni, A.; Colasanti, A.; Colasanti, P.; Mastrocinique, M.; Riccio, P.; G., R. Photochem. Photobiol. 1994, 59, 529.

(20) Thomas, C.; MacGill, R. S.; Miller, G. C.; Pardini, R. S. Photochem. Photobiol. 1992, 55, 47.

(21) Vandenbogaerde, A. L.; Cuveele, J. F.; Proot, P.; Himpens, B. E.; Merlevede, W. J.; deWitte, P. A. J. Photochem. Photobiol., B 1997, 38, 136.

(22) Weller, M.; Trepel, M.; Grimmel, C.; Schabet, M.; Bremen, D.; Krajewski, S.; Reed, J. C. Neurol. Res. 1997, 19, 459.

(23) Mirossay, L.; Mirossay, A.; Kocisova, E.; Radvakova, I.; Miskovsky, P.; Mojzis, J. Physiol. Res. 1999, 48, 135.

(24) Park, J.; English, D. S.; Wannemuehler, Y.; Carpenter, S.; Petrich, J. W. Photochem. Photobiol. 1998, 68, 593.

(25) Gai, F.; Fehr, M. J.; Petrich, J. W. J. Am. Chem. Soc. 1993, 115, 3384.

(26) Gai, F.; Fehr, M. J.; Petrich, J. W. J. Phys. Chem. 1994, 98, 8352.

(27) Gai, F.; Fehr, M. J.; Petrich, J. W. J. Phys. Chem. 1994, 98, 5784.

(28) Das, K.; English, D. S.; Fehr, M. J.; Smirnov, A. V.; Petrich, J. W. J. Phys. Chem. 1996, 100, 18275.

(29) Das, K.; English, D. S.; Petrich, J. W. J. Phys. Chem. A 1997, 101, 3241.

(30) Das, K.; English, D. S.; Petrich, J. W. J. Am. Chem. Soc. 1997, 119, 2763.

(31) Das, K.; Smirnov, A. V.; Snyder, M. D.; Petrich, J. W. J. Phys. Chem. B 1998, 102, 6098.

(32) Das, K.; Dertz, E.; Paterson, J.; Zhang, W.; Kraus, G. A.; Petrich, J. W. J. Phys. Chem. B 1998, 102, 1479.

(33) Das, K.; Ashby, K. D.; Wen, J.; Petrich, J. W. J. Phys. Chem. B 1999, 103, 1581.

(34) English, D. S.; Das, K.; Ashby, K. D.; Park, J.; Petrich, J. W.; Castner, E. W. J. Am. Chem. Soc. 1997, 119, 11585.

(35) English, D. S.; Das, K.; Zenner, J. M.; Zhang, W.; Kraus, G. A.; Larock, R. C.; Petrich, J. W. J. Phys. Chem. A. 1997, 101, 3235.

(36) English, D. S.; Zhang, W.; Kraus, G. A.; Petrich, J. W. J. Am. Chem. Soc. 1997, 119, 2980.

(37) Smirnov, A. V.; Das, K.; English, D. S.; Wan, Z.; Kraus, G. A.; Petrich, J. W. J. Phys. Chem. A 1999, 103, 7949.

(38) Fehr, M. J.; Mccloskey, M. A.; Petrich, J. W. J. Am. Chem. Soc. 1995, 117, 1833.

(39) Sureau, F.; Miskovsky, P.; Chinsky, L.; Turpin, P. Y. J. Am. Chem. Soc. 1996, 118, 9484.

(40) Chaloupka, R.; Sureau, F.; Kocisova, E.; Petrich, J. W. Photochem. Photobiol. 1998, 68, 44.

(41) Petrich, J. W. Int. Rev. Phys. Chem. 2000, 19, 479.

(42) Chowdhury, P. K.; Das, K.; Datta, A.; Liu, W. Z.; Zhang, H. Y.; Petrich, J. W. J. Photochem. Photobiol., A 2002, 154, 107.

(43) Halder, M.; Chowdhury, P. K.; Gordon, M. S.; Petrich, J. W.; Das, K.; Park, J.; Alexeev, Y. Adv. Photochem. 2005, 28, 1.

(44) English, D. S.; Das, K.; Petrich, J. W. Abstr. Pap. Am. Chem. Soc. 1997, 213, 405.

(45) Wen, J.; Chowdhury, P.; Wills, N. J.; Wannemuehler, Y.; Park, J.; Kesavan, S.; Carpenter, S.; Kraus, G. A.; Petrich, J. W. Photochem. Photobiol. 2002, 76, 153.

(46) Immitzer, B.; Etzlstorfer, C.; Obermuller, P. A.; Sonnleitner, M.; Schutz, G. J.; Falk, H. Monatsh. Chem. 2000, 131, 1039.

(47) Dumas, S.; Eloy, D.; Jardon, P. New J. Chem. 2000, 24, 711.

(48) Dumas, S. Thesis. 2000, Universite Joseph Fourier--Grenoble 1.

(49) Darmanyan, A. P.; Jenks, W. S.; Eloy, D.; Jardon, P. J. Phys. Chem. B 1999, 103, 3323.

(50) Murov, S. L.; Carmichael, I.; Hug, G. L. Handbook of Photochemistry, 2nd Ed.; Marcel Dekker, Inc.: New York, 1993.

CHAPTER IV. MARISTENTORIN, A NOVEL PIGMENT FROM THE POSITIVELY PHOTOTACTIC MARINE CILIATE Maristentor dinoferus, IS STRUCTURALLY RELATED TO HYPERICIN AND STENTORIN

A paper published in the Journal of Physical Chemistry B

Prasun Mukherjee[1], D. Bruce Fulton[2], Mintu Halder[1], Xinxin Han[1], Daniel W. Armstrong[1], Jacob W. Petrich[1,*], and Christopher S. Lobban[3,*]

Abstract

The photoreceptor pigment of the heterotrich ciliate, Maristentor dinoferus, has been characterized. It is structurally similar to those of Stentor coeruleus and Blepharisma japonicum but differs significantly in that it bears no aromatic hydrogens. The structure of the pigment, maristentorin, is based upon the hypericin skeleton, and its spectra are nearly identical to those of hypericin but shifted toward the red. Within experimental error, its fluorescence lifetime is identical to that of hypericin, ~ 5.5 ns in dimethylsulfoxide. It is remarkable that while the pigments are structurally similar in S. coeruleus and M. dinoferus, in the former there is an abrupt photophobic response, whereas in the latter there is a slow

---

[1] Department of Chemistry, Iowa State University, Ames, Iowa 50011.
[2] Department of Biochemistry, Biophysics, and Molecular Biology, Iowa State University, Ames, Iowa 50011.
[3] Division of Natural Sciences, University of Guam, UOG Station, Mangilao, Guam 96923.
[*] Author to whom correspondence should be addressed.

response toward light. The roles of the hypericin-like pigments in the heterotrich ciliates are discussed as potentially analogous in Maristentor.

Introduction

Several protozoa in a group of heterotrich ciliate families known collectively as stentorids have photoreceptor pigments that are not related to either rhodopsins (in animals) or to any of the photoreceptive pigments in photosynthetic eukaryotes [1-4]. Rather, they are structurally related to the hypericin group of naphthodianthrone quinone pigments. Hypericin is both toxic and medicinal, causing hypericism in animals and serving a variety of human needs including cancer and depression therapies. Hypericin occurs in the flowers of phylogenetically advanced species of Hypericum, including St. John's Wort (H. perforatum) [3,5]. Hypericum spp. apparently do not use hypericin as a photoreceptor, but both hypericin and the stentorid pigments are toxic to potential predators or pathogens in their respective environments, in part through increasing photosensitivity [3,6].

Structures have been determined for pigments from only two heterotrichs to date. Stentor coeruleus contains stentorin, which is very similar to hypericin [7], while Blepharisma japonicum is colored by several blepharismins and oxyblepharismins, which have the ring structure modified by a "carbon bridge," [2,8-10] (Figure IV.1). The ciliate pigments occur in cortical granules just below the cell membrane. The pigments in S. coeruleus and B. japonicum are involved in the organisms' abrupt photophobic responses [1,2,11,12]. They are also involved in defense reactions, in which a cloud of pigment is released from a patch of cortical granules to deter raptorial ciliate predators [13-15]. Other heterotrichs are known to have spectrally similar pigments but the structures have not been determined. Some other

Stentor spp. have both pigment and symbiotic green algae (zoochlorellae) and are positively phototactic, but neither their photobiology nor their pigment structure has been studied.

A recently discovered marine ciliate, Maristentor dinoferus [16,17], is prominently pigmented and also contains some 600 endosymbiotic golden algal cells (zooxanthellae) (Figure IV.2). It resembles Stentor but was placed in its own family within the stentorid group [18]. It is positively phototactic. Initial observations on the Maristentor pigment [16,17] showed that the pigment is fluorescent and has a UV-visible absorption spectrum similar to stentorin and hypericin. Here we report the structure of the chromophore and spectral properties of the pigment. Maristentorin is interesting both as a novel analog of hypericin and as a new member of the multifunctional pigments from stentorids.

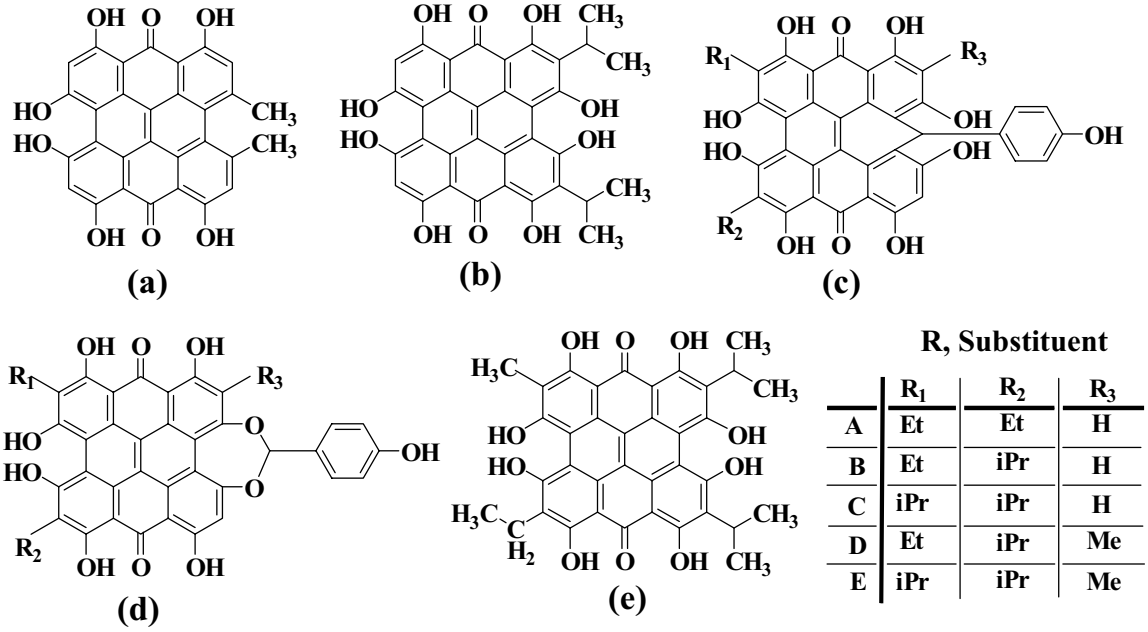

	R_1	R_2	R_3
A	Et	Et	H
B	Et	iPr	H
C	iPr	iPr	H
D	Et	iPr	Me
E	iPr	iPr	Me

Figure IV.1. Structures of (a) hypericin, (b) stentorin, (c) blepharismins, (d) oxyblepharismins, and (e) a plausible form for maristentorin.

Figure IV.2. Portrait of Maristentor. The pigment is concentrated around the nucleus, just below the cap.

Materials and Methods

Materials. The solvents from Aldrich were used (freshly opened) without further purification. Silica gel was purchased from Sorbent Technologies, Atlanta, GA having porosity 60 Å and particle size 32 – 63 μm (230 – 450 Mesh).

Bulk Harvest of Maristentor. Seaweed (Padina) bearing dense populations of the ciliate was collected in gallon bags at a site in Apra Harbor, Guam, 3-5 m below low water [16,17]. During transport to the laboratory, many ciliate cells left the seaweed surface and were swimming; these were decanted into glass dishes. The seaweed and remaining ciliates were transferred to glass dishes with the minimum exposure to air. Dishes were kept at ambient temperatures (28-30 °C) and light (indirect daylight). Under these conditions the ciliates gather on the lighted side of the dish just below the surface, and settle on the glass. When the water is poured out the other side of the dish, the ciliates remain stuck to the glass. Excess water and detritus were wiped from the bottom of the dish. The ciliate cells were then rinsed from the glass with 75% ethanol. Extracts, including cell debris, were shipped chilled to Ames, Iowa for analysis. The solution containing cells in 75% ethanol was centrifuged (7500 rpm for 20 minutes). The residue was resuspended in acetone to extract the pigment. This process was repeated five times. Solid compound recovered after acetone extraction was used to perform the silica gel column chromatography.

Chromatography. The compound obtained after acetone extraction was purified by silica gel column chromatography using a varying composition of mobile phase from 5:1 to 3:1 methylene chloride to methanol.

Steady-State and Time-Resolved Measurements. Steady state excitation and emission spectra were obtained on a Spex Fluoromax with a 4-nm bandpass and corrected for lamp

spectral intensity and detector response. In all fluorescence measurements, a 1-cm path-length quartz cuvette was used. The apparatus for time correlated single photon counting is described elsewhere [19]. Fluorescence decay kinetics were recorded by exciting the sample at 407 nm and collecting emission at > 500 nm with a cut-off filter. A maximum of 10,000 counts was collected at the peak channel.

Mass Spectroscopy. Electrospray mass spectra were obtained using the single quadrupole Shimadzu LCMS-2010 mass spectrometer (Shimadzu Corp. Kyoto, Japan). The mass range was from 50 to 1000 Daltons. 5 μL loop injection was performed for all experiments. The mass spectrometer was operated in the negative ion mode after proper tuning with known standards. The sample was dissolved in acetone.

NMR Spectroscopy. NMR spectra were collected on a Bruker Avance DRX 500 spectrometer equipped with a 5 mm $^{1}H/^{13}C/^{15}N$ gradient probe and operating at ^{1}H frequency of 499.867 MHz. Samples of maristentorin for NMR were dissolved in acetone-d_6. Chemical shifts were internally referenced to the methyl frequency of tetramethylsilane (TMS). All spectra were recorded at 298 K. One dimensional ^{1}H (8 scans, sweep width 9000 Hz) and ^{1}H-decoupled ^{13}C spectra (1024 scans, sweep width 24000 Hz) were acquired using standard experimental protocols. Two dimensional double quantum filtered correlation spectroscopy (DQF-COSY) [20], $^{1}H–^{13}C$ heteronuclear single quantum coherence (HSQC) spectroscopy [21], and $^{1}H–^{13}C$ heteronuclear multiple bond correlation spectroscopy (HMBC) [22] spectra were acquired. Pulse sequences utilizing PFG coherence selection were used for all three two dimensional experiments. The DQF-COSY spectra consisted of 2048 x 256 complex points with ^{1}H sweep width of 9000 Hz and 16 scans per free induction decay (FID). The HSQC and HMBC consisted of 1024 x 128 complex points with ^{1}H sweep width of 4006 Hz and ^{13}C

sweep width of 18855 Hz over identical spectral windows for each experiment. Exactly 32 and 160 scans per FID were used for the HSQC and HMBC spectra, respectively. A transfer delay of 60 ms corresponding to a long range coupling constant of 8.3 Hz was used in the HMBC experiment. All NMR spectra were processed and analyzed using Broker Xwinnr 2.6 software.

Results

Two major pigments were separated chromatographically from the ethanol extract of ciliate cells. One has characteristic hypericin-like emission and excitation spectra (Figure IV.3), the other porphyrin-like spectra (Figure IV.4). The former, the maristentorin, has a single-exponential fluorescence lifetime in DMSO of 5.5 ± 0.2 ns (Figure IV.5), which is within experimental error identical to that of hypericin. The latter pigment is most likely a chlorophyll from the symbiotic green algae, the ~600 zooxanthellae in each ciliate.

When the maristentorin was subjected to analysis by electrospray mass spectrometry in the negative ion mode, it yielded a major peak at 619 m/z (Figure IV.6), corresponding to a molar mass of 620. This molecular mass differs from the structure proposed in Figure IV.1e by one methylene group. The presence of the methyl group was indicated by subsequent NMR measurements, and we reconcile the discrepancy by suggesting that a methylene group is lost during the ionization process.

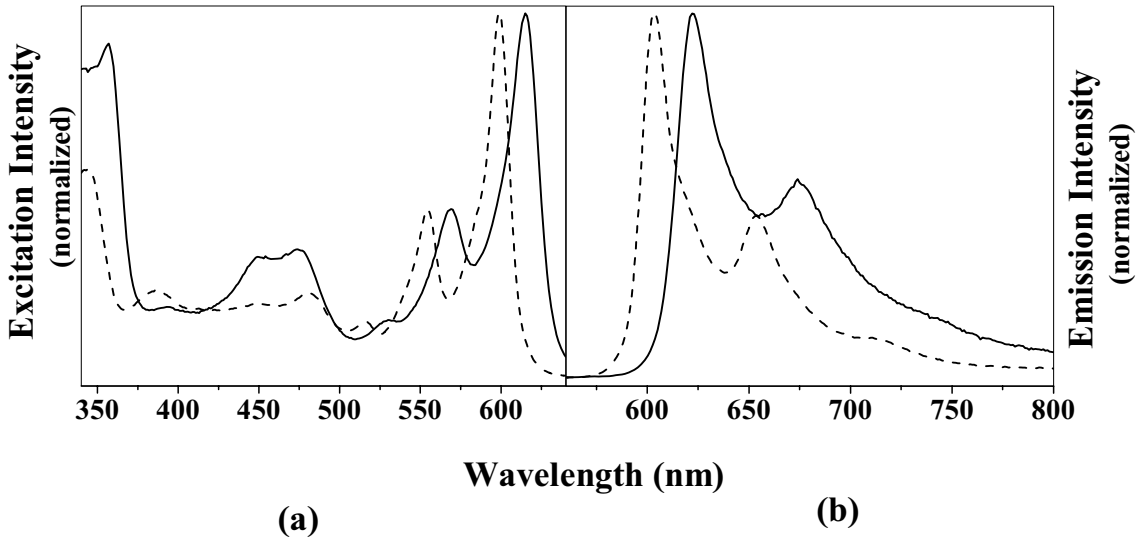

Figure IV.3. Normalized steady state (a) excitation and (b) emission spectra of maristentorin (solid line) and hypericin (dashed line) in DMSO. The excitation wavelength for the emission spectra is 550 nm. For the excitation spectra, the emission monochromator is set to 650 nm.

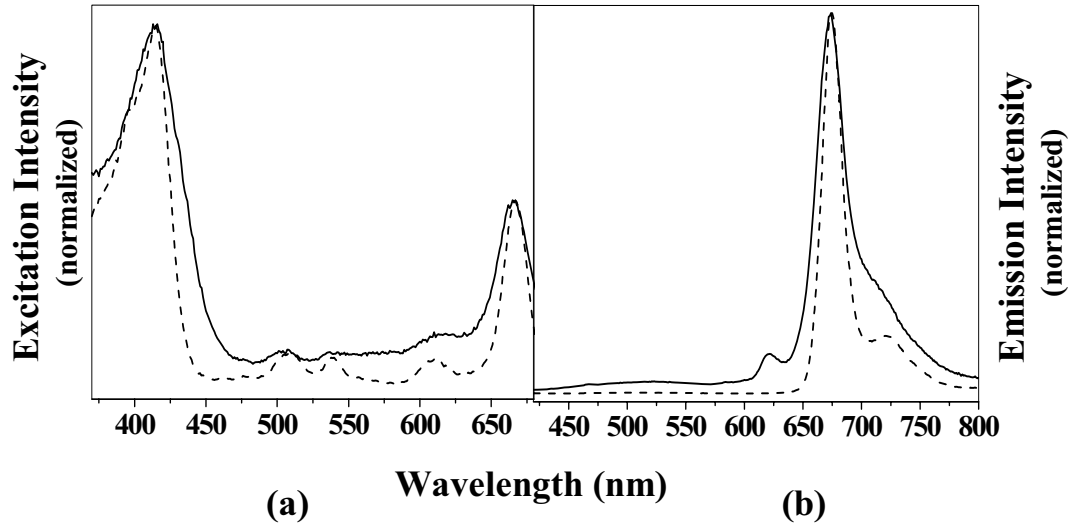

Figure IV.4. Normalized steady state excitation and emission spectra of a porphyrin-like pigment obtained from Maristentor in DMSO (solid line). For purposes of comparison, the spectra of pyropheophorbide dissolved in DMSO (dashed line) are presented. The spectra are normalized to the reddest absorption maximum. For the emission spectra, the sample is excited at 410 nm and for the excitation spectra, the emission monochromator is set to 700 nm.

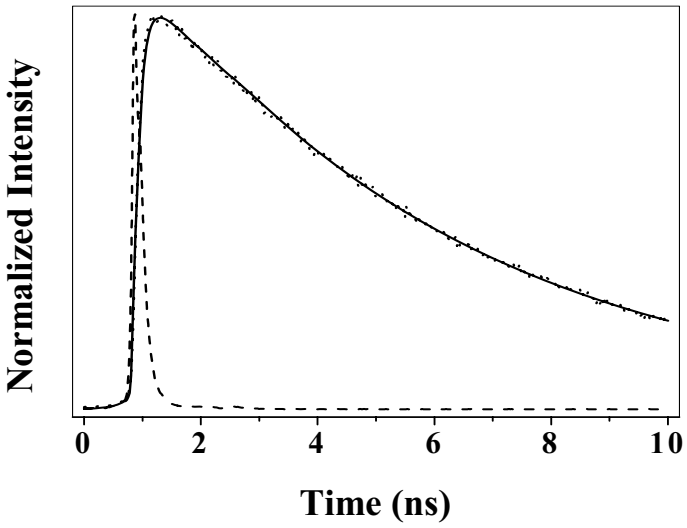

Figure IV.5. Fluorescence decay of maristentorin in DMSO. The sample is excited at 407 nm and emission is collected at wavelengths greater than 500 nm with a cut-off filter. The decay is well described by a single exponential with $\tau_F = 5.5 \pm 0.2$ ns (based on the average of four measurements). For comparison, fluorescence lifetime of hypericin in DMSO was found to be 5.6 ± 0.2 ns [23].

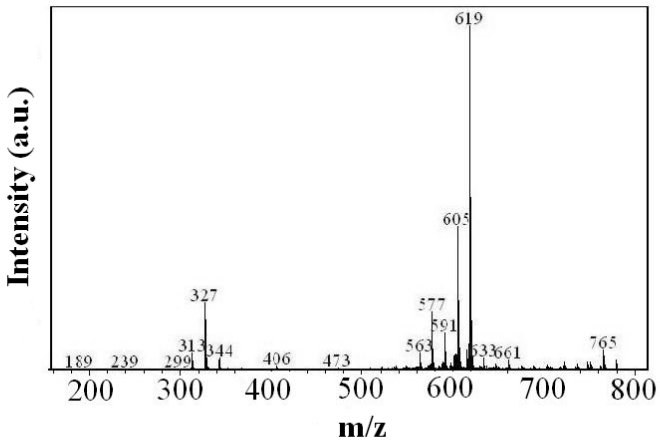

Figure IV.6. Electrospray mass spectra of maristentor in the negative ion mode. The sample is dissolved in acetone. The dominant peak in the spectrum is at 619 m/z. This corresponds to a molecular mass that is one methylene group less than the suggested structure in Figure IV.1e. We believe that a methylene group is lost during the ionization process. The presence of the methyl group is borne out by the NMR spectra in Figure IV.10.

NMR spectroscopy provided the key in determining the maristentorin structure. Figure IV.7 presents a one-dimensional ^{1}H NMR spectrum of maristentorin in acetone-d_6 acquired on a Bruker Avance DRX 500 NMR spectrometer. The lines at 15.6 and 15.4 ppm are due to the presence of the peri hydroxyl groups as were observed for all related pigments, namely hypericin, stentorin and blepharismin (Table IV.1). The spectrum also shows similar splitting for isopropyl groups as was found in stentorin [7] and blepharismin [8]. The major difference in the maristentorin spectrum is the appearance of a singlet at 2.4 ppm (comparable to hypericin) [24], a triplet at 1.3 ppm, and a quartet at 3.1 ppm. We assign these peaks to methyl and an ethyl groups, respectively. Most importantly, the absence of signal at ~ 7 ppm clearly indicates the absence of any aromatic protons in maristentorin and is not consistent with the 619 m/z mentioned above. There are two lines due to aromatic hydrogens in hypericin (indicative of four aromatic protons), whereas only one is present in stentorin and blepharismin (indicative of two aromatic protons). The doublet due to aromatic hydrogens in blepharismin are from the extra phenyl ring, which is attached to the seven-membered ring. ^{1}H chemical shift values for all four pigments discussed here are tabulated in Table IV.1.

Figure IV.8 presents a one-dimensional ^{13}C NMR spectrum of maristentorin in acetone-d_6. The spectrum shows the presence of five alkyl carbons (δ = 10 – 30 ppm), nine aromatic carbons (δ = 100 – 140 ppm), and five carbonyl carbons (δ = 160 – 200 ppm). The smaller and larger peaks correspond to one and two carbons, respectively, in the region δ = 100 – 140 ppm. We have seen half the number of carbon peaks for aromatic and carbonyl carbons in maristentorin because of the structural symmetry. The total numbers of aromatic

and carbonyl carbons in maristentorin are 18 and 10, respectively. The hydroxyl groups tend to have carbonyl characteristics, suggesting tautomeric forms.

Figure IV.9 presents the two-dimensional COSY spectrum of maristentorin in acetone-d_6. The peak at 1.5 ppm is correlated with the peak at 4.2 ppm, whereas the peak at 1.3 ppm is in correlation with the peak at 3.1 ppm; these data confirm the presence of isopropyl and ethyl groups in maristentorin.

Finally, Figure IV.10 presents two-dimensional HSQC (panels a and c) and HMBC (panels b and d) spectra of maristentorin in acetone-d_6. The same contour levels are used to generate the spectra in panels a and c. Panel a shows the correlation of ^{1}H NMR peaks with ^{13}C alkyl peaks. In the HSQC experiment, there is no correlation between ^{1}H peaks with aromatic carbons, as shown in panel c. Panels b and d show the multiple bond correlation between ^{1}H and ^{13}C alkyl signals. All peaks from alkyl groups in the ^{1}H spectrum are correlated with aromatic carbons. The most compelling evidence for the existence of a methyl group in the structure is the strong correlation between the ^{1}H peak at 2.4 ppm and the ^{13}C peak at ~ 113.5 ppm.

Discussion

Structure.

Upon the basis of the data presented above and upon analogy with stentorin [7,25,26] (Figure IV.1b), we propose the structure for maristentorin given in Figure IV.1e where the isopropyl groups are cis to the axis containing the carbonyl groups. We cannot, however, exclude the possibility of the trans isomer. The possibility of the isopropyl groups being on the same anthracene ring is virtually eliminated by consideration of biosynthetic pathways,

since hypericin is produced in vivo through the polyketide pathway, [27] and this is presumably the pathway in the stentorids.

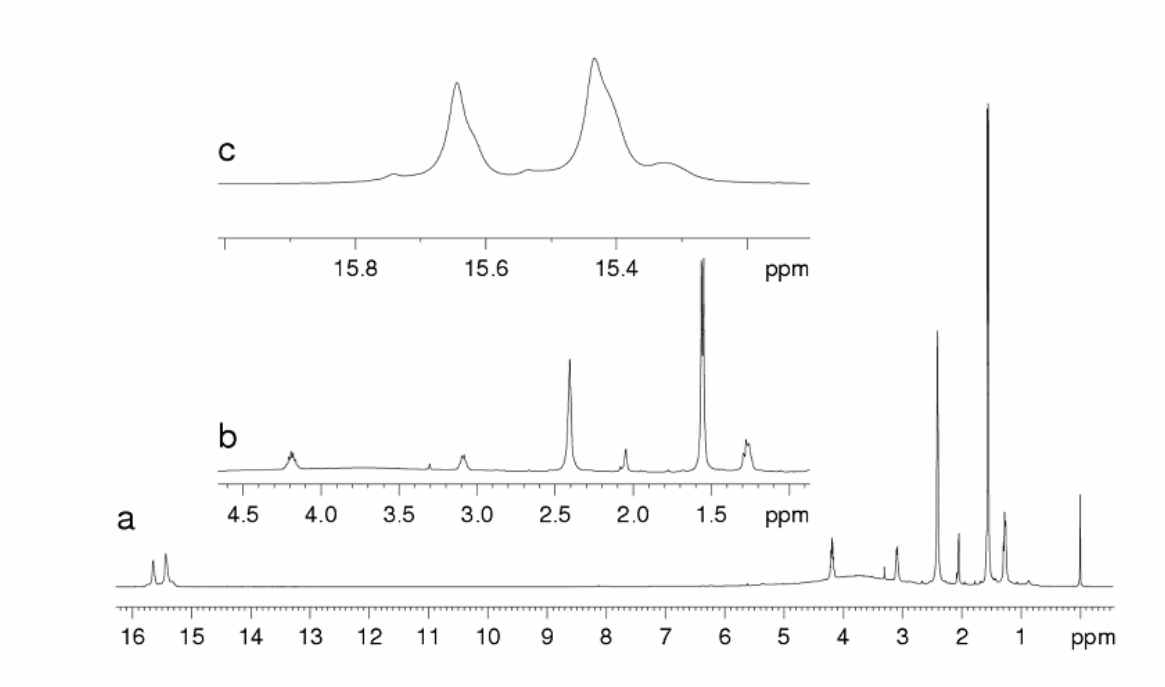

Figure IV.7. One-dimensional ^{1}H NMR spectrum of maristentorin in acetone-d_6 acquired on a Bruker Avance DRX 500 NMR spectrometer. Chemical shifts are internally referenced to the methyl frequency of TMS.

Phylogenetic Considerations.

There are two isopropyl groups in stentorin and the most common forms of blepharismin and oxyblepharismin, and three alkyl groups in maristentorin. Blepharismin and oxyblepharismin have several derivatives with different substitutions; all have a p-hydroxybenzylidene "carbon bridge." The less common forms have ethyl and/or methyl in addition to or instead of isopropyl, but there are never more than three substituents [2] (Figure IV.1).

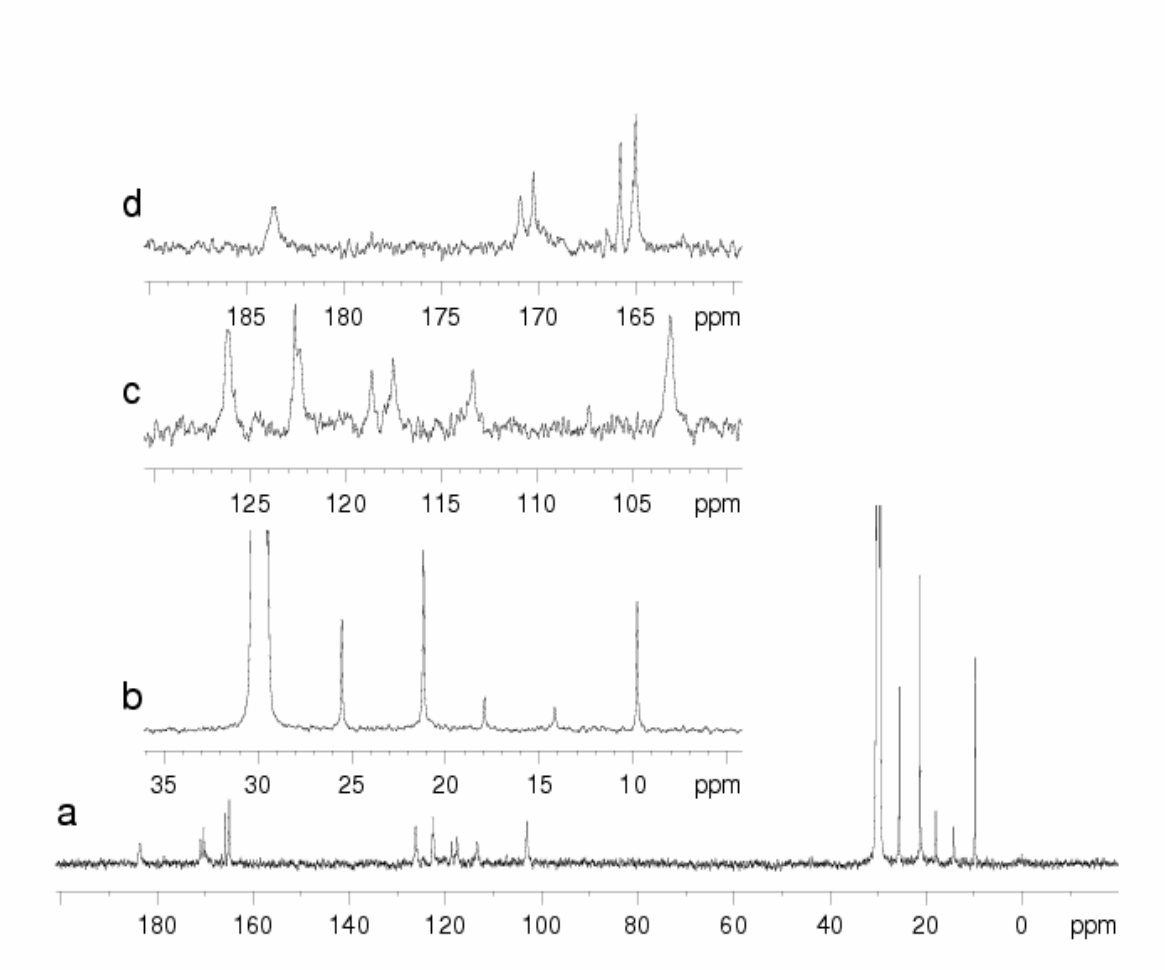

Figure IV.8. One-dimensional ^{13}C NMR spectrum of maristentorin in acetone-d_6. Chemical shifts are referenced to the solvent peak (at ~ 30 ppm).

We now have several similar, presumably homologous molecules from heterotrich ciliates (stentorin, blepharismin/oxyblepharismin and their derivatives, and maristentorin). The phylogeny of the heterotrichs is understood from only a few species [18], and additional members of the stentorin group can be expected. Besides the stentorids mentioned so far, other stentorids such as some Folliculinidae have bluish pigments, some of which appear spectrally similar to stentorin. While S. coeruleus has stentorin, other species of Stentor have cortical pigments of other colors, and the structures of these have not yet been determined.

Still other Stentor species have colorless cortical granules; these may contain unrelated compounds, such as the resorcinolic toxin climacostol in Climacostomum virens [28] that, like stentorin and blepharismin, acts as a predator deterrent. Pigments with hypericin/stentorin-like action spectra have been reported in two non-stentorid ciliates, the heterotrich Fabrea salina (Climacostomidae) and the hymenostome Ophryoglena flava (Ophryoglenidae) "although rhodopsin-like photoreceptors have also been suggested" for the photomovement of these ciliates [2,29]. It will be important in the context of phylogeny to establish whether these pigments in unrelated ciliates are hypericin analogues or not, as well as whether other species of Stentor have stentorin-like pigments or not.

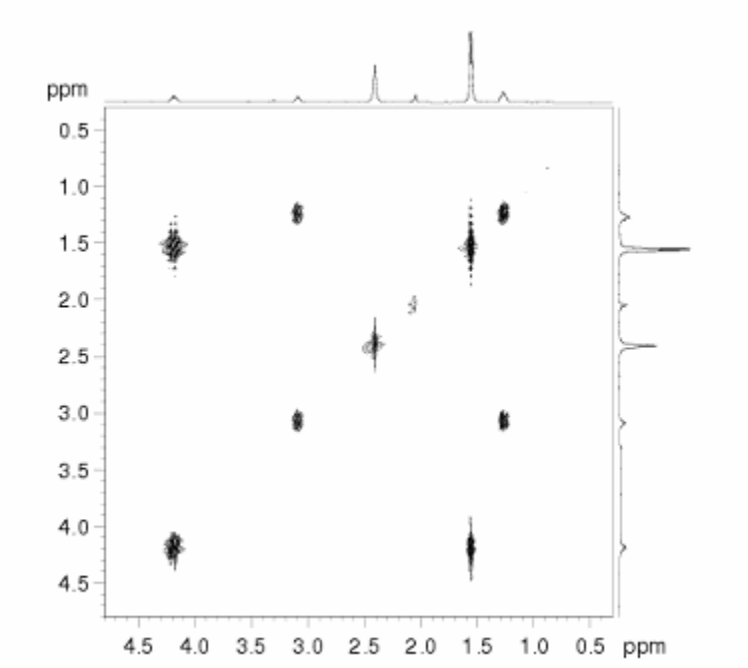

Figure IV.9. Two-dimensional COSY spectrum of maristentorin in acetone-d_6. The peak at 1.5 ppm is correlated with the peak at 4.2 ppm, whereas the peak at 1.3 ppm correlates with the peak at 3.1 ppm; these data confirm the presence of isopropyl and ethyl groups in maristentorin.

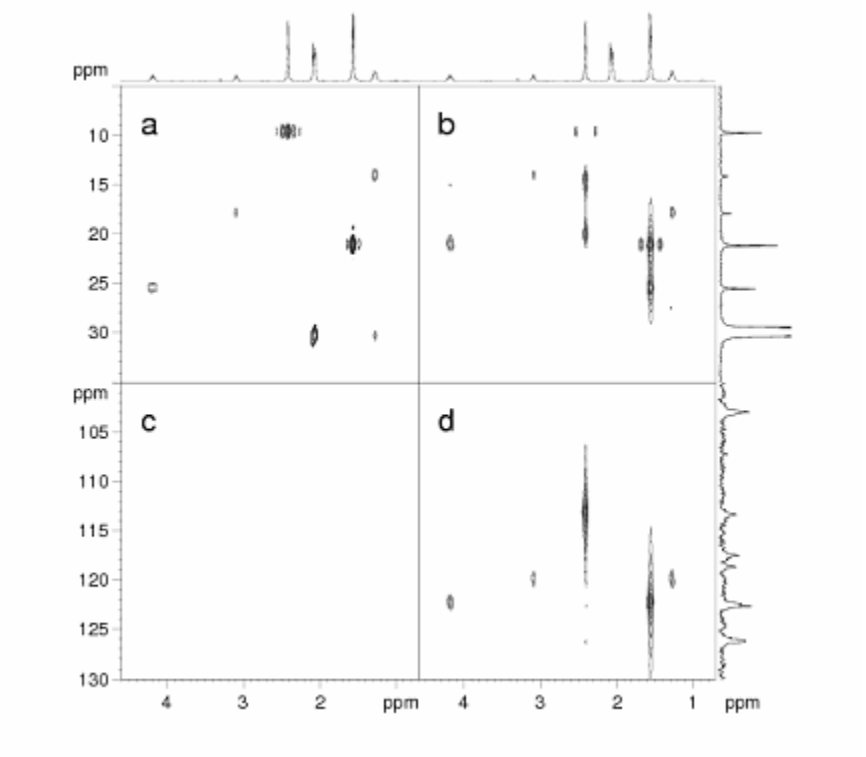

Figure IV.10. Two-dimensional (a, c) HSQC and (b, d) HMBC spectra of maristentorin in acetone-d_6. The same contour levels are used to generate the spectra in panels a and c.

Possible Roles of Maristentorin

Maristentor has a large amount of pigment, and it must serve one or several roles. No role has yet been established, but the chemical similarity of maristentorin to stentorin and blepharismin suggests potentially similar biological functions, including light perception and defense against predators or UV irradiation. However, there are differences between Maristentor and Stentor that may provide illuminating comparisons. Most importantly, while both pigments may be involved in light detection, the results are quite different. Whereas S. coeruleus avoids light—in some strains very abruptly changing direction when encountering a light spot [2,30]— Maristentor, with its cargo of algal symbionts, moves toward

light and does not change direction abruptly. Some Stentor (but not S. coeruleus) also have algal symbionts (zoochlorellae), and are positively phototactic. Some of these species

Table IV.1. ^{1}H Chemical Shift Values (δ, ppm) for Hypericin [24], Stentorin [7], Blepharismin [8] and Maristentorin in Different Solvents[a]

Compound	Hypericin/ acetone-d_6	Hypericin/ DMSO-d_6	Stentorin/ DMSO-d_6	Blepharismin/ acetone-d_6	Maristentorin/ acetone-d_6
phenolic OH	14.82	14.74	15.3	14.8	15.6
	14.27	14.09	14.7	14.11	15.4
				9.72	
aromatic H	7.35 (s)	7.46 (s)	6.9 (s)	6.81 (s)	
	6.62 (s)	6.59 (s)		6.11 (d)	
				6.06 (d)	
non-aromatic H				7.07 (s)	
methylene					3.1 (q)
methyne			4.0 (septet)	3.89 (m)	4.2 (septet)
methyl	2.78 (s)	2.75 (s)	1.5 (d)	1.44 (d)	1.5 (d)
				1.41 (d)	1.3 (t)
					2.4 (s)

[a] The letters in the parentheses are the multiplicity of the signal.

(e.g., S. amethystinus, S. fuliginosus) have cortical pigments, but others (e.g., S. polymorphus) have colorless cortical granules [31]. S. amethystinus and S. araucanus would be particularly interesting for comparison with Maristentor, since their pigment colors are similar and they have zoochlorellae.

There are no known ciliate predators of Maristentor comparable to those that attack Stentor and Blepharisma in freshwaters (but the ciliate fauna of the reefs is barely known); however, fish predation of seaweeds on the reefs is significant. Maristentor occurs on various seaweeds and on rocks, and its clustering behavior should make it visible to foraging fish. If maristentorin is toxic or distasteful to fish, it could serve as a feeding deterrent, in which case its role in making the cells macroscopically visible could act as warning coloration.

The UV absorbption of blepharismin led Giese [32] to propose that it serves a protective role in Blepharisma, which is very light sensitive, and such a function could be useful to Maristentor, at least for shallow-water populations. Maristentor can redistribute its pigment: during the day specimens in bright light concentrate it around the macronucleus, and away from the zooxanthellae [16,17]. Maristentor's ability to move both pigment granules and algal symbionts within the host cell appears to be unique among the stentorids and provides the association more options than simply moving in response to environmental conditions.

Finally, an additional role for maristentorin is suggested by the work of Schlichter et al. [33] on deep-water corals, in which fluorescent pigment in the coral cells below the zooxanthellae enhanced photosynthesis of the algae. The fluorescence peak for maristentorin is close to the red absorbance of chlorophyll, and it is possible that it may serve as means of trapping and transferring light energy. None of these possible functions have yet been tested but remain for interesting future work on the biological side.

Conclusions

The photoreceptor pigment of the heterotrich ciliate, Maristentor, has been characterized. It is structurally similar to those of Stentor and Blepharisma but differs significantly in that it bears no aromatic hydrogens. The structure of the pigment, maristentorin, is based upon the hypericin skeleton, and its spectra are nearly identical to those of hypericin but shifted towards the red. Within experimental error, its fluorescence lifetime is identical to that of hypericin, ~ 5.5 ns in DMSO. It is remarkable that while the pigments are structurally similar in Stentor and Maristentor, in the former they give rise to an abrupt photophobic response; and in the latter, to a nonabrupt photophilic response. Clearly the immediate environment of the chromophore, for example the protein to which it is attached, modulates its photoinduced properties. Such a modulation of physical properties was seen for hypericin itself in complex with the glutathione S-transferase isoforms A1-1 and P1-1 [34,35]. Hypericin in complex with the former gives rise to significant oxidative damage; while in complex with the latter, almost none. It will be interesting to study the photophysical properties of the pigments in the heterotrich ciliates in complex with their respective proteins.

Acknowledgements

The authors thank Professor P.-S. Song for his interest in the project. P. M. thanks S. Giri for technical assistance. Professor M. S. Hargrove gave us access to his centrifuge and K. Harrata performed the mass spectroscopic experiments. C.L. thanks M. Schefter for assistance with the field collections, C. Kohlert-Schupp for preliminary HPLC data, and NIGMS RISE grant GM 63682 for support of professional development.

References

(1) Song, P.-S. J. Photosci. 1999, 6, 37.

(2) Song, P.-S. Hypericin-like photoreceptors. In Handbook of Photosensory Receptors; Spudich, J. L., Briggs, W. R., Eds.; Wiley VCH: Weinheim 2005.

(3) Falk, H. Angew. Chem., Int. Ed. 1999, 38, 3117.

(4) Sgarbossa, A.; Checcucci, G.; Lenci, F. Photochem. Photobiol. Sci. 2002, 1, 459.

(5) Piovan, A.; Filippini, R.; Caniato, R.; Borsarini, A.; Bini Maleci, L.; Cappelletti, E. M. Phytochemistry 2004, 65, 411.

(6) Maron, J. L.; Vila, M.; Arnason, J. Ecology 2004, 85, 3243.

(7) Tao, N.; Orlando, M.; Hyon, J. S.; Gross, M.; Song, P.-S. J. Am. Chem. Soc. 1993, 115, 2526.

(8) Checcucci, G.; Shoemaker, R. S.; Bini, E.; Cerny, R.; Tao, N.; Hyon, J. S.; Gioffre, D.; Ghetti, F.; Lenci, F.; Song, P. S. J. Am. Chem. Soc. 1997, 119, 5762.

(9) Plaza, P.; Mahet, M.; Martin, M. M.; Angelini, N.; Malatesta, M.; Checcucci, G.; Lenci, F. Photochem. Photobiol. Sci. 2005, 4, 754.

(10) Spitzner, D.; Höfle, G.; Klein, I.; Pohlan, S.; Ammermann, D.; Jaenicke, L. Tetrahedon Lett. 1998, 39, 4003.

(11) Song, P.-S. Biochim. Biophys. Acta 1981, 639, 1.

(12) Fabczak, H. Acta Protozool. 2000, 39, 171.

(13) Miyake, A.; Harumoto, T.; Salvi, B.; Rivola, V. Eur. J. Protistol. 1990, 25, 310.

(14) Miyake, A.; Harumoto, T.; Iio, H. Eur. J. Protistol. 2001, 37, 77.

(15) Harumoto, T.; Miyake, A.; Ishikawa, N.; Sugibayashi, R.; Zenfuku, K.; Iio, H. Eur. J. Protistol. 1998, 34, 458.

(16) Lobban, C. S.; Schefter, M.; Simpson, A. G. B.; Pochon, X.; Pawlowski, J.; Foissner, W. Mar. Biol. 2002, 140, 411.

(17) Lobban, C. S.; Schefter, M.; Simpson, A. G. B.; Pochon, X.; Pawlowski, J.; Foissner, W. Mar. Biol. 2002, 141, 207.

(18) Miao, W.; Simpson, A. G. B.; Fu, C.; Lobban, C. S. J. Eukaryotic Microbiol. 2005, 54, 11.

(19) Chowdhury, P. K.; Halder, M.; Sanders, L.; Calhoun, T.; Anderson, J. L.; Armstrong, D. W.; Song, X.; Petrich, J. W. J. Phys. Chem. B 2004, 108, 10245.

(20) Shaw, A. A.; Salaun, C.; Dauphin, J.-F.; Ancian, B. J. Magn. Reson., Ser. A 1996, 120, 110.

(21) Kontaxis, G.; Stonehouse, J.; Laue, E. D.; Keeler, J. J. Magn. Reson., Ser. A 1994, 111, 70.

(22) Ruiz-Cabello, J.; Vuister, G. W.; Moonen, C. T. W.; van Gelderen, P.; Cohen, J. S.; van Zijl, P. C. M. J. Magn. Reson. 1992, 100, 282.

(23) Wen, J.; Chowdhury, P.; Wills, N. J.; Wannemuehler, Y.; Park, J.; Kesavan, S.; Carpenter, S.; Kraus, G. A.; Petrich, J. W. Photochem. Photobiol. 2002, 76, 153.

(24) Smirnov, A.; Fulton, D. B.; Andreotti, A.; Petrich, J. W. J. Am. Chem. Soc. 1999, 121, 7979.

(25) Cameron, D. W.; Riches, A. G. Tetrahedron Lett. 1995, 36, 2331.

(26) Cameron, D. W.; Riches, A. G. Aust. J. Chem. 1997, 50, 409.

(27) Thomson, R. H. Naturally occurring quinones.; Academic Press: London, 1957.

(28) Masaki, M. E.; Hiro, S.; Usuki, Y.; Harumoto, T.; Terazima, M. N.; Buonanno, F.; Miyake, A.; Iio, H. Tetrahedron 2004, 60, 7041.

(29) Marangoni, R.; Lucia, S.; Colombetti, G. Photomovements in ciliates. In CRC Handbook of Organic Photochemistry and Photobiology.; Horspool, W., Lenci, F., Eds.; CRC Press: Boca Raton, FL, 2004; Vol. 122; p 1.

(30) Tartar, V. The Biology of Stentor; Pergamon Press: London, England, 1961.

(31) Foissner, W.; Wölfl, S. J. Plankton Res. 1994, 16, 255.

(32) Giese, A. C. Blepharisma: The Biology of a Light-Sensitive Protozoan; Stanford University Press: Palo Alto, CA, 1973.

(33) Schlichter, D.; Meier, U.; Fricke, H. W. Oecologia 1994, 99, 124.

(34) Lu, W. D.; Atkins, W. M. Biochemistry 2004, 43, 12761.

(35) Halder, M.; Chowdhury, P. K.; Das, R.; Mukherjee, P.; Atkins, W. M.; Petrich, J. W. J. Phys. Chem. B 2005, 109, 19484.

CHAPTER V. ASSESSING THE ROLES OF THE CONSTITUENTS OF IONIC LIQUIDS IN DYNAMIC SOLVATION: COMPARISON OF AN IONIC LIQUID IN MICELLAR AND BULK FORM

A paper published in the Journal of Physical Chemistry A

Prasun Mukherjee[1], Jeffrey A. Crank[2], Mintu Halder[1], Daniel W. Armstrong[2], and Jacob W. Petrich[1,*]

Abstract

Dynamic solvation of the dye, coumarin 153, is compared in an ionic liquid that forms micelles in water against the bulk solvent. This provides the unprecedented opportunity of investigating the behavior of the ionic liquid in two globally different configurations. It is proposed that the imidazolium moiety is in both cases responsible for the majority of the solvation, which manifests itself in the first 100 ps. Exploiting the use of ionic liquids capable of accommodating specific structures thus provides a deeper insight into how solutes interact with these fascinating and interesting solvents (at least those that are imidazolium based) that are gaining ever increasing interest in the scientific community.

---

[1] Department of Chemistry, Iowa State University, Ames, Iowa 50011.

[2] Department of Chemistry and Biochemistry, University of Texas, Arlington, Box 19065, Arlington, Texas 76019

[*] Author to whom correspondence should be addressed.

Introduction

Room temperature ionic liquids, most commonly comprised of organic cations and inorganic anions, are receiving an increasing amount of attention because of their utility as environmentally friendly, "green" solvents and because of a host of practical applications to which they are amenable [1-4]. The importance of ionic liquids has consequently stimulated considerable interest in their dynamic solvation properties, both in the experimental [5-25] and the theoretical arenas [26-32]. An intriguing aspect of certain ionic liquids, which has only recently become appreciated, is their ability to promote micelle formation or to form micelles themselves [33-36]. Major questions regarding dynamic solvation by ionic liquids deal with whether the organic cation or the inorganic anion solvate preferentially on different time scales, the role of the correlated motion of the ion pairs and their lifetime, and the importance of translational motion of the ions relative to dipolar relaxation [23-25]. Here, we attempt to address some of these questions by studying the solvation of the dye, coumarin 153, in a bulk ionic liquid and its corresponding micelle in water (Figure V.1). Because coumarin 153 is only sparingly soluble and weakly fluorescent in water, a clear distinction can be made between its fluorescent properties in the bulk ionic liquid and that in the micelles formed from the ionic liquid. Sarkar and coworkers [37] have compared the solvation dynamics of coumarin 153 in an ionic liquid with that of coumarin 153 in Brij-35 micelles in the same ionic liquid. This comparison suffers because coumarin 153 is soluble in both systems and only modest differences can be observed. Hara et al. have performed a detailed study of the effect of pressure on the solvation of coumarin 153 in micelles [38].

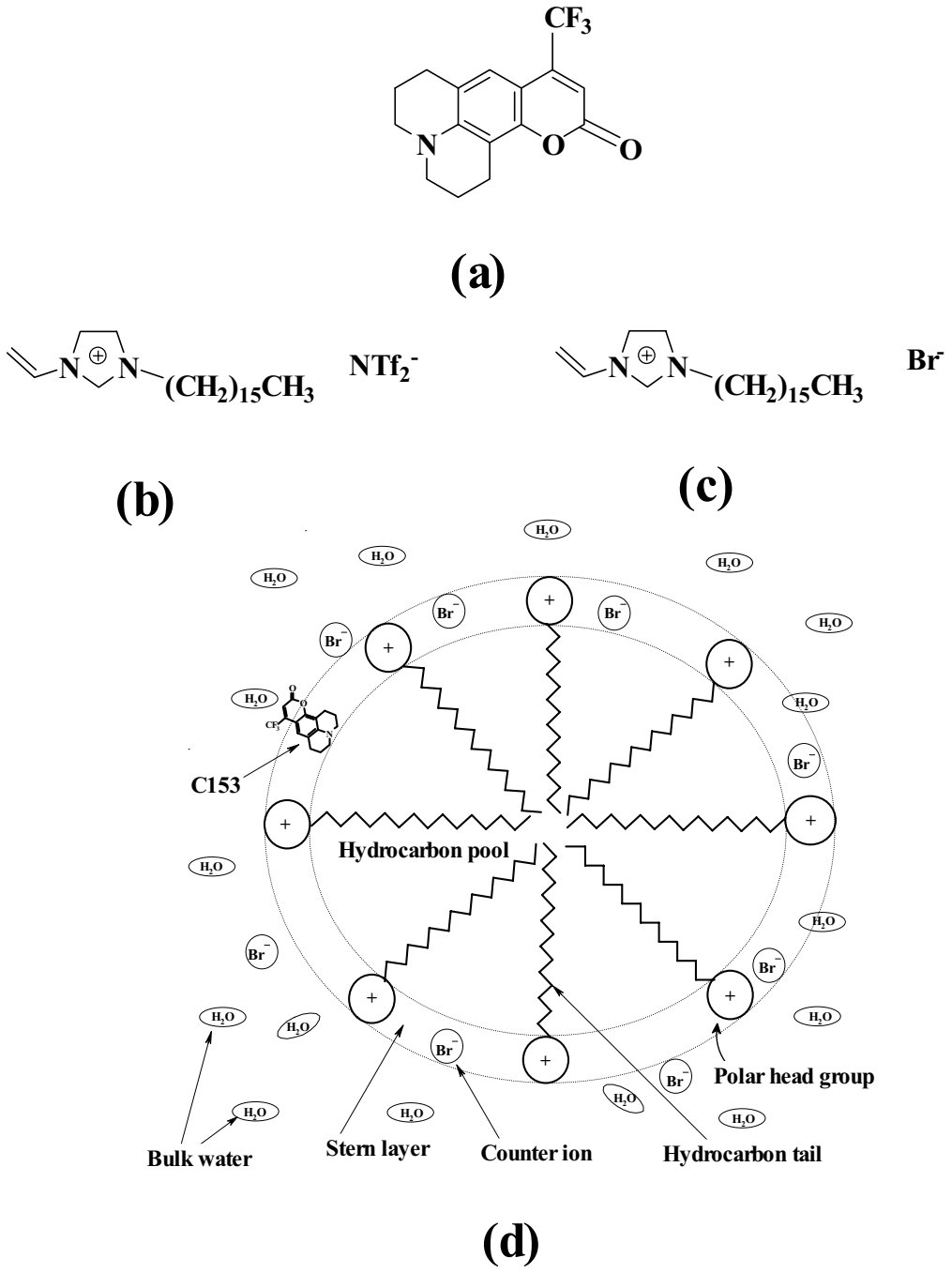

Figure V.1. Structures of the (a) solvation probe, coumarin 153 (C153), and the two ionic liquids, (b) 1-cetyl-3-vinylimidazolium NTf_2 ($[CVIM^+][NTf_2^-]$; NTf_2^- = $(CF_3SO_2)_2N^-$) (melting point: 39°C), and (c) 1-cetyl-3-vinylimidazolium bromide ($[CVIM^+][Br^-]$) (melting point: 69°C). The bromide salt forms micelles in water. Also provided is a schematic diagram (d) of the micelle formed by $[CVIM^+][Br^-]$ in water indicating the proposed location of C153 in the Stern layer.

Materials and Methods

Ionic Liquid Synthesis. 1-cetyl-3-vinylimidazolium bromide was synthesized by reacting 1 molar equivalent of 1-vinylimidazole and 1-bromohexadecane. The mixture was heated to 65°C and stirred for 4 hr. The bromide salt was then dissolved in water and heated to 50°C for hot extraction. Eight extractions were performed with ethyl acetate to remove impurities. The ionic liquid was then allowed to crystallize in the aqueous solution to purify the product further. The ionic liquid was then filtered and dried under vacuum. Anion exchange of 1-cetyl-3-vinylimidazolium bromide to 1-cetyl-3-vinylimidazolium bis[(trifluoromethyl)-sulfonyl]imide (NTf_2) was achieved by first dissolving the bromide salt in water. Next an equimolar amount of lithium bis[(trifluoromethyl)sulfonyl]imide was dissolved in water and added to the bromide salt solution and stirred until the aqueous layer became clear. The NTf_2 salt was then dissolved in methylene chloride and extracted with water eight times. A rotary evaporator was used to remove the excess methylene chloride. The NTf_2 salt was then placed under vacuum overnight to achieve complete dryness. Viscosity measurements for the solvents studied were taken with a ViscoLab 4000 piston-style viscometer from Cambridge Applied Systems.

CMC Determination. The critical micelle concentration (CMC) was found by plotting surface tension (dyn/cm) against concentration (mM). Surface tension measurements were taken using a Fischer Model 20 Surface Tensiometer. All glassware used was cleaned by chromic acid, rinsed with deionized water, and dried in an oven. Concentrations between 0 and 1×10^{-3} M of 1-cetyl-3-vinylimidazolium bromide were prepared in aqueous solution and heated to 39°C. Measurements were taken at 39°C to circumvent solubility problems that occur at room temperature. An average of 4 measurements was taken to obtain the

surface tension at each concentration of the ionic liquid. At 21° C, CMC = 2.6 x 10^{-5} M; at 39° C, CMC = 3.2 x 10^{-5} M.

Determination of the Micellar Aggregation Number. The aggregation number (the average number of surfactant molecules per micelle) can be estimated by optical techniques proposed by Turro and Yekta [39] and later modified by De Schryver and coworkers [40]. We employ the latter method, where the micellar aggregation number is obtained by exploiting the vibronic fine structure of pyrene emission. Pyrene was recrystallized several times from absolute ethanol before use. Three stock solutions were prepared of concentrations 0.2 × 10^{-3} , 10 × 10^{-3} , and 4 × 10^{-2} M pyrene in ethanol, cetyl pyridinium chloride in water, and [$CVIM^+$][Br^-] in water. For all measurements, pyrene and surfactant concentrations were kept constant at ~ 2 × 10^{-6} M and ~ 4 × 10^{-3} M. Six solutions were prepared with increasing quencher concentration from 0 to 0.5 × 10^{-3} M. Samples were excited at 337 nm for emission spectra. The aggregation number can be determined using equations V.1 and V.2

$$\ln\left(\frac{I_0}{I_Q}\right)=\frac{[Q_{mic}]}{[mic]} \qquad \text{(V.1)}$$

where I_0 is the emission intensity at a particular wavelength in the absence of added quencher and I_Q is the corresponding emission intensity in the presence of quencher and micelle concentrations of $[Q_{mic}]$ and [mic] respectively. The mean aggregation number, <a>, is given by

$$\langle a\rangle=\frac{[S_{tot}]-CMC}{[mic]} \qquad \text{(V.2)}$$

Cetyl pyridinium chloride can also form micelles, so in the present case the $[Q_{mic}]$ is not exactly equal to the total quencher concentration, $[Q_{tot}]$. The $[Q_{mic}]$ were calculated using

$$[Q_{mic}]=(1-\alpha)[Q_{tot}] \quad \text{(V.3)}$$

where,

$$\alpha=\frac{CMC}{[S_{tot}]} \quad \text{(V.4)}$$

A plot of $\ln\frac{I_0}{I_Q}$ against $[Q_{mic}]$ yields a straight line with a slope of 1/[mic] (equation V.1). Multiplying the slope with the difference between the total surfactant concentration and the critical micellar concentration (CMC) gives the mean aggregation number (equation V.2). Calculations can be performed using the intensity of either band I or band III. We have chosen the emission intensity of band I (at ~ 373 nm) or band III (at ~ 384 nm) for determining the aggregation number of the micelle. The results obtained from both bands were identical. The mean aggregation number of $[CVIM^+][Br^-]$ micelle at 39°C was found to be 25.

Preparation of Micellar Solutions. The critical micelle concentration (CMC) of $[CVIM^+][Br^-]$ in water was found to be 3.2×10^{-5} M at 39°C, see above. For all experiments in micellar systems, the C153 concentration was kept at ~ 8×10^{-6} M in ~ 4×10^{-3} M $[CVIM^+][Br^-]$ (~125 times CMC) and a 500:1 surfactant-to-C153 ratio was maintained. Under these conditions there is one C153 molecule for every 20 micelles, thus minimizing the possibility of association or contact between the C153 probes.

Preparation of Solutions for Stern-Volmer Quenching Experiments. For quenching of C153 in methanol, two stock solutions were prepared of concentrations 2×10^{-4} M C153 in methanol and 0.1 M potassium iodide in methanol. For all measurements, C153 concentrations were kept constant at ~ 2×10^{-6} M. Six solutions were prepared with

increasing quencher concentration from 0 to 0.4 M. Similar quenching experiments were performed in micellar environment by preparing three stock solutions of concentrations 2×10^{-4} M, 4×10^{-2} M and 0.1 M, of C153 in methanol, $[CVIM^+][Br^-]$ in water and potassium iodide in water. For all measurements, C153 and surfactant concentrations were kept constant at $\sim 2 \times 10^{-6}$ M and $\sim 4 \times 10^{-3}$ M. Six solutions were prepared with increasing quencher concentration from 0 to 2×10^{-2} M. Samples were excited at 420 nm for taking the emission spectra.

Steady-State Optical Measurements. Steady-state excitation and emission spectra were recorded with a SPEX Fluoromax with a 4-nm bandpass and were corrected for detector response. A 1-cm pathlength quartz cuvette was used for the measurements except for $[CVIM^+][Br^-]$ as a pure solvent. For this system, a 5-mm pathlength quartz cuvette was used. During spectroscopic measurements, the quartz cuvettes were kept tightly sealed so as to prevent moisture from being absorbed by the ionic liquids. The steady-state spectra can be used to compute the reorganization energy, λ [23,24]

$$\lambda = \hbar \frac{\int_0^\infty d\nu [\sigma_a(\nu) - \sigma_f(\nu)]\nu}{\int_0^\infty d\nu [\sigma_a(\nu) + \sigma_f(\nu)]} \qquad \text{(V.5)}$$

The $\sigma_{a,f}$ are the absorption (or excitation) and emission spectral line-shapes, respectively.

Time-Resolved Measurements. The apparatus for the time-correlated single-photon counting measurements is described in detail elsewhere [23,24]. The instrument response function had a full-width–at-half-maximum (FWHM) of $\leq$ 100 ps. A 1-cm pathlength quartz cuvette was used for all the time-resolved measurements except for $[CVIM^+][Br^-]$ as pure solvent. A 5-mm pathlength quartz cuvette was used for this solvent. To construct the time-

resolved spectra, a series of decays (~3,000 counts in the peak channel) were collected over as much of the fluorescence spectrum as possible, typically from 470 nm to 610 nm at 10 nm intervals. They were fit to a maximum of three exponentials. Transient spectra were reconstructed from these fits by normalizing to the steady state spectra:

$$S(\lambda,t) = D(\lambda,t)\frac{S_0(\lambda)}{\int_0^\infty D(\lambda,t)} \qquad \text{(V.6)}$$

$D(\lambda,t)$ is the wavelength-resolved fluorescence decay, and $S_0(\lambda)$ is the steady-state emission intensity at a given wavelength. We have employed the traditional approach of fitting the time-resolved spectra to a log-normal function, from which we extract the peak frequency, $\nu(t)$, as a function of time.

The solvation dynamics were described by the normalized correlation function:

$$C(t) = \frac{\nu(t) - \nu(\infty)}{\nu(\text{"t = 0"}) - \nu(\infty)} \qquad \text{(V.7)}$$

ν("t = 0") is the frequency at zero time [24,41]. $\nu(\infty)$ is the frequency at "infinite time," the maximum of the steady-state fluorescence spectrum. $\nu(t)$ is determined by taking the maxima from the lognormal fits as the emission maximum. In most of the cases, however, the spectra are broad, so there is some uncertainty in the exact position of the emission maxima. Thus, we have considered the range of the raw data points in the neighborhood of the maximum to estimate an error for the maximum obtained from the lognormal fit. Depending on the width of the spectrum (i.e. "zero-time", steady-state, or time-resolved emission spectrum), we have determined the typical uncertainties as follows: "zero-time" ~ steady-state (~ ± 100 cm^{-1}) < time-resolved emission (~ ± 200 cm^{-1}). We use these uncertainties to compute error bars for the C(t).

Finally, in generating the C(t), the first point was obtained from the "zero-time" spectrum. The second point was taken at the maximum of the instrument response function, which, having a full-width at half-maximum of ≤ 100 ps, was taken to be ~100 ps. Fractional solvation at 100 ps was calculated using f (t = 100 ps) = 1 − C (t = 100 ps).

Polarized fluorescence traces were collected in order to obtain anisotropy decay parameters. 10,000 counts were collected in the peak channel of the trace whose polarization was aligned parallel to that of the excitation pulse. We could not detect any polarized fluorescence from coumarin 153 dissolved in [$CVIM^+$][Br^-] (solvent). This might be due to scattering arising from the opaque, solid substance formed at 69°C.

Results

Steady-state spectra and representative wavelength-resolved decays are presented in Figures V.2 and V.3, respectively. Figure V.4 provides the solvation relaxation functions, C(t). Relevant spectroscopic and relaxation parameters are summarized in Tables V.1 and V.2. Examination of Figure V.4 and Table V.1 indicates the following.

1. Temperature does not significantly (within 10%) change the fractional solvation at 100 ps or the average solvation time for either bulk [$CVIM^+$][NTf_2^-] or for micellar [$CVIM^+$][Br^-].

2. The fractional solvation of bulk [$CVIM^+$][NTf_2^-] and micellar [$CVIM^+$][Br^-] are comparable: 0.70, 0.62; 0.77, 0.78 respectively. There is roughly 10% more unresolved solvation occurring in the micelle. It is unclear how much of this additional solvation occurs because of the difference in the anion or because of the difference between the bulk or micellar systems. In order to respond to this question, it is crucial to study bulk [$CVIM^+$][Br^-].

3. It is to be noted that of the systems considered here, only [$CVIM^+$][Br^-] forms micelles in water and that bulk [$CVIM^+$][Br^-] forms an opaque solid that is suitable for measurements of spectra and lifetimes, but scatters light to such a degree that it is not suitable for obtaining measurements of polarized fluorescence. Nonetheless, it is striking that in the solid bulk, [$CVIM^+$][Br^-] still has f_{100ps} as great as 0.50. For example, Maroncelli and coworkers, using an instrument response of 25 ps, found that for the imidazolium ionic liquid, [$DMPIM^+$][NTf_2^-] whose glass transition temperature is ~ 191 K, 0.54 of the solvation is missed at 323 K whereas only 0.17 is missed at 238 K [11].

4. The fluorescence anisotropies (Table V.2) computed from the polarized fluorescence data indicate a single exponential decay for bulk [$CVIM^+$][NTf_2^-]. On the other hand, for micellar [$CVIM^+$][Br^-], the anisotropy decay is dominated by a subpicosecond component and accompanied by a very long component whose duration could not be determined on the time-scale employed for the measurement. The former is attributed to rapid restricted movement of the coumarin 153; and the slower, to overall tumbling of the micelle.

5. Stern-Volmer quenching data indicate that coumarin 153 is quenched more easily when it is embedded in micellar [$CVIM^+$][Br^-] than in methanol solution (Figure V.5).

Discussion

The above results lead us to suggest that:

1. Coumarin 153 is located in the Stern layer of the [$CVIM^+$][Br^-]. This seems reasonable since coumarin 153 is expected to be more soluble in a polarizable environment dominated by imidazolium than a long, nonpolarizable hydrocarbon chain. It is also well known that coumarin 153 is sparingly soluble and weakly fluorescent in bulk water. More concrete

justification of this assignment is given by the anisotropy and the quenching data. The fluorescence anisotropy is dominated by a rapid phase, which is consistent with a mobile coumarin probe located near the micellar surface. This is also confirmed by the quenching data. Coumarin 153 is more strongly quenched in the micelle, whose cationic head groups exert a coulombic attraction upon the anionic quencher, I^-.

2. The same entity is responsible for the majority of the solvation in both bulk $[CVIM^+][NTf_2^-]$ and micellar $[CVIM^+][Br^-]$. We suggest, as we have elsewhere [23-25], that it is the imidazolium cation. It has been proposed that the NTf_2^- may play a major role in solvation because of its polarizability and flexibility [17,24]. At least in this example, that does not seem to be the case: f_{100ps} is slightly larger for micellar $[CVIM^+][Br^-]$ than for bulk $[CVIM^+][NTf_2^-]$.

3. The slightly enhanced f_{100ps} observed in micellar $[CVIM^+][Br^-]$ is attributed to water molecules that are localized near the Stern layer. The average solvation time is considerably shorter in micellar $[CVIM^+][Br^-]$ than in bulk $[CVIM^+][NTf_2^-]$, about 70 ps as opposed to 300 ps. The former solvation time is nowhere near that of bulk water, where solvation is essentially complete after 1 ps [42,43]. It is known, however, that water in confined environments produces solvation that is significantly slower than that of bulk [43,44]; and thus, the average solvation time observed for micellar $[CVIM^+][Br^-]$ is consistent with the presence of water molecules that are confined by the Stern layer. It is also possible, however, that the slower solvation in the bulk solvents arises at least in part from the higher viscosity of these systems (Table V.1).

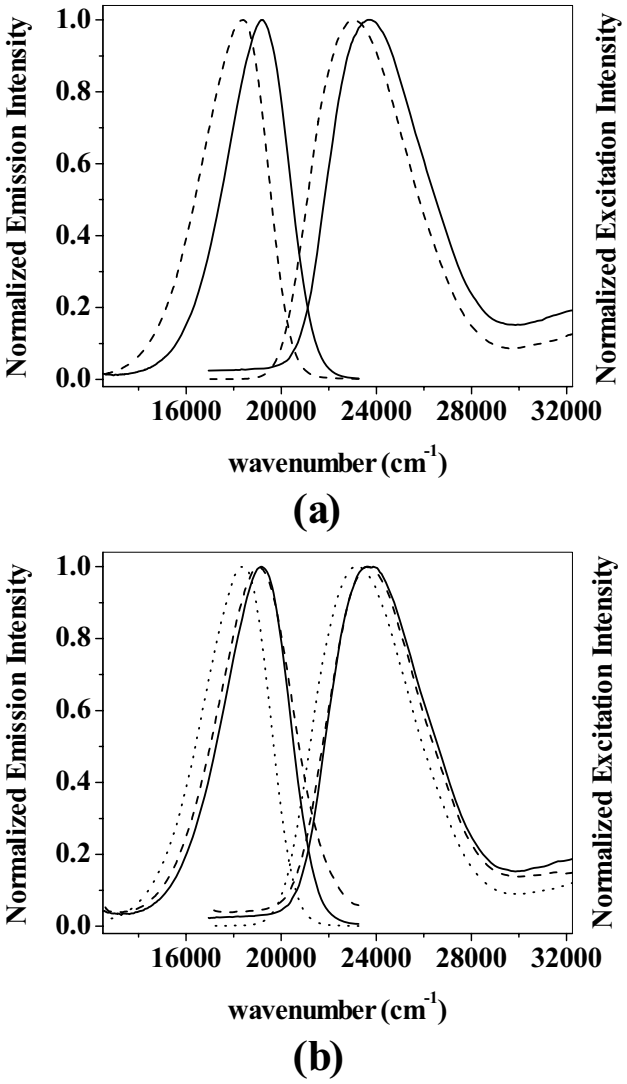

Figure V.2. (a) Normalized excitation and emission spectra of C153 in [CVIM$^+$][NTf$_2^-$] (solid line) and in [CVIM$^+$][Br$^-$] under micellar conditions (dashed line) at 39°C; (b) Normalized excitation and emission spectra of coumarin 153 in [CVIM$^+$][NTf$_2^-$] (solid line), in [CVIM$^+$][Br$^-$] (dashed line), and in [CVIM$^+$][Br$^-$] under micellar conditions (dotted line) at 69°C.

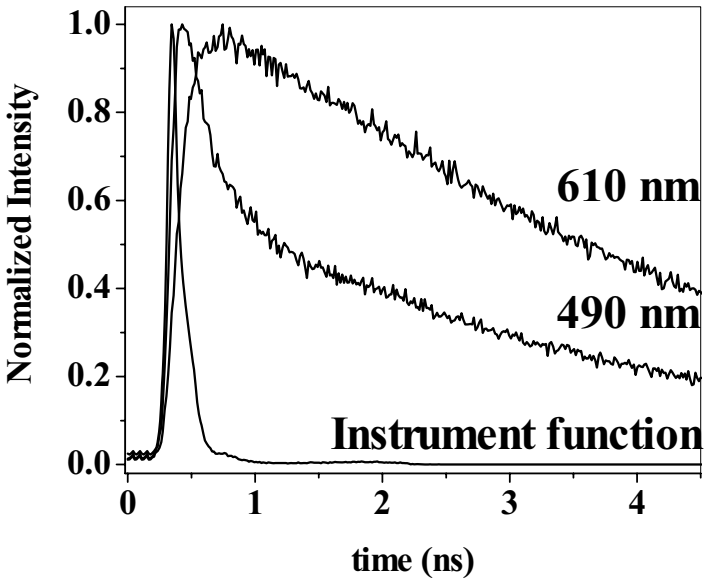

Figure V.3. Representative wavelength-resolved decays for C153 at 490 and 610 nm in [CVIM$^+$][Br$^-$] under micellar conditions at 39°C. A typical instrument response function is shown. The decay at blue end of the spectrum decays faster than that of at the red end of the spectrum. The decay at the red end of the spectrum shows a growing component. The decays used to construct the time-resolved emission spectra were typically collected over a range of wavelengths from 470 to 610 nm at 10 nm intervals, a total of fifteen decays were used to generate the time-resolved emission spectra, from which the C(t) values were calculated.

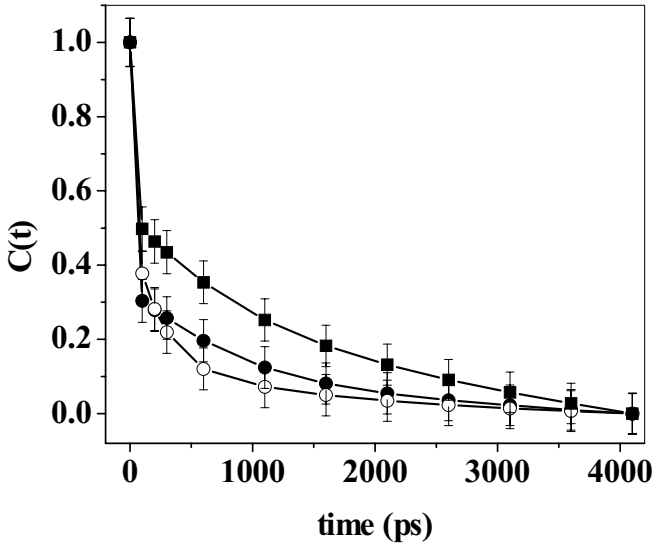

(a)

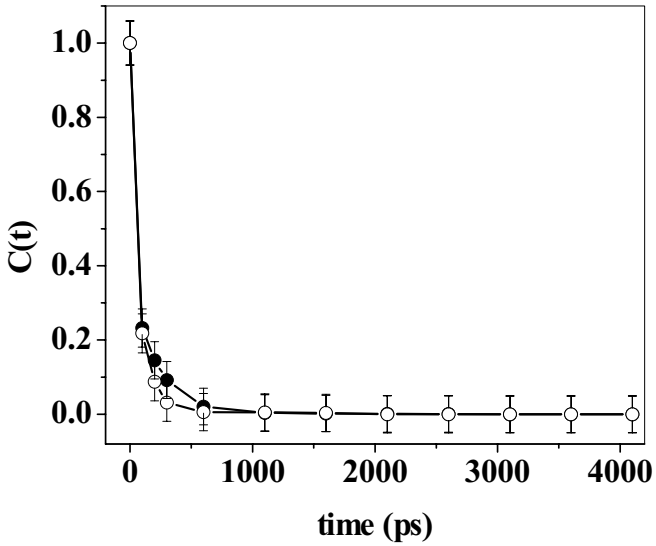

(b)

Figure V.4. C(t) curves for C153. (a) [CVIM$^+$][NTf$_2^-$] (bulk solvent) at 39°C (solid circles); [CVIM$^+$][NTf$_2^-$] (bulk solvent) at 69°C (open circles); and [CVIM$^+$][Br$^-$] (bulk solvent) at 69°C (squares). (b) [CVIM$^+$][Br$^-$] (micelle) at 39°C (solid circles); and [CVIM$^+$][Br$^-$] (micelle) at 69°C (open circles). In all cases, the initial fast component of solvation occurs within our instrumental time resolution. See Table V.1.

Table V.1. Solvation of coumarin 153 in bulk and micellar ionic liquid systems

System	η (cP)	$\lambda_{t=0}$ (cm^{-1})	λ_{SS} (cm^{-1})	f_{100ps}	a_1[a]	τ_1 (ps)	τ_2 (ps)	$\langle\tau\rangle$ (ns)
$[CVIM^+][NTf_2^-]$ bulk (39°C)	124 ± 2.5	1924	2590	0.70	0.67	1	1130	0.37
$[CVIM^+][NTf_2^-]$ bulk (69°C)	37.5 ± 0.8	1906	2616	0.62	0.44	2	1180	0.28
$[CVIM^+][Br^-]$ bulk (69°C)	solid	1985	2716	0.50	0.46	0.3	1420	0.77
$[CVIM^+][Br^-]$ micelle (39°C)	0.67 ± 0.01	1854	2720	0.77	0.63	2	220	0.08
$[CVIM^+][Br^-]$ micelle (69°C)	0.37 ± 0.01	1898	2748	0.78	0.44	2	110	0.06

[a] The solvation relaxation functions, C(t), are in all cases but one fit to a sum of two decaying exponentials: $C(t) = a_1 \exp(-t/\tau_1) + a_2 \exp(-t/\tau_2)$, where $a_1 + a_2 = 1$. The exception is $[CVIM^+][NTf_2^-]$ bulk at 69°C, where there is an intermediate time constant of 190 ps with a weight of 0.38. The average solvation time, $\langle\tau\rangle$, is given by the sum of the products of the preexponential factors and the time constants. Although we fit the C(t) to a sum of exponentials, we do not intend to suggest that this presents an accurate physical description of the solvation process. Finally, we note that the magnitude of τ_1, and consequently that of $\langle\tau\rangle$, is an estimate obtained essentially from only two data points, that at "zero-time" and that at 100 ps. Consequently, the very early time process may be considerably more complicated or represented by a much shorter time constant.

Table V.2. Fluorescence anisotropy of coumarin 153 in bulk solvents and micellar systems

System	r_0 [a]	$\tau^{(r)}_1$ (ns)	r_1	$\tau^{(r)}_2$ (ns)	r_2	$\langle\tau^{(r)}\rangle$ [a] (ns)
$[CVIM^+][NTf_2^-]$ bulk (39°C)	0.32 ± 0.03	3.5	0.32	----	----	3.5
$[CVIM^+][NTf_2^-]$ bulk (69°C)	0.29 ± 0.02	1.6	0.29	----	----	1.6
$[CVIM^+][Br^-]$ micelle (39°C)	0.24 ± 0.02	0.46	0.23	> 20	0.01	----
$[CVIM^+][Br^-]$ micelle (69°C)	0.22 ± 0.03	0.24	0.18	> 20	0.04	----

[a] The errors for r_0 are based on the average of three measurements. The bulk solvents yielded a single-exponential anisotropy decay. The fitting parameters are estimated to be accurate to approximately ± 15%. An average anisotropy decay time is not computed for the micellar systems, since the longer decay components could not be accurately determined on the time scale used, 12 ns full scale.

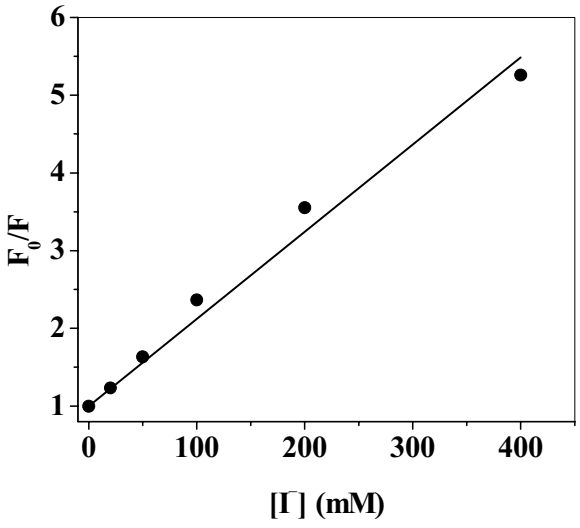

(a)

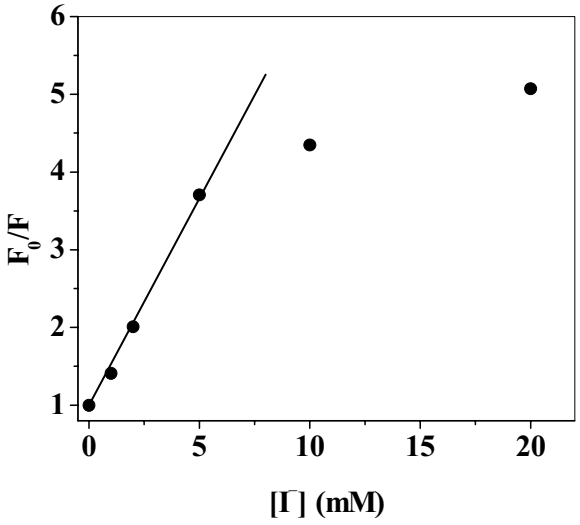

(b)

Figure V.5. Stern-Volmer quenching plots of C153 in (a) methanol and (b) $[CVIM^+][Br^-]$ micelle. K_{SV} values were found to be 10 M^{-1} for C153 in methanol and 530 M^{-1} for $[CVIM^+][Br^-]$ micelle. For the micellar system we have fit only the initial linear portion of the data. The very efficient quenching of C153 fluorescence in micelle is indicative of the presence of probe molecule in the Stern layer of the micelle (see text). All experiments were done at 39°C.

Conclusions

As noted above, our previous work on ionic liquids has led us to conclude that the organic cation is most often responsible for the early-time dynamic solvation events [23-25]. Here we compare the micellar system formed by 1-cetyl-3-vinylimidazolium bromide in water against the bulk bromide solvent and the NTf_2^- solvent (Figure V.1). Given that coumarin 153 is sparingly soluble in both water and nonpolar hydrocarbons, it is most likely that it is located in the Stern layer of the micelle formed by 1-cetyl-3-vinylimidazolium bromide. If this is so, the immediate environment of the coumarin is predominantly the imidazolium cation and an outer sphere of associated water molecules and bromide ions (Figure V.1d). Table V.1 and Figure V.4 indicate that the fractional solvation in the micelles is, within experimental error, slightly greater than or equal to that in the bulk ionic liquids. We interpret this result as indicative of predominant solvation in both cases by the imidazolium cation. This assignment, however, is tentative since it is based only upon the value of the fractional solvation at 100 ps. In order to make it definitive, solvation studies need to be performed either on a variety of ionic liquids and counter anions or with superior time resolution so that the form of the C(t) function may be compared. Finally, the average solvation time in the micelles is considerably smaller than that of the bulk solvents, which we interpret in terms of the contribution of localized water molecules.

Exploiting the use of ionic liquids capable of accommodating specific structures provides a deeper insight into how solutes interact with these fascinating and interesting solvents that are gaining ever increasing interest in the scientific community.

Acknowledgements

We thank Professor Xueyu Song of Iowa State University and Dr. Nitin Chattopadhyay, Jadavpur University, Kolkata, India, for stimulating comments. Dr. Lindsay Sanders Headley kindly provided viscosity measurements. DWA and JC acknowledge the support of this work by the National Institutes of Health, NIH RO1 GM53825-11.

References

(1) Seddon, K. R. Nature (Materials) 2003, 2, 363.

(2) Anderson, J. L.; Ding, J.; Welton, T.; Armstrong, D. W. J. Am. Chem. Soc. 2002, 124, 14247.

(3) Anderson, J. L.; Armstrong, D. W.; Wei, G.-T. Anal. Chem. 2006, 78, 2893.

(4) Pandey, S. Anal. Chim. Acta 2006, 556, 38.

(5) Karmakar, R.; Samanta, A. J. Phys. Chem. A 2002, 106, 6670.

(6) Karmakar, R.; Samanta, A. J. Phys. Chem. A 2002, 106, 4447.

(7) Karmakar, R.; Samanta, A. J. Phys. Chem. A 2003, 107, 7340.

(8) Ingram, J. A.; Moog, R. S.; Ito, N.; Biswas, R.; Maroncelli, M. J. Phys. Chem. B 2003, 107, 5926.

(9) Ito, N.; Arzhantsev, S.; Maroncelli, M. Chem. Phys. Lett. 2004, 396, 83.

(10) Ito, N.; Arzhantsev, S.; Heitz, M.; Maroncelli, M. J. Phys. Chem. B 2004, 108, 5771.

(11) Arzhantsev, S.; Ito, N.; Heitz, M.; Maroncelli, M. Chem. Phys. Lett. 2003, 381, 278.

(12) Arzhantsev, S.; Hui, J.; Baker, G. A.; Naoki, I.; Maroncelli, M. "Solvation dynamics in ionic liquids, results from ps and fs emission spectroscopy." Femtochemistry VII, 2005.

(13) Arzhantsev, S.; Hui, J.; Naoki, I.; Maroncelli, M. Chem. Phys. Lett. 2006, 417, 524.

(14) Hyun, B.-R.; Dzyuba, S. V.; Bartsch, R. A.; Quitevis, E. L. J. Phys. Chem. A 2002, 106, 7579.

(15) Giraud, G.; Gordon, C. M.; Dunkin, I. R.; Wynne, K. J. Chem. Phys. 2003, 119, 464.

(16) Cang, H.; Li, J.; Fayer, M. D. J. Chem. Phys. 2003, 119, 13017.

(17) Shirota, H.; Funston, A. M.; Wishart, J. F.; Castner, E. W., Jr. J. Chem. Phys. 2005, 122, 184512.

(18) Rajian, J. R.; Li, S.; Bartsch, R. A.; Quitevis, E. L. Chem. Phys. Lett. 2004, 393, 372.

(19) Shirota, H.; Castner, E. W., Jr. J. Phys. Chem. A 2005, 109, 9388.

(20) Weingärtner, H.; Knocks, A.; Schrader, W.; Kaatze, U. J. Phys. Chem. A 2001, 105, 8646.

(21) Daguenet, C.; Dyson, P. J.; Krossing, I.; Oleinikova, A.; Slattery, J.; Wakai, C.; Weingartner, H. J. Phys. Chem. B, accepted.

(22) Ito, N.; Huang, W.; Richert, R. J. Phys. Chem. B 2006, 110, 4371.

(23) Chowdhury, P. K.; Halder, M.; Sanders, L.; Calhoun, T.; Anderson, J. L.; Armstrong, D. W.; Song, X.; Petrich, J. W. J. Phys. Chem. B 2004, 108, 10245.

(24) Headley, L. S.; Mukherjee, P.; Anderson, J. L.; Ding, R.; Halder, M.; Armstrong, D. W.; Song, X.; Petrich, J. W. J. Phys. Chem. A 2006, 110, 9549.

(25) Halder, M.; Headley, L. S.; Mukherjee, P.; Song, X.; Petrich, J. W. J. Phys. Chem. A 2006, 110, 8623.

(26) Margulis, C. J.; Stern, H. A.; Berne, B. J. J. Phys. Chem. B 2002, 106, 12017.

(27) Shim, Y.; Duan, J.; Choi, M. Y.; Kim, H. J. J. Chem. Phys. 2003, 119, 6411.

(28) Znamenskiy, V.; Kobrak, M. N. J. Phys. Chem. B 2004, 108, 1072.

(29) Kobrak, M. N.; Znamenskiy, V. Chem. Phys. Lett. 2004, 395, 127.

(30) Del Popolo, M. G.; Voth, G. A. J. Phys. Chem. B 2004, 108, 1744.

(31) Morrow, T. I.; Maginn, E. J. J. Phys. Chem. B 2002, 106, 12807.

(32) Hu, Z.; Margulis, C. J. Proc. Natl. Acad. Sci. U. S. A. 2006, 103, 831.

(33) Anderson, J. L.; Pino, V.; Hagberg, E. C.; Sheares, V. V.; Armstrong, D. W. Chem. Commun. 2003, 19, 2444.

(34) Trewyn, B. G.; Whitman, C. M.; Lin, V. S. Y. Nano Lett. 2004, 4, 2139.

(35) Miskolczy, Z.; Sebok-Nagy, K.; Biczok, L.; Gokturk, S. Chem. Phys. Lett. 2004, 400, 296.

(36) Merrigan, T. L.; Bates, E. D.; Dorman, S. C.; Davis, J. H., Jr. Chem. Commun. 2000, 2051.

(37) Chakraborty, A.; Seth, D.; Chakrabarty, D.; Setua, P.; Sarkar, N. J. Phys. Chem. A 2005, 109, 11110.

(38) Hara, K.; Baden, N.; Kajimoto, O. J. Phys.: Condens. Matter 2004, 16, S1207.

(39) Turro, N. J.; Yekta, A. J. Am. Chem. Soc. 1978, 100, 5951.

(40) Stam, J. v.; Depaemelaere, S.; De Schryver, F. C. J. Chem. Ed. 1998, 75, 93.

(41) Fee, R. S.; Maroncelli, M. Chem. Phys. 1994, 183, 235.

(42) Jimenez, R.; Fleming, G. R.; Kumar, P. V.; Maroncelli, M. Nature 1994, 369, 471.

(43) Vajda, S.; Jimenez, R.; Rosenthal, S. J.; Fidler, V.; Fleming, G. R.; Castner, E. W., Jr. J. Chem. Soc., Faraday Trans. 1995, 91, 867.

(44) Pal, S. K.; Peon, J.; Bagchi, B.; Zewail, A. H. J. Phys. Chem. B 2002, 106, 12376.

CHAPTER VI. DYNAMIC SOLVATION IN PHOSPHONIUM IONIC LIQUIDS: COMPARISON OF BULK AND MICELLAR SYSTEMS AND CONSIDERATIONS FOR THE CONSTRUCTION OF THE SOLVATION CORRELATION FUNCTION, C(t)

A paper published in the Journal of Physical Chemistry B

Prasun Mukherjee[1], Jeffrey A. Crank[2], Pritesh S. Sharma[2], Aruna B. Wijeratne[2], Ramkrishna Adhikary[1] , Sayantan Bose[1] , Daniel W. Armstrong[2],

and Jacob W. Petrich[1,*]

Abstract

Dynamic solvation of the dye, coumarin 153, is studied in a phosphonium ionic liquid: hexadecyl tributyl phosphonium bromide, $[(C_4)_3C_{16}P^+][Br^-]$. It forms micelles in water, and the bulk also exists as a liquid under our experimental conditions. This system permits a comparison with an imidazolium ionic liquid studied earlier, which also formed micelles in water (J. Phys. Chem. A 2006, 110, 10725-10730). We conclude that our analysis of the comparable situation in a phosphonium liquid is not as definitive as we had proposed earlier, i.e., that the majority of the early-time solvation arises from the organic cation. Part of the difficulty in performing this analysis is most likely due to the amount of water that is associated with the micelle. In the course of this work, we have focused on the calculation of

[1] Department of Chemistry, Iowa State University, Ames, Iowa 50011.

[2] Department of Chemistry and Biochemistry, University of Texas, Arlington, Box 19065 Arlington, Texas 76019.

[*] Author to whom correspondence should be addressed.

the solvation correlation function, C(t), and investigated how it depends upon the methods with which the "zero-time" spectrum is constructed.

Introduction

Room temperature ionic liquids, most commonly comprised of organic cations and inorganic anions, are receiving an increasing amount of attention because of their utility as environmentally friendly, "green" solvents and because of a host of practical applications to which they are amenable [1-4]. The importance of ionic liquids has consequently stimulated considerable interest in their dynamic solvation properties [5-34]. A special issue of the The Journal of Physical Chemistry has recently been devoted to ionic liquids [35]. Major questions regarding dynamic solvation by ionic liquids deal with whether the organic cation or the inorganic anion solvate preferentially on different time scales, the role of the correlated motion of the ion pairs and their lifetime, and the importance of translational motion of the ions relative to dipolar relaxation [23-25]. Previously, we attempted to address some of these questions by studying the solvation of the dye, coumarin 153, in a bulk imidazolium ionic liquid, 1-cetyl-3-vinylimidazolium bromide ($[CVIM^+][Br^-]$) and its corresponding micelle in water [36]. (There is a growing body of work on the subject of ionic liquids in micelles, microemulsions and related systems [37-43].) Because coumarin 153 is only sparingly soluble and weakly fluorescent in water, a clear distinction can be made between its fluorescent properties in the bulk ionic liquid and those in the micelles formed from the ionic liquid. We concluded from this study that the same entity is responsible for the majority of the solvation in both the bulk and micellar $[CVIM^+][Br^-]$ ionic liquid, namely as we have suggested elsewhere [23-25], that it is the imidazolium cation. This study was, however, limited: first,

because bulk [CVIM$^+$][Br$^-$] could only be studied as an opaque solid at the temperatures at which we investigated the micelle; second, because the study only considered ionic liquids based upon imidazolium. In this work, we investigate a phosphonium ionic liquid (Figure VI.1), which forms micelles in water and for which the bulk also exists as a liquid under our experimental conditions: hexadecyl tributyl phosphonium bromide, [$(C_4)_3C_{16}P^+$][Br$^-$] (melting point of 58-60°C). As a result of this study, our earlier conclusions have been tempered and, most importantly, we present conclusions dealing with the construction of the solvation correlation function, C(t).

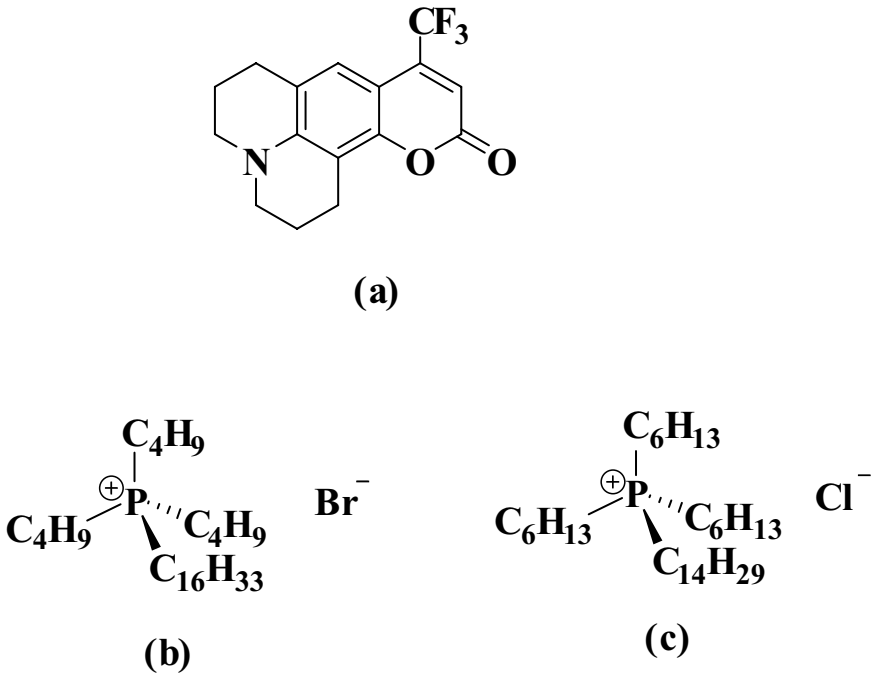

Figure VI.1. Structures of the solvation probe (a) coumarin 153 (C153) and the two ionic liquids studied in this work: (b) hexadecyl tributyl phosphonium bromide [$(C_4)_3C_{16}P^+$][Br$^-$], melting point = 58-60°C and (c) tetradecyl trihexyl phosphonium chloride [$(C_6)_3C_{14}P^+$][Cl$^-$] (liquid at room temperature). [$(C_4)_3C_{16}P^+$][Br$^-$] forms micelles in water.

Materials and Methods

Preparation and Purification/Decolorization of Low-Melting Phosphonium Halide Organic Salts. Phosphonium halide ionic liquids (ILs) were donated by Cytec Inc. and were decolorized according to the procedure described elsewhere [44]. A conventional column used for flash-chromatography was packed with the following compounds: celite on the bottom to trap charcoal particles; flash chromatographic silica gel and alumina in the middle for decolorization and removal of polar and inorganic impurities; and charcoal on the top for decolorizing. The column was treated with CH_2Cl_2 (3 × 200 ml). The RTIL was dissolved in CH_2Cl_2 (200 mL) and passed through the column. Then dichloromethane (200 mL) was passed in order to elute the remainder of the ionic liquid. To purge the ionic liquid through the column, N_2 gas was passed over the column. In order to obtain some visible change in color during the decolorization, the aforementioned procedure (the passage of the RTIL dissolved in CH_2Cl_2) was repeated for more than 15 times. Also, during each of the repetitions, the column was treated with CH_2Cl_2 (200 mL). The eluted solution was then concentrated under reduced pressure and finally by heating at 60 °C in vacuo over night. Structures were verified by ^{1}H-NMR and ESI-MS. The water contents of the RTILs were measured by coulometric Karl Fischer Titration (Mettler Toledo DL 39).

CMC Determination. The critical micelle concentration (CMC) was found by plotting surface tension (dynes/cm) vs. concentration (M). Surface tension measurements were taken using a Fischer Model 20 surface tensiometer. All glassware used was cleaned by chromic acid, rinsed with deionized water, and dried in an oven. Concentrations between 0 and 0.1 M of hexadecyl tributyl phosphonium bromide were prepared in aqueous solution at room temperature. An average of 3 measurements was taken to represent the surface tension at

each concentration of IL. The CMC value of $[(C_4)_3C_{16}P^+][Br^-]$ micelle was found to be 2×10^{-3} M at room temperature.

Determination of the Micellar Aggregation Number. The aggregation number (the average number of surfactant molecules per micelle) can be estimated by optical techniques proposed by Turro and Yekta [45] and later modified by De Schryver and coworkers [46]. As before [36], we employ the latter method, where the micellar aggregation number is obtained by exploiting the vibronic fine structure of pyrene emission. Pyrene was recrystallized several times from absolute ethanol before use. Three stock solutions were prepared of concentrations 2×10^{-4}, 10×10^{-3}, and 5×10^{-2} M pyrene in ethanol, cetyl pyridinium chloride in water, and $[(C_4)_3C_{16}P^+][Br^-]$ in water. For all measurements, pyrene and surfactant concentrations were kept constant at ~ 2×10^{-6} M and ~ 2×10^{-2} M. Six solutions were prepared with increasing quencher concentration from 0 to 0.5×10^{-3} M. Samples were excited at 337 nm. The aggregation number was determined by the same procedure we have employed elsewhere. Calculations can be performed using the intensity of either band I or band III of pyrene emission. We have chosen the emission intensity of band I (at ~ 373 nm) and band III (at ~ 384 nm) for determining the aggregation number of the micelle. The results obtained from both bands were identical. The mean aggregation number of $[(C_4)_3C_{16}P^+][Br^-]$ micelle at room temperature was found to be 40.

Preparation of Micellar Solutions. The critical micelle concentration (CMC) of $[(C_4)_3C_{16}P^+][Br^-]$ in water was found to be 2×10^{-3} M at 22°C, see above. For all experiments in micellar systems, the C153 concentration was kept at ~ 6×10^{-6} M in ~ 2×10^{-2} M $[(C_4)_3C_{16}P^+][Br^-]$ (10 times CMC) and a ~ 3330:1 surfactant-to-C153 ratio was

maintained. Under these conditions there is one C153 molecule for every 75 micelles, thus minimizing the possibility of aggregation.

Preparation of Solutions for Stern-Volmer Quenching Experiments. We initially attempted to perform quenching experiments with iodide anion, as we did in our previous work. We were not able to attain concentrations of I^- higher than 3 mM due to solubility problems and consequently were not able to obtain enough data to determine quenching constants. We thus opted for N,N-dimethyl aniline (DMA) to quench C153 fluorescence in this system. For quenching of C153 in bulk solvent, a stock solution of 2×10^{-4} M C153 in acetonitrile was used. The corresponding quenching experiment in micellar environments was performed by preparing two stock solutions: 2×10^{-4} M C153 in acetonitrile and 5×10^{-2} M $[(C_4)_3C_{16}P^+][Br^-]$ in water. For all measurements, the C153 and surfactant concentrations were kept constant at ~ 2×10^{-6} M and ~ 5×10^{-3} M (2.5 times CMC) and an 830:1 surfactant-to-C153 ratio was maintained. Under these conditions there is one C153 molecule for every 18 micelles, thus minimizing the possibility of aggregation. Seven solutions were prepared with increasing quencher concentration from 0 to 10×10^{-3} M. We could not increase the quencher concentration above 10×10^{-3} M due to precipitation of the surfactant at higher DMA concentration. Emission spectra were obtained using an excitation wavelength of 420 nm. The control experiment was performed in acetonitrile rather than in bulk $[(C_4)_3C_{16}P^+][Br^-]$ owing to the difficulties imposed in preparing solutions by the high viscosity of the bulk and the rather small quantities available to us of the purified material.

Steady-State Optical Measurements. Steady-state excitation and emission spectra were recorded with a SPEX Fluoromax-2 with a 2-nm bandpass and were corrected for detector

response. A 1-cm pathlength quartz cuvette was used for the measurements. During spectroscopic measurements, the quartz cuvettes were kept tightly sealed so as to prevent moisture from being absorbed by the ionic liquids. The steady-state spectra can be used to compute the reorganization energy, λ [24]:

$$\lambda = \hbar \frac{\int_0^\infty \mathbf{d}\nu[\sigma_a(\nu) - \sigma_f(\nu)]\nu}{\int_0^\infty \mathbf{d}\nu[\sigma_a(\nu) + \sigma_f(\nu)]} \qquad \textbf{(VI.1)}$$

The $\sigma_{a,f}$ are the absorption (or excitation) and emission spectral line-shapes, respectively.

Time-Resolved Measurements. The apparatus for the time-correlated single-photon counting measurements is described in detail elsewhere [23]. The instrument response function had a full-width–at-half-maximum (FWHM) of ≤ 100 ps. A 1-cm pathlength quartz cuvette was used for all the time-resolved measurements. To construct the time-resolved spectra, a series of decays (~3,000 counts in the peak channel for the data presented here, i.e., the 4- and 20-ns full-scale windows) were collected over as much of the fluorescence spectrum as possible, typically from 470 nm to 610 nm at 10-nm intervals. They were fit to a maximum of three exponentials. Transient spectra were reconstructed from these fits in the standard manner [23,36]. We have employed the traditional approach of fitting the time-resolved spectra to a log-normal function, from which we extract the peak frequency, ν(t), as a function of time.

The solvation dynamics were described by the normalized correlation function:

$$\mathbf{C(t)} = \frac{\nu(\mathbf{t}) - \nu(\text{"}\infty\text{"})}{\nu(\text{"}\mathbf{t = 0}\text{"}) - \nu(\text{"}\infty\text{"})} \qquad \textbf{(VI.2)}$$

ν("t = 0") is the frequency at zero time, as calculated by the method of Fee and Maroncelli [47]. ν("∞") is the frequency at "infinite time," which may be taken as the maximum of the

steady-state fluorescence spectrum if solvation is more rapid than the population decay of the probe. $\nu(t)$ is determined by taking the maxima from the lognormal fits as the emission maximum. In most of the cases, however, the spectra are broad, so there is some uncertainty in the exact position of the emission maxima. Thus, we have considered the range of the raw data points in the neighborhood of the maximum to estimate an error for the maximum obtained from the lognormal fit. Depending on the width of the spectrum (i.e. "zero-time", steady-state, or time-resolved emission spectrum), we have determined the typical uncertainties as follows: "zero-time" ~ steady-state (~ $\pm$ 100 cm^{-1}) < time-resolved emission (~ $\pm$ 200 cm^{-1}). We use these uncertainties to compute error bars for the C(t). Finally, in generating the C(t), the first point was obtained from the "zero time" spectrum. The second point was taken at the maximum of the instrument response function, which, having a full-width at half-maximum of $\leq$ 100 ps, was taken to be ~100 ps. Fractional solvation at 100 ps was calculated using f (t = 100 ps) = 1 – C (t = 100 ps).

Results

C153 is sparingly soluble in water, and hence must be located in the micelles formed by $[(C_4)_3C_{16}P^+][Br^-]$. In order to characterize its location therein, we constructed Stern-Volmer plots using N,N-dimethyl aniline (DMA) as a quencher. Figure VI.2 presents the Stern-Volmer plots of C153 quenched by DMA in acetonitrile and micelles formed by $[(C_4)_3C_{16}P^+][Br^-]$. K_{SV} values were 60 M^{-1} for C153 in acetonitrile and 390 M^{-1} for $[(C_4)_3C_{16}P^+][Br^-]$ micelle. The greater K_{SV} value in micelle compared to that in bulk might be attributed to greater accessibility of C153 to the quencher in the micelle. We suppose this is due to the close proximity of C153 and DMA, the latter being preferentially located in the

Stern layer of the micelle. This situation is comparable to that of [CVIM$^+$][Br$^-$], where C153 is quenched more efficiently in the micelle than in the bulk reference solvent [36]. In both cases, C153 is interpreted to be located in the Stern layer, in proximity to the cation, and exposed to water molecules hydrating the micelle.

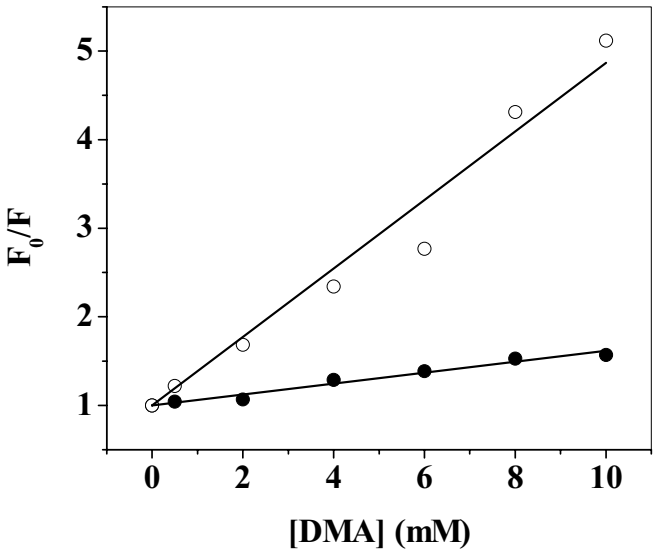

Figure VI.2. Stern-Volmer quenching plots of C153 by N,N-dimethyl aniline (DMA) in acetonitrile (solid circles) and [$(C_4)_3C_{16}P^+$][Br^-] micelles (open circles). K_{SV} values were found to be 60 M^{-1} for C153 in acetonitrile and 390 M^{-1} for [$(C_4)_3C_{16}P^+$][Br^-] micelle. All experiments were done at room temperature. DMA is negligibly soluble in water, and based on NMR [48] and fluorescence [49] measurements in CTAB micelles, it has been concluded that DMA resides in the head group region of the micelles. We expect the same location of DMA in [$(C_4)_3C_{16}P^+$][Br^-] micelles. The very efficient quenching of C153 fluorescence by DMA (most likely by electron transfer from DMA to C153 [50,51]) indicates that the probe molecules are accessible to the quencher.

Time-resolved spectra are presented in Figure VI.3 for C153 in bulk [$(C_4)_3C_{16}P^+$][Br^-] at 100 ps, 4 ns, and 20 ns. The corresponding "steady-state" and "time-zero" spectra are also included. Note that the 4 and 20-ns spectra cross the "steady-state" spectrum, indicating that this spectrum does not adequately report on the completed solvation of C153, as would usually be expected.

Figure VI.4 illustrates this phenomenon more extensively by presenting the solvation relaxation or correlation functions, C(t), for bulk $[(C_4)_3C_{16}P^+][Br^-]$ (66°C) and $[(C_4)_3C_{16}P^+][Br^-]$ under micellar conditions (at room temperature and 66°C) for increasingly larger time windows: 4- and 20- ns. Relevant spectral parameters are summarized in Table VI.1. A salient feature is that the fraction of rapid solvation and the average solvation time decrease and increase, respectively, as the time-window of the experiment is increased. This phenomenon is intimately related to the fact, which has been mentioned above, and noticed elsewhere for related systems [10,11], that the spectrum at a given time may be more red shifted than the "equilibrium" spectrum. We see this clearly in the comparison of the 4-ns, 20-ns and equilibrium spectra of Figure VI.3. (We attempted to construct the C(t) on an 80-ns time scale as well. The 80-ns spectrum we obtained was red of the 20-ns spectrum, but since the number of counts at 80-ns was so limited, <10, we do not take this result to be quantitative.)

Fluorescence anisotropy decay parameters for bulk $[(C_4)_3C_{16}P^+][Br^-]$ and for its micelles in water are presented in Table VI.2. Figure VI.5 presents the polarized fluorescence decays for $[(C_4)_3C_{16}P^+][Br^-]$ under micellar conditions at room temperature. The fluorescence anisotropy decay parameters of the room temperature micellar system are comparable to those of the bulk ionic liquid. Nonetheless, the fractional solvation at 100 ps, f_{100ps}, of the former is 0.5 whereas that of the latter is 0.3 (as measured with a 20-ns window). The difference in fractional solvation between the bulk and micellar forms of the phosphonium ionic liquid is considerably larger than that for the imidazolium ionic liquid we investigated earlier, which was within about 10% of each other.

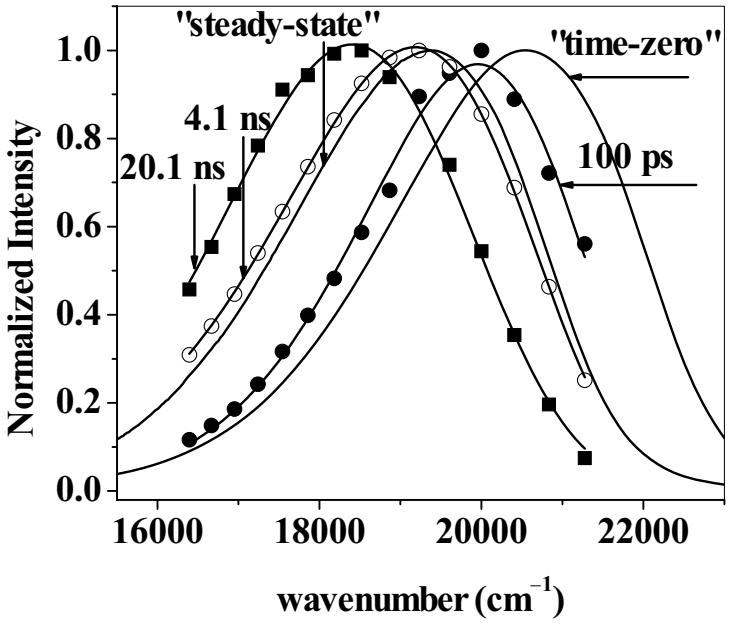

Figure VI.3. Time-resolved fluorescence emission spectra of C153 in bulk $[(C_4)_3C_{16}P^+][Br^-]$ (66°C) at 100 ps, 4.1 ns and 20.1 ns. Corresponding "steady-state" and "time-zero" spectra are also included. Note that the 4.1- and 20.1-ns spectra cross the "steady-state" spectrum, indicating that this spectrum does not adequately report on the completed solvation of C153, as would usually be expected.

Discussion

Bulk Solvent versus Micellar System.

As indicated directly above, there are significant differences between the fractional solvation at early times for the bulk and micellar forms of $[(C_4)_3C_{16}P^+][Br^-]$. In addition, the average solvation time of the bulk at 66°C is at least three times as long as that in the micellar environment at room temperature on the 20-ns time scale (Table VI.1). The enhanced f_{100ps} in micelles is most likely a result of aqueous solvation. As in the case of the imidazolium ionic liquid [36], quenching experiments indicate that it is likely that C153 resides in the Stern layer of the $[(C_4)_3C_{16}P^+][Br^-]$ micelle. Such a probe location can also explain why the average solvation time is considerably longer in bulk $[(C_4)_3C_{16}P^+][Br^-]$ compared to

that of the micellar. In bulk water, solvation is essentially complete after 1 ps [52,53]; but water in confined environments gives rise to slower solvation response [53,54], which has been argued to arise from a dynamic equilibrium between bound and free water molecules [55-60]. (We do not, however, subscribe to the idea of "biological water" which some of these latter references argue for [61].) Consequently, we suggest that the water responsible for the relatively rapid solvation response in the micelles is colocalized in the Stern layer with C153.

It is well to note that temperature can have rather profound effects on the structure of micelles and, consequently, the solvation dynamics at their interfaces. The temperature dependence of the structure and hydration number of triton X-100 (TX-100) micelles was demonstrated by Streletzky and Phillies [62], who reported an increase in hydration number of micelle with increase in temperature. The temperature dependence of the solvation dynamics in micelles was studied in triton X-100 (TX-100) using 4-aminophthalimide (4-AP) as a fluorescent probe where an increase in temperature from 283 K to 323 K results ~ 8-times decrease in average solvation time. From this study the authors also concluded that temperature dependent change of structure and hydration number in TX-100 micelle appears to be playing a minor role in their measurements of solvation dynamics [63]. And finally, the temperature dependent effects on solvation dynamics of C153 and C151 are significant in TX-100 micelles and moderate in Brij-35 micelles [64]. In this work the authors emphasized the effect of micellar size and hydration on solvation dynamics in micellar media.

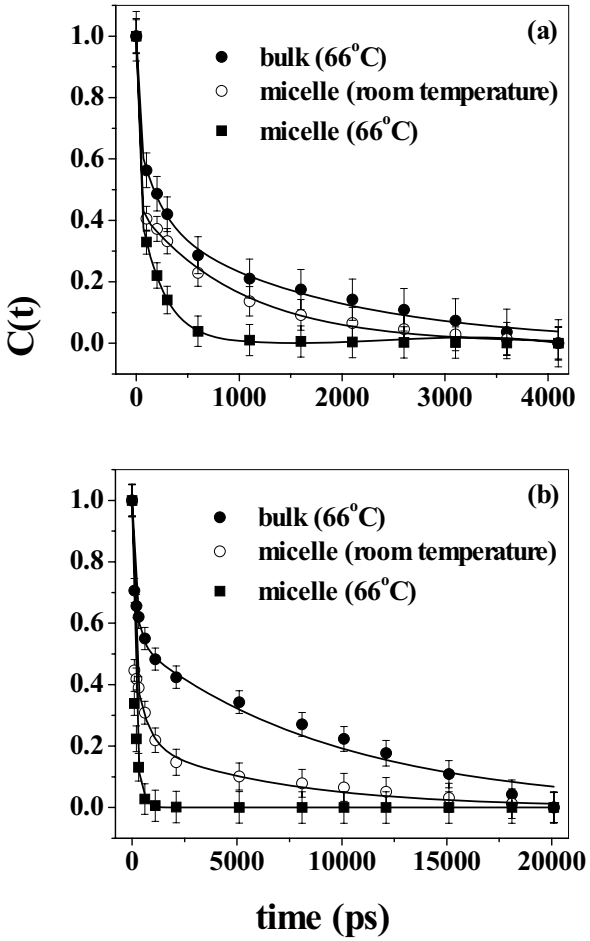

Figure VI.4. C(t) curves for C153 in:
(a) bulk $[(C_4)_3C_{16}P^+][Br^-]$ (66°C) (solid circles) [C(t) = 0.30 exp(–t/0.63 ps) + 0.29 exp(–t/210 ps) + 0.41 exp(–t/1730 ps)], $[(C_4)_3C_{16}P^+][Br^-]$ under micellar conditions at room temperature (open circles) [C(t) = 0.56 exp(–t/20 ps) + 0.44 exp(–t/1000 ps)] and at 66°C (solid squares) [C(t) = 0.48 exp(–t/0.35 ps) + 0.52 exp(–t/230 ps)], with a time window of 4 ns.
(b) bulk $[(C_4)_3C_{16}P^+][Br^-]$ (66°C) (solid circles) [C(t) = 0.22 exp(–t/2.5 ps) + 0.24 exp(–t/300 ps) + 0.54 exp(–t/9700 ps)], $[(C_4)_3C_{16}P^+][Br^-]$ under micellar conditions at room temperature (open circles) [C(t) = 0.49 exp(–t/1.3 ps) + 0.30 exp(–t/590 ps) + 0.21 exp(–t/7000 ps)] and at 66°C (solid squares) [C(t) = 0.45 exp(–t/0.13 ps) + 0.55 exp(–t/210 ps)], with a time window of 20 ns.
In all cases the initial fast component occurs within our instrumental time resolution. Most importantly, there is a dependence of f_{100ps} and the average solvation time on the choice of the time scale of the experiment for the bulk $[(C_4)_3C_{16}P^+][Br^-]$ (66°C) and $[(C_4)_3C_{16}P^+][Br^-]$ under micellar conditions at room temperature. This effect is more pronounced in the bulk compared to that in the micellar system. However, no such effect was observed for $[(C_4)_3C_{16}P^+][Br^-]$ under micellar conditions at 66°C on changing the time scale from 4 ns to 20 ns, indicating faster solvation in this system.

Table VI.1. Solvation of Coumarin153 in Bulk and Micellar Phosphonium Ionic Liquid Systems [a]

					4-ns window			20-ns window		
system	η (cP)	wt. % H_2O	$\lambda_{t=0}$ (cm^{-1})[b]	λ_{SS} (cm^{-1})[b]	f100ps	<τ> (ns)	ν("∞") (cm^{-1})	f100ps	<τ> (ns)	ν("∞") (cm^{-1})
$[(C_4)_3C_{16}P^+][Br^-]$ bulk (66°C)	268 ± 2	0.2	1920	2480	0.44 ± 0.06	0.77	19180	0.29 ± 0.04	5.3	18410
$[(C_4)_3C_{16}P^+][Br^-]$ micelle (room temp.)	1.11 ± 0.01	------	1980	2740	0.59 ± 0.04	0.45	18080	0.55 ± 0.04	1.6	17840
$[(C_4)_3C_{16}P^+][Br^-]$ micelle (66°C)	0.44 ± 0.01	------	1920	2660	0.67 ± 0.04	0.12	18130	0.66 ± 0.04	0.12	18130
$[(C_6)_3C_{14}P^+][Cl^-]$ bulk (purified) (58°C)	80 ± 1	0.3	1970	2660	0.41 ± 0.05	0.70	19160	0.33 ± 0.04	3.9	18610
$[(C_6)_3C_{14}P^+][Cl^-]$ bulk (unpurified) (58°C)	234 ± 2	0.3	1960	2460	------	------	------	0.34 ± 0.05	4.9	18900
$[(C_6)_3C_{14}P^+][Cl^-]$ bulk (58°C) [c]	230 [d]	0.1	1960	2930	------	------	------	0.03	6.7 ± 1.7	18540

[a] The solvation relaxation functions, C(t), are fit to a sum of two or three exponentially decaying functions, where we attribute no particular physical significance to the choice of the functional form employed. The average solvation time <τ> is calculated as $\langle\tau\rangle=\sum_i a_i\tau_i$, where the a_i are the amplitudes of the exponential functions normalized to sum to unity. C(t) is fit from its value at unity, i.e., starting at "t = 0"; consequently the early part of its decay is determined by only two points, and the <τ> that we report must be considered an upper limit. The fractional solvation at 100 ps is defined in the text and elsewhere [24,36].

[b] The reorganization energies calculated using equation VI.1 from either the zero-time spectrum ("t = 0"), obtained using the method of Fee and Maroncelli [47], or from the equilibrium spectrum (SS).

[c] Ref. [11]. [d] Ref. [65].

Table VI.2. Fluorescence Anisotropy of C153 in Bulk Solvent and Micellar Systems [a]

System	r_0	r_1	$\tau^{(r)}_1$ (ps)	r_2	$\tau^{(r)}_2$ (ps)	$\langle\tau^{(r)}\rangle$ (ps)
$[(C_4)_3C_{16}P^+][Br^-]$ bulk (66°C)	0.22 ± 0.02	0.09 ± 0.01	260 ± 70	0.13 ± 0.02	3000 ± 400	1900 ± 600
$[(C_4)_3C_{16}P^+][Br^-]$ micelle (room temperature)	0.35 ± 0.03	0.15 ± 0.02	200 ± 80	0.20 ± 0.02	1700 ± 400	1100 ± 500
$[(C_4)_3C_{16}P^+][Br^-]$ micelle (66°C)	0.25 ± 0.04	0.25 ± 0.04	360 ± 80	------	------	360 ± 80

[a] The errors are based on the average of three measurements. Fluorescence anisotropy decays are fit to the form: $r_0 = r_1 \exp(-t/\tau^{(r)}_1) + r_2 \exp(-t/\tau^{(r)}_2)$. In all cases $\chi^2 \leq 1.3$. All experiments were done on a time scale of 12 ns.

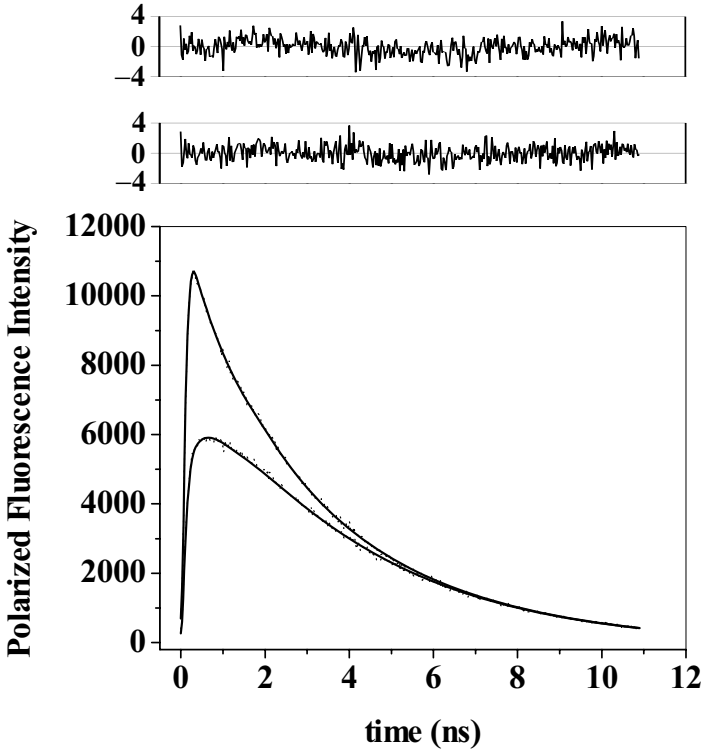

Figure VI.5. Representative polarized fluorescence decay of C153 in $[(C_4)_3C_{16}P^+][Br^-]$ under micellar conditions at room temperature. Fitting parameters are given in Table VI.2.

Phosphonium Ionic Liquids, their Properties, and the Construction of the Solvation Correlation Function, C(t)

Our results for the solvation dynamics of bulk $[(C_4)_3C_{16}P^+][Br^-]$ at 66°C provide a solvation correlation function, C(t), that has a component that is complete within 100 ps and that has a slower evolution over the course of an 20-ns time window. Such a result for a long-chain phosphonium halide ionic liquid is contrary to the report of Maroncelli and coworkers, who find that for $[(C_6)_3C_{14}P^+][Cl^-]$ essentially all of the solvation can be resolved, very little solvation has occurred by 100 ps, and that the average solvation time is 6.7 ns [11] (Table VI.1). The authors attributed the slower dynamics to the presence of nonpolarizable longer alkyl chains in the ionic liquid.

This discrepancy led us to check the integrity of our experimental system by studying the solvation dynamics of $[(C_6)_3C_{14}P^+][Cl^-]$ ourselves as a control experiment. Our results were consistent with those obtained for $[(C_4)_3C_{16}P^+][Br^-]$, namely there was a rapid component of solvation occurring within 100 ps and the average solvation time was 3.9 ns, faster than that reported [11] (Table VI.1). From this result, we concluded that at least some of the observed differences could be attributed to sample quality. Considerable discussion has been given to the effect of impurities on the properties of ionic liquids [44,66,67]. The role of water on the physical properties of ionic liquids is well known, and an excellent study is provided by Bright and coworkers [67]. This work indicates that the solvation probe, PRODAN, is highly sensitive to water content. On the other hand, Ito et al. [10] have shown that coumarin 153 is fortuitously insensitive to the presence of water, most likely owing to its hydrophobic character. In any case, the amount of water present in our sample (0.3 % by

weight, Table VI.1) provides only a minor perturbation in the results for PRODAN [67] and thus is expected to have a negligible effect on C153, based on the work of Ito et al. [10].

On the other hand, the $[(C_6)_3C_{14}P^+][Cl^-]$ we obtained from Cytec has a yellowish tint and a viscosity of 230 cP at 58°C. Maroncelli and coworkers obtained their sample from Cytec as well, reported similar sample properties, and performed their measurements with unpurified samples. Our purification procedure produces a colorless solvent with a viscosity of 80 cP at 58°C (Table VI.1). The purified solvent is ~3 times less fluorescent than the unpurified solvent when excited at 420 nm at room temperature. The solvation dynamics, however, are not drastically different from those obtained with the unpurified liquid. We have seen a lengthening in the longer solvation component in the unpurified solvent compared to that in the purified one (see the caption to Figure VI.6 and Table VI.1), which is in accordance with the higher viscosity of the unpurified solvent.

While it is possible that some of these minor differences that we observe result from solvent purity and viscosity, there are, however, other more general factors that may explain the contrast between our results and those of Maroncelli and coworkers: namely how C(t) is computed. How accurately the solvation correlation function, C(t), is constructed depends critically upon the quantities used in the denominator of equation VI.2. We have already indicated how sensitive the results can be to the choice of the time-window used to collect the data—namely, the effect upon $\nu(\infty)$ or, more precisely, $\nu(\text{“}\infty\text{”})$; but the determination of $\nu(\text{“0”})$ has its own idiosyncrasies. $\nu(\text{“0”})$ is the maximum of the estimated “zero-time” spectrum of the fluorescent probe after it has undergone intramolecular events contributing to its relaxation and before it has been altered by interactions with the solvent. The construction of the “zero-time” spectrum, which thus assumes such a time-scale separation of events, has

been described by Fee and Maroncelli [47], and we have shown that it is consistent with an independent method we have proposed, which compares the experimentally and theoretically determined reorganization energies in solvents over a wide range of polarities and indicates that 2068 cm^{-1} of "solvation" in coumarin 153 is intramolecular [24]. This value is consistent with the reorganization energies obtained from the "zero-time" spectra cited in Table VI.1, which are ~1950 cm^{-1}.

To gain insight into the apparent discrepancy between our results and those of Maroncelli and coworkers [11] we again considered the solvation of C153 in $[(C_6)_3C_{14}P^+][Cl^-]$. The required inputs for the calculation of the "zero-time" spectrum are the absorption (or excitation) spectrum of C153 in a nonpolar solvent and the corresponding spectrum in the polar solvent under investigation—in this case, the phosphonium ionic liquid. Also required is the emission spectrum of C153 in the nonpolar solvent. We used hexane as the nonpolar solvent to calculate the zero-time spectrum in polar solvents, while Maroncelli and coworkers used 2-methyl butane. Calculated "zero-time" peak frequencies using different spectra from different sources and obtained under different conditions are presented in Table VI.3. As indicated, the value of ν("0") is subject to the differences in the polar absorption/excitation spectra, the excitation wavelength, the nonpolar solvent, and even the fitting procedure used to obtain the spectral maximum. The data indicate that these factors can produce a difference of up to 350 cm^{-1} in the position of the "zero-time" spectrum, which can represent ~20 % of the total Stokes shift at 20-ns. Such factors must be taken into consideration when analyzing data or comparing results from different laboratories. Ideally, the reorganization energy, λ, may be the best parameter to use for the computation of C(t) because it is an integrated measure of the solvation dynamics (equation VI.1). The

construction of λ, however, requires high quality spectra, which are typically not provided by the traditional methods of spectral construction of 10-20 wavelength-resolved transients such as those illustrated in Figure VI.3.

We note, notwithstanding all the considerations enumerated above, that if the C(t) of Maroncelli and coworkers is normalized to begin at the end of the rapid component we observe, then their C(t) is within experimental error very similar to ours for both the purified and unpurified phosphonium liquid (Figure VI.6b and caption).

Finally, taking into consideration all of these issues, we believe that the full method of Fee and Maroncelli for obtaining the zero-time spectrum is the soundest available. The details of this method are clearly described in their paper [47], are briefly alluded to above, and provide the basis for the construction of an entire emission spectrum. In this paper, Fee and Maroncelli provide a simple equation for approximating the position of the zero-time spectrum:

$$\nu^{P}_{em}(0) = \nu^{P}_{abs} - (\nu^{nP}_{abs} - \nu^{nP}_{em}), \qquad \text{(VI.3)}$$

where P and nP refer to polar and nonpolar solvents, respectively. This approximate method has been employed by some workers, but we find that if it is successful in predicting the position of the "zero-time" spectrum, this success lies in using midpoint (rather than peak) frequencies in Equation VI.3: $\nu_{md} = (\nu_+ + \nu_-)/2$, where ν_+ and ν_- are the midpoint frequencies at the blue and red edges of the spectrum, respectively. Also, in order to be consistent, this procedure recommends the use of midpoint frequencies in the construction of C(t). The literature is often murky on these important details. We find that if midpoint frequencies are

not employed, the approximation always provides a lower value (by at least a few hundred wavenumbers) for the peak maximum of the zero-time spectrum than the full method. We have illustrated this for the systems investigated here in Table VI.4, which provides a comparison of the positions of the zero-time spectrum for the solvents studied here using the rigorous method and the approximate method with peak and midpoint frequencies. Equation VI.3 is a quick and useful way of estimating the position of the zero-time spectrum [37,68], but we suggest that it is no substitute for using the full method—especially when quantitative interpretations of C(t) are required.

For completeness, it has been suggested that the zero-time and steady-state frequencies could be obtained by rearranging Equation VI.2 to

$$\nu(t) = C(t)[\nu(0) - \nu(\infty)] + \nu(\infty), \qquad \text{(VI.4)}$$

expressing C(t) in terms of some function such as a sum of exponentials, using a curve-fitting procedure to extract the required parameters [69,70]. We find that this procedure yields unphysical results (such as negative steady-state frequencies) if all parameters are permitted to vary. It always yields severely red-shifted zero-time spectra. We suggest that such a fitting procedure will not produce an accurate result unless the time resolution of the experiment is adequate for resolving most of the solvation response in the first place.

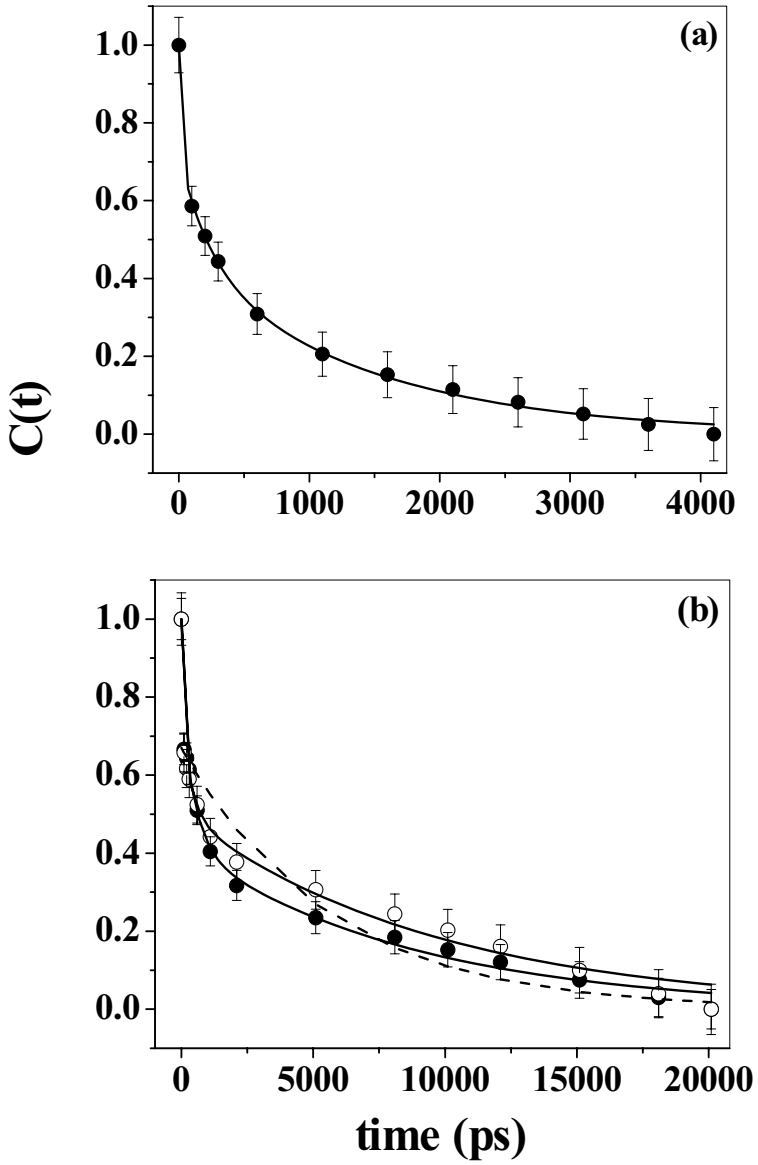

Figure VI.6. Solvation correlation functions for C153 in bulk $[(C_6)_3C_{14}P^+][Cl^-]$ (58°C) with (a) 4-ns and (b) 20-ns full-scale time windows. This system serves as a model system in our study. Solid circles: purified $[(C_6)_3C_{14}P^+][Cl^-]$; open circles: unpurified $[(C_6)_3C_{14}P^+][Cl^-]$. The dashed line in panel (b) was constructed using the stretched exponential, C(t) = 0.67 $[\exp(-t/2400\ ps)]^{0.43}$, based upon the parameters obtained by Maroncelli and coworkers [11], with the exception that the preexponential factor was normalized to our curves at the point at which the initial rapid component of solvation had been completed, namely 100 ps. For purified $[(C_6)_3C_{14}P^+][Cl^-]$, C(t) [4-ns] = [0.28 exp(–t/2.8 ps) + 0.27 exp(–t/240 ps) + 0.45 exp(–t/1420 ps)] and C(t) [20-ns] = [0.23 exp(–t/2.5 ps) + 0.35 exp(–t/530 ps) + 0.42 exp(–t/8850 ps)]. For unpurified $[(C_6)_3C_{14}P^+][Cl^-]$, C(t) [20-ns] = [0.28 exp(–t/2.5 ps) + 0.22 exp(–t/410 ps) + 0.50 exp(–t/9710 ps)].

Table VI.3. "Zero-time" Spectral Parameters for C153 in $[(C_6)_3C_{14}P^+][Cl^-]$

Spectral maxima [a]	nonpolar solvent [b]	ν("0") (cm^{-1}) [a]
ν_{ex} = 23590 cm^{-1} [c]	hexane	20710
ν_{abs} = 23430 cm^{-1} [d, 11]	hexane	20560
ν_{ex} = 23590 cm^{-1} [c]	2-methyl butane	20630
ν_{abs} = 23430 cm^{-1} [d, 11]	2-methyl butane	20420 [e]

[a] Peak maxima of the excitation (ν_{ex}) (or absorption (ν_{abs})) and "zero time" (ν("0")) spectra of C153 in $[(C_6)_3C_{14}P^+][Cl^-]$ obtained from lognormal fitting. The spectra of C153 in 2-methyl butane and $[(C_6)_3C_{14}P^+][Cl^-]$ were generously provided by Mark Maroncelli. Excitation spectra in our laboratory were collected at an emission wavelength of 600 nm. Unless otherwise indicated, the data were obtained with the purified phosphonium liquid.

[b] Nonpolar solvent employed to obtain the excitation or absorption and emission spectra used for the construction of the "zero-time" spectrum. The $\nu_{ex/abs}$ and ν_{em} peak frequencies of C153 are very similar in hexane and 2-methyl butane. ν_{ex} (hexane) = 25710 cm^{-1}, ν_{em} (hexane) = 22370 cm^{-1} and ν_{abs} (2-methyl butane) = 25700 cm^{-1}, ν_{em} (2-methyl butane) = 22300 cm^{-1}.

[c] An excitation wavelength of 420 nm was used for the determination of the "zero-time" emission spectrum.

[d] An excitation wavelength of 427 nm was used for the determination of the "zero-time" emission spectrum using an unpurified sample [11].

[e] "Zero-time" emission maximum, ν("0") = 20360 cm^{-1}, obtained by Maroncelli and coworkers [11].

Table VI.4. Comparison of "Zero-Time" Spectral Positions (cm^{-1}) Using Different Methods

System	$\nu(0)$ [a] full peak	$\nu(0)$ [b] approx peak	$\Delta\nu$ [c] full peak – approx peak	$\nu(0)$ [d] approx mid	$\Delta\nu$ [e] full peak – approx mid	$\nu(0)$ [f] full mid	$\Delta\nu$ [g] full mid – approx mid
$[(C_4)_3C_{16}P^+][Br^-]$ bulk, 66°C	20560	20130	430	20300	260	20340	40
$[(C_4)_3C_{16}P^+][Br^-]$ micelle, room temperature	20020	19540	480	19730	290	19770	40
$[(C_4)_3C_{16}P^+][Br^-]$ micelle, 66°C	20200	19650	550	19910	290	19950	40
$[(C_6)_3C_{14}P^+][Cl^-]$ bulk, purified, 58°C	20710	20250	460	20450	260	20460	10
$[(C_6)_3C_{14}P^+][Cl^-]$ bulk, unpurified, 58°C	20550	20080	470	20230	320	20240	10

[a] Maximum of zero-time spectrum obtained from lognormal fitting using the full Fee and Maroncelli procedure.

[b] Maximum of zero-time spectrum using the Fee and Maroncelli approximation, Equation VI.3, where peak frequencies are employed.

[c] Difference between the methods employing the full procedure and the approximation using peak frequencies.

[d] Position of zero-time spectrum using the Fee and Maroncelli approximation, Equation VI.3, where midpoint frequencies are employed, $\nu_{md} = (\nu_+ + \nu_-)/2$, where ν_+ and ν_- are the midpoint frequencies at the blue and red edges of the spectrum, respectively. The midpoint values are recommended by Fee and Maroncelli [47].

[e] Difference between the methods employing the full procedure using peak maxima and the approximation using midpoint frequencies.

[f] Midpoint position of the zero-time spectrum using the full Fee and Maroncelli procedure.

[g] Difference between the methods employing the full procedure and the approximation using midpoint frequencies. The smaller deviation should not affect the value of the total Stokes shift and the nature of C(t) significantly because in this case one should also consider the midpoint frequencies from the lognormal fits of different time resolved spectra.

Conclusions

In studying a phosphonium ionic liquid that can form micelles in water, we conclude that our analysis of the comparable situation in an imidazolium liquid [36] is not as definitive as we had proposed: namely that the majority of the early-time solvation arises from the organic cation. Part of the difficulty in performing this analysis is most likely due to the amount of water that is associated with the micelle.

In the course of this work, we have found that the calculation of the solvation correlation function, C(t) is surprisingly dependent upon the methods with which the zero-time spectrum is constructed. An interesting means of validating such spectral construction may ultimately be based upon computing C(t) using dielectric spectra, as we have done elsewhere [25]. Finally, we have noted in another context, that of solvation by a protein environment [61], how important an accurate computation of C(t) is for the interpretation of the experimental results.

Acknowledgements

We thank Professor Mark Maroncelli for sharing his data for coumarin 153 in 2-methyl butane and in the phosphonium chloride and for helpful comments. We thank Professor Xueyu Song for helpful comments.

References

(1) Seddon, K. R. Nature (Materials) 2003, 2, 363.

(2) Anderson, J. L.; Ding, J.; Welton, T.; Armstrong, D. W. J. Am. Chem. Soc. 2002, 124, 14247.

(3) Anderson, J. L.; Armstrong, D. W.; Wei, G.-T. Anal. Chem. 2006, 78, 2893.

(4) Pandey, S. Anal. Chim. Acta 2006, 556, 38.

(5) Karmakar, R.; Samanta, A. J. Phys. Chem. A 2002, 106, 6670.

(6) Karmakar, R.; Samanta, A. J. Phys. Chem. A 2002, 106, 4447.

(7) Karmakar, R.; Samanta, A. J. Phys. Chem. A 2003, 107, 7340.

(8) Ingram, J. A.; Moog, R. S.; Ito, N.; Biswas, R.; Maroncelli, M. J. Phys. Chem. B 2003, 107, 5926.

(9) Ito, N.; Arzhantsev, S.; Maroncelli, M. Chem. Phys. Lett. 2004, 396, 83.

(10) Ito, N.; Arzhantsev, S.; Heitz, M.; Maroncelli, M. J. Phys. Chem. B 2004, 108, 5771.

(11) Arzhantsev, S.; Ito, N.; Heitz, M.; Maroncelli, M. Chem. Phys. Lett. 2003, 381, 278.

(12) Arzhantsev, S.; Hui, J.; Baker, G. A.; Naoki, I.; Maroncelli, M. "Solvation dynamics in ionic liquids, results from ps and fs emission spectroscopy." Femtochemistry VII, 2005.

(13) Arzhantsev, S.; Hui, J.; Naoki, I.; Maroncelli, M. Chem. Phys. Lett. 2006, 417, 524.

(14) Hyun, B.-R.; Dzyuba, S. V.; Bartsch, R. A.; Quitevis, E. L. J. Phys. Chem. A 2002, 106, 7579.

(15) Giraud, G.; Gordon, C. M.; Dunkin, I. R.; Wynne, K. J. Chem. Phys. 2003, 119, 464.

(16) Cang, H.; Li, J.; Fayer, M. D. J. Chem. Phys. 2003, 119, 13017.

(17) Shirota, H.; Funston, A. M.; Wishart, J. F.; Castner, E. W., Jr. J. Chem. Phys. 2005, 122, 184512.

(18) Rajian, J. R.; Li, S.; Bartsch, R. A.; Quitevis, E. L. Chem. Phys. Lett. 2004, 393, 372.

(19) Shirota, H.; Castner, E. W., Jr. J. Phys. Chem. A 2005, 109, 9388.

(20) Weingärtner, H.; Knocks, A.; Schrader, W.; Kaatze, U. J. Phys. Chem. A 2001, 105, 8646.

(21) Wakai, C.; Oleinikova, A.; Ott, M.; Weingärtner, H. J. Phys. Chem. B 2005, 109, 17028.

(22) Ito, N.; Huang, W.; Richert, R. J. Phys. Chem. B 2006, 110, 4371.

(23) Chowdhury, P. K.; Halder, M.; Sanders, L.; Calhoun, T.; Anderson, J. L.; Armstrong, D. W.; Song, X.; Petrich, J. W. J. Phys. Chem. B 2004, 108, 10245.

(24) Headley, L. S.; Mukherjee, P.; Anderson, J. L.; Ding, R.; Halder, M.; Armstrong, D. W.; Song, X.; Petrich, J. W. J. Phys. Chem. A 2006, 110, 9549.

(25) Halder, M.; Headley, L. S.; Mukherjee, P.; Song, X.; Petrich, J. W. J. Phys. Chem. A 2006, 110, 8623.

(26) Margulis, C. J.; Stern, H. A.; Berne, B. J. J. Phys. Chem. B 2002, 106, 12017.

(27) Shim, Y.; Duan, J.; Choi, M. Y.; Kim, H. J. J. Chem. Phys. 2003, 119, 6411.

(28) Znamenskiy, V.; Kobrak, M. N. J. Phys. Chem. B 2004, 108, 1072.

(29) Kobrak, M. N.; Znamenskiy, V. Chem. Phys. Lett. 2004, 395, 127.

(30) Del Popolo, M. G.; Voth, G. A. J. Phys. Chem. B 2004, 108, 1744.

(31) Morrow, T. I.; Maginn, E. J. J. Phys. Chem. B 2002, 106, 12807.

(32) Hu, Z.; Margulis, C. J. Proc. Natl. Acad. Sci. U. S. A. 2006, 103, 831.

(33) Lang, B.; Angulo, G.; Vauthey, E. J. Phys. Chem. A 2006, 110, 7028.

(34) Samanta, A. J. Phys. Chem. B 2006, 110, 13704.

(35) J. Phys. Chem. B 2007, 111, 4639-5029 (special issue).

(36) Mukherjee, P.; Crank, J. A.; Halder, M.; Armstrong, D. W.; Petrich, J. W. J. Phys. Chem. A 2006, 110, 10725.

(37) Adhikari, A.; Sahu, K.; Dey, S.; Ghosh, S.; Mandal, U.; Bhattacharyya, K. J. Phys. Chem. B 2007, 111, 12809.

(38) Chakrabarty, D.; Seth, D.; Chakraborty, A.; Sarkar, N. J. Phys. Chem. B 2005, 109, 5753.

(39) Chakraborty, A.; Seth, D.; Chakrabarty, D.; Setua, P.; Sarkar, N. J. Phys. Chem. A 2005, 109, 11110.

(40) Seth, D.; Chakraborty, A.; Setua, P.; Sarkar, N. Langmuir 2006, 22, 7768.

(41) Seth, D.; Chakraborty, A.; Setua, P.; Sarkar, N. J. Phys. Chem. B 2007, 111, 4781.

(42) Gao, Y.; Li, N.; Zheng, L.; Bai, X.; Yu, L.; Zhao, X.; Zhang, J.; Zhao, M.; Li, Z. J. Phys. Chem. B 2007, 111, 2506.

(43) Eastoe, J.; Gold, S.; Rogers, S. E.; Paul, A.; Welton, T.; Heenan, R. K.; Grillo, I. J. Am. Chem. Soc. 2005, 127, 7302.

(44) Earle, M. J.; Gordon, C. M.; Plechkova, N. V.; Seddon, K. R.; Welton, T. Anal. Chem. 2007, 79, 758.

(45) Turro, N. J.; Yekta, A. J. Am. Chem. Soc. 1978, 100, 5951.

(46) Stam, J. v.; Depaemelaere, S.; De Schryver, F. C. J. Chem. Ed. 1998, 75, 93.

(47) Fee, R. S.; Maroncelli, M. Chem. Phys. 1994, 183, 235.

(48) Eriksson, J. C.; Gillberg, G. Acta Chem. Scand. 1996, 20, 2019.

(49) Weidemaier, K.; Tavernier, H. L.; Fayer, M. D. J. Phys. Chem. B 1997, 101, 9352.

(50) Chakraborty, A.; Chakrabarty, D.; Harza, P.; Seth, D.; Sarkar, N. Chem. Phys. Lett. 2003, 382, 508.

(51) Kumbhakar, M.; Nath, S.; Mukherjee, T.; Pal, H. J. Chem. Phys. 2004, 120, 2824.

(52) Jimenez, R.; Fleming, G. R.; Kumar, P. V.; Maroncelli, M. Nature 1994, 369, 471.

(53) Vajda, S.; Jimenez, R.; Rosenthal, S. J.; Fidler, V.; Fleming, G. R.; Castner, E. W., Jr. J. Chem. Soc., Faraday Trans. 1995, 91, 867.

(54) Pal, S. K.; Peon, J.; Bagchi, B.; Zewail, A. H. J. Phys. Chem. B 2002, 106, 12376.

(55) Nandi, N.; Bagchi, B. J. Phys. Chem. B 1997, 101, 10954.

(56) Nandi, N.; Bagchi, B. J. Phys. Chem. A 1998, 102, 8217.

(57) Nandi, N.; Bhattacharyya, K.; Bagchi, B. Chem. Rev. 2000, 100, 2013.

(58) Bhattacharya, K. Acc. Chem. Res. 2003, 36, 95.

(59) Pal, S. K.; Zewail, A. H. Chem. Rev. 2004, 104, 2099.

(60) Ghosh, S.; Mandal, U.; Adhikari, A.; Dey, S.; Bhattacharya, K. Int. Rev. Phys. Chem. 2007, 26, 421.

(61) Halder, M.; Mukherjee, P.; Bose, S.; Hargrove, M. S.; Song, X.; Petrich, J. W. J. Chem. Phys. 2007, 127, 055101.

(62) Streletzky, K.; Phillies, G. D. J. Langmuir 1995, 11, 42.

(63) Sen, P.; Mukherjee, S.; Halder, A.; Bhattacharyya, K. Chem. Phys. Lett. 2004, 385, 357.

(64) Kumbhakar, M.; Goel, T.; Mukherjee, T.; Pal, H. J. Phys. Chem. B 2004, 108, 19246.

(65) Bradaric, C. J.; Downard, A.; Kennedy, C.; Robertson, A. J.; Zhou, Y. Green Chem. 2003, 5, 143.

(66) Seddon, K. R.; Stark, A.; Torres, M.-J. Pure Appl. Chem. 2000, 72, 2275.

(67) Baker, S. N.; Baker, G. A.; Munson, C. A.; Chen, F.; Bukowski, E. J.; Cartwright, A. N.; Bright, F. V. Ind. Eng. Chem. Res. 2003, 42, 6457.

(68) Sahu, K.; Mondal, S. K.; Ghosh, S.; Roy, D.; Sen, P.; Bhattacharyya, K. J. Phys. Chem. B 2006, 110, 1056.

(69) Maroncelli, M.; Fleming, G. R. J. Chem. Phys. 1987, 86, 6221.

(70) Horng, M. L.; Gardecki, J. A.; Papazyan, A.; Maroncelli, M. J. Phys. Chem. 1995, 99, 17311.

CHAPTER VII. CHARACTERIZATION OF THE INTERACTIONS OF FLUORESCENT PROBES WITH PROTEINS: COUMARIN 153 AND 1,8-ANS IN COMPLEX WITH HOLO- AND APOMYOGLOBIN

A paper published in Photochemistry and Photobiology

Prasun Mukherjee[1], Mintu Halder[1], Mark S. Hargrove[2], and Jacob W. Petrich[1,*]

Abstract

In order to provide a thorough characterization of a system with which to study the dielectric response of a protein, a well defined system complex of a fluorescent probe and protein is required. We have argued that such a system is provided by coumarin 153 and apomyoglobin (Photochem. Photobiol. 79, 440-446 (2004)). In order to demonstrate further that coumarin 153 exhibits negligible nonspecific binding to the surface of apomyoglobin, we study its interactions with both the apo and holo proteins. We further make a similar comparison with 8-anilino-1-naphthalenesulfonic acid, for which an NMR structure with apomyoglobin has been obtained. Our results confirm the appropriateness of the system of coumarin 153 and apomyoglobin for the investigation of solvation by the protein matrix.

Reprinted with permission from Photochemistry and Photobiology, 2006, 82(6), 1586–1590.
[1] Department of Chemistry, Iowa State University, Ames, Iowa 50011.
[2] Departments of Biochemistry, Biophysics, and Molecular Biology Iowa State University, Ames, Iowa 50011.
[*] Author to whom correspondence should be addressed.

Introduction

Studies of the solvation dynamics of proteins offer a powerful tool in understanding the local dielectric response. Considerable effort in both the theoretical and experimental domains has been devoted to the study of solvation dynamics in protein environments [1-21]. Such effort is motivated not only by the intrinsic interest of proteins but also because proteins furnish the most challenging test for understanding solvation in a heterogeneous environment. We have argued elsewhere that the myoglobin system is particularly interesting in this regard, and we have argued that it is particularly suited to this type of study [22]. Early investigations of solvation in myoglobin suggested that a slow relaxation (~1 ns) exists in myoglobin [19, 20] in contrast to different polar solvents. This may not be unexpected because of the structural constraints present in the protein environment.

Previous work involving the myoglobin used different fluorescent probes such as anilinonaphthalene sulfonates (ANS), 2,6-ANSDMA and DANCA [19, 20]. Recently we have furnished a characterization of the binding of the fluorescence probe, coumarin 153 (C153, Figure VII.1) with apomyoglobin (apoMb) [22]. Much of the work presented here is motivated by these results. In this report we have characterized the binding of two structurally dissimilar probes namely, ANS and C153, with both holo and apomyoglobin. Comparison of the binding of the probe molecules with holo and apoMb can substantiate the difference in the nature of interaction in these two different environments. The choice of the systems was based on the following considerations. First, the structure of myoglobin and their mutants have been determined with high resolution. Second, the structure of the complex between apoMb and ANS is known.

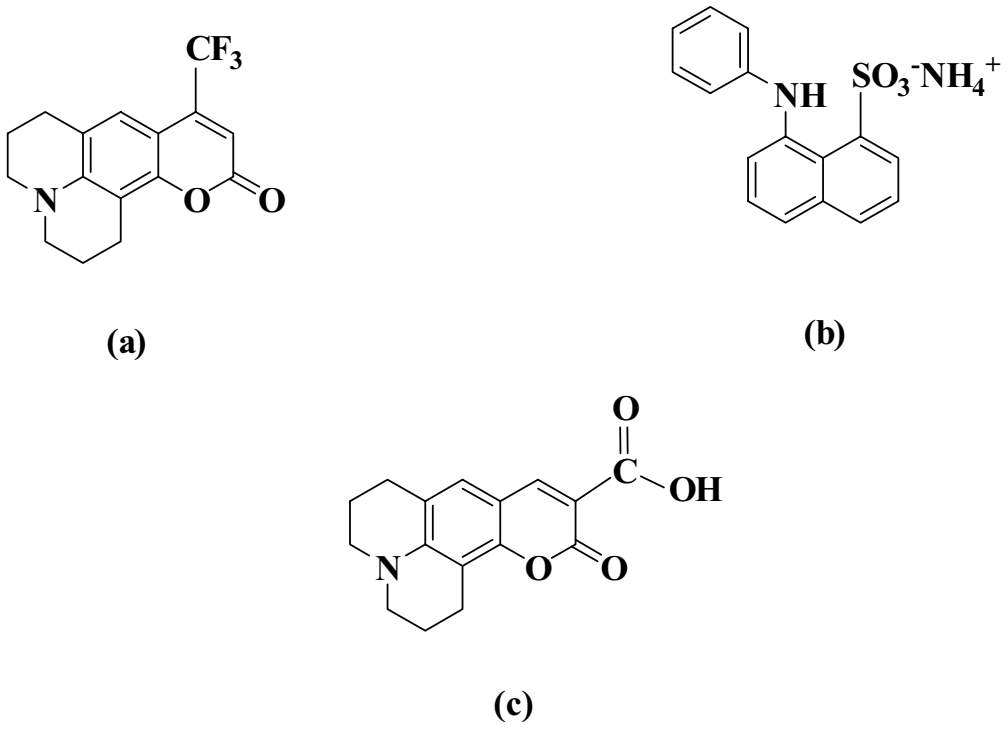

Figure VII.1. Structures of the fluorescent probe molecules studied: (a) coumarin 153, (b) ammonium salt of 8-anilino-1-naphthalenesulfonic acid and (c) coumarin 343.

Materials and Methods

C153 was purchased from Exciton Inc. (Dayton, OH) and used without further purification. Ammonium salt of 8-anilino-1-naphthalenesulfonic acid was purchased from Fluka and used without further purification. C343 was purchased from Acros Organics and was used without further purification. Horse heart myoglobin (Mb) was purchased from Sigma. ApoMb was prepared using a method described elsewhere [23]. C153 has very low solubility in water. A stock solution of C153 was prepared by adding a microliter amount of a concentrated solution of C153 in methanol to water. That is, concentrated C153/MeOH was added to water, keeping the organic content < 0.3 % (v/v) in the final solution. To

prepare a 5×10^{-5} M solution of C153/water, 5 µL of 20×10^{-3} M C153/MeOH solution was added to 2 ml of water. The resulting solution was sonicated. The stock solution of ANS was prepared in water. All samples were equilibrated for about 2 hours before taking the steady state measurements. The protein/C343 solutions were equilibrated overnight to ensure maximum interaction with protein.

Binding constant measurements by fluorescence titrations. Two stock solutions of apoMb and C153 or ANS were prepared, each having concentration 5×10^{-5} M. For experiments with C343 the concentrations of stock protein and probe solutions were 1×10^{-6} M respectively. From these stock solutions, seven 200 µL samples were prepared by increasing the mole fraction of the probe molecule X, 0.1, 0.2, 0.25, 0.5, 0.75, 0.8 and 0.9. For the experiments involving C153 and ANS, the concentration of probe molecule varies from 5×10^{-6} M ($X_{probe} = 0.1$) to 4.5×10^{-5} M ($X_{probe} = 0.9$) keeping [Protein] + [Probe] = 5×10^{-5} M. In the C343 solutions, the concentration of probe varies from 1×10^{-7} M ($X_{C343} = 0.1$) to 9×10^{-7} M ($X_{C343} = 0.9$) keeping [Protein] + [C343] = 1×10^{-6} M. After the samples were equilibrated for about 2 hours (for C153 and ANS) and overnight (for C343) to ensure complete complex formation, the steady-state fluorescence spectra were taken. The fluorescence intensities were plotted against the mole fraction of the probe molecule, the maximum in both cases occurred at a mole fraction of 0.5, indicating the binding stoichiometry between apoMb and C153/ANS as 1:1. (C153 has a very low solubility in water, and ANS has a very low quantum yield in water (0.004) [24]. The apoMb itself does not fluoresce in the region where the complex emits. So, the fluorescence intensities are

directly proportional to the concentration of protein-probe complex.) The binding constant, K_B, was calculated using the following equation [25].

$$K_B = \frac{I \times I_0}{(I_0 - I)(I_0[\text{apoMb}]_T - I[\text{probe}]_T)} \qquad \text{(VII.1)}$$

I_0 is the maximum fluorescence intensity at X = 0.5, and I is the fluorescence intensity at any other mole fraction. The subscript T indicates the total concentration of either apoMb or the probe molecule. The dissociation constant K_D of the complex is calculated as the reciprocal of calculated K_B value. The same procedure was also adopted for holoMb-probe interaction.

Steady-state measurements. Steady-state absorbance spectra were obtained on Perkin Elmer Lambda 18 double beam UV-visible spectrophotometer with 1-nm resolution. Solutions of holoMb were prepared by dissolving known amount of protein in 10 mM phosphate buffer solution. The concentration of apoMb was determined spectrophotometrically using the extinction coefficient 15.2 $mM^{-1}cm^{-1}$ at 280 nm [22]. Steady-state fluorescence spectra were obtained on a Spex Fluoromax with a 4-nm bandpass and corrected for lamp spectral intensity and detector response. For both fluorescence and absorption measurements, a 3-mm path-length quartz cuvette was used.

Results and Discussion

The binding of C153 and ANS with holoMb and apoMb has been characterized using Job's plots. Representative plots of complex formation between C153/holoMb and C153/apoMb are shown in Figure VII.2a. The corresponding data for ANS binding are given in Figure VII.2b. In the case of holoMb, the fluorescence intensity increases with the mole fraction of C153, which suggests binding of the probe molecule to the protein surface. The

occurrence of the maxima at mole fraction 0.5 in apoMb is a clear indication of 1:1 complex formation between C153 and apoMb. A similar trend in fluorescence intensity is observed in the case of ANS binding to apoMb (Fig. VII.2b) indicating a 1:1 binding stoichiometry. For the apoMb/C153 complex we have obtained a dissociation constant of 18 ± 6 μM. For the apoMb/ANS complex we obtain 10 ± 5 μM.

For the ANS/holoMb system we observe an inflection in the fluorescence intensity around 0.5 mole fraction of ANS, indicating 1:1 binding of ANS to holoMb. This gives a dissociation constant of 6 ± 2 μM, using equation VII.1. It would thus appear that ANS binds more tightly with holoMb than with apoMb (6 μM for ANS-holoMb as opposed to 10 μM for ANS-apoMb), which is physically unreasonable because in holoMb the major binding site, the heme pocket, is occupied. This apparent discrepancy may be rectified by consideration of the fluorescence quantum yields. The quantum yield of ANS in the protein environments are calculated with respect to that of ANS in MeOH, which is taken as 0.21 [26]. We thus measure the fluorescence quantum yield of ANS to be 0.67 in apoMb and 0.0065 in holoMb. Taking these values into account, the dissociation constant for the holoMb/ANS complex is approximately 600 μM. That holoMb forms a weak 1:1 complex with ANS but not with C153 may be attributed to the presence of charged group in ANS, which can interact with ionized surface residues but not the nonpolar hemepocket.

Representative fluorescence spectra are shown in Figures VII.3 and VII.4. Upon binding to apoMb the fluorescence intensity of ANS and C153 increases drastically compared to the bulk aqueous solvent, and the peak maximum shifts to the blue, which indicates binding of the probe molecules to the heme pocket. For C153 binding to holoMb, the fluorescence intensity increases with increase in mole fraction of C153. The peak

maxima at ~550 nm indicate that the probe molecule is exposed to the polar aqueous environment while fixed to the protein surface. Most interestingly, the fluorescence intensity of C153 was found to be equal in holoMb and apoMb with the C153 mole fraction 0.9 (Figure VII.3). This observation unambiguously points toward binding of C153 to the holoMb surface. The slight change in the intensity values in these two cases might be attributed to the experimental error associated with these measurements.

Finally, there is a significant Stokes shift of bound probe molecule in apoMb with respect to that in bulk polar solvents. This clearly demonstrates the difference between the heme pocket and the bulk solvent. The steady-state spectra can be used to compute the reorganization energy, λ, by means of [14]

$$\lambda = \hbar \frac{\int_0^\infty \mathrm{d}\upsilon [\sigma_a(\upsilon) - \sigma_f(\upsilon)]\upsilon}{\int_0^\infty \mathrm{d}\upsilon [\sigma_a(\upsilon) + \sigma_f(\upsilon)]} \qquad \text{(VII.2)}$$

The $\sigma_{a,f}$ are the absorption (or excitation) and emission spectral line-shapes, respectively. The reorganization energy is widely used as a measure of the strength of interactions between a chromophore and its surrounding dielectric media in solvation dynamics studies. It is usually taken as half of the Stokes shift. This estimation is accurate if the excitation and emission spectra are Gaussian, but it becomes unreliable if they are not. The reorganization energies for the apoMb/C153 and apoMb/ANS complexes were found to be 2290 cm^{-1} and 3400 cm^{-1}, the corresponding values in C153/methanol and ANS/water were found to be 2885 cm^{-1} and 4650 cm^{-1} (Table VII.1). This clearly demonstrates the presence of the probe molecules in two completely different environments.

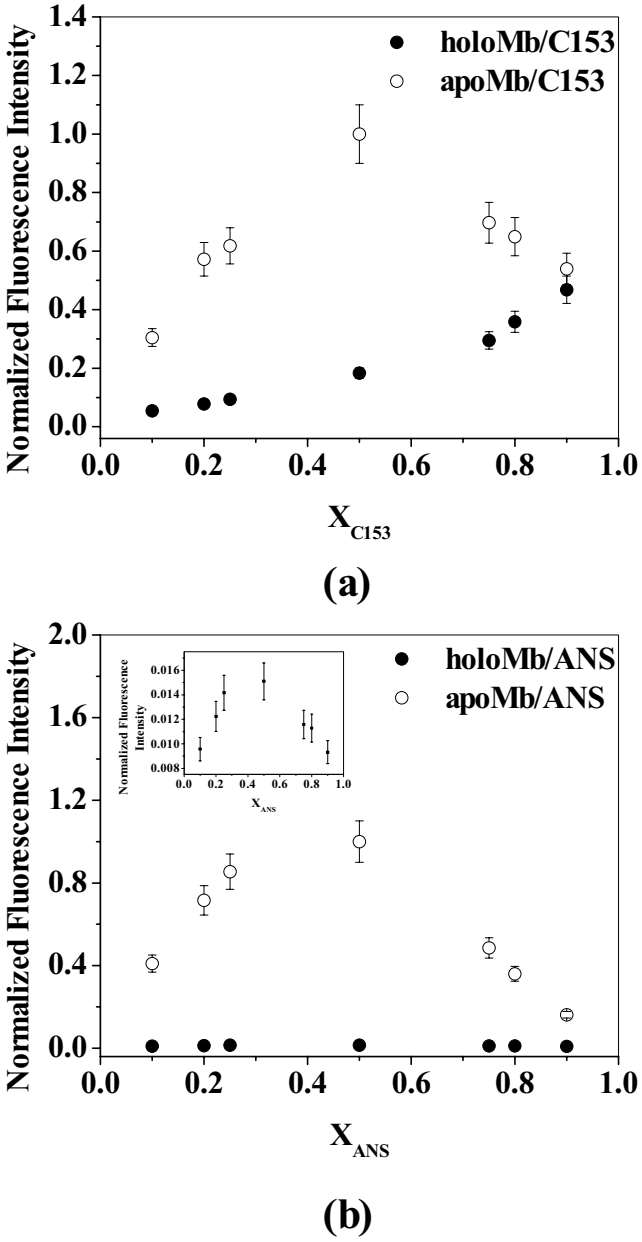

Figure VII.2. Job's plot for the complex formation of (a) C153 and (b) ANS with holoMb (solid circles) and apoMb (open circles); (inset), the Job's plot for the holoMb/ANS system on an expanded ordinate scale to accentuate the weak 1:1 binding. With holoMb, the fluorescence intensity increases with the mole fraction of C153, indicating binding of the probe molecule to the protein surface. The occurrence of the maxima at mole fraction 0.5 in apoMb is a clear indication of 1:1 complex formation between C153/ANS and apoMb. The data presented are an average of three measurements. The calculated dissociation constant for the complex apoMb/C153 is 18 ± 6 μM, the corresponding value for apoMb/ANS is 10 ± 5 μM. The data are normalized to the fluorescence intensity of apoMb/probe at the probe mole fraction of 0.5.

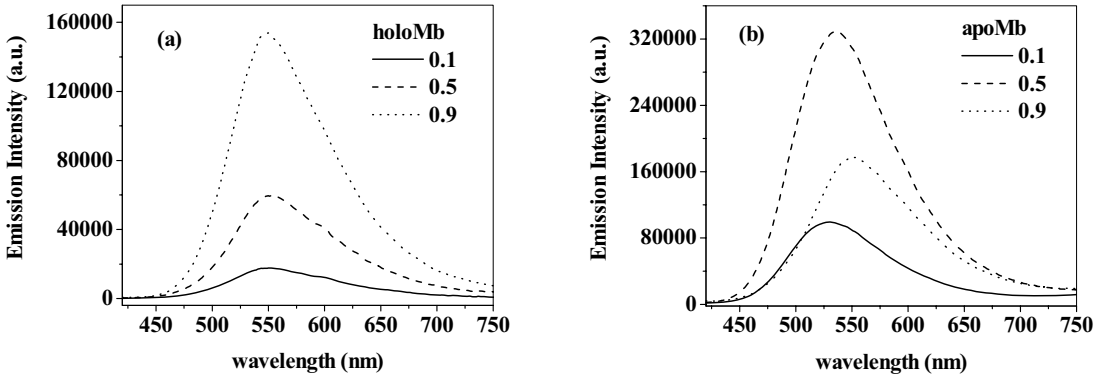

Figure VII.3. Representative fluorescence spectra for C153 with (a) holoMb and (b) apoMb. The solid, dashed, and dotted lines are for C153 at mole fractions of 0.1, 0.5 and 0.9, respectively. Most interestingly, within experimental error the fluorescence intensity of C153 is found to be equal in holoMb and apoMb with the C153 mole fraction 0.9. This points toward the binding of C153 on the surface of the protein. The excitation wavelength for the emission spectra is 407 nm.

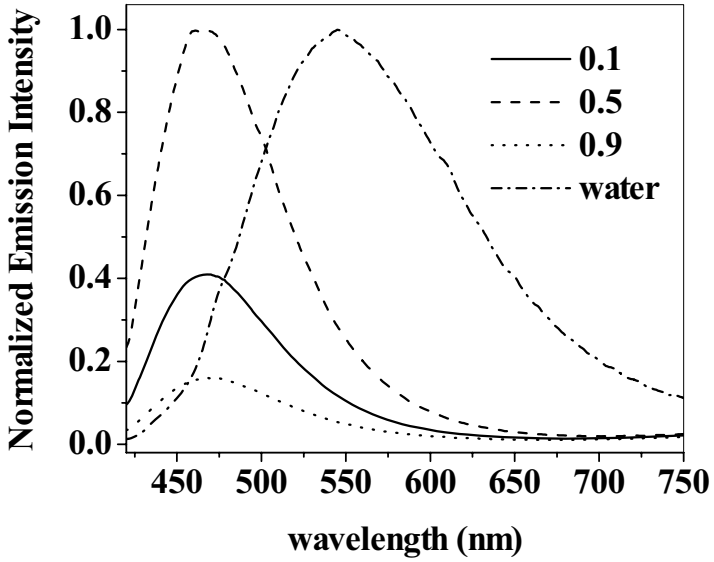

Figure VII.4. Representative fluorescence spectra for ANS in apoMb. The solid, dashed and dotted lines are for ANS mole fraction 0.1, 0.5 and 0.9 respectively. The excitation wavelength for the emission spectra was 407 nm. For purposes of comparison, the spectrum of ANS in water is also presented, and arbitrarily normalized to a peak intensity of unity.

Table VII.1. Binding of fluorescent probes to myoglobin

system	K_D (μM)	λ_{SS} (cm^{-1}) [b]
ANS/H_2O	------	4650 ± 100
ANS/holoMb	600	2865 ± 20
ANS/apoMb	10 ± 5	3400 ± 15
C153/MeOH	------	2885 ± 10
C153/holoMb	surface binding	2770 ± 25
C153/apoMb	18 ± 6 [a]	2290 ± 20
C343/H_2O	------	2030 ± 10
C343/holoMb	------	2130 ± 20
C343/apoMb	------	1950 ± 25

[a] In our earlier work [22], we report 5.65 ± 0.25 μM (from a Job's plot) and 13 ± 2 μM (from capillary electrophoresis) for the C153/apoMb complex.
[b] Computed from equation VII.2.

Comparison of the reorganization energy of apoMb/C153 with that of C153/methanol is not optimal, of course, because the protein/probe complex is in water and thus the proper comparison is with C153 in water. Such a comparison is, however, prohibited because of the negligible solubility of C153 in water. To this end, we attempted a comparison based upon coumarin 343 (C343, Figure VII.1). As Figure VII.5 and Table VII.1 demonstrate, this comparison was not fruitful because the enhanced solubility of C343 in water does not permit it to partition well between the protein and bulk water. Also, the dipole moment change of C343 upon electronic excitation is apparently not as large as that of C153; and consequently the reorganization energy of C343 in water is less than that of C153 in methanol, the less polar solvent: 2030 as opposed to 2885 cm^{-1}, respectively. What this failed comparison does demonstrate, however, is that the presence of the carboxylic acid group in C343 eliminates its ability to bind specifically to the heme pocket of apoMb and that this group

when ionized (pK_a = 4.65 [27]), provides an interaction for surface binding to the holo protein, as observed at 0.9 mole fraction in Figure VII.5.

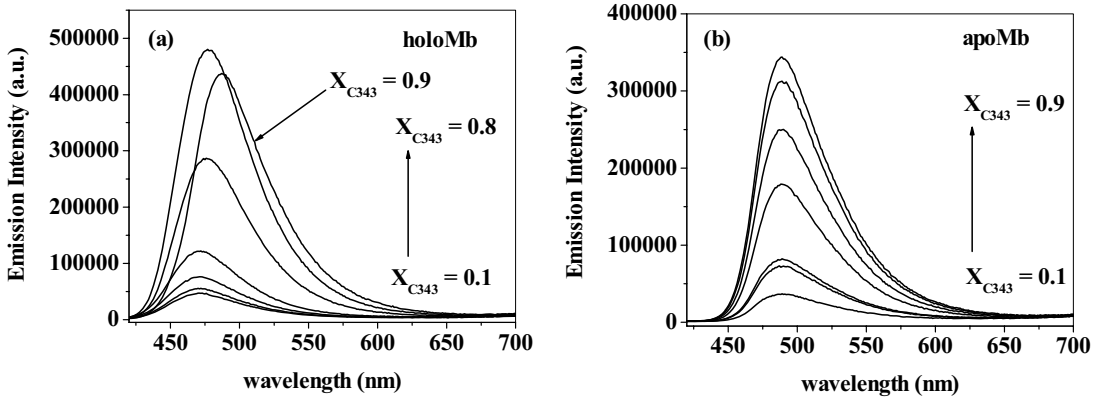

Figure VII.5. Fluorescence spectra for C343 with (a) holoMb and (b) apoMb. For apoMb, the fluorescence increases as indicated by the vertical arrow with mole fraction x = 0.1, 0.2, 0.25, 0.5, 0.75, 0.8. 0.9, indicating that there is no significant interaction between the protein and C343. For holoMb, the fluorescence intensity increases for the same progression of mole fractions up 0.8. At x = 0.9, however, there is a decrease in intensity and a shift, indicative of protein/probe interaction.

Conclusions

Elsewhere [22] we had argued that the apoMb/C153 complex was ideal for studying the solvation dynamics of a protein. This was based on the extensive characterization of C153 as a solvation probe [21, 28-36] and also on our results from molecular dynamics simulations, Job's plots, capillary electrophoresis, circular dichroism, and an array of steady-state and time-resolved measurements that C153 bound specifically to the apoMb hemepocket. In order to respond to remaining skepticism, the measurements discussed here were undertaken to explicitly demonstrate that the interaction between apoMb and C153 is not a surface interaction. If it were a surface interaction, then the Job's plots for the apo and holo proteins would be, if not identical, at least very similar.

The existence of an NMR structure for the apoMb/ANS complex [37] incited us to study the behavior of C153 and ANS with both the apo protein–and the holo protein as well. Here, we have concluded that the two fluorophores bind comparably well to the apo protein, which is consistent with the NMR data. We have also concluded that ANS exhibits a 1:1 binding with the holo protein, presumably because of its charge. Consequently, the complex of apoMb with C153 (and possibly with ANS) provides an extremely promising means for studying the protein dielectric response.

Acknowledgements

We thank Drs. Pramit Chowdhury and Suman Kundu and Ms. Puspita Halder for their helpful comments and assistance.

References

1. Zheng, C., Wong, C.F., McCammon, J.A., Wolynes, P.G. (1989) Classical and Quantum Aspects of Ferrocytochrome c. Chem. Scripta 29A, 171-179.
2. Simonson, T. (2002) Gaussian Fluctuations and Linear Response in an Electron Transfer Protein. Proc. Natl. Acad. Sci. U. S. A. 99, 6544-6549.
3. Warshel, A., Russel, S.T. (1984) Calculation of Electrostatic Interactions in Biological Systems and in Solutions. Q. Rev. Biol. 17, 283.
4. Sharp, K.A., Honig, B. (1990) Electrostatic Interactions in Macromolecules: Theory and Applications. Ann. Rev. Biophys. Chem. 19, 301.
5. Schutz, C.N., Warshel, A. (2001) What are the Dielectric "Constants" of Proteins and How to Validate Electrostatic Models? Proteins: Struc. Func. Gen. 44, 400.

6. Simonson, T. (2001) Macromolecular Electrostatics: Continuum Models and Their Growing Pains. Curr. Opin. Struc. Biol. 11, 243.

7. Nakamura, H. (1996) Roles of Electrostatic Interaction in Proteins. Q. Rev. Biophys. 29, 1.

8. Brooks, C.L., Karplus, M., Pettitt, B.M. (1987) Proteins: A Theoretical Perspective of Dynamics, Structure, and Thermodynamics. Adv. Chem. Phys. 71, 1.

9. Sheppard, R.J., Grant, E.H., South, G.P. (1978) Dielectric Behavior of Biological Molecules, first edition. Oxford University Press, Clarendon.

10. Pethig, R. (1992) Protein-Water Interactions Determined by Dielectric Methods. Ann. Rev. Phys. Chem. 43, 177.

11. Nandi, N., Bhattacharyya, K., Bagchi, B. (2000) Dielectric relaxation and solvation dynamics of water in complex chemical and biological systems. Chem. Rev. 100, 2013-2045.

12. Homoelle, B.J., Edington, M.D., Diffey, W.M., Beck, W.F. (1998) Stimulated Photon-Echo and Transient-Grating Studies of Protein-Matrix Solvation Dynamics and Interexciton-State Radiationless Decay in Phycocyanin and Allophycocyanin. J. Phys. Chem. B 102, 3044-3052.

13. Fraga, E., Loppnow, G.R. (1998) Proteins as Solvents: Blue Copper Proteins as a Molecular Ruler for Solvent Effects on Resonance Raman Intensities. J. Phys. Chem. B 102, 7659-7665.

14. Jordanides, X.J., Lang, M.J., Song, X., Fleming, G.R. (1999) Solvation dynamics in protein environments studied by photon echo spectroscopy. J. Phys. Chem. B 103, 7995-8005.

15. Pal, S.K., Peon, J., Zewail, A.H. (2002) Ultrafast surface hydration dynamics and expression of protein functionality: alpha-Chymotrypsin. Proc. Natl. Acad. Sci. U. S. A. 99, 15297-15302.

16. Pal, S.K., Peon, J., Bagchi, B., Zewail, A.H. (2002) Biological water: Femtosecond dynamics of macromolecular hydration. J. Phys. Chem. B 106, 12376-12395.

17. Peon, J., Pal, S.K., Zewail, A.H. (2002) Hydration at the surface of the protein Monellin: Dynamics with femtosecond resolution. Proc. Natl. Acad. Sci. U. S. A. 99, 10964-10969.

18. Pal, S.K., Peon, J., Zewail, A.H. (2002) Biological water at the protein surface: Dynamical solvation probed directly with femtosecond resolution. Proc. Natl. Acad. Sci. U. S. A. 99, 1763-1768.

19. Pierce, D.W., Boxer, S.G. (1992) Dielectric Relaxation in a Protein Matrix. J. Phys. Chem. 96, 5560-5566.

20. Bashkin, J.S., Mclendon, G., Mukamel, S., Marohn, J. (1990) Influence of Medium Dynamics on Solvation and Charge Separation Reactions - Comparison of a Simple Alcohol and a Protein Solvent. J. Phys. Chem. 94, 4757-4761.

21. Changenet-Barret, P., Choma, C.T., Gooding, E.F., DeGrado, W.F., Hochstrasser, R.M. (2000) Ultrafast dielectric response of proteins from dynamic Stokes shifting of coumarin in calmodulin. J. Phys. Chem. B 104, 9322-9329.

22. Chowdhury, P.K., Halder, M., Sanders, L., Arnold, R.A., Liu, Y., Armstrong, D.W., Kundu, S., Hargrove, M.S., Song, X., Petrich, J.W. (2004) The Complex of Apomyoglobin with the Fluorescent Dye, Coumarin 153. Photochem. Photobiol. 79, 440-446.

23. Hargrove, M.S., Singleton, E.W., Quillin, M.L., Ortiz, L.A., Phillips, G.N., Olson, J.S., Mathews, A.J. (1994) His(64)(E7)-]Tyr Apomyoglobin as a Reagent for Measuring Rates of Hemin Dissociation. J. Biol. Chem. 269, 4207-4214.

24. Stryer, L. (1965) The interaction of a naphthalene dye with apomyoglobin and apohemoglobin: A fluorescent probe of non-polar binding sites. J. Mol. Biol. 13, 482-495.

25. Williams, K.R., Adhyaru, B., Pierce, R., Schulman, S.G. (2002) The binding constant of complexation of bilrubin to bovine serum albumin. J. Chem. Ed. 79, 115-116.

26. Kitamura, N., Sakata, N., Kim, H.-B., Habuchi, S. (1999) Energy gap dependence of the nonradiative rate constant of 1-anilino-8-naphthalene sulfonate in reverse micelles. Anal. Sci. 15, 413-419.

27. Riter, R.E., Undiks, E.P., Levinger, N.E. (1998) Impact of counterion on water motion in aerosol OT reverse micelles. J. Am. Chem. Soc. 120, 6062-6067.

28. Maroncelli, M., Fleming, G.R. (1987) Picosecond Solvation Dynamics of Coumarin-153 - the Importance of Molecular Aspects of Solvation. J. Chem. Phys. 86, 6221-6239.

29. Horng, M.L., Gardecki, J.A., Papazyan, A., Maroncelli, M. (1995) Subpicosecond measurements of polar solvation dynamics: Coumarin 153 revisited. J. Phys. Chem. 99, 17311.

30. Lewis, J.E., Maroncelli, M. (1998) On the (uninteresting) dependence of the absorption and emission transition moments of coumarin 153 on solvent. Chem. Phys. Lett. 282, 197-203.

31. Muhlpfordt, A., Schanz, R., Ernsting, N.P., Farztdinov, V., Grimme, S. (1999) Coumarin 153 in the gas phase: optical spectra and quantum chemical calculations. Phys. Chem. Chem. Phys. 1, 3209-3218.

32. Jiang, Y., McCarthy, P.K., Blanchard, D.J. (1994) The role of multiple electronic states in the dissipative energy dynamics of coumarin 153. Chem. Phys. 183, 249-267.

33. Flory, W.C., Blanchard, D.J. (1998) Excitation energy-dependent transient spectral relaxation of coumarin 153. Appl. Spectrosc. 52, 82-90.

34. Palmer, P.M., Chen, Y., Topp, M.R. (2000) Simple water clusters of coumarins 151 and 152A studied by IR-UV double resonance spectroscopy. Chem. Phys. Lett. 318, 440-447.

35. Chen, Y., Palmer, P.M., Topp, M.R. (2002) Infrared spectroscopy of jet-cooled, electronically excited clusters of coumarin 151: Excited-state interactions and conformational relaxation. Int. J. Mass. Spectrosc. 220, 231-251.

36. Agmon, N. (1990) Dynamic Stokes shift in coumarin: Is it only relaxation? J. Phys. Chem. 94, 2959-2963.

37. Cocco, M.J., Lecomte, J.T.J. (1994) The Native State of Apomyoglobin Described by Proton NMR Spectroscopy: Interaction with the Paramagnetic Probe HyTEMPO and the Fluorescent Dye ANS. Protein Sci. 3, 267.

CHAPTER VIII. SOLVATION DYNAMICS IN PROTEIN ENVIRONMENTS: COMPARISON OF FLUORESCENCE UPCONVERSION MEASUREMENTS OF COUMARIN 153 IN MONOMERIC HEMEPROTEINS WITH MOLECULAR DYNAMICS SIMULATIONS

A paper published in the Journal of Chemical Physics

Mintu Halder[1], Prasun Mukherjee[1], Sayantan Bose[1], Mark S. Hargrove[2], Xueyu Song[*,1], and Jacob W. Petrich[*,1]

Abstract

The complexes of the fluorescence probe coumarin 153 with apomyoglobin and apoleghemoglobin are used as model systems to study solvation dynamics in proteins. Time-resolved Stokes shift experiments are compared with molecular dynamics simulations, and very good agreement is obtained. Solvation of the coumarin probe is very rapid with approximately 60% occurring within 300 fs and is attributed to interactions with water (or possibly to the protein itself). Differences in the solvation relaxation (or correlation) function, C(t), for the two proteins are attributed to differences in their heme pockets.

---

[1] Department of Chemistry, Iowa State University, Ames, Iowa 50011.
[2] Departments of Biochemistry, Biophysics, and Molecular Biology, Iowa State University, Ames, Iowa 50011.
[*] Author to whom correspondence should be addressed.

Introduction

It has been well established by numerous experimental and theoretical studies that solvation dynamics in polar solvents can be described by linear response theory [1-4]. In general, the full frequency dependent dielectric function of the polar solvent (and, perhaps, even of ionic solvents [5]) gives a good description of the solvation dynamics from the ultra-fast regime to that of diffusive relaxation. Some direct and successful comparisons between theory and experiments have been established [1,4-6]. Such success is achieved largely because the dielectric fluctuations of polar solvents can be described accurately by simple linear response models, such as the dielectric continuum model [7,8]. On the other hand, the structure and function of a protein are determined by a delicate balance of different interactions, mainly of noncovalent nature. Among these, the correct description of electrostatic interactions is critical in the understanding of protein properties. To date, much effort has been put to the investigation of their static role in the structure and function of a protein, and considerable progress has been made with this approach for the analysis of structural stability, molecular recognition and drug design, the efficiency of enzyme catalysis, and other properties [9]. For many elementary processes occurring in a protein its dynamical dielectric response is also important. A prime example is that electron and energy transfers in photosynthesis are modulated by the dielectric medium of a protein complex [7]. Studies of these dynamical responses have been a very active field, both theoretically and experimentally [10-18]; but in spite of considerable efforts towards the understanding of the dielectric relaxation processes in proteins [2,19], up to now a reliable estimate for the dielectric response function of proteins is still lacking.

For example, a range of experiments has been performed to study dielectric relaxation in proteins; but the results have been very disparate. Early studies suggested that slow relaxation, than for that of tryptophan in bulk water, and they argue that the slow relaxation arises from the water molecules constrained on the protein surface on the nanosecond time scale, exists in myoglobin [10], in contrast to polar solvents. This may not be unexpected owing to structural constraints, but the role of a protein's interior motions in its dielectric relaxation is presently unclear from various experimental studies [11,12,14]. Homoelle et al. have suggested that the dynamical fluctuations observed in phycobiliproteins involve the interior motions of the protein substantially [11]. Fraga and Loppnow [20] have shown that the resonance Raman spectra are affected by the different residue compositions of the blue copper proteins from different species. On the other hand, experimental and theoretical studies of lysozyme suggest that significant contributions of the observed dynamical fluctuations come from the surrounding water solvent and the water molecules attached on the protein surface [12]. As another example, Zewail and coworkers used tryptophan as a probe to study solvation dynamics in proteins [14-18,21] and have reported slow relaxation from which they inferred the presence of "biological water": water molecules in the immediate vicinity of a surface believed to have different properties from those of bulk water [2,22]. For example, they report that the dynamics are significantly slower for the surface tryptophan residues in Subtilisin Carlsberg [16] and in monellin [14,17]. The changes in fluorescence emission maxima that they report for Subtilisin and monellin are, however 1,440 cm^{-1} and 960 cm^{-1}, respectively. Given this difference of 480 cm^{-1} for the two surface tryptophans, it would seem that there is also a considerable relaxation arising from the different amino acids neighboring them.

These differences in the interpretations of various experiments are in no small part due to the lack of a reliable dielectric response function for the studied proteins from either experiments or computer simulations. Studies of the solvation dynamics in proteins, nevertheless, offer the best means of investigating the dielectric response. In this work, we discuss the solvation dynamics of the complexes of coumarin 153 (C153, Figure VIII.1) with the monomeric hemeproteins, apomyoglobin and apoleghemoglobin, in water.

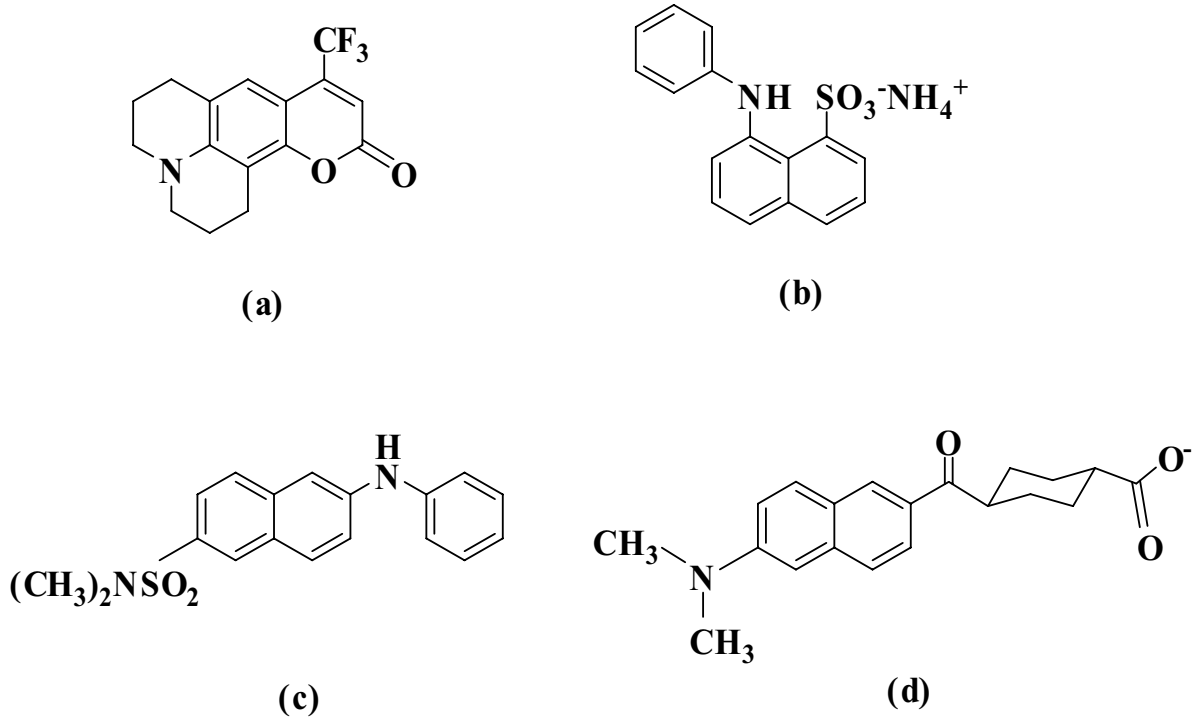

Figure VIII.1. Structures of the fluorescent probe molecules: (a) coumarin 153 (C153), (b) the ammonium salt of 8-anilino-1-naphthalenesulfonic acid (1,8-ANS), (c) anilino-2-aminonaphthalene-6-dimethylsulfonamide (2,6-ANSDMA) and (d) 2′-(N,N-dimethylamino)-6-naphthoyl-4-trans-cyclohexanoic acid (DANCA). The structures for ANSDMA and DANCA were incorrectly transmitted in reference [23].

There are four main considerations for the choice of this system.

First, coumarin 153 (C153) is a well characterized and widely used chromophore for solvation dynamics studies [24,25].

Second, we have experimentally obtained a binding constant of ~ 6 μM for coumarin 153 and apomyoglobin and have characterized the complex [23,26]. In fact, one of our motivations for using coumarin to probe the hemepocket was the existence of an NMR structure of the dye ANS, a molecule similar to coumarin (Figure VIII.1), in the hemepocket of apomyoglobin [27]. Binding studies based upon a Job's plot analysis, circular dichroism, fluorescence depolarization, capillary electrophoresis, and molecular dynamics simulations indicate that coumarin indeed is in the hemepocket (Figure VIII.2). Furthermore, the coumarin's rotation in the hemepocket is very slow compared to the relaxation time scale of interest (see Figure 2 of ref. [23]). Finally, for the H64Y/V68F double mutant of myoglobin the reorganization energy increases by 5 cm^{-1} and for the H64W mutant it decreases by 90 cm^{-1}, on the other hand, a surface mutant D112N, has, within experimental error, the same reorganization energy as the wild type. This confirms the presence of coumarin in the hemepocket as opposed to the surface.

Third, while myoglobin and leghemoglobin share a common globin fold, they have differences in their hemepockets [28], the region to be probed by the coumarin. For example, the F-helix is oriented in such a way that in myoglobin HisF8 (His93) eclipses the pyrrole nitrogens of the porphyrin but in leghemoglobin it is staggered with respect to them. In the myoglobin proximal hemepocket, SerF7 facilitates a hydrogen bonding network that drives HisF8 into a conformation that destabilizes ligand affinity. The opposite is true in leghemoglobin, which lacks SerF7 and contains a proximal hemepocket that destabilizes ligand binding. The two proteins exhibit differences on the distal sides of their heme pockets as well. The leghemoglobin distal pocket is larger and more flexible than those of most other

hemoglobins and contains a combination of HisE7 (His64) and TyrB10 not found naturally in any other hemoglobin.

Fourth, we can produce a broad range of mutant proteins in which one or several amino acids are strategically replaced, so as to test how specific substitutions can affect solvation dynamics.

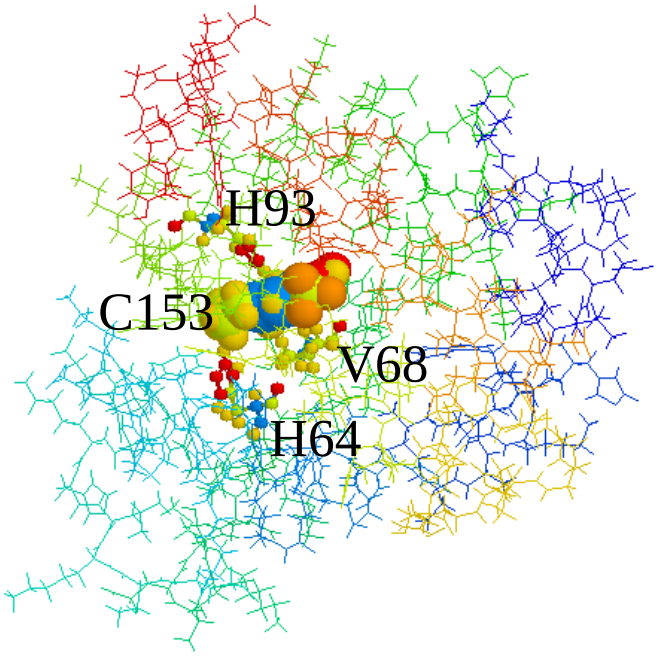

Figure VIII.2. A snapshot of equilibrated C153-apomyoglobin in water from 3-ns molecular dynamics simulations using CHARMM22 force field. The C153 is shown in a space-filling model, and two histidine residues in the hemepocket are also shown with stick and ball models. His93 is the proximal histidine belonging to the F helix and is also referred to as HisF8. His64 is the distal histidine, also referred to as HisE7.

Materials and Methods

C153 was purchased from Exciton Inc. (Dayton, OH) and used without further purification. Horse heart myoglobin (Mb) was purchased from Sigma. Apoproteins were prepared using a method described elsewhere [29]. C153 has very low solubility in water. A stock solution of C153 was prepared by adding a microliter amount of a concentrated solution of C153 in methanol to water. That is, concentrated C153/MeOH was added to water, keeping the organic content < 0.3 % (v/v) in the final solution. To prepare a 5×10^{-5} M solution of C153/water, 5 μL of 20×10^{-3} M C153/MeOH solution was added to 2 ml of water. The resulting solution was sonicated. For fluorescence upconversion experiments a stock solution of C153/MeOH was added to 1.2 ml of ~ 1.2×10^{-3} M apoprotein solution keeping the organic content < 3 % (v/v) in the final solution with 1:1 protein to C153 ratio. All samples were equilibrated for about 2 hours before taking the steady state and time resolved measurements. For soybean leghemoglobin (Lba), ammonium sulfate was added to 30% saturation and centrifuged at 14000 rpm for 10 min. The protein in the supernatant was then precipitated by slowly adding ammonium sulfate (to avoid local denaturation) to 90% saturation followed by centrifugation at 14000 rpm for 10 min. The pellets were resuspended in 20mM Tris buffer, pH 8.0 and then loaded onto a Phenyl Sepharose (Sigma) column which was pre-equilibrated with 2 M ammonium sulfate in 20 mM Tris buffer, pH 8.0. The protein was eluted with 0.4 M ammonium sulfate. The eluted protein was dialysed into 20 mM Tris buffer, pH 8.0. The dialysed protein was loaded onto a DEAE (Phramacia column) and eluted with 75 mM NaCl in 20 mM Tris buffer, pH 8.0. The eluted protein was concentrated to ~1 mL and then it was run through a size exclusion column and washed with 10 mM phosphate buffer, pH 7.0.

Steady-state measurements. Steady-state absorbance spectra were obtained on a Hewlett-Packard 8453 UV-visible spectrophotometer with 1-nm resolution. All samples were prepared in 10 mM phosphate buffer solution. The concentrations of apoproteins were determined spectrophotometrically using the extinction coefficient 15.2 $mM^{-1}cm^{-1}$ at 280 nm [23]. Steady-state fluorescence spectra were obtained on a Spex Fluoromax-2 with a 4-nm bandpass and corrected for lamp spectral intensity and detector response. For both fluorescence and absorption measurements, a 3-mm path-length quartz cuvette was used. The adequacy of the correction factors and the calibration of our fluorometer were checked against the tabulations of Gardecki and Maroncelli [30].

Time-resolved measurements. The apparatus for fluorescence upconversion measurements is described elsewhere [31]. The instrument response function had a full-width–at-half-maximum (FWHM) of 300 fs. A rotating sample cell was used. To construct the time-resolved spectra from upconversion measurements, a series of decays were collected typically from 480 nm to 560 nm at 10-nm intervals. Transients were fit to sums of exponentials, and time-dependent spectra were reconstructed from these fits by normalizing to the steady-state spectra:

$$S(\lambda,t) = D(\lambda,t)\frac{S_0(\lambda)}{\int_0^\infty D(\lambda,t)} \qquad \text{(VIII.1)}$$

$D(\lambda,t)$ is the wavelength-resolved fluorescence decay, and $S_0(\lambda)$ is the steady-state emission intensity at a given wavelength. We have employed the traditional approach of fitting the time-resolved spectra to a log-normal function [24,31], from which we extract the peak frequency, $\nu(t)$, as a function of time.

The solvation dynamics were described by the normalized correlation function:

$$C(t) = \frac{\nu(t) - \nu(\infty)}{\nu(\text{"t = 0"}) - \nu(\infty)} \qquad \text{(VIII.2)}$$

ν("t = 0") is the frequency at "zero time." [5,32,33] ν(∞) is (usually [34]) the frequency at "infinite time," the maximum of the steady-state fluorescence spectrum. ν(t) is determined by taking the maxima from the lognormal fits as the emission maximum. In most of the cases, however, the spectra are broad, so there is some uncertainty in the exact position of the emission maxima. Thus, we have considered the range of the raw data points in the neighborhood of the maximum to estimate an error for the maximum obtained from the lognormal fit. Depending on the width of the spectrum (i.e. "zero-time", steady-state, or time-resolved emission spectrum), we have determined the typical uncertainties as follows: "zero-time" ~ steady-state (~ ± 100 cm^{-1}) < time-resolved emission (~ ± 200 cm^{-1}). We use these uncertainties to compute error bars for the C(t). Finally, in generating the C(t), the first point was obtained from the "zero-time" spectrum. The second point was taken at the maximum of the instrument response function. Fractional solvation at 300 fs is given by f (t = 300 fs) = 1 − C (t = 300 fs).

Molecular dynamics simulations. The starting configurations of horse heart myoglobin (HHMB) and leghemoglobin (LEGMB) are from the protein DATA BANK (PDB id 1WLA and 1BIN) with TIP3P water models. To have a reasonable starting point for the C153-protein complex the heme is replaced by C153 and then energy minimization is used to obtain the starting configuration of the C153-protein complex. Standard constant pressure-temperature MD was performed using the ORAC package [35] with the Amber force field [36]. In all simulations, short-range non-bonded interactions were calculated up to a 10 Å cutoff, whereas long-range electrostatic interactions were treated by the SPME method using a very

fine grid, 128 points per axis, with periodic boundary conditions, and Ewald convergence parameter of 0.43 $Å^{-1}$. Three different Nosé-Hoover thermostats were coupled to solute, solvent, and total center of mass. An external pressure of 0.1 MPa was applied all along the trajectory. A five time-step rRESPA [37] algorithm with times of 0.5-1.0-2.0-4.0-12.0 fs was used with bond constraints on hydrogen covalent bonds handled by a Shake-Rattle-like algorithm. The final system was first equilibrated with velocity rescaling for 60 ps at 50 K and 80 ps at 300 K. Following this initial equilibration, we ran the system for one additional nanosecond at constant temperature (T = 300 K) and pressure (P = 0.1 MPa). To achieve full relaxation, the simulation box was entirely flexible for the first 300 ps, whereas for the remainder of the run, only isotropic changes of the box were allowed [35]. Finally, the system was simulated for an additional 10 ns. As we have demonstrated in our previous work [23], an equilibrium configuration for C153 in the heme-pocket of the protein can be found and experimental measurements seem to support our interpretation. Using the equilibrated configuration, additional 12-ns trajectories are generated and are used for the calculation of solvation correlations functions.

Using the charges of C153 in the ground and excited states [4], the solvation correlation function can be obtained within the linear response theory [38] as

$$C(t) = \frac{< \delta\Delta E(t)\delta\Delta E(0) >}{< \delta\Delta E(0)\delta\Delta E(0) >}, \qquad \text{(VIII.3)}$$

where $\delta\Delta E(t) = \Delta E(t) - < \Delta E(t) >$, and $\Delta E(t)$ is the interaction energy difference between C153 in its excited state and ground state with surrounding protein and water molecules at time t. The symbol $< \cdots >$ denotes the ensemble average in the simulation.

Results

Representative wavelength resolved traces obtained on an ~10-ps time scale by means of fluorescence upconversion are shown in Figure VIII.3. Figure VIII.4 provides the time-resolved emission spectra at 300 fs and 10.3 ps along with the steady-state and "zero-time" spectra. Figure VIII.5 presents the solvation correlation functions, C(t). The C(t) obtained from molecular dynamics simulations are also compared with the experimental data in Figure VIII.5. Relevant fitting parameters are summarized in Table VIII.1. The salient results are:

1. Almost 60 % of the solvation is complete in both apoMb and apoLba within the time resolution of our instrument (300 fs).
2. The initial faster solvation is followed by a slower response, which is slower in apoLba than in apoMb by about a factor of 4 (Table VIII.1).
3. There is excellent agreement between the C(t) from fluorescence upconversion experiments and those obtained from molecular dynamics simulations.

Discussion

The rapidity of the solvation in both the proteins studied here suggests that water is playing a dominant role, which is consistent with the report by Fleming and coworkers [12] that solvation in the lysozyme/eosin system is dominated by water. (Solvation in bulk water is characterized largely by an ~30-fs component and is complete in ~15 ps. [6,39]) The remainder of the solvation can be attributed to motions of the protein matrix or coupled protein-water [40] motions. The protein's contribution to solvation should not be neglected. For example, Nilsson and Halle have simulated the Stokes shift in the protein monellin [41] and have

discussed how to separate the relative contributions of protein and water. They find a significant protein component, at least 25%. Li et al. [40] find that the relative protein and water contributions can vary substantially with the conformational substate of myoglobin: sometimes the protein contribution can even be larger than water. Both Nilsson and Halle [41] and Li et al. [40] find that the protein contribution also has an ultrafast component. Li et al. also found that, in disagreement with the "biological water" picture, protein motion (or protein-water motion) was essential for the slow (~50-100-ps) time-scale Stokes shifts. This feature was independent of the dynamics apparent from the protein and water Stokes shift contributions.

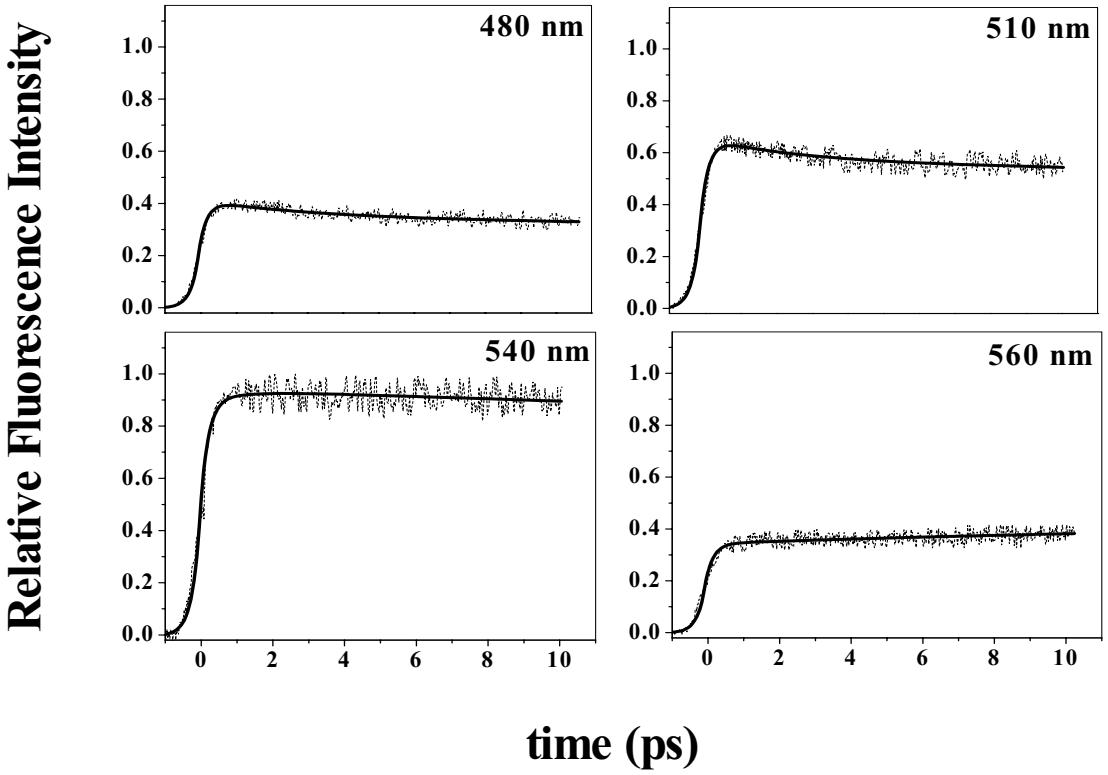

Figure VIII.3. Fluorescence upconversion traces obtained for C153 in apoMb at the indicated wavelengths. The maximum intensity of the traces are given relative to the most intense, i.e., that at 540 nm. The decays used to construct the time-resolved emission spectra were typically collected over a range of wavelengths from 480 to 560 nm at 10 nm intervals, a total of eight or nine decays was used to generate the time-resolved emission spectra, from which the C(t) were calculated.

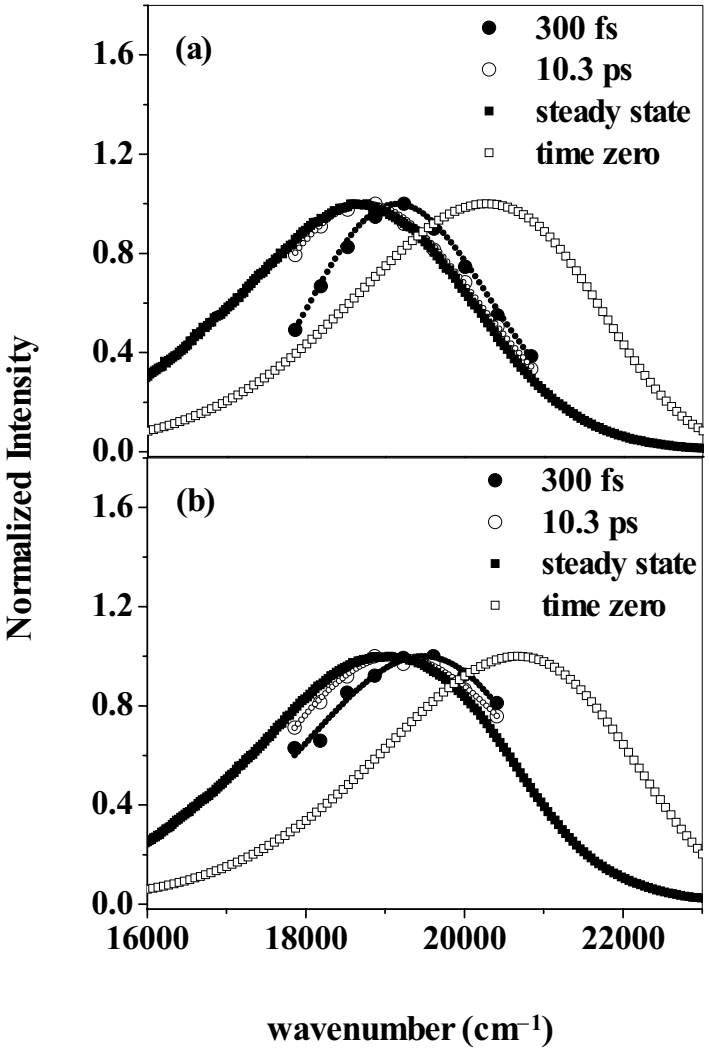

Figure VIII.4. Normalized time resolved emission spectra for C153 in (a) apoMb and (b) apoLba at 300 fs and 10.3 ps. Corresponding steady-state and "zero-time" spectra are included. Almost 60 % of the solvation is complete in both systems within the time resolution of our instrument (300 fs).

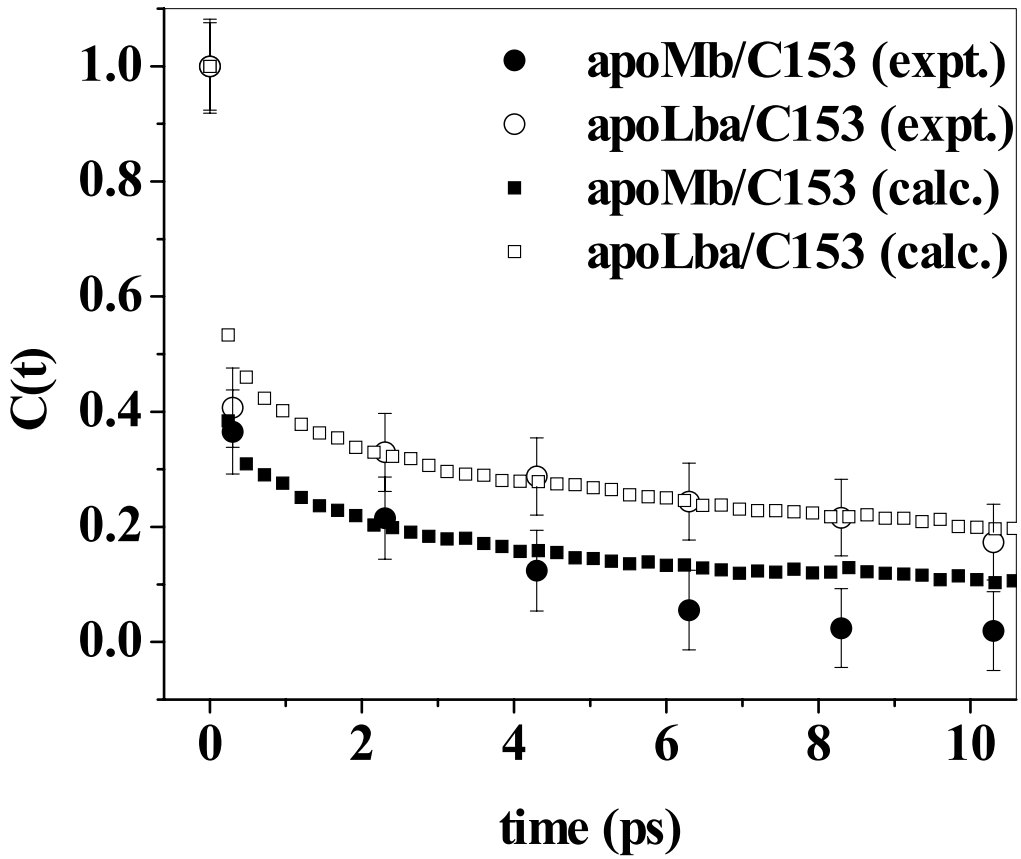

Figure VIII.5. Comparison of C(t) for C153 in apoMb and apoLba obtained from fluorescence upconversion experiments with those obtained from molecular dynamics simulations. In both proteins, the initial fast component occurs within the time resolution of our instrument.

Our results are, however, at odds with those of previous attempts to exploit the myoglobin system to study the solvation response of proteins. These studies [10] used the fluorescent probes, 2,6-ANSDMA and DANCA (Figure VIII.1). The former probe molecule afforded a single exponential response of 9.1 ns; the latter, a more complicated response with both shorter and longer response times. The discrepancy between the results for these two probe molecules as well as the predominance of the long-lived response time caused us to search for other probes. We consequently opted for coumarin 153, which not only has been studied in a very wide range of solvents and in the gas phase, but whose excited-state

solvation has been demonstrated not to involve any contributions other than those from S_1 [24,25].

Table VIII.1. Solvation of C153 in Two Hemeproteins (20°C)[a]

System	f_{300fs}	a_1[b]	τ_1	τ_2	a_1 calc	τ_1 calc	τ_2 calc	$\langle\tau\rangle$	$\langle\tau\rangle$ calc	ν("0")[c]	λ("0")[d]	$\lambda(\infty)$[d]
apoMb	0.64	0.59	0.02	3.4	0.73	0.14	9.3	1.4	2.6	20,260	1,850	2,450
apoLba	0.59	0.60	0.09	13	0.60	0.19	13	5.3	5.3	20,660	1,840	2,590

[a] Unless otherwise indicated, the parameter refers to that experimentally obtained. The time constants are in picoseconds and the frequencies and reorganization energies are given in wavenumbers.

[b] The solvation relaxation functions, C(t), are in both cases fit to a sum of two decaying exponentials, $C(t) = a_1 \exp(-t/\tau_1) + a_2 \exp(-t/\tau_2)$, where $a_1 + a_2 = 1$. C(t) is fit from its value at unity, i.e., starting at "t = 0"; consequently the early part of its decay is determined by only two points. The τ_1 we report are thus upper limits for the early portion of the relaxation. The average solvation time was calculated according to equation: $\langle\tau\rangle = \sum_i a_i \tau_i$.

[c] For apoMb/C153, ν("0") − $\nu(\infty)$ = 1530 cm^{-1}; for apoLba/C153, ν("0") − $\nu(\infty)$ = 1600 cm^{-1}. The "zero-time" spectra were calculated according to the method described elsewhere [5,32,33]. We use the "zero-time" spectrum in our analysis (Figure VIII.4), and not any approximation for obtaining its maximum. We use hexane as the nonpolar solvent for the "zero-time" calculation.

[d] The reorganization energy, discussed elsewhere [12,31,33], at "t = 0" and at steady state.

Our results are also at odds with those of other studies [16,18], from which it is suggested that aqueous solvation in proteins is much slower than that in bulk water. This slow solvation is attributed to "biological water": [2,22] in restricted environments, water is proposed to solvate on a much slower time scale, tens to hundreds of picoseconds, as opposed to ~1 ps [2]. We note, however, that an accurate determination of C(t) depends upon appropriate values for $\nu(0)$ and $\nu(\infty)$. The latter is usually given by the equilibrium spectrum. This is not, however, true in the case of very slowly relaxing solvents, as has been demonstrated in the case of certain ionic liquids: [34] for example, here the emission spectrum at ~3 times the

fluorescence lifetime of the probe is red-shifted to that of the equilibrium spectrum. The appropriate value for $\nu(0)$ is not obtained from the emission spectrum obtained immediately upon optical excitation with infinite time resolution, even if such an experiment were possible, but that arising from the spectrum of a vibrationally relaxed excited state that has been fully solvated by its internal motions but that has not yet responded to the surrounding solvent. Fee and Maroncelli [32] have described a robust, model independent, and simple procedure for generating this "zero-time" spectrum (ν("0")); and we have checked its validity using a different method for estimating the "zero-time" reorganization energy [33]. Finally, Li et al. [40] have compared experiments and simulations for protein solvation and note a significant discrepancy between theory and experiment: namely, a very rapid early relaxation is obtained in the simulations but is absent in the experiments. We suggest, based on our results and others to which we refer, that these authors are in fact simulating the solvation appropriately and are, rather, missing the rapid dynamics in their experiment and its analysis.

Conclusions

The results presented here attest to the utility of coumarin 153 as a probe of protein dynamics, as we suggested in earlier work [23,26]. Since the late 1980s, coumarin 153 has proved to be the most useful and reliable probe of solvation dynamics, has been exhaustively studied, and has successfully withstood numerous challenges to this title [24,25]. Its priority in this arena can be attributed to its large Stokes shift (crucial for acquiring an accurate estimate of C(t)), relative rigidity, nonreactivity in the excited state, and that its spectral features arise from only one electronic state. The solvation relaxation functions, C(t), obtained from complexes of coumarin 153 with apomyoglobin and apoleghemoglobin by means of

fluorescence upconversion experiments and molecular dynamics simulations are in excellent agreement. Solvation of the coumarin probe is very rapid with approximately 60% occurring within 300 fs and is attributed to interactions with water and possibly the protein. The hemepockets of myoglobin and leghemoglobin differ considerably [28] as we note in the Introduction, and this manifests itself in both the experimental results and the molecular dynamics simulations.

The literature concerning protein dielectric relaxation contains conflicting reports and conclusions. Our results are in good agreement with those obtained by Fleming and coworkers [12], who find that the initial solvation dynamics of the lysozyme/eosin complex are identical to those of eosin in bulk water. Our results are, however, rather different from those obtained in other studies. Notably, the dynamics we observe are much more rapid than those reported in other work involving monomeric hemeproteins [10]. We suggest that the probes used, ANSDMA and DANCA (Figure VIII.1), are not ideal probes of solvation. They are much more flexible than coumarin, and they are likely to undergo excited-state charge transfer reactions, which could seriously complicate the interpretation of solvation dynamics. This class of chromophores is notable for its dual emission from locally-excited and charge-transfer states [42].

We suggest that owing to their methods of analyzing the Stokes shift data, other workers have exaggerated the amount of the slowly relaxing component of solvation that they attribute to "biological water" [2,16,18,22]. While it is possible that water molecules may be tightly bound to the protein surface and in this way contribute to slower solvation events, we propose that there is no cogent evidence for excluding ultrafast solvation from bulk water.

Finally, we stress the importance of accurately obtaining the "zero-time" spectrum. Its knowledge is fundamental to an accurate construction of the solvation relaxation function.

Acknowledgements

The authors thank Mr. Jordan Witmer for assistance in preparing the monomeric hemeproteins, Drs. Pramit Chowdhury and Lindsay Sanders Headley for their early work on this problem, and Professor Dongping Zhong for discussing his data. We thank Professors Kankan Bhattacharyya, Mark Maroncelli, and Graham Fleming for their comments on the manuscript. XS thanks the NSF for support from grant CHE0303758.

References

[1] **X. Song, AIP Conf. Proc. 492, 417 (1999); C. P. Hsu, X. Y. Song, and R. A. Marcus, J. Phys. Chem. B 101, 2546 (1997).**

[2] **N. Nandi, K. Bhattacharyya, and B. Bagchi, Chem. Rev. 100, 2013 (2000).**

[3] **J. D. Simon, Acc. Chem. Res. 21, 128 (1988); G. R. Fleming and P. G. Wolynes, Phys. Today 43(5), 36 (1990); P. F. Barbara and W. Jarzeba, in Advances in Photochemistry, edited by D. H. Volman, G. S. Hammond, and K. Gollnick (John Wiley & Sons, 1990); M. Maroncelli, J. Mol. Liq. 57, 1 (1993); J. T. Hynes, in Ultrafast Dynamics of Chemical Systems (1994), Vol. 7, pp. 345; G. R. Fleming and M. H. Cho, Annu. Rev. Phys. Chem. 47, 109 (1996); R. M. Stratt and M. Maroncelli, J. Phys. Chem. 100, 12981 (1996); E. W. Castner, Jr. and M. Maroncelli, J. Mol. Liq. 77, 1 (1998); S. Mukamel, Principles of Nonlinear Optical Spectroscopy, First Edition ed. (Oxford University Press, New York, 1995).**

[4] **X. Song and D. Chandler, J. Chem. Phys. 108, 2594 (1998).**

[5] M. Halder, L. S. Headley, P. Mukherjee, X. Song, and J. W. Petrich, J. Phys. Chem. A 110, 8623 (2006).

[6] M. J. Lang, X. J. Jordanides, X. Song, and G. R. Fleming, J. Chem. Phys. 110, 5884 (1999).

[7] R. A. Marcus and N. Sutin, Biochim. Biophys. Acta 811, 265 (1985).

[8] G. King and A. Warshel, J. Chem. Phys. 91, 3647 (1989); J. S. Bader, R. A. Kuharski, and D. Chandler, Abstr. Pap. - Am. Chem. Soc. 199, 65 (1990).

[9] M. F. Perutz, Science 210, 1187 (1978); A. Warshel and S. T. Russel, Q. Rev. Biol. 17, 283 (1984); K. A. Sharp and B. Honig, Annu. Rev. Biophys. Chem. 19, 301 (1990); H. Nakamura, Q. Rev. Biophys. 29, 1 (1996).

[10] D. W. Pierce and S. G. Boxer, J. Phys. Chem. 96, 5560 (1992); J. S. Bashkin, G. Mclendon, S. Mukamel, and J. Marohn, J. Phys. Chem. 94, 4757 (1990).

[11] B. J. Homoelle, M. D. Edington, W. M. Diffey, and W. F. Beck, J. Phys. Chem. B 102, 3044 (1998).

[12] X. J. Jordanides, M. J. Lang, X. Song, and G. R. Fleming, J. Phys. Chem. B 103, 7995 (1999).

[13] C. L. Brooks, M. Karplus, and B. M. Pettitt, Adv. Chem. Phys. 71, 1 (1987); M. Marchi, J. N. Gehlen, D. Chandler, and M. Newton, J. Am. Chem. Soc. 115, 4178 (1993).

[14] S. K. Pal, J. Peon, B. Bagchi, and A. H. Zewail, J. Phys. Chem. B 106, 12376 (2002).

[15] D. P. Zhong, S. K. Pal, D. Q. Zhang, S. I. Chan, and A. H. Zewail, Proc. Natl. Acad. Sci. U. S. A. 99, 13 (2002).

[16] S. K. Pal, J. Peon, and A. H. Zewail, Proc. Natl. Acad. Sci. U. S. A. 99, 1763 (2002).

[17] J. Peon, S. K. Pal, and A. H. Zewail, Proc. Natl. Acad. Sci. U. S. A. 99, 10964 (2002).

[18] W. Qiu, Y.-T. Kao, L. Zhang, Y. Yang, L. Wang, W. E. Stites, D. Zhong, and A. H. Zewail, Proc. Natl. Acad. Sci. U. S. A. 103, 13979 (2006); W. Qiu, L. Zhang, O. Okobiah, Y. Yang, L. Wang, D. Zhong, and A. H. Zewail, J. Phys. Chem. B. 110, 10540 (2006).

[19] R. J. Sheppard, E. H. Grant, and G. P. South, Dielectric Behavior of Biological Molecules, first edition. (Oxford University Press, Clarendon, 1978); R. Pethig, Annu. Rev. Phys. Chem. 43, 177 (1992).

[20] E. Fraga and G. R. Loppnow, J. Phys. Chem. B 102, 7659 (1998).

[21] W. Lu, J. Kim, W. Qiu, and D. Zhong, Chem. Phys. Lett. 388, 120 (2004).

[22] K. Bhattacharyya and B. Bagchi, J. Phys. Chem. A 104, 10603 (2000); K. Sahu, S. K. Mondal, S. Ghosh, D. Roy, P. Sen, and K. Bhattacharyya, J. Phys. Chem. B 110, 1056 (2006); S. K. Pal, D. Mandal, D. Sukul, S. Sen, and K. Bhattacharyya, J. Phys. Chem. B 105, 1438 (2001); S. Guha, K. Sahu, D. Roy, S. K. Mondal, S. Roy, and K. Bhattacharyya, Biochemistry 44, 8940 (2005).

[23] P. K. Chowdhury, M. Halder, L. Sanders, R. A. Arnold, Y. Liu, D. W. Armstrong, S. Kundu, M. S. Hargrove, X. Song, and J. W. Petrich, Photochem. Photobiol. 79, 440 (2004).

[24] M. Maroncelli and G. R. Fleming, J. Chem. Phys. 86, 6221 (1987).

[25] M. L. Horng, J. A. Gardecki, A. Papazyan, and M. Maroncelli, J. Phys. Chem. 99, 17311 (1995); J. E. Lewis and M. Maroncelli, Chem. Phys. Lett. 282, 197 (1998); S. A. Kovalenko, J. Ruthmann, and N. P. Ernsting, Chem. Phys. Lett. 271, 40 (1997); A. Muhlpfordt, R. Schanz, N. P. Ernsting, V. Farztdinov, and S. Grimme, Phys. Chem.

Chem. Phys. 1, 3209 (1999); P. Changenet-Barret, C. T. Choma, E. F. Gooding, W. F. DeGrado, and R. M. Hochstrasser, J. Phys. Chem. B 104, 9322 (2000); Y. Jiang, P. K. McCarthy, and D. J. Blanchard, Chem. Phys. 183, 249 (1994); W. C. Flory and D. J. Blanchard, Appl. Spectrosc. 52, 82 (1998); P. M. Palmer, Y. Chen, and M. R. Topp, Chem. Phys. Lett. 318, 440 (2000); Y. Chen, P. M. Palmer, and M. R. Topp, Int. J. Mass. Spectrosc. 220, 231 (2002); N. Agmon, J. Phys. Chem. 94, 2959 (1990); M. Maroncelli, R. S. Fee, C. F. Chapman, and G. R. Fleming, J. Phys. Chem. 95, 1012 (1991).

[26] P. Mukherjee, M. Halder, M. Hargrove, and J. W. Petrich, Photochem. Photobiol. 82, 1586 (2006).

[27] M. J. Cocco and J. T. J. Lecomte, Protein Sci. 3, 267 (1994).

[28] S. Kundu, B. Snyder, K. Das, P. Chowdhury, J. Park, J. W. Petrich, and M. S. Hargrove, Proteins: Struct., Funct., Genet. 46, 268 (2002); S. Kundu and M. S. Hargrove, Proteins: Struct., Funct., Genet. 50, 239 (2003).

[29] M. S. Hargrove, E. W. Singleton, M. L. Quillin, L. A. Ortiz, G. N. Phillips, J. S. Olson, and A. J. Mathews, J. Biol. Chem. 269, 4207 (1994).

[30] J. A. Gardecki and M. Maroncelli, Appl. Spectrosc. 52, 1179 (1998).

[31] P. K. Chowdhury, M. Halder, L. Sanders, T. Calhoun, J. L. Anderson, D. W. Armstrong, X. Song, and J. W. Petrich, J. Phys. Chem. B 108, 10245 (2004).

[32] R. S. Fee and M. Maroncelli, Chem. Phys. 183, 235 (1994).

[33] L. S. Headley, P. Mukherjee, J. L. Anderson, R. Ding, M. Halder, D. W. Armstrong, X. Song, and J. W. Petrich, J. Phys. Chem. A 110, 9549 (2006).

[34] S. Arzhantsev, N. Ito, M. Heitz, and M. Maroncelli, Chem. Phys. Lett. 381, 278 (2003); N. Ito, S. Arzhantsev, M. Heitz, and M. Maroncelli, J. Phys. Chem. B 108, 5771 (2004).

[35] M. Marchi and P. Procacci, Chem. Phys. 108, 5194 (1999).

[36] D. A. Pearlman, D. A. Case, J. W. Caldwell, W. S. Ross, T. E. Cheatham, III, S. DeBolt, D. Ferguson, S. Seibel, and P. Kollman, Comput. Phys. Commun. 91, 1 (1995).

[37] M. E. Tuckerman, B. Berne, and G. J. Martyna, Chem. Phys. 97, 1992 (1990).

[38] M. Maroncelli and G. R. Fleming, J. Chem. Phys. 89, 5044 (1988).

[39] R. Jimenez, G. R. Fleming, P. V. Kumar, and M. Maroncelli, Nature 369, 471 (1994).

[40] T. Li, A. A. Hassanali, Y.-T. Kao, D. Zhong, and S. J. Singer, J. Am. Chem. Soc. 129, 3376 (2007).

[41] L. Nilsson and B. Halle, Proc. Natl. Acad. Sci. U. S. A. 102, 13867 (2005).

[42] J. R. Lakowicz, Principles of fluorescence spectroscopy, 2nd ed. (Springer, New York, 2004).

CHAPTER IX. GENERAL CONCLUSIONS

Owing to the diverse applications in widespread antitumor and antiviral activities the primary photophysical processes of hypericin has been extensively studied in bulk organic solvents. It has been concluded that upon light absorption there is an intramolecular hydrogen atom transfer followed by an intermolecular proton transfer. However to further understand the photodynamic action of hypericin it is important to study the interaction of hypericin with different macromolecules. Interaction of hypericin with two different isoforms, A1-1 and P1-1, of Glutathione S-transferase (GST) proteins has been studied in chapter III. The results are compared to our previous study of hypericin/HSA interaction. It has been demonstrated that hypericin binds to GST proteins with submicromolar affinity with a binding stoichiometry of hypericin: GST = 2:1. Most importantly two GST isoforms tune the hypericin photophysics differently. While there is extensive singlet oxygen generation when hypericin binds A1-1 this pathway is suppressed in the corresponding P1-1 complex. These results were understood based on a kinetic scheme in which the triplet state of hypericin decays by two competing processes, namely, interaction with ground state oxygen to produce singlet oxygen and ionization by liberating a proton, the latter being modulated by different protein environment. Although intramolecular H-atom transfer is impeded in both complexes, the triplet state of hypericin is still capable to liberate proton to the environment.

Understanding the photomovements in ciliates is a fascinating topic. Two photoreceptor pigments have been characterized earlier from Stentor coeruleus and Blepharisma japonicum. While it is suggested that similar pigments might exist in other ciliates the structures of these are not characterized. The photoreceptor pigment from heterotrich marine ciliate, Maristentor dinoferus, has been characterized in chapter IV. The

major pigment in the ciliate was found to be structurally similar to hypericin and stentorin but differs in the fact that it bears no aromatic hydrogens. The structure of the pigment is based on hypericin skeleton and the fluorescence spectra identical to those of hypericin but shifted towards the red. Fluorescence lifetime of the isolated pigment was found to be ~ 5.5 ns in DMSO which is identical to the corresponding value of hypericin. It is interesting to note that although the structures of stentorin and maristentorin are similar, while Stentor coeruleus shows an abrupt photobhobic response, Maristentor dinoferus exhibits a slow photophilic response. Clearly the immediate environment of these pigments in the corresponding species is different which might play an important role in the photoresponse in these ciliates. Such different behavior has been demonstrated in our study involving GST-hypericin interactions where the photophysics of hypericin was strongly modulated in the presence of two different isofroms of GST proteins, namely, A1-1 and P1-1.

Room temperature ionic liquids (RTILs) are gaining attention in the scientific community owing to their potential for use as "green solvents". Consequently it is of interest to understand the nature of dynamic solvation in this fascinating class of solvent. One of the outstanding questions is to understand the role of the constituent ions in the solvation response. Earlier based on a comparison between an ionic liquid with its neutral organic counterpart we have demonstrated that the early time solvation response is dominated by the cation response. To further gain insight into this we have attempted to compare the solvation response of coumarin 153 (C153) in a bulk imidazolium based ionic liquid with its micelle in water where the cationic part is responsible to form the micelle. This gives us an opportunity to compare the solvation response in two widely separated environments, namely the bulk and micellar environments. In chapter V we have demonstrated that while C153 resides in

the Stern layer of the micelle, the extent of faster solvation was found to be very similar in bulk and micellar environment. Based on this we suggested that the initial faster solvation response (≤ 100 ps) is dominated by the imidazolium cation. However, the average solvation time was found to be considerably faster in the micellar environment compared to the bulk which was understood as being the contribution of localized water molecules in the Stern layer of the micelle.

The study undertaken in chapter V is limited because this was based on only imidazolium based ionic liquid; also the bulk solvent exists as an opaque solid at the experimental temperature. To achieve a firmer conclusion, this study should be extended to other classes of ionic liquids. Towards this goal we have undertaken similar studies in a phosphonium based ionic liquid, results are presented in chapter VI. From this study it emerges that our interpretation regarding the cation dependence on the early time solvation response is not as definitive as we had proposed earlier. Part of the difficulty in the comparison is probably associated with the water molecules which are colocalized with C153 in the Stern layer of the micelle. During this study we have also realized that our results on phosphonium based ionic liquids are somewhat in disagreement with previously published results. Towards this point we have extensively discussed the possible sources of discrepancy based on the calculation of "zero-time" spectrum and focused on the importance of special precaution while comparing data obtained from different laboratories. We note that more physical insight on the nature of the solvation response in phosphonium based ionic liquids should await results from dielectric calculations.

To understand the dielectric relaxation in protein environment it is required to characterize a model system in which solvation dynamics could be studied and hence can be

compared to the theoretical calculations. Previously based on Job's plot analysis, caplillary electrophoresis, circular dichroism, molecular dynamics simulation, steady-state fluorescence and time-resolved fluorescence anisotropy experiments we have proposed that the complex of C153 with apomyoglobin (apoMb) provides such a model system. It has been demonstrated that C153 binds to the heme pocket of the protein with 1:1 binding stoichiometry. To further explore the nature of this binding especially to demonstrate that this binding involves negligible non-specific interaction (that is, surface binding) we have undertaken Job's plot analysis in apoprotein and compared the results with those obtained with the holoprotein. The data from these experiments are discussed in chapter VII. Similar experiments were also extended to apoMb-ANS complex, ANS being known to bind to the heme pocket of the apoprotein. The nature of the Job's plot in apoMb was found to be similar with both C153 and ANS which differs from that of in the holoMb. This extensively demonstrates that C153 binds specifically to the hydrophobic heme pocket of the protein molecule and consequently validates its use to study the dielectric relaxation of proteins.

Following the characterization of apoMb-C153 complex as a potential system to study the dielectric response of proteins we have undertaken solvation dynamics experiments of C153 in apoMb and compared the experimental results with that obtained from theoretical calculations. Similar experiments were also extended to another similar monomeric hemeprotein apoleghemoglobin (apoLba). Our results from these experiments are discussed in chapter VIII. Experimental results were found to be in very good agreement with theoretical calculations. Approximately 60 % of the C153 solvation was found to be very rapid and occurs within 300 femtoseconds. The very fast solvation response was attributed to bulk type solvation. The possibility of the protein contribution was also discussed. The

difference in the longer solvation response was attributed to the difference in the heme pocket of apoMb and apoLba. The importance of the construction of the "zero-time" spectrum is discussed while arguing against the presence of special type of water, namely, "biological water".

VITA

NAME OF AUTHOR: Prasun Mukherjee

DATE AND PLACE OF BIRTH: December 14, 1979, Guwahati, India

DEGREES AWARDED:
B. S. in Chemistry, Alipurduar College, North Bengal University, 2000
M. S. in Chemistry, Indian Institute of Technology, Bombay, 2003

HONORS AND AWARDS:
The Chevron Phillips Travel Award, 2006
ISU Teaching Excellence Award, 2006
The Proctor & Gamble Fellowship in Analytical Chemistry, 2007

PROFESSIONAL EXPERIENCE:
Teaching and Research Assistant, Department of Chemistry, Iowa State University, 2003-2006
Research Assistant, Department of Chemistry, Iowa State University, 2006-2008

PROFESSIONAL PUBLICATIONS:
1. Sambhu N. Datta, Prasun Mukherjee and Praket P. Jha. "Ab Initio Quantum Chemical Investigation of the Spin States of Some Chain and Monocyclic Diradicals." J. Phys. Chem. A, 2003, 107, 5049-5057.
2. M. Halder, P. K. Chowdhury, R. Das, P. Mukherjee, W. M. Atkins and J. W. Petrich. "Interaction of Glutathione S-Transferase with Hypericin: A Photophysical Study." J. Phys. Chem. B, 2005, 109, 19484-19489.
3. Prasun Mukherjee, D. Bruce Fulton, Mintu Halder, Xinxin Han, Daniel W. Armstrong, Jacob W. Petrich and Christopher S. Lobban. "Maristentorin, a novel pigment from the positively phototactic marine ciliate Maristentor dinoferus, is structurally related to hypericin and stentorin." J. Phys. Chem. B, 2006, 110, 6359-6364.
4. M. Halder, L. S. Headley, P. Mukherjee, X. Song and J. W. Petrich. "Experimental and Theoretical Investigations of Solvation Dynamics of Ionic Fluids: Appropriateness of Dielectric Theory and the Role of DC Conductivity." J. Phys. Chem. A, 2006, 110, 8623-8626.
5. Lindsay Sanders Headley, Prasun Mukherjee, Jared L. Anderson, Rongfang Ding, Mintu Halder, Daniel W. Armstrong, Xueyu Song and Jacob W. Petrich. "Dynamic Solvation in Imidazolium-Based Ionic Liquids on Short Time Scales." J. Phys. Chem. A, 2006, 110, 9549-9554.
6. Prasun Mukherjee, Jeffrey A. Crank, Mintu Halder, Daniel W. Armstrong and Jacob W. Petrich. "Assessing the Roles of the Constituents of Ionic Liquids in Dynamic Solvation: Comparison of an Ionic Liquid in Micellar and Bulk Form." J. Phys. Chem. A, 2006, 110, 10725-10730.
7. Prasun Mukherjee, Mintu Halder, Mark S. Hargrove and Jacob W. Petrich. "Characterization of the Interactions of Fluorescent Probes with Proteins: Coumarin 153 and

1,8-ANS in complex with Holo- and Apomyoglobin." Photochem. Photobiol., 2006, 82, 1586-1590.

8. Mintu Halder, Prasun Mukherjee, Sayantan Bose, Mark S. Hargrove, Xueyu Song and Jacob W. Petrich. "Solvation dynamics in protein environments: Comparison of fluorescence upconversion measurements of coumarin 153 in monomeric hemeproteins with molecular dynamics simulations." J. Chem. Phys., 2007, 127, 055101-055106.

9. Christopher S. Lobban, Steven J. Hallam, Prasun Mukherjee and Jacob W. Petrich. "Photophysics and Multifunctionality of Hypericin-Like Pigments in Heterotrich Ciliates: A Phylogenetic Perspective." Photochem. Photobiol., 2007, 83, 1074-1094.

10. Jun Xu, Jun Wang, Mike Mitchell, Prasun Mukherjee, Malika Jeffries-EL, Jacob W. Petrich and Zhiqun Lin. "Organic–Inorganic Nanocomposites Prepared by Grafting Conjugated Polymers onto Quantum Dots." J. Am. Chem. Soc., 2007, 129, 12828-12833.

11. Prasun Mukherjee, Ramkrishna Adhikary, Mintu Halder, Jacob W. Petrich and Pavol Miskovsky. "Accumulation and Interaction of Hypericin in Low Density Lipoprotein (LDL): A Photophysical Study." Photochem. Photobiol., (in press).

12. Prasun Mukherjee, Jeffrey A. Crank, Pritesh S. Sharma, Aruna B. Wijeratne, Ramkrishna Adhikary, Sayantan Bose, Daniel W. Armstrong and Jacob W. Petrich. "Dynamic Solvation in Phosphonium Ionic Liquids: Comparison of Bulk and Micellar Systems and Considerations for the Construction of the Solvation Correlation Function, C(t)." J. Phys. Chem. B, 2008, 112, 3390-3396.

13. Ramkrishna Adhikary, Sayantan Bose, Prasun Mukherjee, Aniket Thite, George A. Kraus, Aruna B. Wijeratne, Pritesh S. Sharma, Daniel W. Armstrong and Jacob W. Petrich. "Influence of Chiral Ionic Liquids on the Excited-State Properties of Naproxen Analogs." J. Phys. Chem. B, (accepted).

14. Holger Schönenbrücher, Ramkrishna Adhikary, Prasun Mukherjee, Thomas A. Casey, Mark A. Rasmussen, Frank D. Maistrovich, Marcus E. Kehrli, Jr., Jürgen A. Richt and Jacob W. Petrich. "Towards a new fluorescence based method for the real-time detection of central nervous system (CNS) tissues on bovine carcasses." J. Agric. Food Chem., (submitted).

15. Prasun Mukherjee, Sayantan Bose, Alyse A. Hurd, Ramkrishna Adhikary, Holger Schönenbrücher, Thomas A. Casey, Mark A. Rasmussen and Jacob W. Petrich. "Monitoring the Accumulation of Lipofuscin in Aging Murine Eyes by Fluorescence Spectroscopy." Photochem. Photobiol., (submitted).